Integrating Metalens Modeling into Multiscale System Simulations

Metalenses Belong to the Category of Flat Lenses

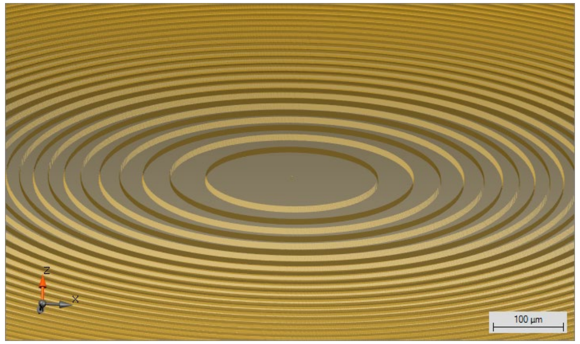

Illustration of a diffractive lens

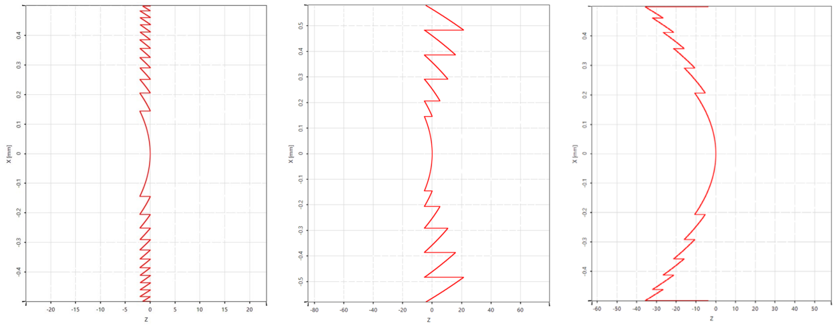

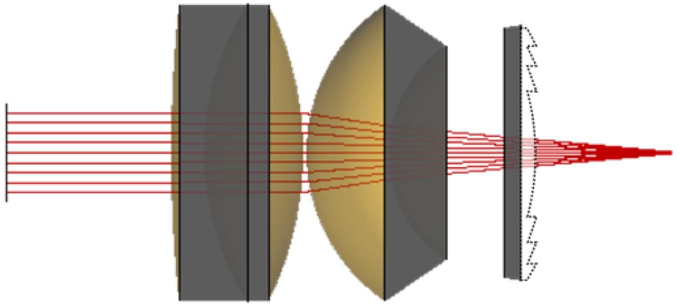

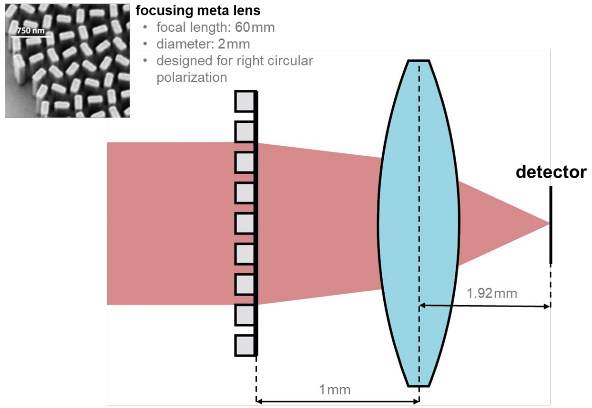

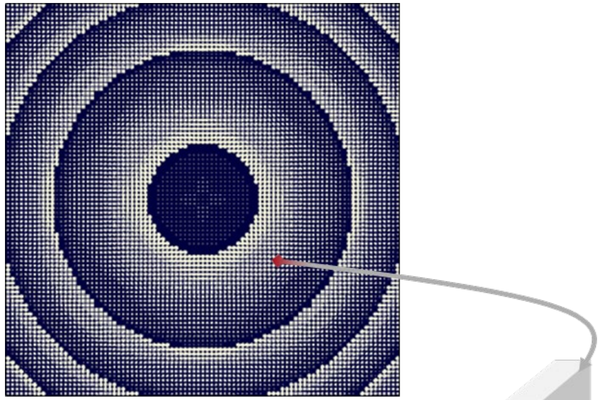

Illustration of a metalens

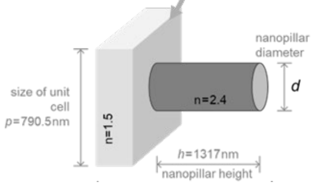

Introduction

Multiscale Optical Modeling and Design Software

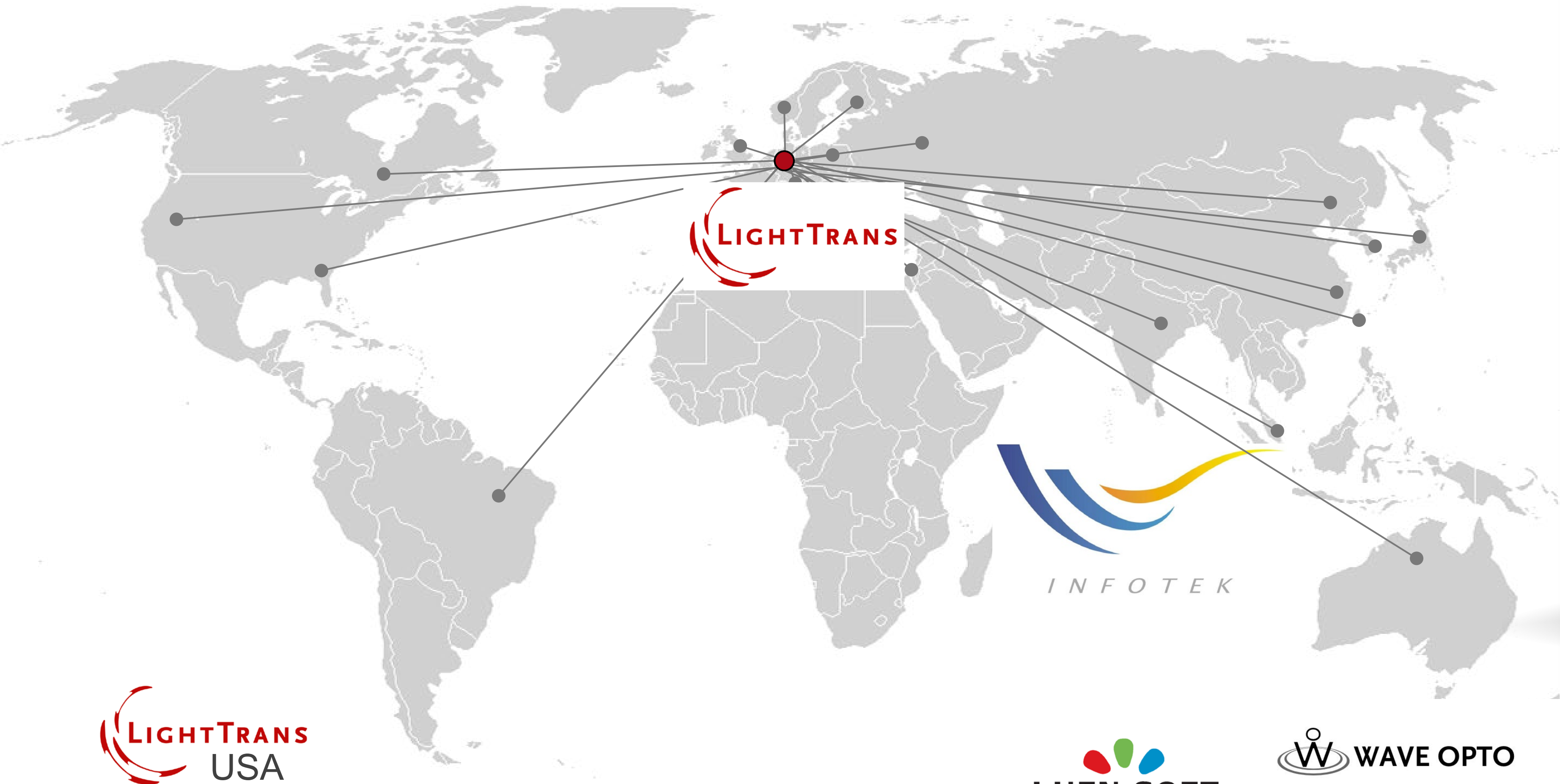

Thousands of licenses sold worldwide

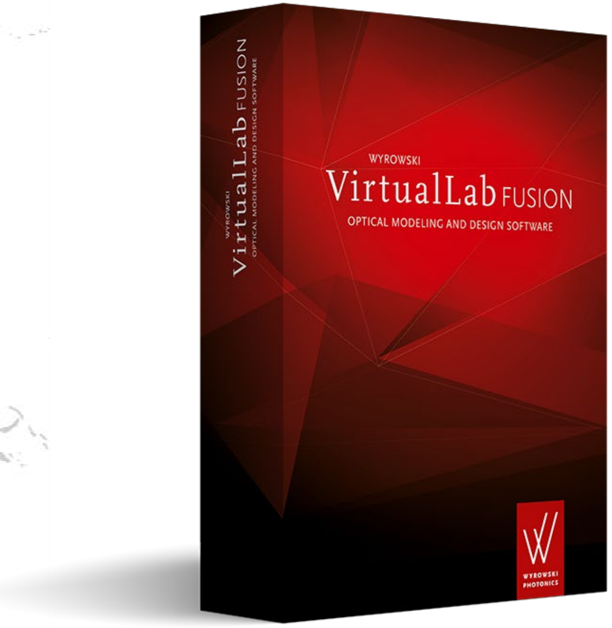

LightTrans USA

LUEN SOFT

WAVE OPTO

T.E.M. Incorporated

Simulation and Design of Flat Lenses using VirtualLab Fusion

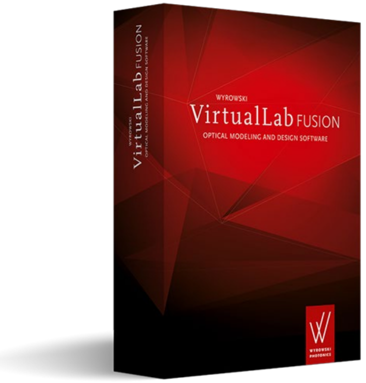

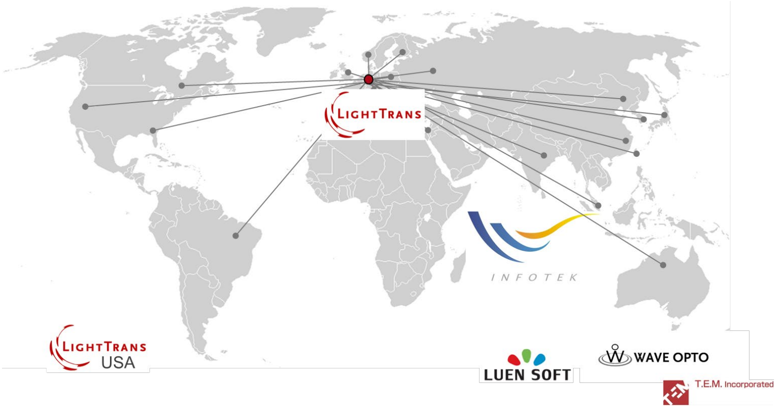

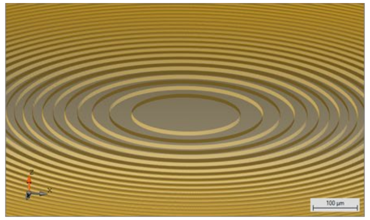

Illustration of a diffractive lens

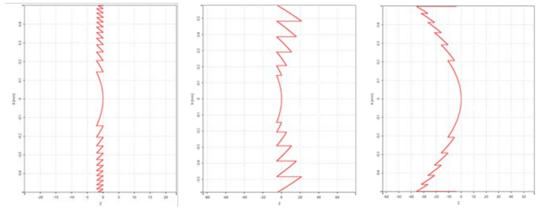

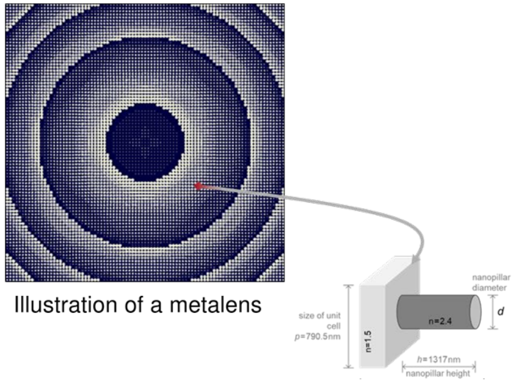

Illustration of a metalens

- VirtualLab Fusion is a multiscale simulation platform that serves a broad spectrum of applications.
- In this paper, we demonstrate the features of VirtualLab Fusion associated with flat lenses, which are planned for release in 2025.
- We aim to address various tasks and challenges faced in software development when integrating flat lenses into lens system design and modeling.

Simulation and Design of Flat Lenses using VirtualLab Fusion

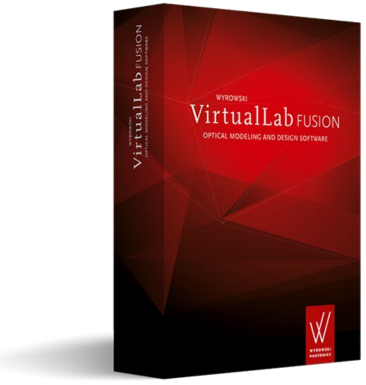

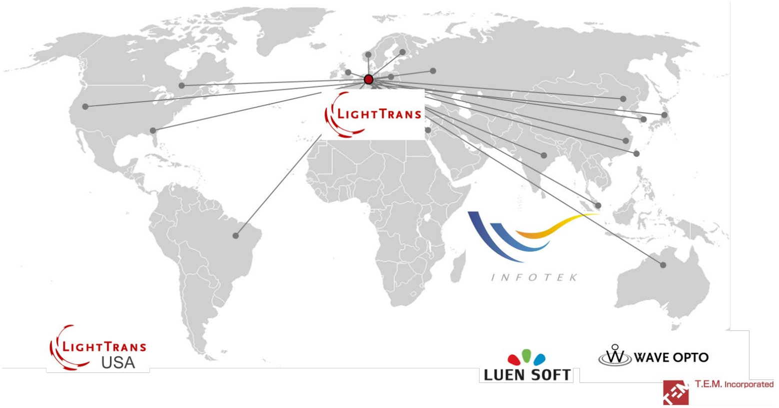

This article offers you

- a range of mathematical concepts,
- a wealth of insights, and
- example simulations and designs.

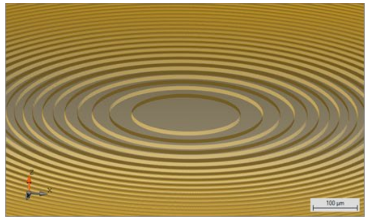
Illustration of a diffractive lens

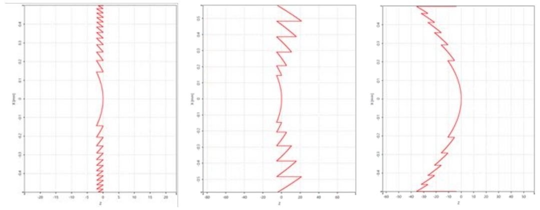

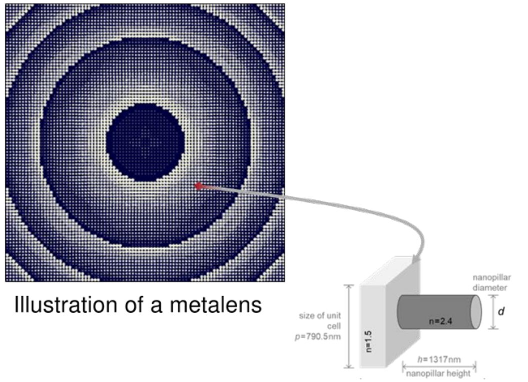

Illustration of a metalens

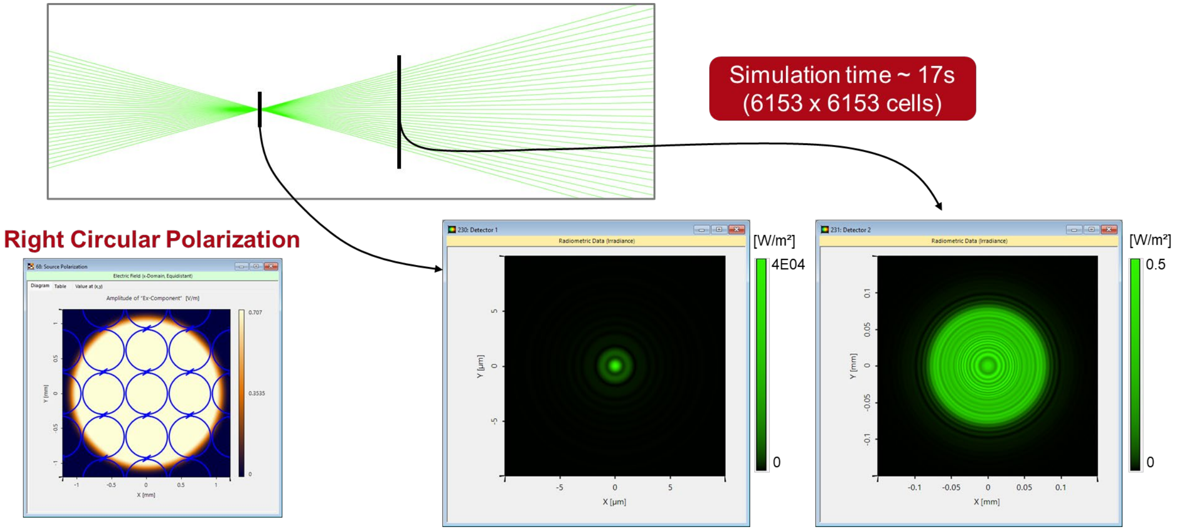

Simulation and Design of Flat Lenses using VirtualLab Fusion

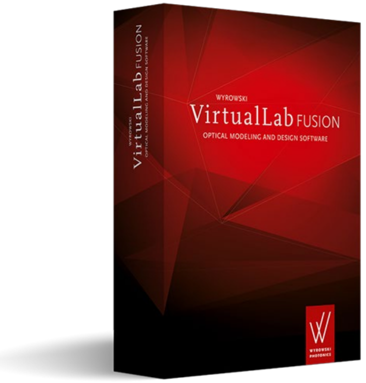

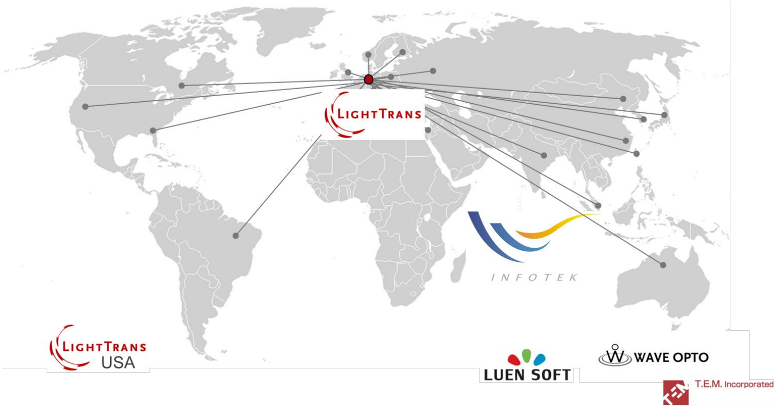

Our objective is to equip you with robust software tools that enable you to investigate the significance and utilization of flat lens technology in your endeavors.

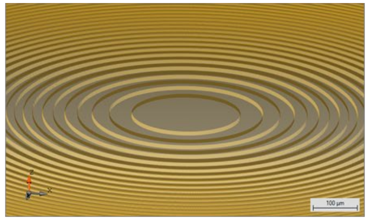

Illustration of a diffractive lens

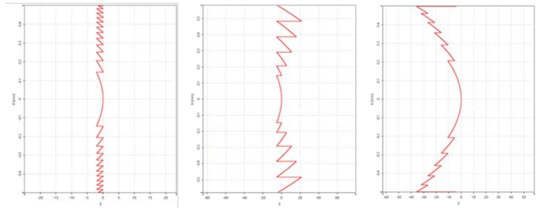

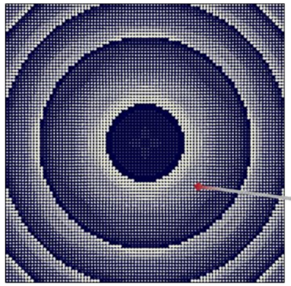

Illustration of a metalens

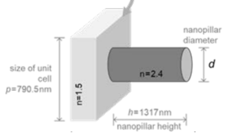

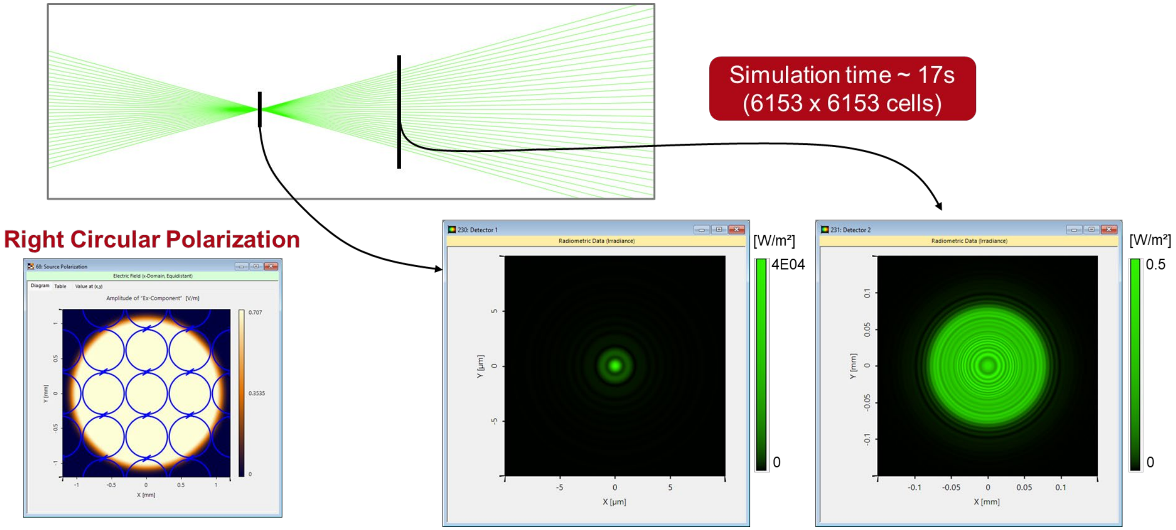

Multiscale Optical Simulation

Metalenses

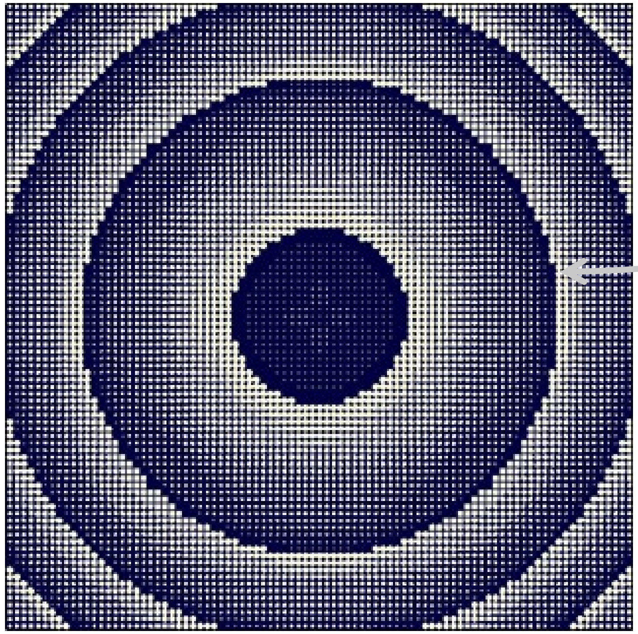

Illustration of a metalens

- Metasurfaces employ nanostructures with a high refractive index, commonly known as meta-atoms or metacells, arranged on a substrate that has a lower refractive index.
- This approach has been recognized for a while, but it has recently gained renewed interest.

P. Lalanne *et al*., J. Opt. Soc. Am. A **16**, 1143-1156 (1999).

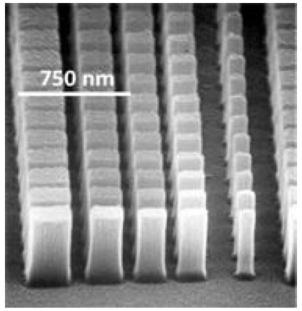

M. Khorasaninejad *et al*., Science **352**, 1190-1194 (2016).

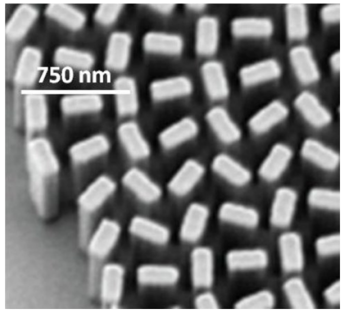

Metalenses: Historical Background and Assessment

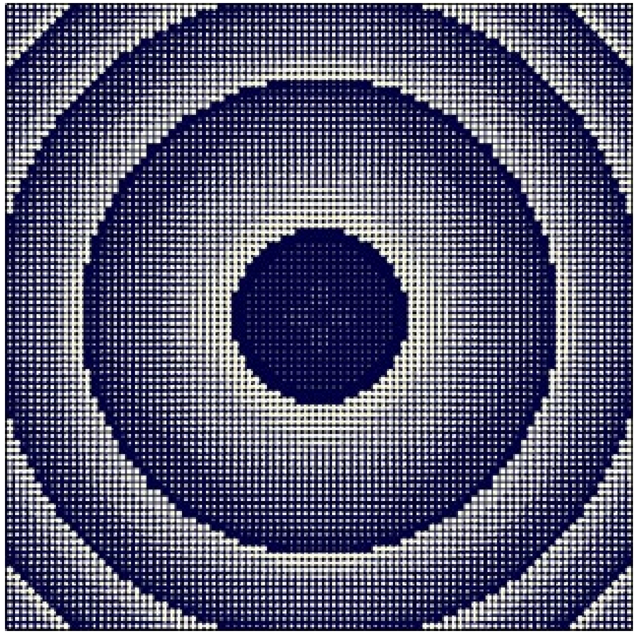

Illustration of a metalens

Recommened for an initial insightful read

LASER & PHOTONICS REVIEWS

2017

Laser Photonics Rev. **11,** No. 3, 1600295 (2017) / **DOI** 10.1002/lpor.201600295

EXPERT OPINION

Abstract The so-called 'flat optics' that shape the amplitude and phase of light with high spatial resolution are presently receiving considerable attention. Numerous journal publications seemingly offer hope for great promises for ultra-flat metalenses with high efficiency, high numerical aperture, broadband operation . . . We temperate the expectation by referring to the current status of metalenses against their historical background, assessing the technical and scientific challenges recently solved and critically identifying those that still stand in the way.

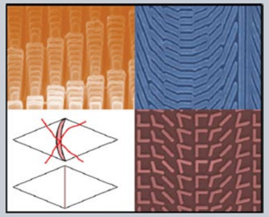

Metalenses at visible wavelengths: past, present, perspectives

Philippe Lalanne[1,*] and Pierre Chavel[2,3,*]

Tutorial

May/Jun 2023 • Vol. 5(3)

ADVANCED PHOTONICS

Wide field-of-view metalens: a tutorial

Fan Yang,[a] Mikhail Y. Shalaginov,[a] Hung-I Lin,[a] Sensong An,[a] Anu Agarwal,[a] Hualiang Zhang,[b] Clara Rivero-Baleine,[c] Tian Gu,[a,d,*] and Juejun Hu[a,d,*]

[a]Massachusetts Institute of Technology, Department of Materials Science and Engineering, Cambridge, Massachusetts, United States
[b]University of Massachusetts Lowell, Department of Electrical and Computer Engineering, Lowell, Massachusetts, United States
[c]Lockheed Martin Corporation, Orlando, Florida, United States
[d]Massachusetts Institute of Technology, Materials Research Laboratory, Cambridge, Massachusetts, United States

… with 220 references

Multiscale Simulation

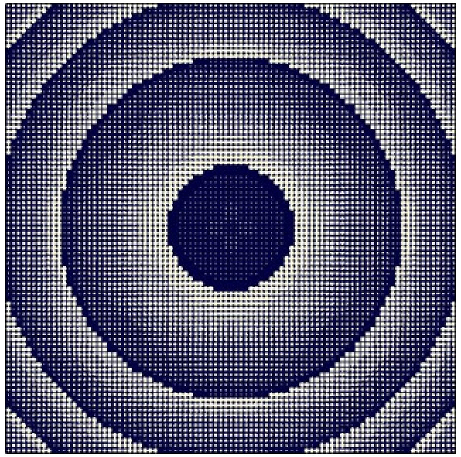

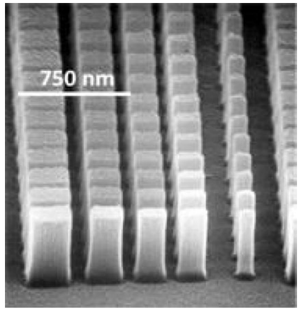

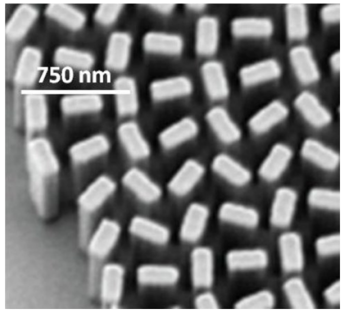

- Given that metasurfaces are composed of nanostructures, it is clear that a geometrical optics approach is unsuitable.
- Instead, it is necessary to utilize electromagnetic field theory based on Maxwell's equations, commonly known as physical optics.

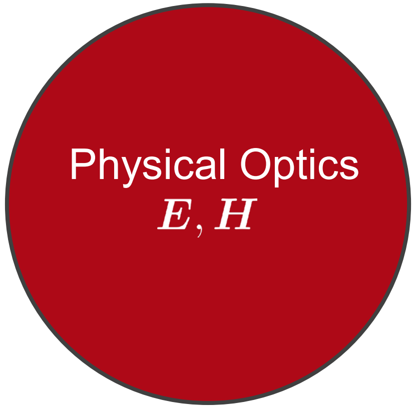

Multiscale Simulation with VirtualLab Fusion

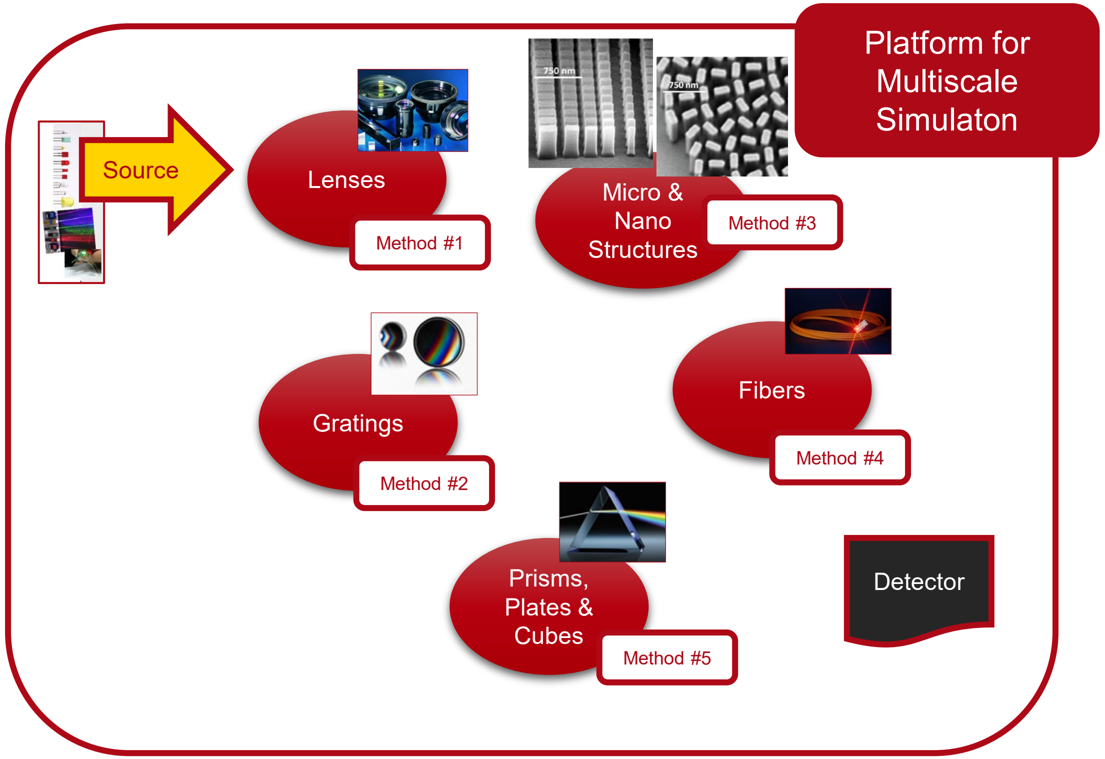

- Given that metasurfaces are composed of nanostructures, it is clear that a geometrical optics approach is unsuitable.
- Instead, it is necessary to utilize electromagnetic field theory based on Maxwell's equations, commonly known as physical optics.
- Modeling optical systems across different scales requires the integration of diverse simulation models within a unified physical optics framework.
- This is the approach that we take with our VirtualLab Fusion software.

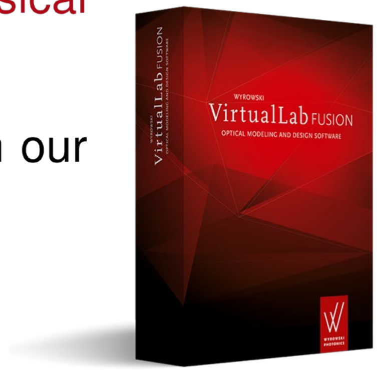

Geometrical Optics for Electromagnetic Fields

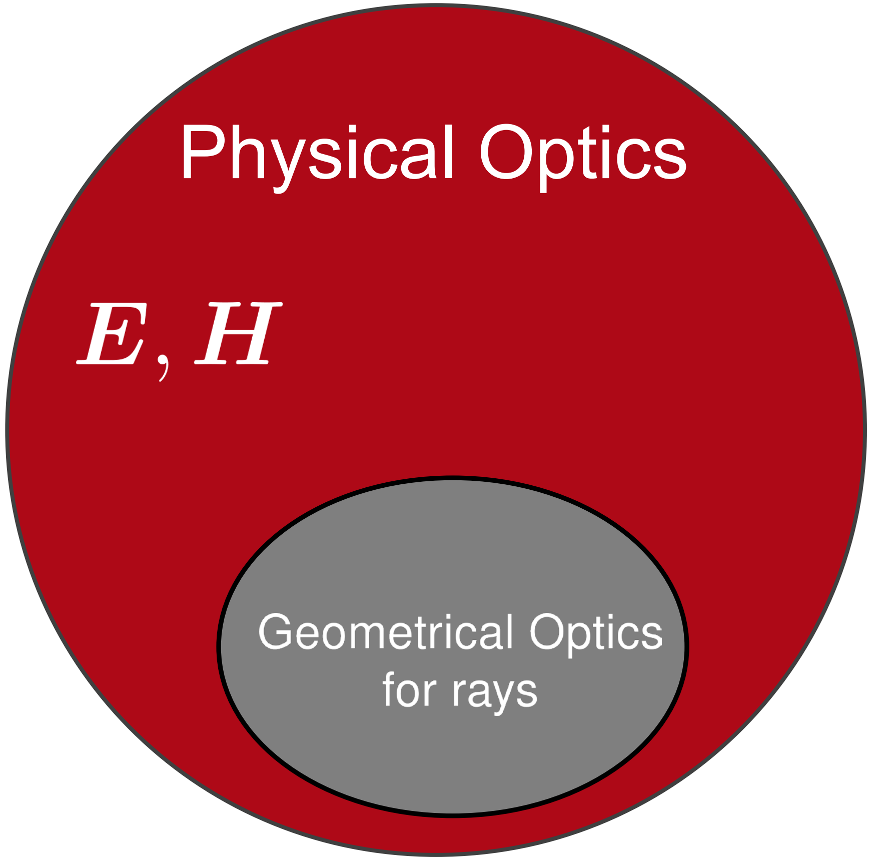

Geometrical Optics for Electromagnetic Fields

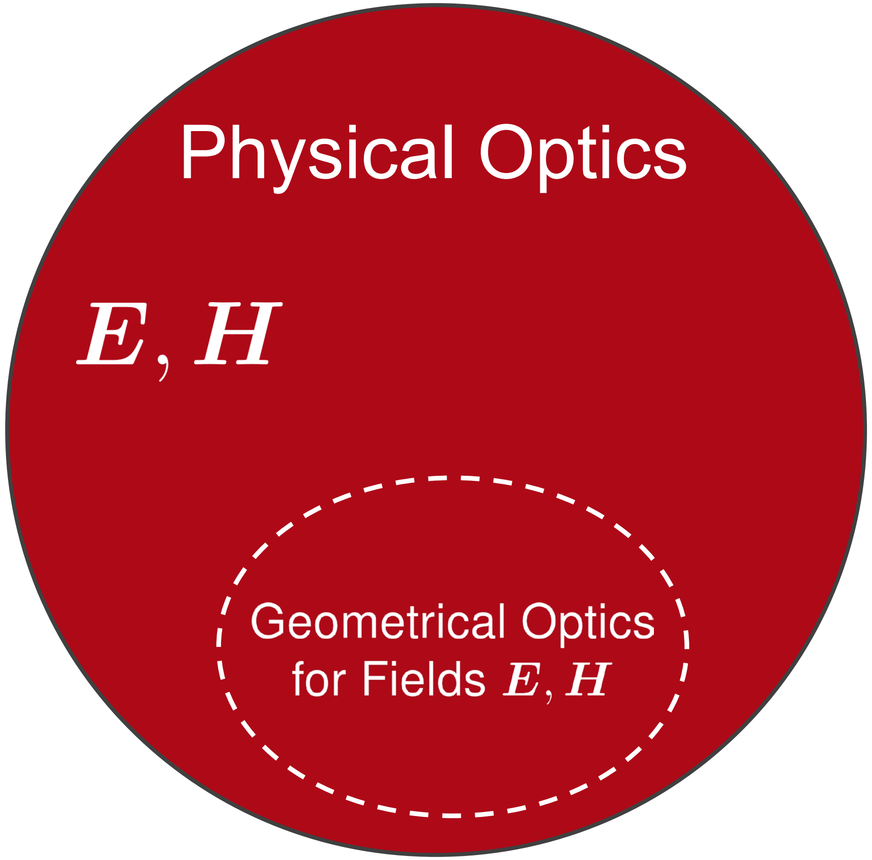

We follow Max Born's and Emil Wolf's advice!

We need to identify that part of physical optics, which deals with the "***geometrical laws relating to the propagation of the 'amplitude vectors' E and H.***"

Citation from 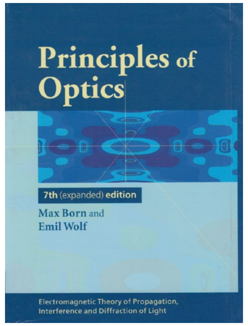

page 125

Multiscale Simulation with VirtualLab Fusion

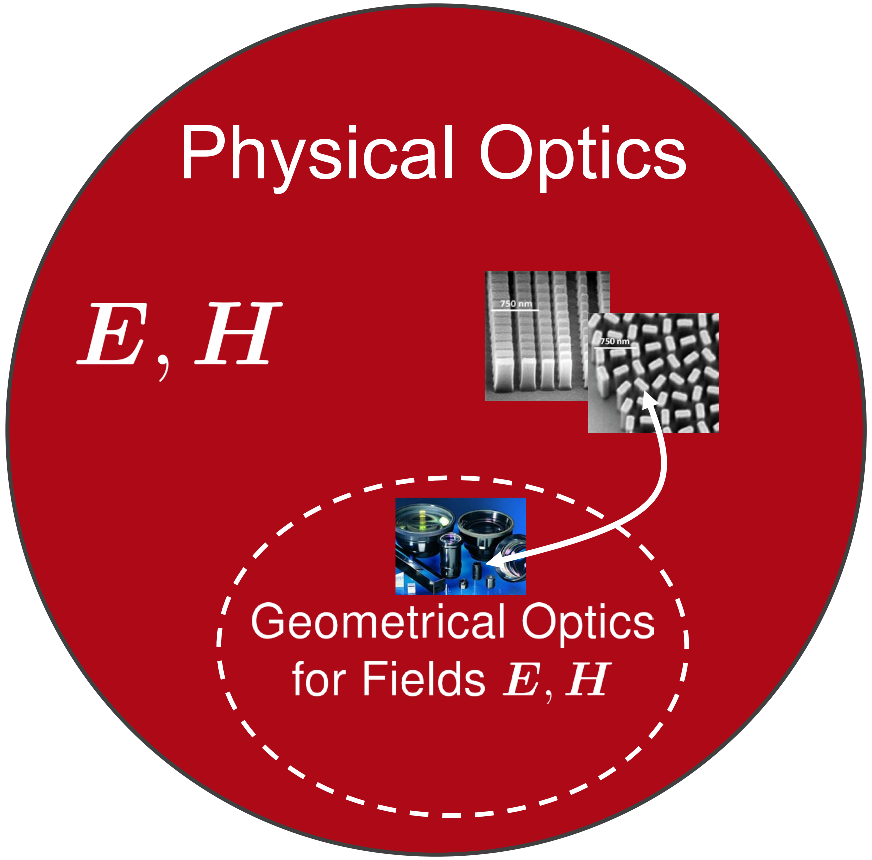

- By employing our unified approach for multiscale simulation, we can seamlessly link the geometrical optics modeling of a traditional lens surface with the sophisticated simulation model for a metalens.
- This leads to unparalleled speed in multiscale simulation when utilizing VirtualLab Fusion.

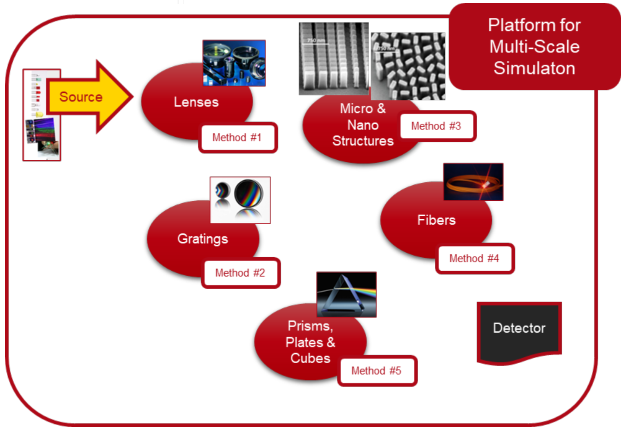

Modeling Scenario: Wafer Inspection System

micro-structured wafer

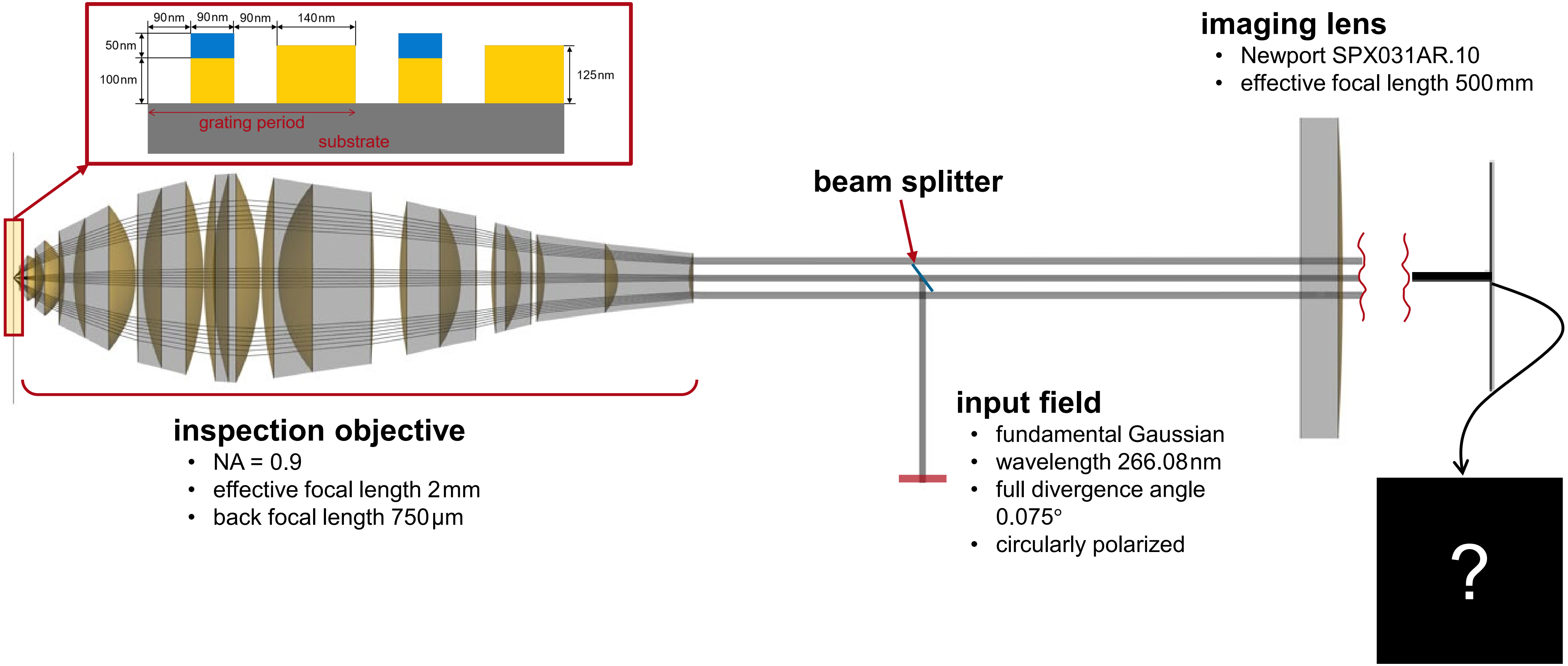

image

imaging lens
- Newport SPX031AR.10
- effective focal length 500 mm

inspection objective
- NA = 0.9
- effective focal length 2 mm
- back focal length 750 µm

input field
- fundamental Gaussian
- wavelength 266.08 nm
- full divergence angle 0.075°
- circularly polarized

Rays Derived from Multiscale Simulation

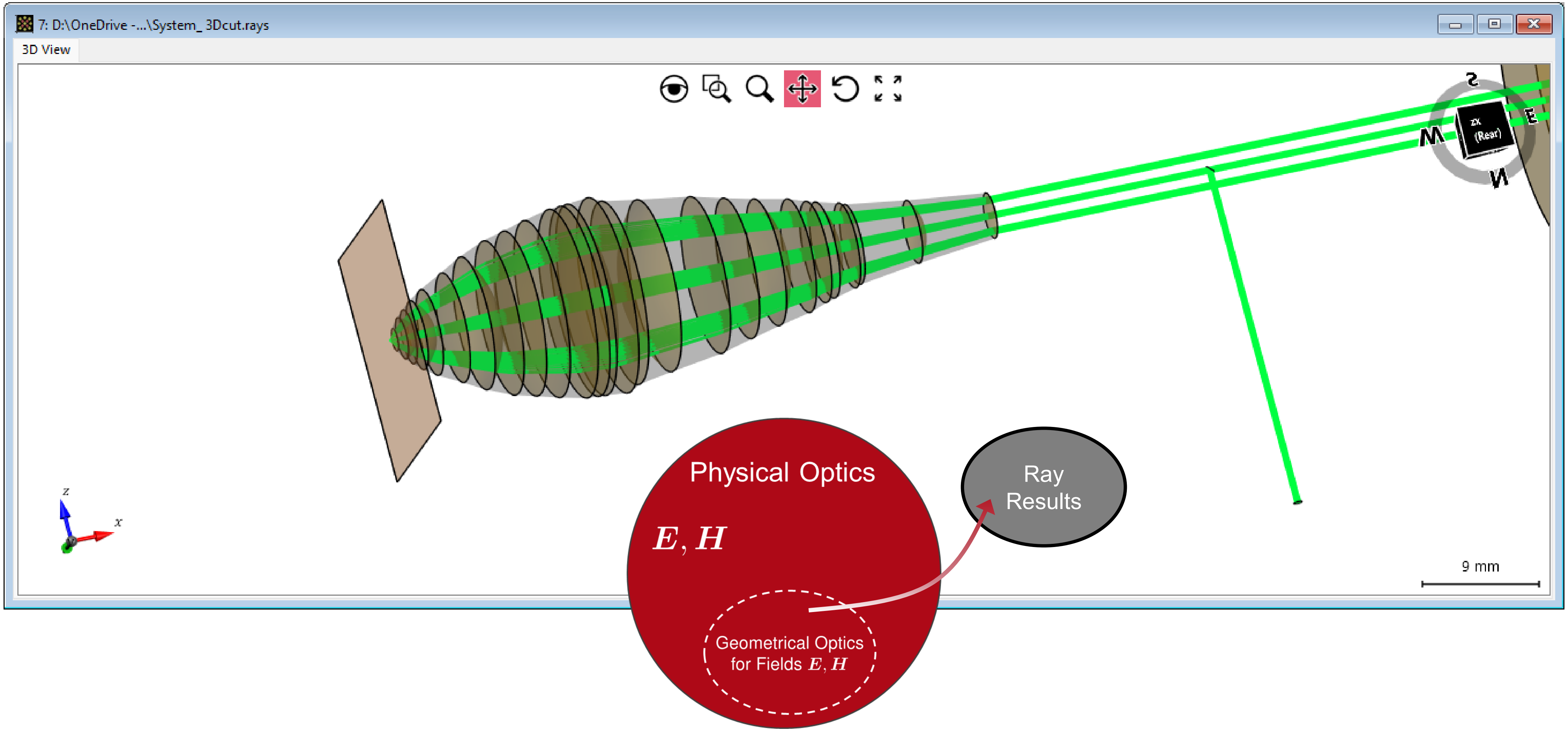

Multiscale Simulation: Focal Spot on Wafer Structure

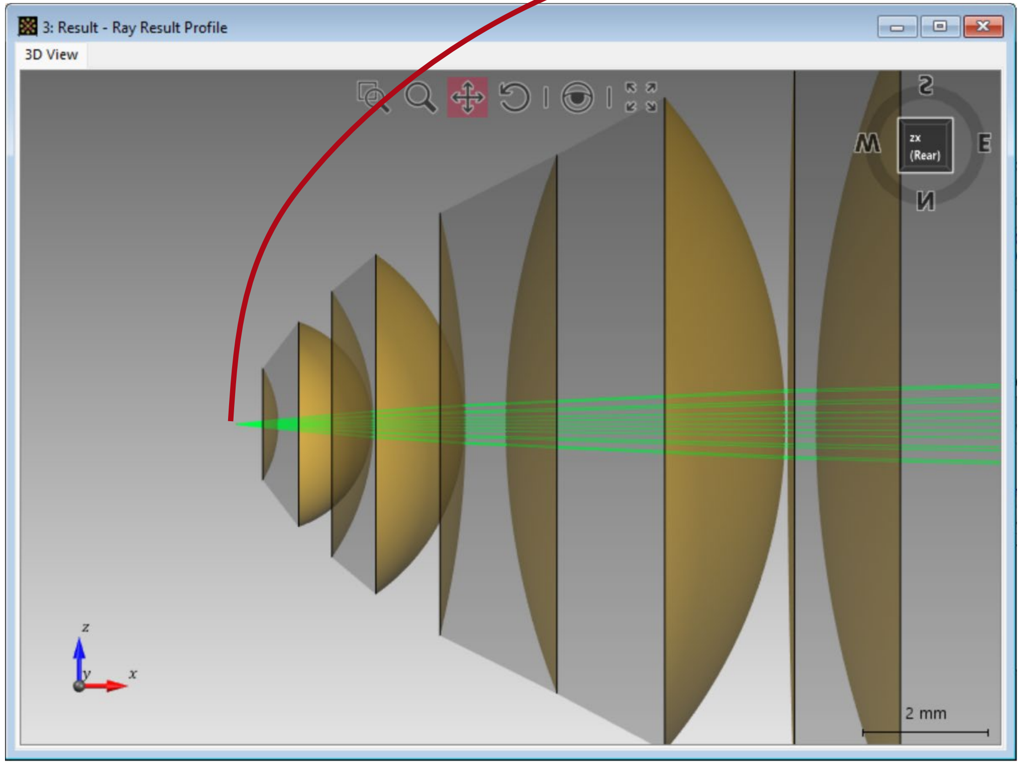

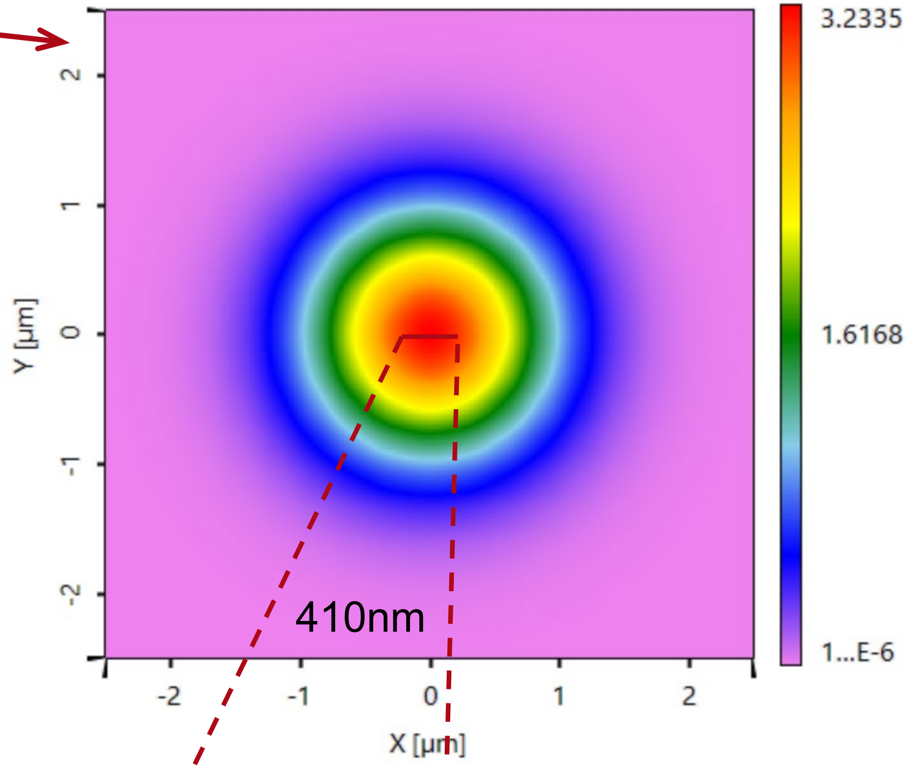

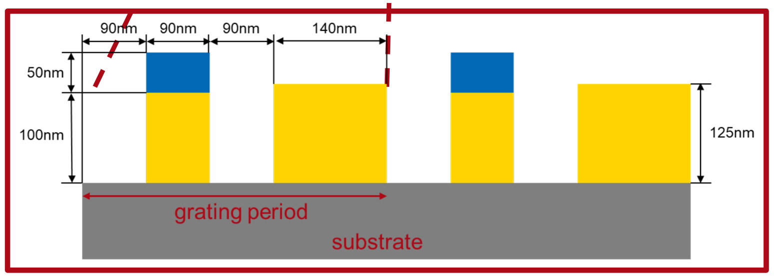

Image Generation through Multiscale Simulation

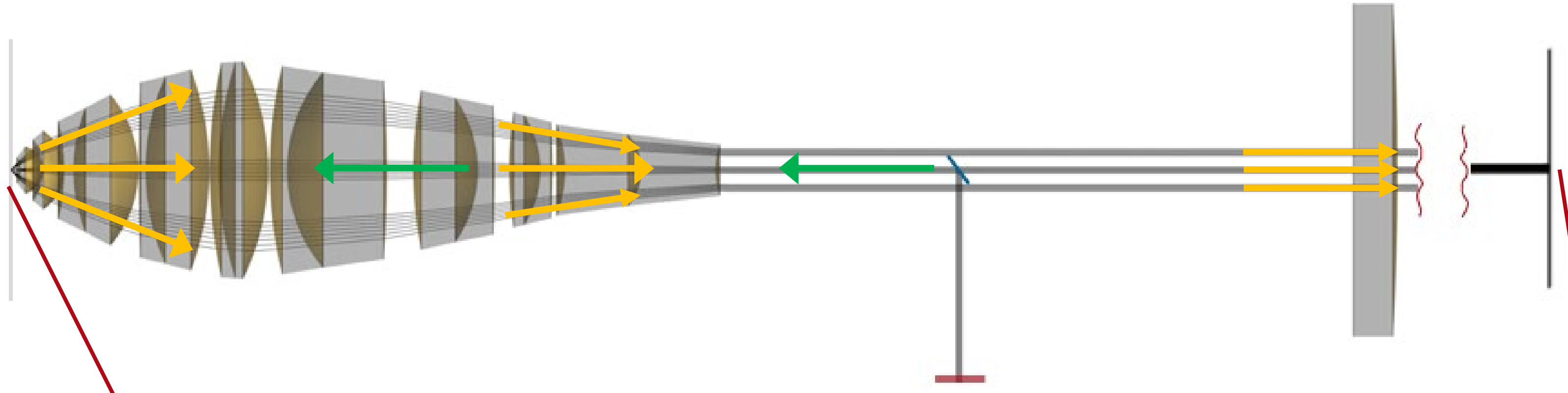

Wafer structure
in focus

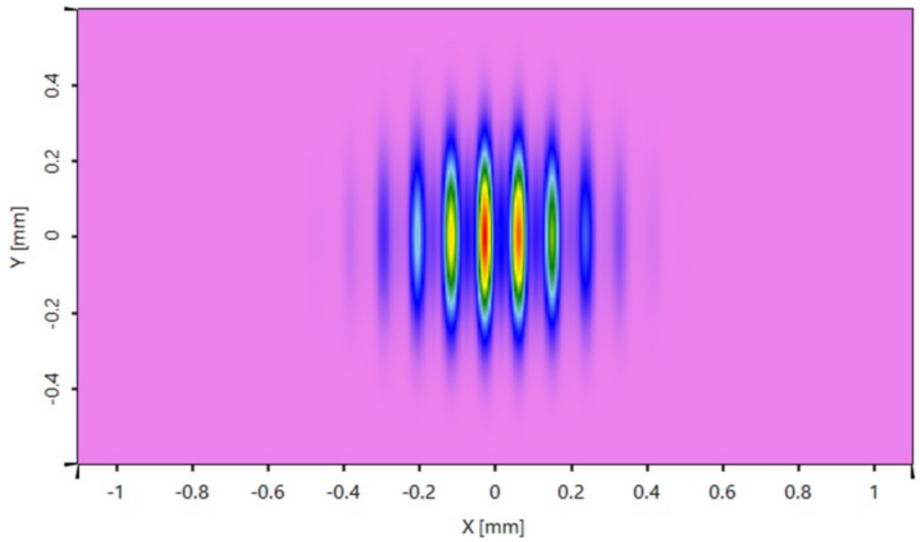

Image Generation through Multiscale Simulation

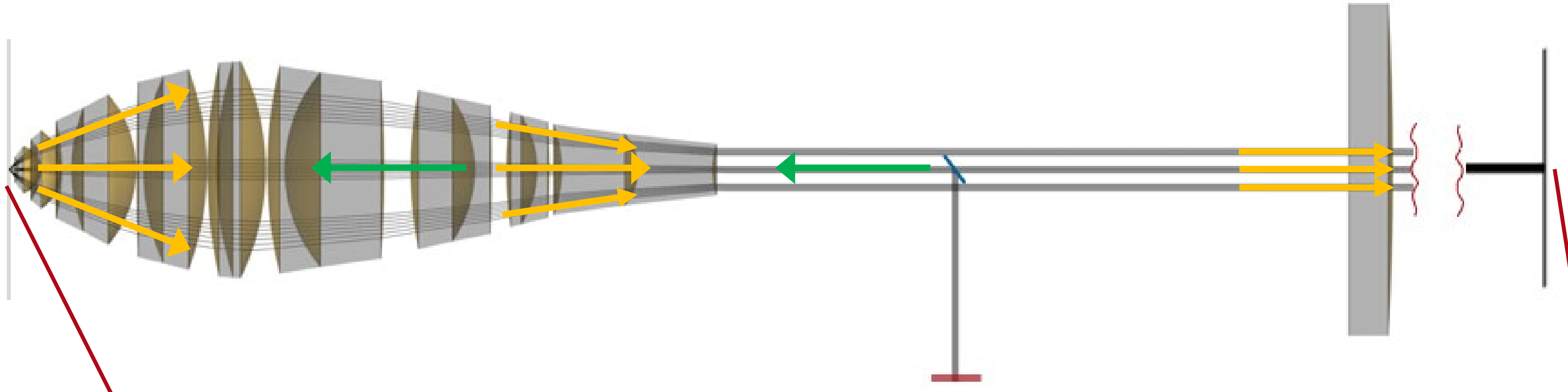

Wafer
structure 1µm
before focus

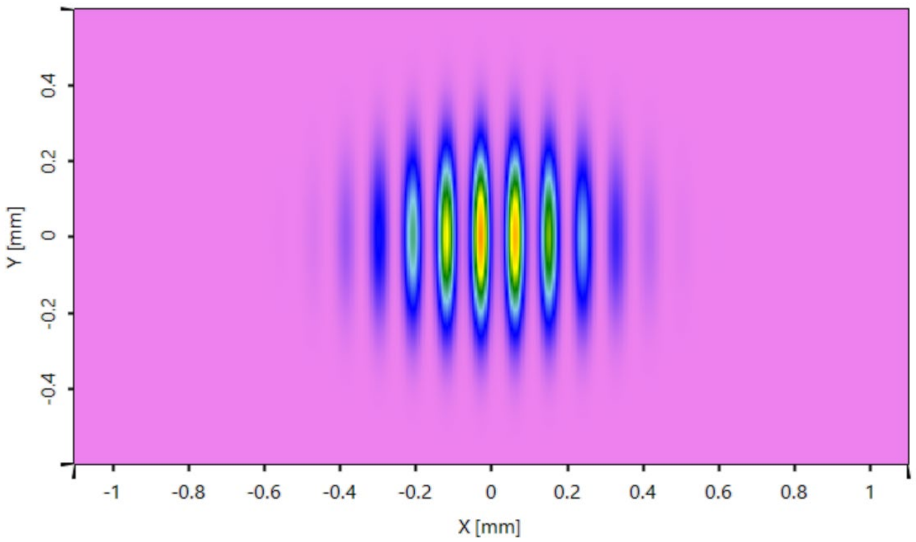

Image Generation through Multiscale Simulation

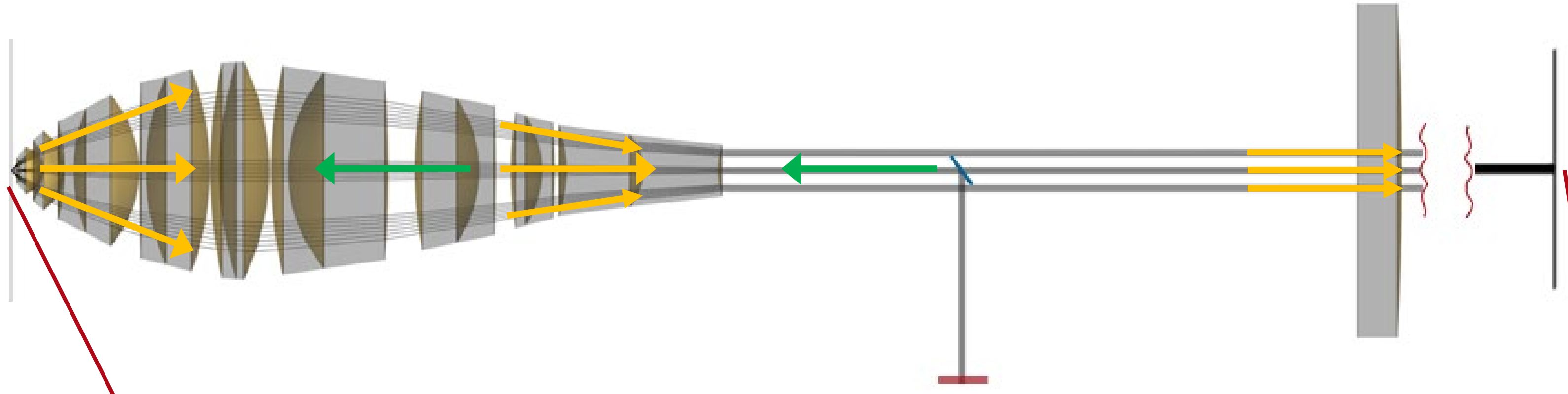

Wafer
structure 2µm
before focus

Siumlation time: seconds

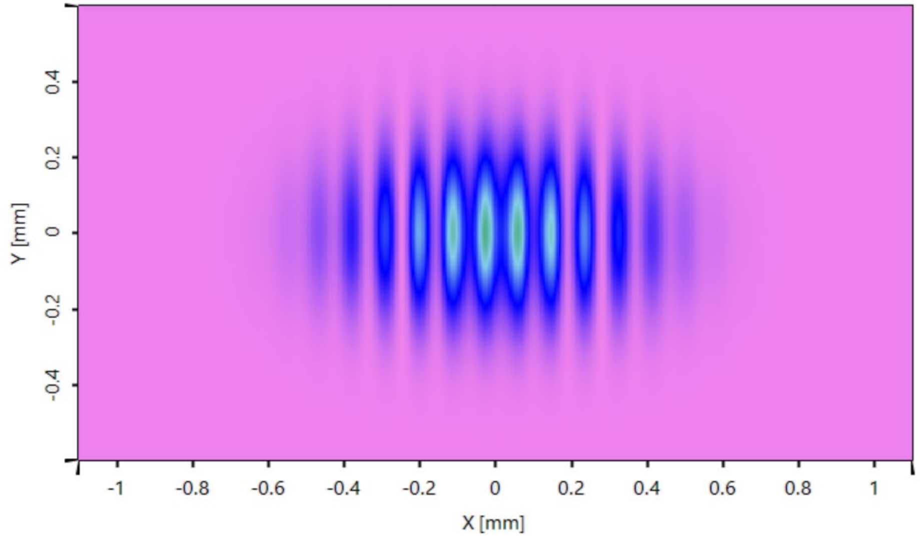

Interoperable Simulation Model for Metalenses

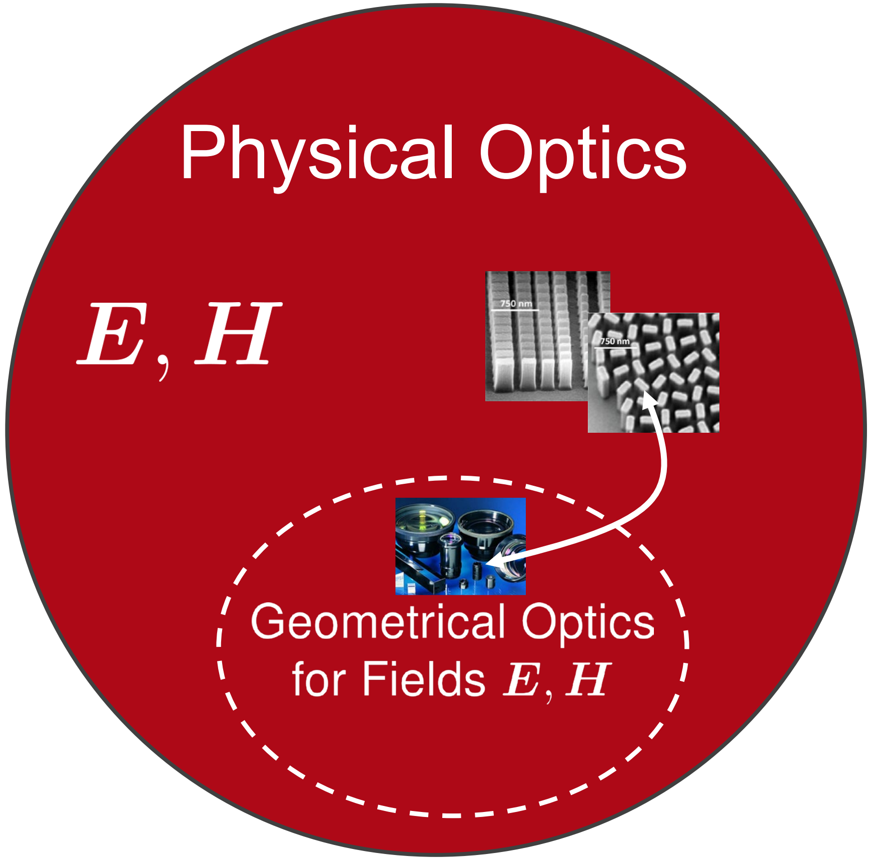

- The primary challenge in integrating metalenses into the multi-scale modeling framework of VirtualLab Fusion is creating a metalens simulation model that can seamlessly interact with the simulation models of other components, such as traditional lenses.

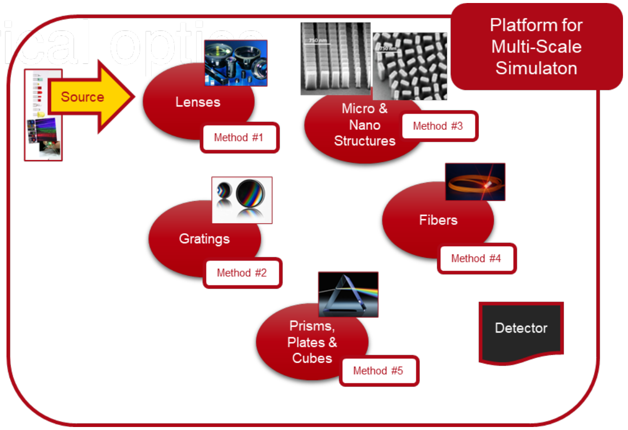

Application Potential of Flat Lenses

Some Basic Observations

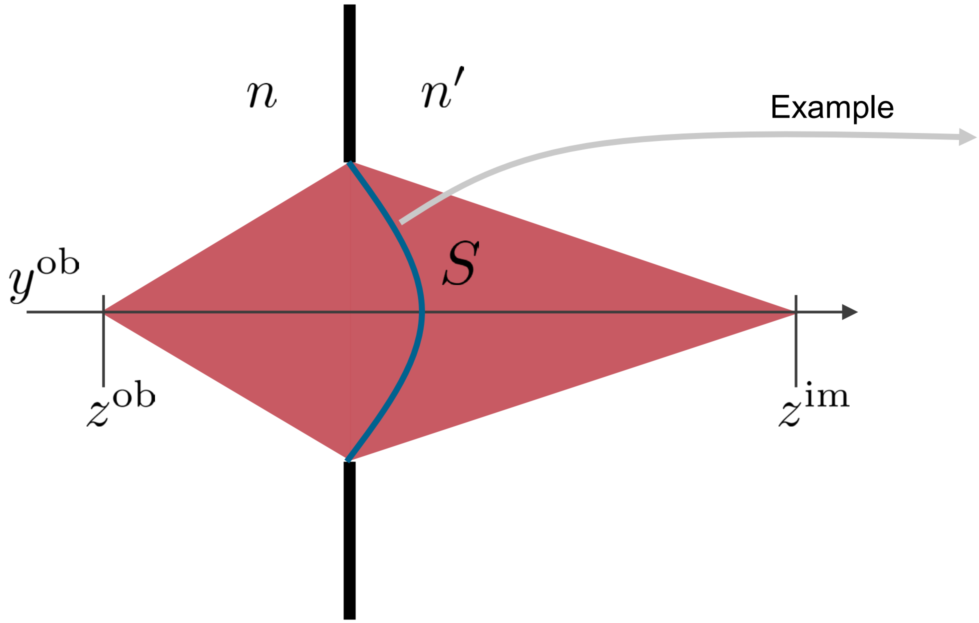

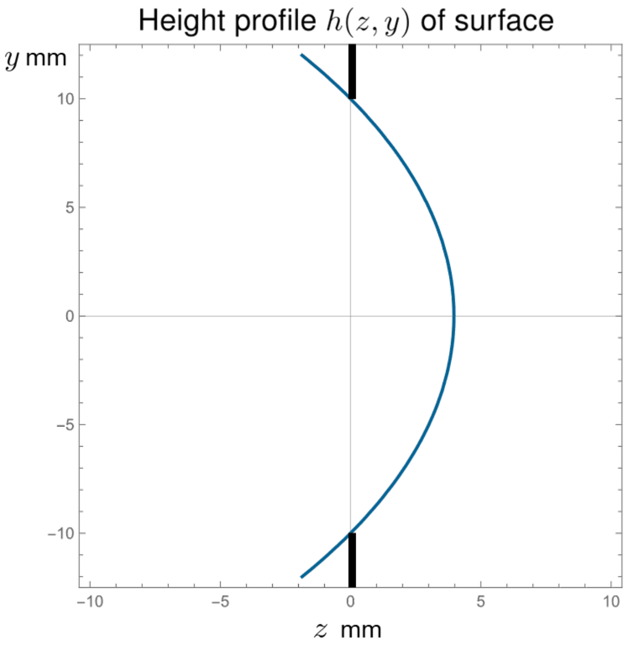

- Wavelength: $532\,\mathrm{nm}$
- Refractive indexes: $n = 1.5$ and $n' = 1$
- Lens radius: $10\,\mathrm{mm}$
- Object position: $z^{\mathrm{ob}} = -50\,\mathrm{mm}$
- Image position: $z^{\mathrm{im}} = 100\,\mathrm{mm}$
- Lateral position: $y^{\mathrm{ob}} = 0\,\mathrm{mm}$

Some Basic Observations

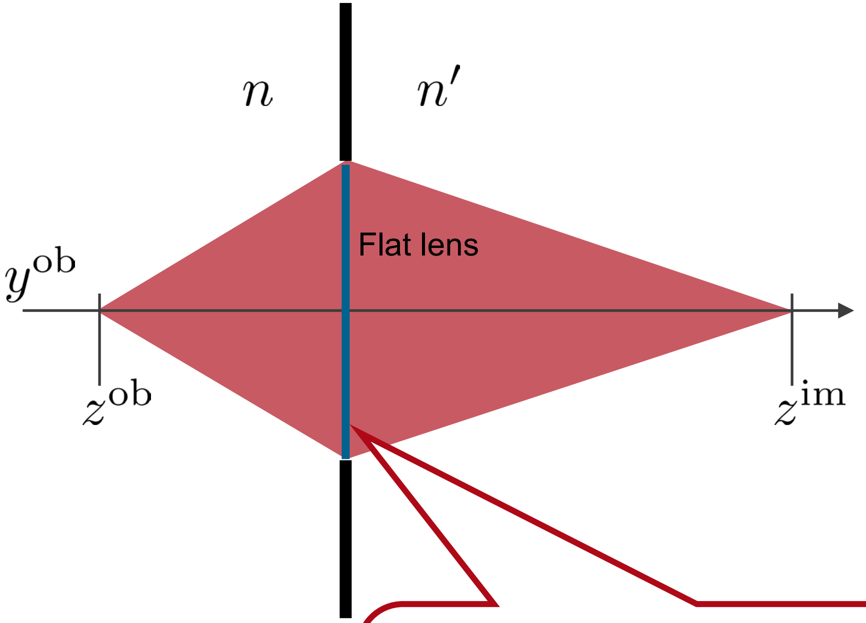

A flat lens does not alter the distances to the object and image planes, hence it does not reduce the system's length.

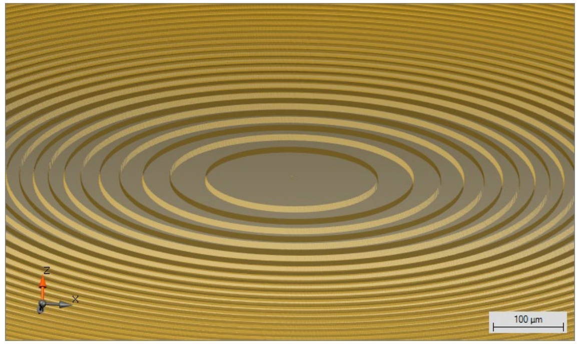

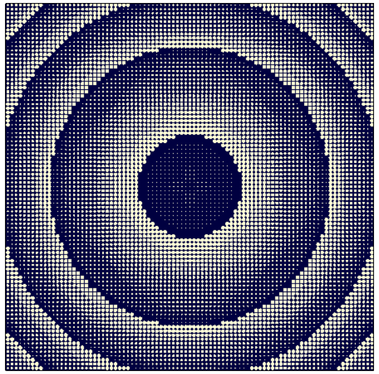

Some Basic Observations

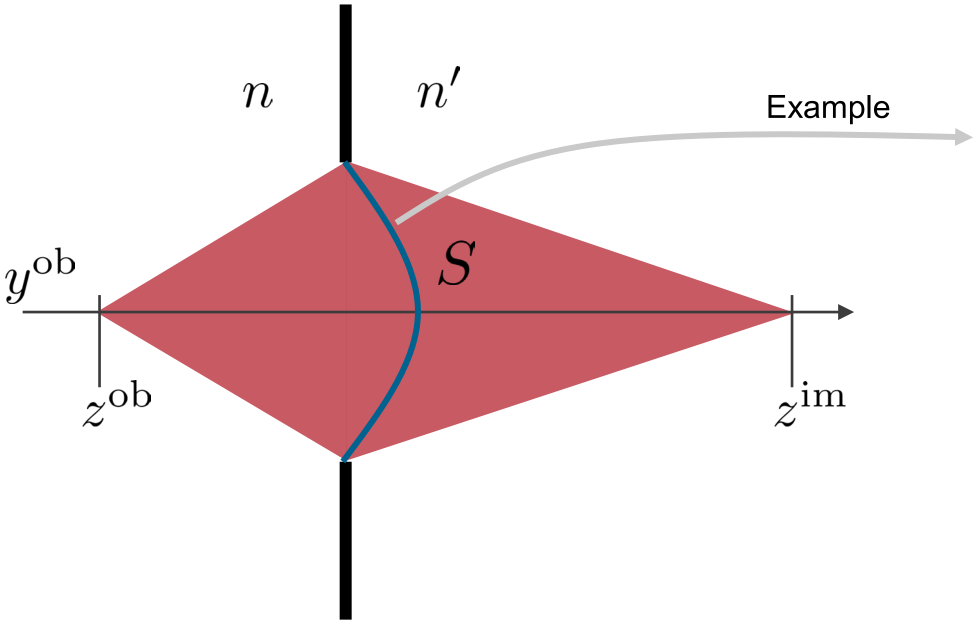

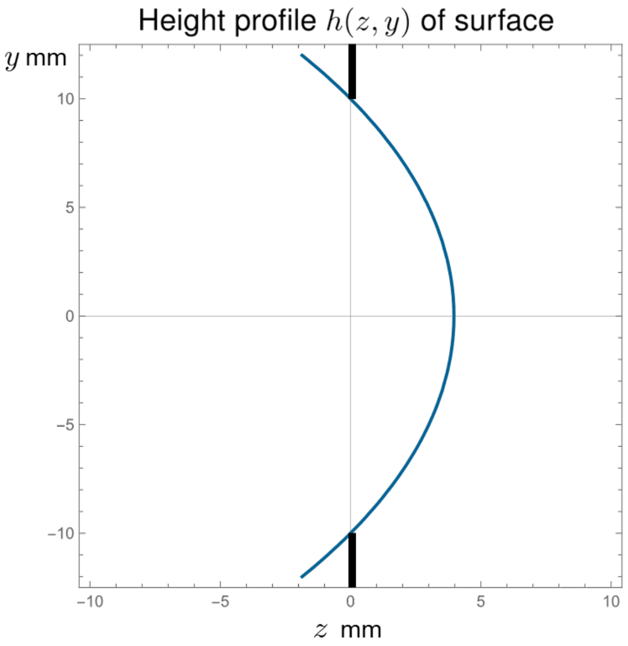

- Wavelength: $532\,\mathrm{nm}$
- Refractive indexes: $n = 1.5$ and $n' = 1$
- Lens radius: $10\,\mathrm{mm}$
- Object position: $z^{\mathrm{ob}} = -50\,\mathrm{mm}$
- Image position: $z^{\mathrm{im}} = 100\,\mathrm{mm}$
- Lateral position: $y^{\mathrm{ob}} = 0\,\mathrm{mm}$

Some Basic Observations

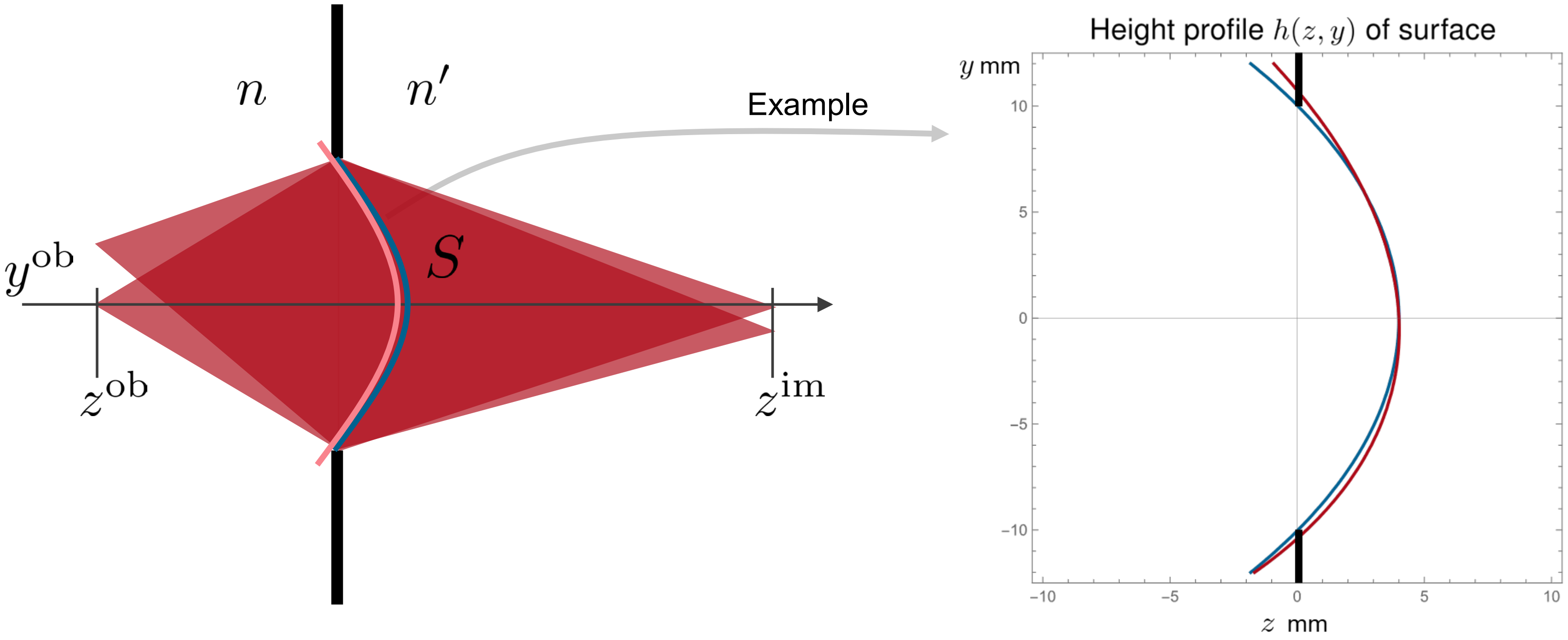

- Wavelength: $532\,\mathrm{nm}$
- Refractive indexes: $n = 1.5$ and $n' = 1$
- Lens radius: $10\,\mathrm{mm}$
- Object position: $z^{\mathrm{ob}} = -50\,\mathrm{mm}$
- Image position: $z^{\mathrm{im}} = 100\,\mathrm{mm}$
- Lateral positions: $y^{\mathrm{ob}} = 0$ and $10\,\mathrm{mm}$

Some Basic Observations

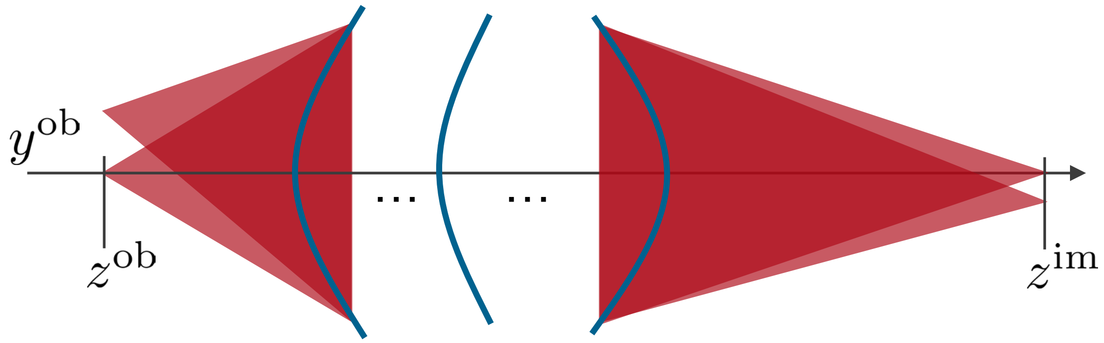

- A single surface cannot accurately image multiple object points.
- Therefore, adding more surfaces to correct aberrations is crucial.
- **There is no evidence to suggest that flat lenses eliminate this requirement.**

Beam Expander Scenario

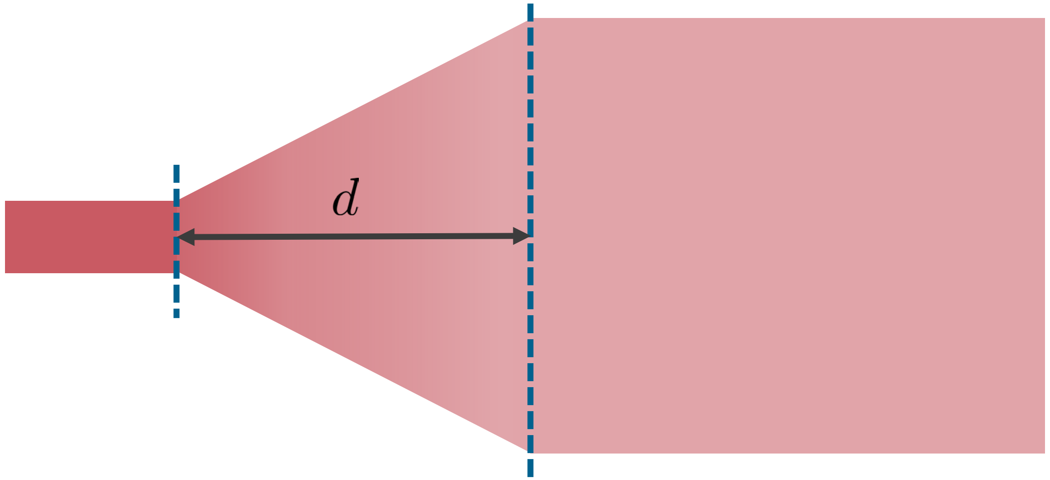

- The use of two lenses is necessary.
- The degree of beam expansion is governed by the distance d between the lenses and their numerical apertures.
- Flattening the lenses does not change that outcome.

Insights on the Capabilities of Flat Lenses

- Flat lenses reduce both the thickness and weight of the lenses.
- The thin design of flat lenses allows for more possibilities in reducing the distance between lens surfaces.
- The fabrication methods for flat lenses vary from those for traditional lenses, which may offer benefits in specific scenarios.
- Flat lenses could provide new opportunities for switchable lenses.
- Replacing thick lens surfaces with flat surfaces changes the aberration dynamics in the system, which may enhance aberration correction possibilities based on the particular scenario.

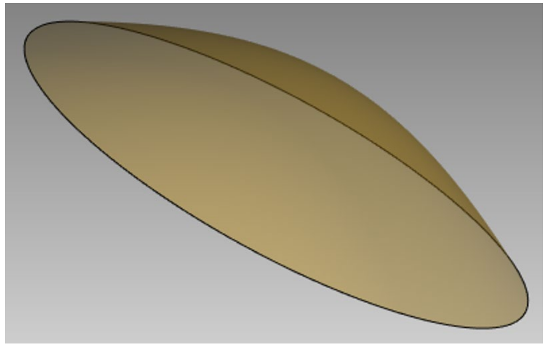

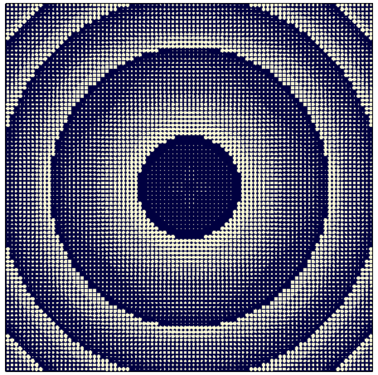

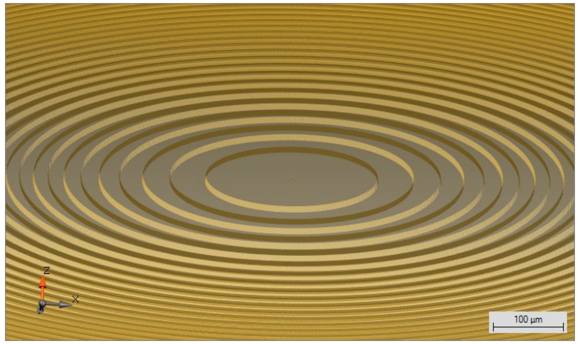

Insights on the Capabilities of Flat Lenses

- Flat lenses reduce both the thickness and weight of the lenses.
- The thin design of flat lenses allows for more possibilities in reducing the distance between lens surfaces.
- The fabrication methods for flat lenses vary from those for traditional lenses, which may offer benefits in specific scenarios.
- Flat lenses could provide new opportunities for switchable lenses.
- Replacing thick lens surfaces with flat surfaces changes the aberration dynamics in the system, which may enhance aberration correction possibilities based on the particular scenario.

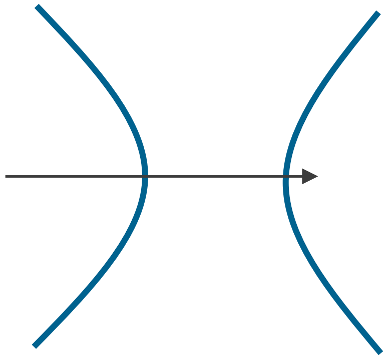

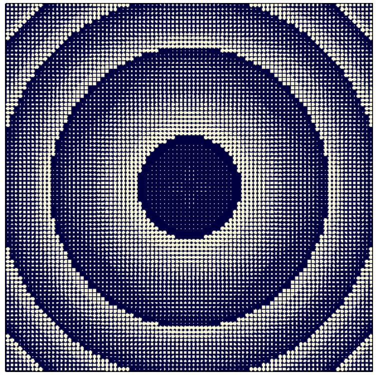

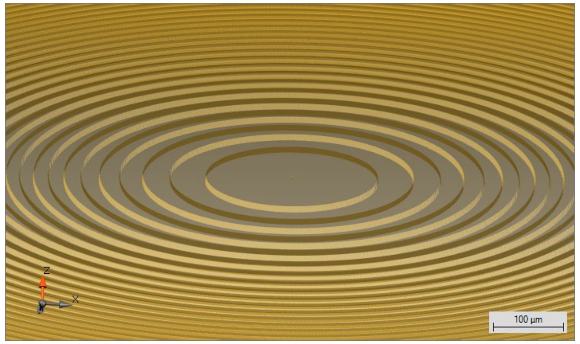

Insights on the Capabilities of Flat Lenses

- Flat lenses reduce both the thickness and weight of the lenses.
- The thin design of flat lenses allows for more possibilities in reducing the distance between lens surfaces.
- The fabrication methods for flat lenses vary from those for traditional lenses, which may offer benefits in specific scenarios.
- Flat lenses could provide new opportunities for switchable lenses.
- Replacing thick lens surfaces with flat surfaces changes the aberration dynamics in the system, which may enhance aberration correction possibilities based on the particular scenario.

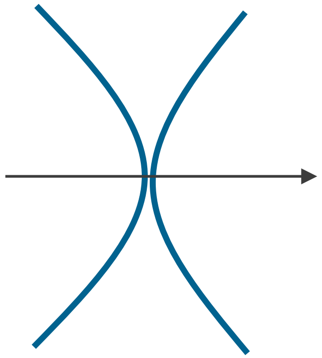

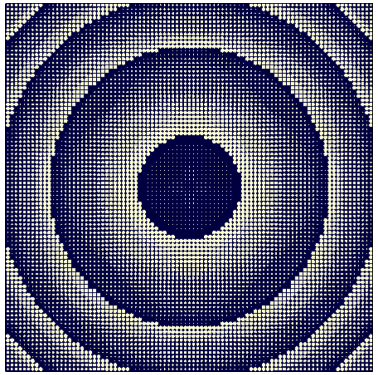

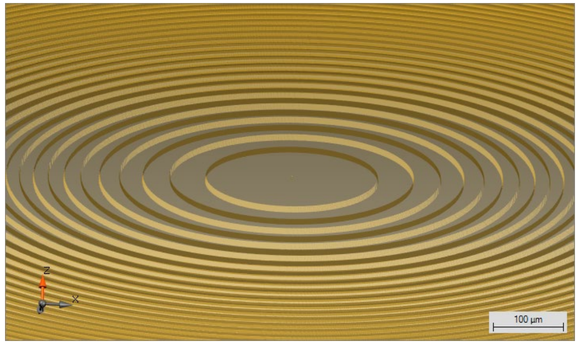

Insights on the Capabilities of Flat Lenses

- Flat lenses reduce both the thickness and weight of the lenses.
- The thin design of flat lenses allows for more possibilities in reducing the distance between lens surfaces.
- The fabrication methods for flat lenses vary from those for traditional lenses, which may offer benefits in specific scenarios.
- Flat lenses could provide new opportunities for switchable lenses.
- Replacing thick lens surfaces with flat surfaces changes the aberration dynamics in the system, which may enhance aberration correction possibilities based on the particular scenario.

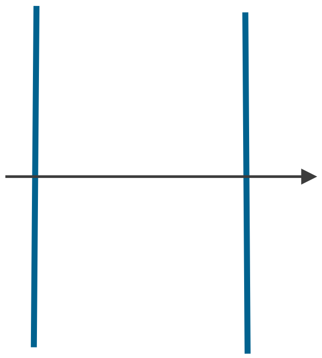

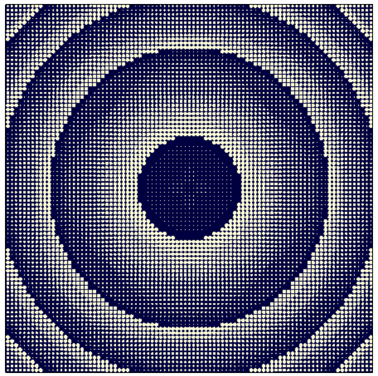

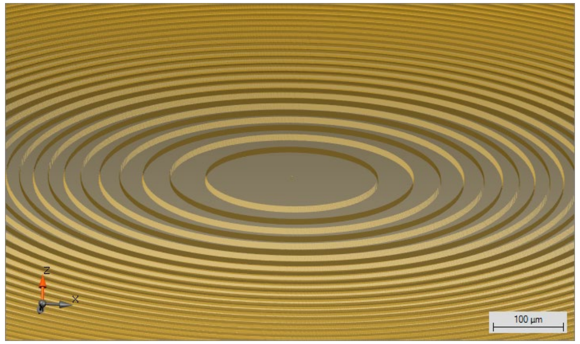

Insights on the Capabilities of Flat Lenses

- Flat lenses reduce both the thickness and weight of the lenses.
- The thin design of flat lenses allows for more possibilities in reducing the distance between lens surfaces.
- The fabrication methods for flat lenses vary from those for traditional lenses, which may offer benefits in specific scenarios.
- Flat lenses could provide new opportunities for switchable lenses.
- Replacing thick lens surfaces with flat surfaces changes the aberration dynamics in the system, which may enhance aberration correction possibilities based on the particular scenario.

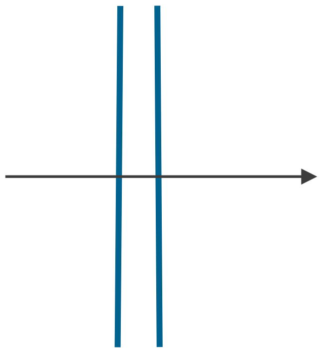

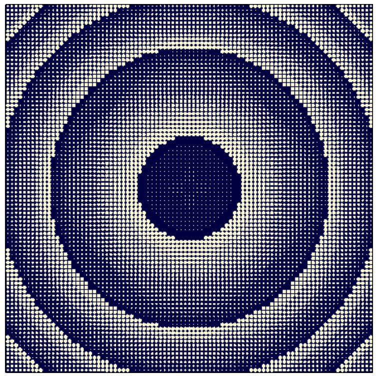

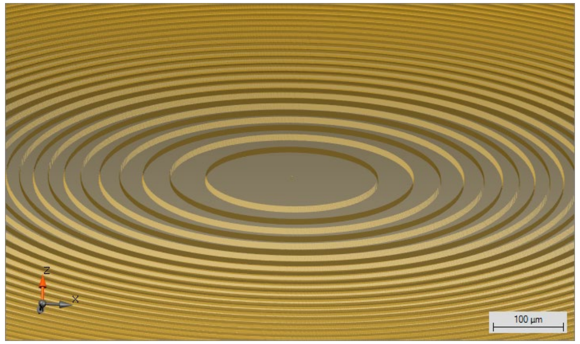

Insights on the Capabilities of Flat Lenses

- Flat lenses reduce both the thickness and weight of the lenses.
- The thin design of flat lenses allows for more possibilities in reducing the distance between lens surfaces.
- The fabrication methods for flat lenses vary from those for traditional lenses, which may offer benefits in specific scenarios.
- Flat lenses could provide new opportunities for switchable lenses.
- Replacing thick lens surfaces with flat surfaces changes the aberration dynamics in the system, which may enhance aberration correction possibilities based on the particular scenario.

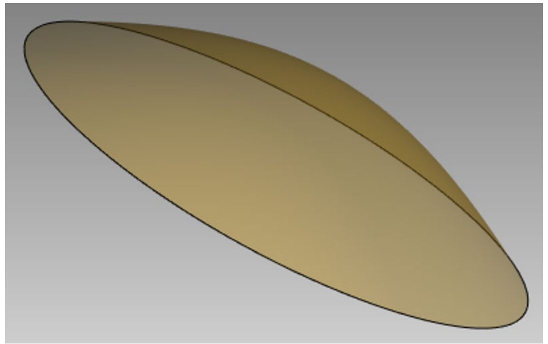

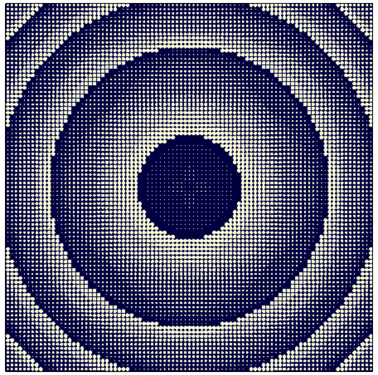

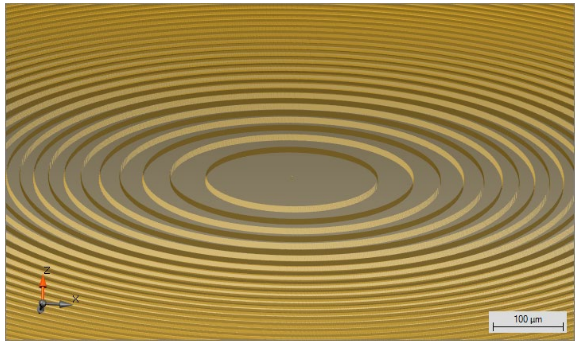

Insights on the Capabilities of Flat Lenses

- Flat lenses reduce both the thickness and weight of the lenses.
- The thin design of flat lenses allows for more possibilities in reducing the distance between lens surfaces.
- The fabrication methods for flat lenses vary from those for traditional lenses, which may offer benefits in specific scenarios.
- Flat lenses could provide new opportunities for switchable lenses.
- Replacing thick lens surfaces with flat surfaces changes the aberration dynamics in the system, which may enhance aberration correction possibilities based on the particular scenario.

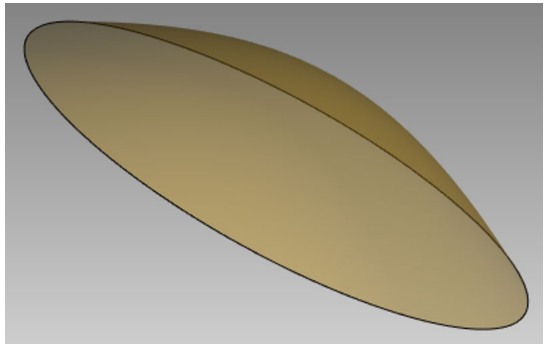

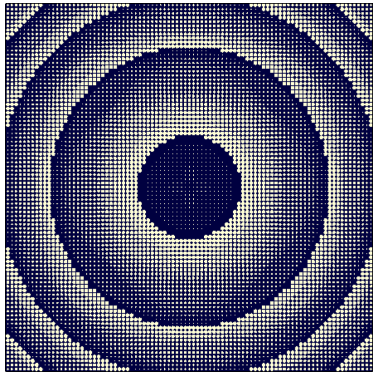

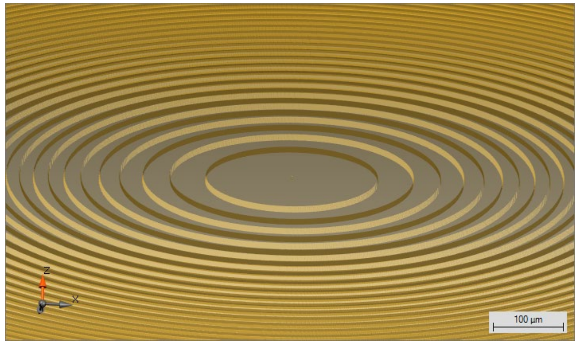

Insights on the Capabilities of Flat Lenses

- Flat lenses reduce both the thickness and weight of the lenses.
- The thin design of flat lenses allows for more possibilities in reducing the distance between lens surfaces.
- The fabrication methods for flat lenses vary from those for traditional lenses, which may offer benefits in specific scenarios.
- Flat lenses could provide new opportunities for switchable lenses.
- Replacing thick lens surfaces with flat surfaces changes the aberration dynamics in the system, which may enhance aberration correction possibilities based on the particular scenario.

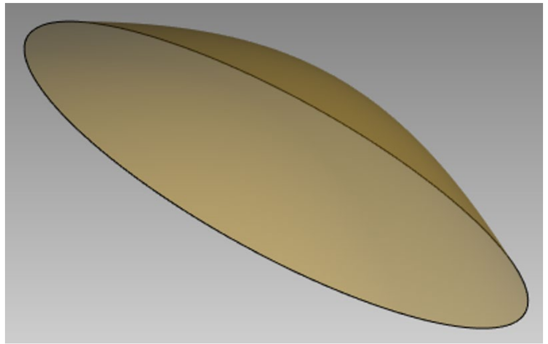

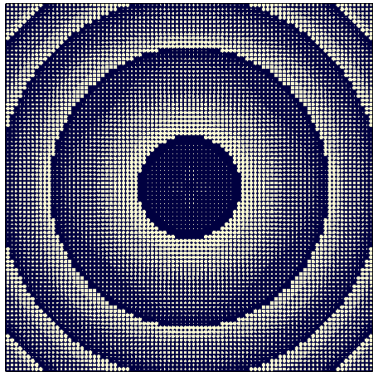

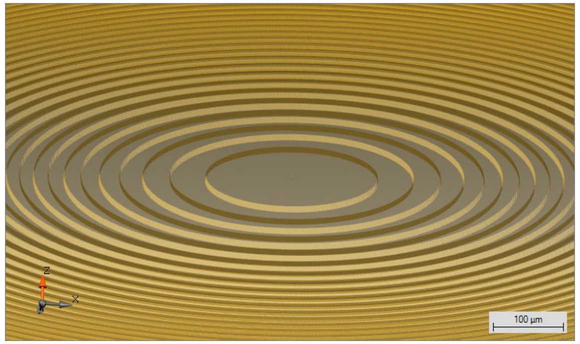

Insights on the Capabilities of Flat Lenses

- Flat lenses reduce both the thickness and weight of the lenses.
- The thin design of flat lenses allows for more possibilities in reducing the distance between lens surfaces.
- The fabrication methods for flat lenses vary from those for traditional lenses, which may offer benefits in specific scenarios.
- Flat lenses could provide new opportunities for switchable lenses.
- Replacing thick lens surfaces with flat surfaces changes the aberration dynamics in the system, which may enhance aberration correction possibilities based on the particular scenario.
- Employing diffractive lenses, which exhibit strong and opposing chromatic aberrations, to counteract the chromatic aberrations of smooth lens surfaces serves as a well-documented instance of this potential.
- Some characteristics of flat lenses, such as its polarization-sensitive function, may be considered beneficial or detrimental depending on their use.
- There is no evidence to suggest that flat lenses, including metalenses, reduce the total length of the system or the number of lens surfaces in optical systems beyond what is possible with aspherical and freeform surfaces.

Insights on the Capabilities of Flat Lenses

- Flat lenses reduce both the thickness and weight of the lenses.
- The thin design of flat lenses allows for more possibilities in reducing the distance between lens surfaces.
- The fabrication methods for flat lenses vary from those for traditional lenses, which may offer benefits in specific scenarios.
- Flat lenses could provide new opportunities for switchable lenses.
- Replacing thick lens surfaces with flat surfaces changes the aberration dynamics in the system, which may enhance aberration correction possibilities based on the particular scenario.
- Employing diffractive lenses, which exhibit strong and opposing chromatic aberrations, to counteract the chromatic aberrations of smooth lens surfaces serves as a well-documented instance of this potential.
- Some characteristics of flat lenses, such as its polarization-sensitive function, may be considered beneficial or detrimental depending on their use.

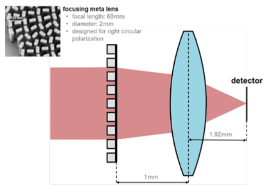

- There is no evidence to suggest that flat lenses, including metalenses, reduce the total length of the system or the number of lens surfaces in optical systems beyond what is possible with aspherical and freeform surfaces.

Insights on the Capabilities of Flat Lenses

- Flat lenses reduce both the thickness and weight of the lenses.
- The thin design of flat lenses allows for more possibilities in reducing the distance between lens surfaces.
- The fabrication methods for flat lenses vary from those for traditional lenses, which may offer benefits in specific scenarios.
- Flat lenses could provide new opportunities for switchable lenses.
- Replacing thick lens surfaces with flat surfaces changes the aberration dynamics in the system, which may enhance aberration correction possibilities based on the particular scenario.
- Employing diffractive lenses, which exhibit strong and opposing chromatic aberrations, to counteract the chromatic aberrations of smooth lens surfaces serves as a well-documented instance of this potential.
- Some characteristics of flat lenses, such as its polarization-sensitive function, may be considered beneficial or detrimental depending on their use.
- There is no evidence to suggest that flat lenses, including metalenses, reduce the total length of the system or the number of lens surfaces in optical systems beyond what is possible with aspherical and freeform surfaces.

Insights on the Capabilities of Flat Lenses

- Flat lenses reduce both the thickness and weight of the lenses.
- The thin design of flat lenses allows for more possibilities in reducing the distance between lens surfaces.

The slim profile of flat lenses is the key factor in their potential for miniaturization

- The fabrication methods for flat lenses vary from those for traditional lenses, which may offer benefits in specific scenarios.
- Flat lenses could provide new opportunities for switchable lenses.
- Replacing thick lens surfaces with flat surfaces changes the aberration dynamics in the system, which may enhance aberration correction possibilities based on the particular scenario.

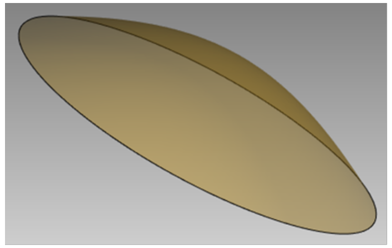

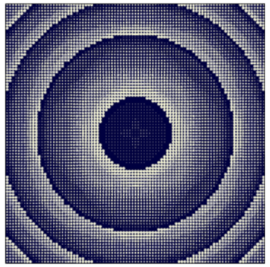

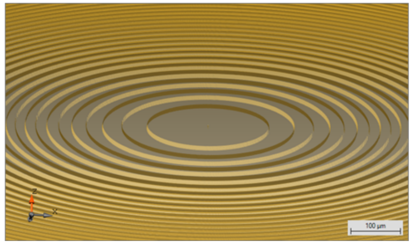

Integrating Flat Lenses into Lens Design Workflows

- Ultimately, flat lenses offer a notable and intriguing **addition to the array of tools for optical design**.
- The usefulness of flat lenses changes significantly based on the context of their application.

It is crucial to integrate flat lens technology into lens design workflows to fully comprehend and utilize their capabilities.

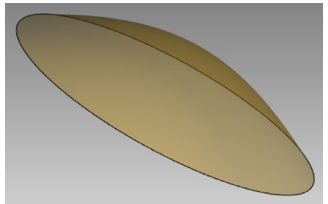

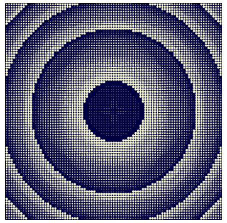

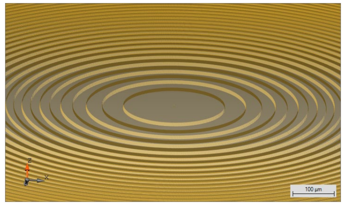

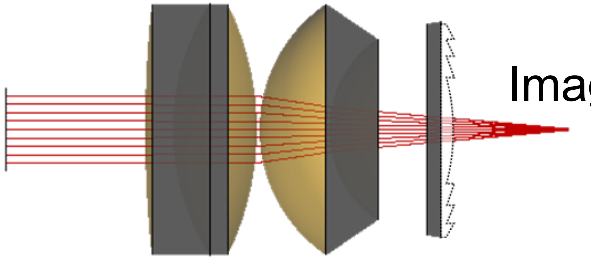

Imaging

Illumination

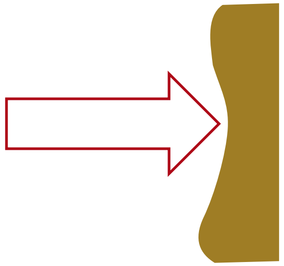

Result radiant intensity

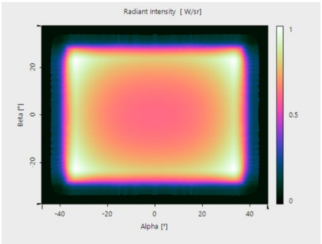

90° X 70°
Diagonal: 114°

Interoperable Simulation Model for Metalenses

The Importance of the Wavefront Phase

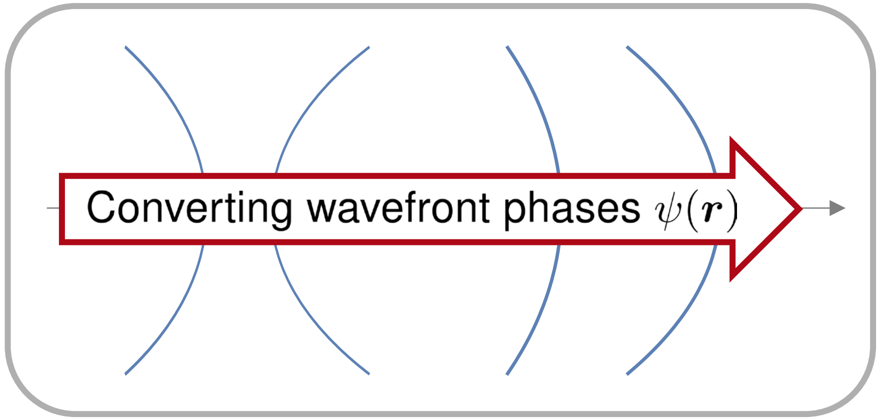

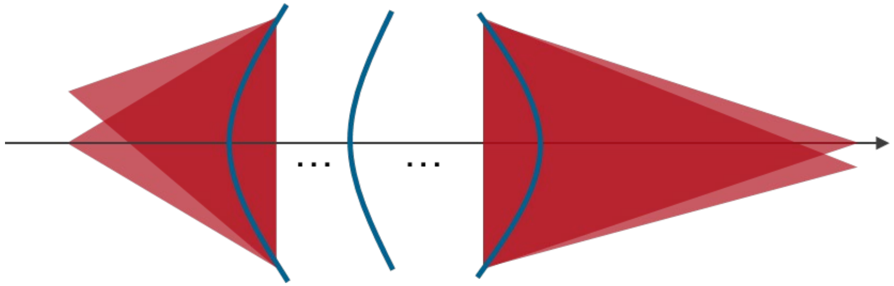

- Lens systems convert wavefronts originating from object points into wavefronts that create the image points.
- Wavefronts are mathematically represented by their corresponding phase function $\psi(\boldsymbol{r})$, which we call the **wavefront phase**.
- The wavefront phase is of pivotal importance in both the design and simulation of lens systems.

The Importance of the Wavefront Phase: Geometrical Optics

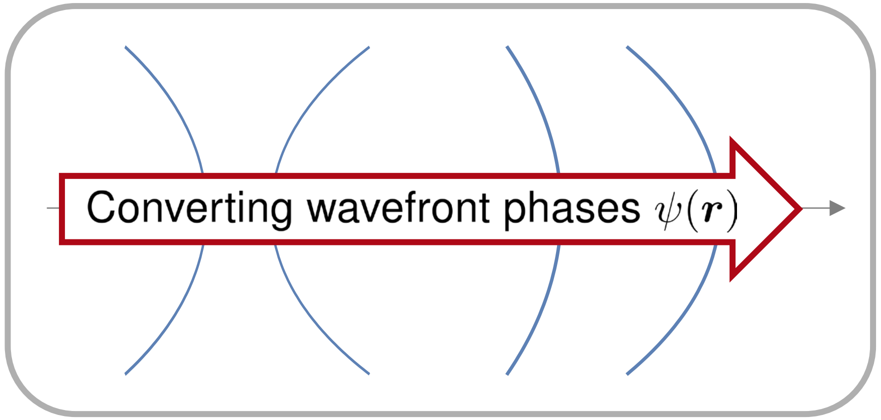

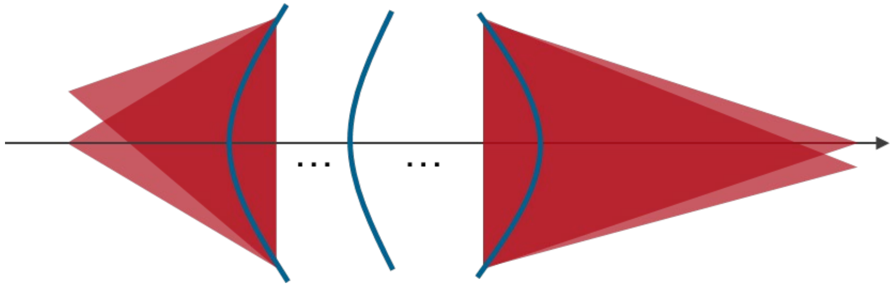

- In geometrical optics, the wavefront phase is directly connected to the local ray direction vector $\hat{s}$ through the equation

$$\hat{\boldsymbol{s}}_{\perp}(\boldsymbol{r}) = \frac{\{\nabla_{\perp}\psi\}(\boldsymbol{r})}{k_0 n}$$

where $_{\perp}$ represents the x and y components, and s_z is determined by $\|\hat{\boldsymbol{s}}\| = 1$.

The Importance of the Wavefront Phase: Physical Optics

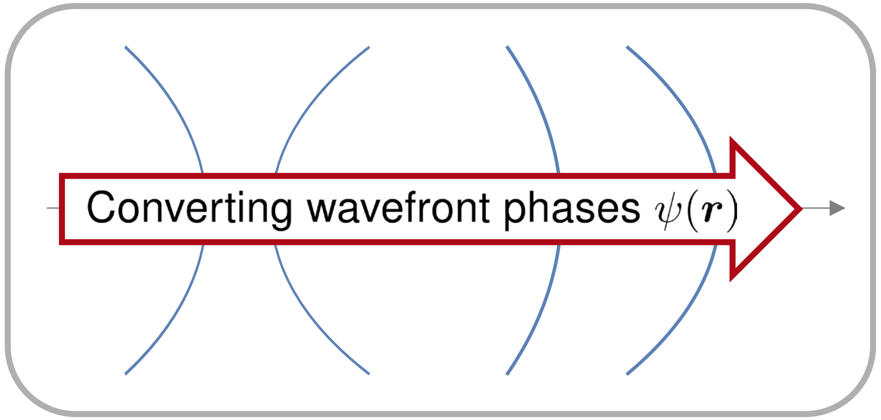

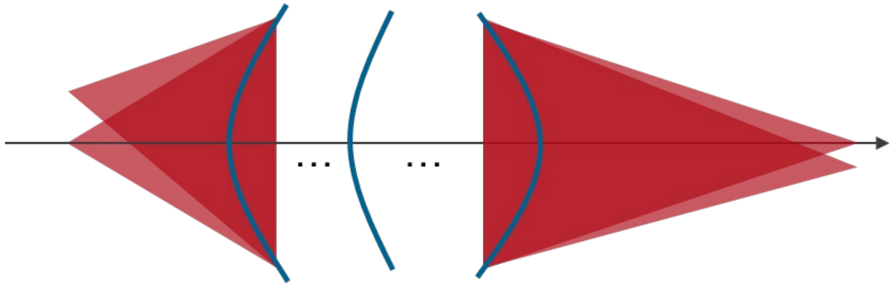

- In physical optics, the wavefront phase retains its crucial significance.
- It is now integrated into the electric field vector $\boldsymbol{E}(\boldsymbol{r})$ through

$$\boldsymbol{E}(\boldsymbol{r}) = \boldsymbol{U}(\boldsymbol{r}) \exp[\mathrm{i}\psi(\boldsymbol{r})]$$

  with

$$U_\ell(\boldsymbol{r}) := |E_\ell(\boldsymbol{r})| \exp[\mathrm{i} \arg U_\ell(\boldsymbol{r})]$$

  for the components $\ell = x, y, z$.

- In multi-scale physical optics simulations, ψ is utilized as a continuous and smooth phase that is shared across all components.
- The electric field components can possess extra phases $\arg U_\ell$, such as a vortex associated with an angular momentum beam.

The Importance of the Wavefront Phase: Physical Optics

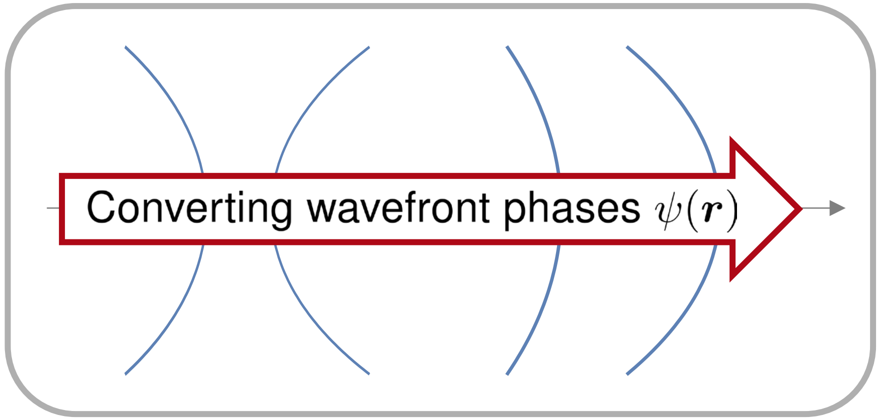

$\arg E(x,y)$ = $\psi(x,y)$ + $\arg U(x,y)$

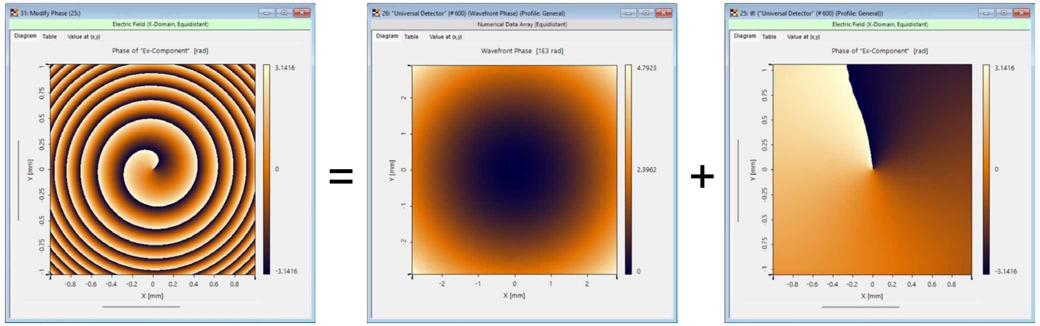

- In physical optics, the wavefront phase retains its crucial significance.
- It is now integrated into the electric field vector $\boldsymbol{E}(\boldsymbol{r})$ through

$$\boldsymbol{E}(\boldsymbol{r}) = \boldsymbol{U}(\boldsymbol{r}) \exp[\mathrm{i}\psi(\boldsymbol{r})]$$

  with

$$U_\ell(\boldsymbol{r}) := |E_\ell(\boldsymbol{r})| \exp[\mathrm{i} \arg U_\ell(\boldsymbol{r})]$$

  for the components $\ell = x, y, z$.

- In multi-scale physical optics simulations, ψ is utilized as a continuous and smooth phase that is shared across all components.
- The electric field components can possess extra phases $\arg U_\ell$, such as a vortex associated with an angular momentum beam.

The Optical Path Length (OPL)

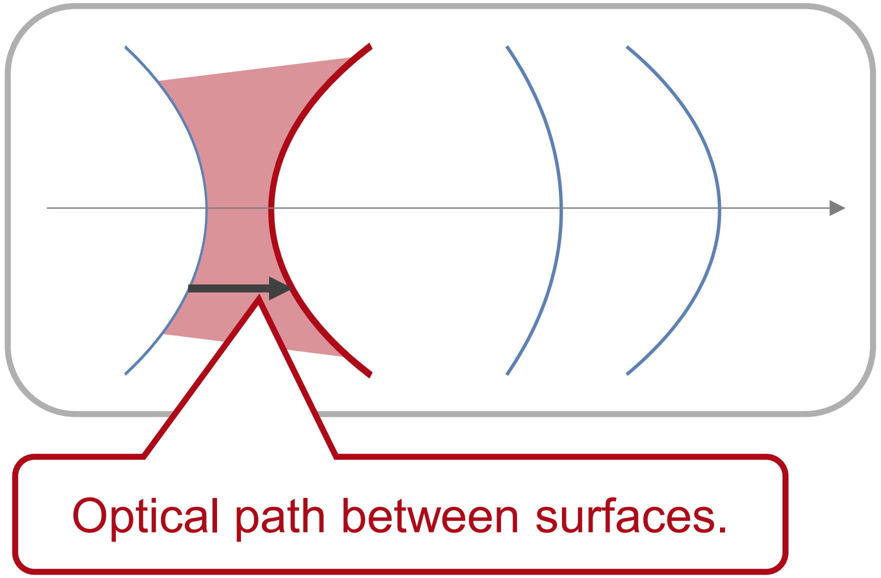

- Conventional lenses modify the wavefront phase through the optical path length (OPL) between their surfaces.
- The phase is derived from the OPL through

$$\psi = k_0 \, \mathsf{OPL} \, .$$

- This outcome is equally valid in the realm of physical optics.
- The resulting phase is continuous and not expressed as modulo 2π, meaning it is unwrapped.
- The variation in the wavefront phase ψ is independent of the polarization of the electric field!

Effect of a Flat Lens on the Wavefront Phase

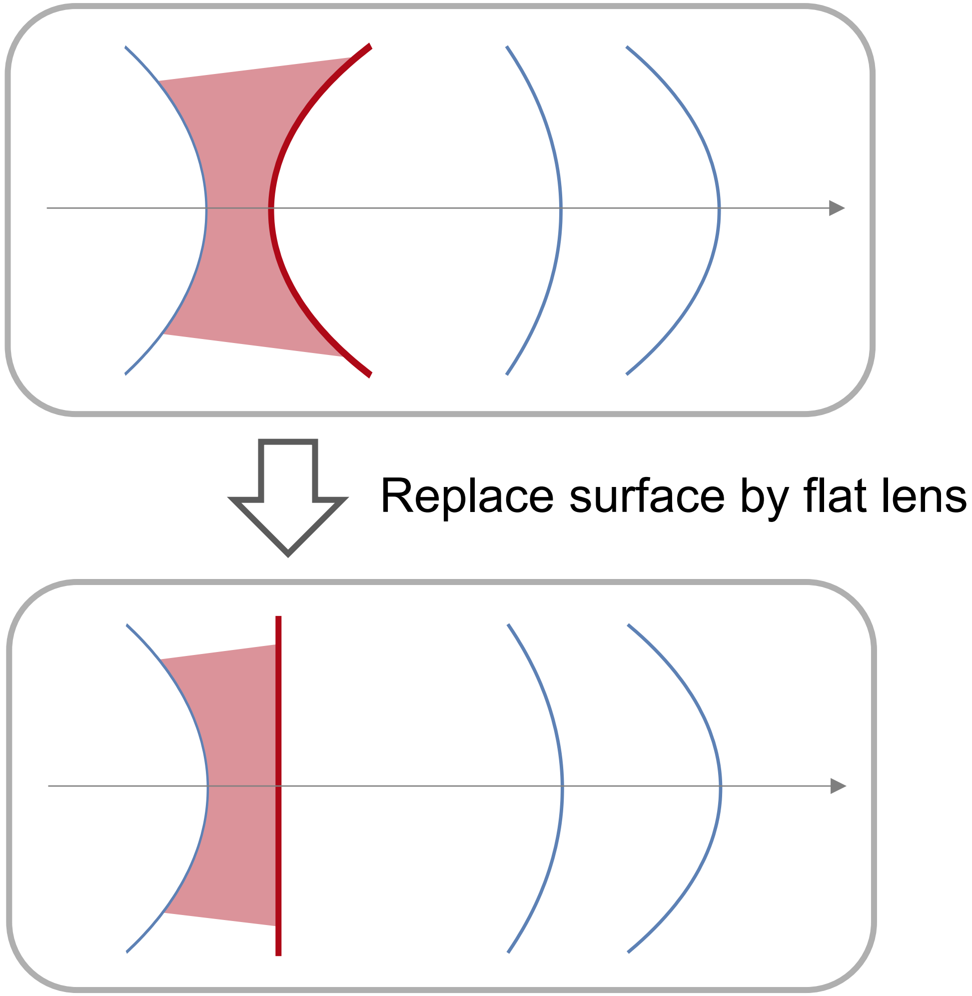

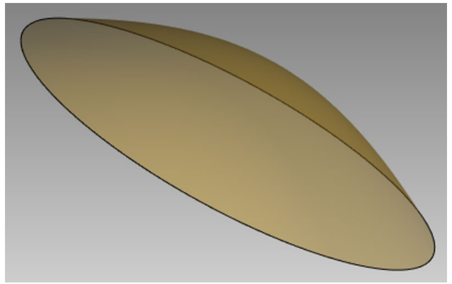

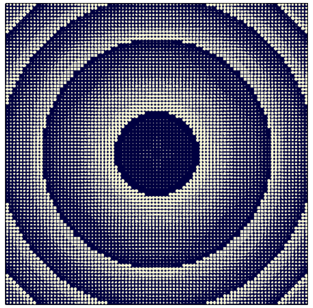

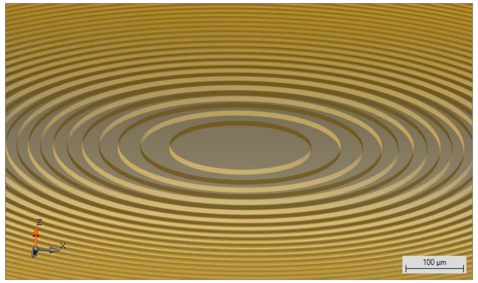

Effect of a Flat Lens on the Wavefront Phase

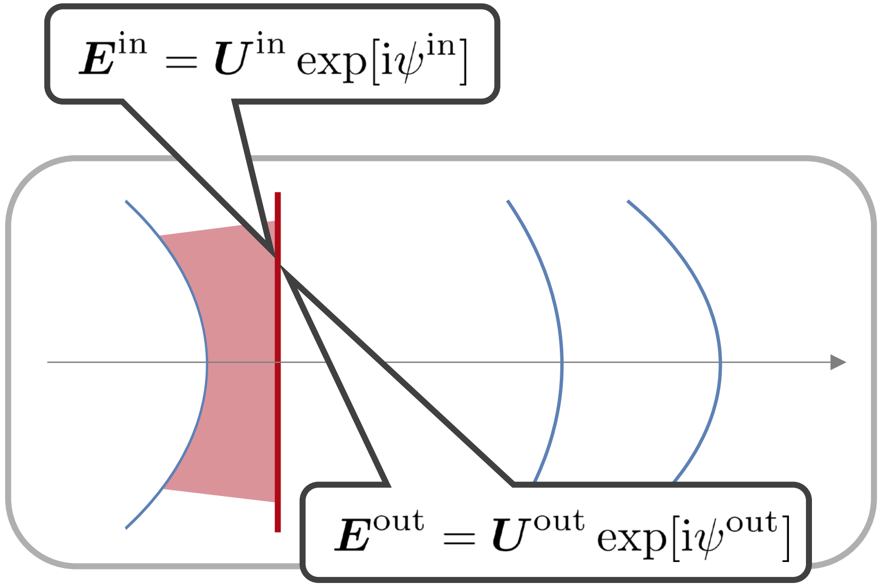

- The influence of the flat lens on the field at any location on its planar surface can be characterized by

$$\boldsymbol{E}_{\perp}^{\mathrm{out}} = \mathbf{M}\boldsymbol{E}_{\perp}^{\mathrm{in}},$$

with $\boldsymbol{E}_{\perp} = (E_x, E_y)$ and the quadratic matrix

$$\mathbf{M} = \begin{pmatrix} M_{xx} & M_{xy} \\ M_{yx} & M_{yy} \end{pmatrix} .$$

Effect of a Flat Lens on the Wavefront Phase

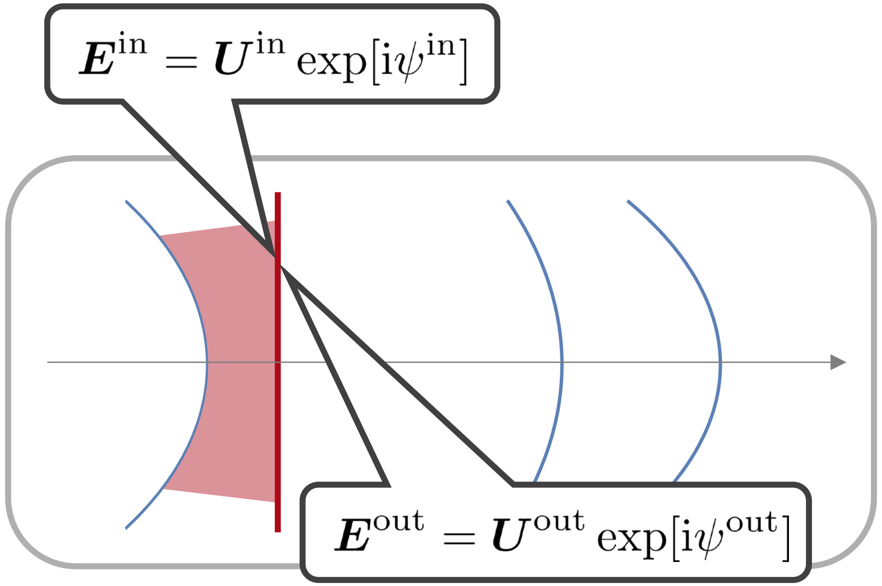

- The influence of the flat lens on the field at any location on its planar surface can be characterized by

$$\boldsymbol{E}^{\text{out}} = \mathbf{M}\boldsymbol{E}^{\text{in}},$$

with the quadratic matrix

$$\mathbf{M} = \begin{pmatrix} M_{xx} & M_{xy} \\ M_{yx} & M_{yy} \end{pmatrix} .$$

Effect of a Flat Lens on the Wavefront Phase

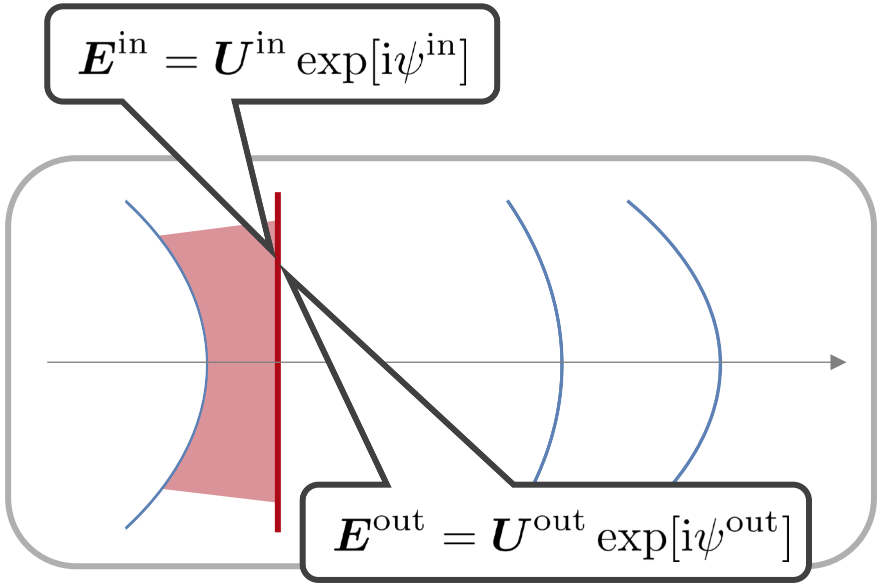

- The influence of the flat lens on the field at any location on its planar surface can be characterized by

$$\boldsymbol{E}^{\mathrm{out}} = \mathbf{M}\boldsymbol{E}^{\mathrm{in}},$$

  with the quadratic matrix

$$\mathbf{M} = \begin{pmatrix} M_{xx} & M_{xy} \\ M_{yx} & M_{yy} \end{pmatrix} .$$

- The values of the matrix **M** can be obtained using any suitable simulation model of the flat lens surface.

Effect of a Flat Lens on the Wavefront Phase

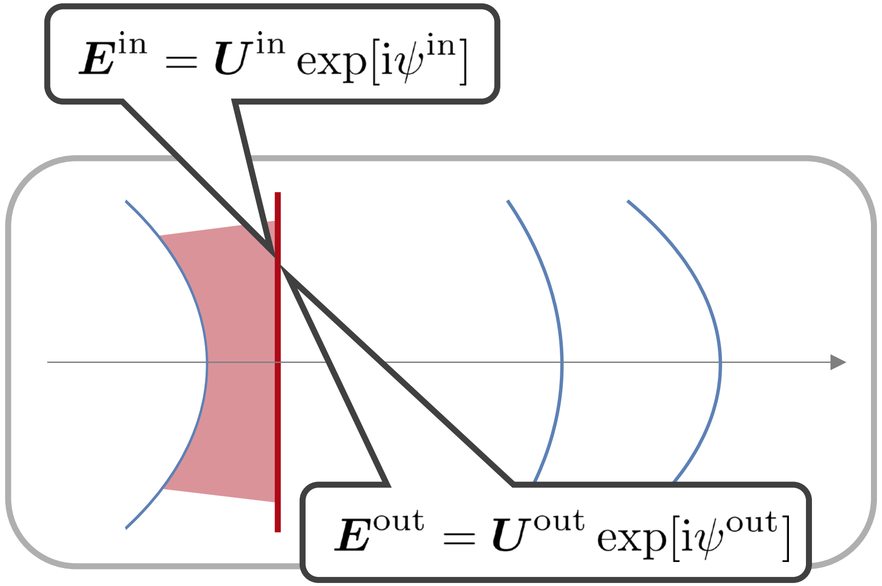

- The wavefront phase ψ^{in} of the incoming field, can be explicitly separated from the matrix multiplication, leading to the expression

$$\boldsymbol{E}^{\mathrm{out}} = \boldsymbol{U}^{\mathrm{out}} \exp[\mathrm{i}\psi^{\mathrm{out}}] = \left(\mathbf{M}\,\boldsymbol{U}^{\mathrm{in}}\right) \exp[\mathrm{i}\psi^{\mathrm{in}}] \,.$$

  where

$$\psi^{\mathrm{out}} = \psi^{\mathrm{in}} + \Psi.$$

- The phase Ψ represents the change of the input wavefront phase due to the flat lens.

- In the case of flat lenses, the phase Ψ is not determined by an OPL between lens surfaces, but rather must be derived from the matrix effect on the input field, represented as $\mathbf{M}\boldsymbol{U}^{\mathrm{in}}$.

Evaluating Matrix M

Wavelength λ of incoming light.

Local direction vector $\hat{\boldsymbol{s}}^{\text{in}}(\boldsymbol{\rho})$.

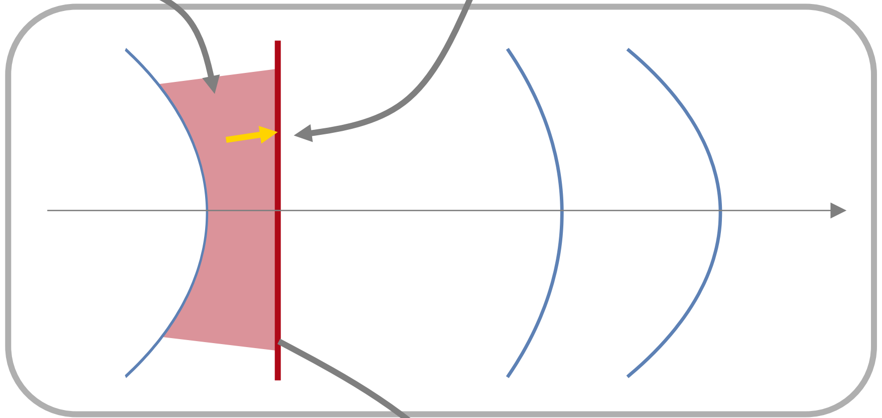

Pillars with varying widths

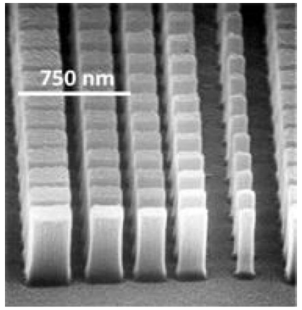

Rotated nanofins

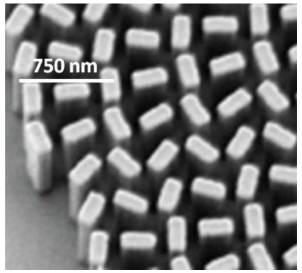

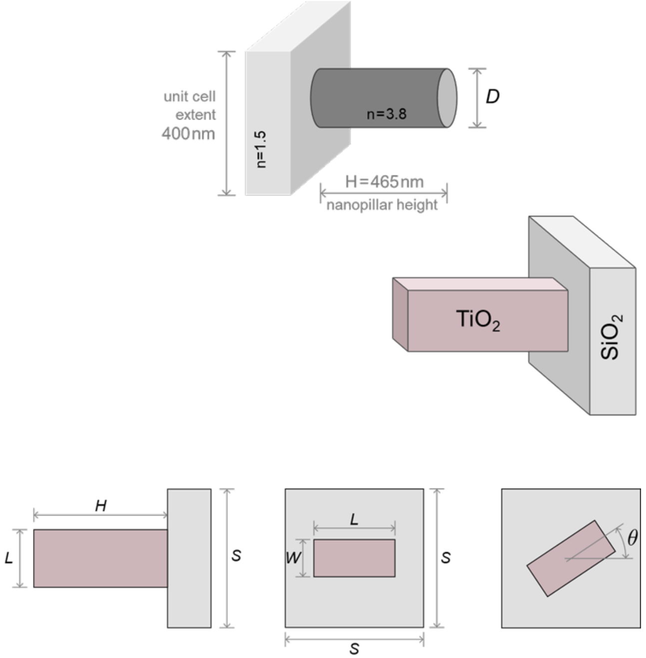

Structure parameter vector $\boldsymbol{p}$,
such as width, height, and rotation angle.

Creating a Neural Network for Modeling and Design

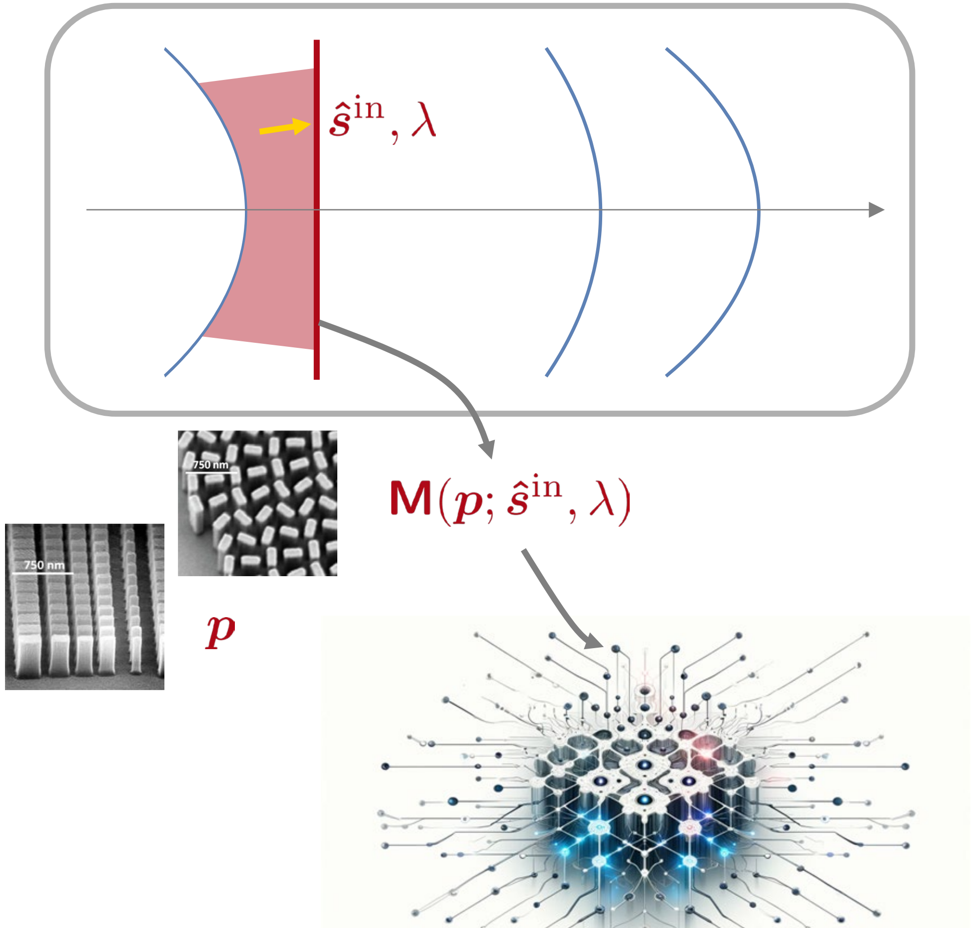

Generated by chatGPT

- In mathematical terms, the dependencies of the matrix are represented by $\mathbf{M}(\boldsymbol{p}; \hat{\boldsymbol{s}}^{\mathrm{in}}, \lambda)$.
- All matrix elements $\mathbf{M}(\boldsymbol{p}; \hat{\boldsymbol{s}}^{\mathrm{in}}, \lambda)$ are evaluated over the parameter space for a selected type of metacell structure, the relevant direction domain, and the specified wavelength range.
- These matrix values function as nodes within a neural network, connecting the parameter space, the directional domain, and the wavelength spectrum.
- This neural network serves as the irreplaceable cornerstone for identifying an appropriate wavefront phase response Ψ, and it establishes the most effective methods for modeling and design.

Creating a Neural Network for Modeling and Design

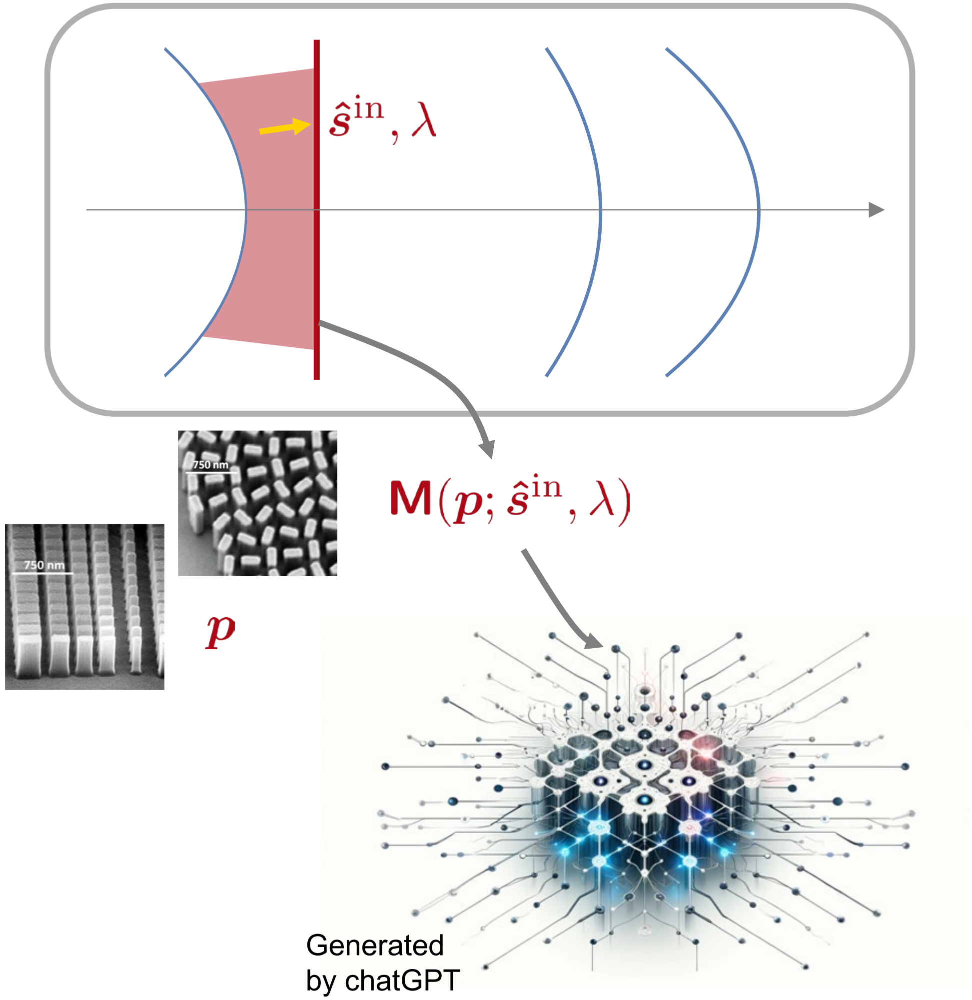

Generated by chatGPT

- It is important to note that this network only needs to be computed once for each type of metacell structure.
- Employing advanced modeling methods on a typical laptop, the time required to set up the neural network varies from a few hours to several days, depending on the number of nodes involved.
- VirtualLab Fusion supports distributed computing, which allows for an almost linear decrease in computation time with the addition of more clients.
- In summary, the network computation is not a practical limitation.

Effect of a Flat Lens on the Input Field: Examples

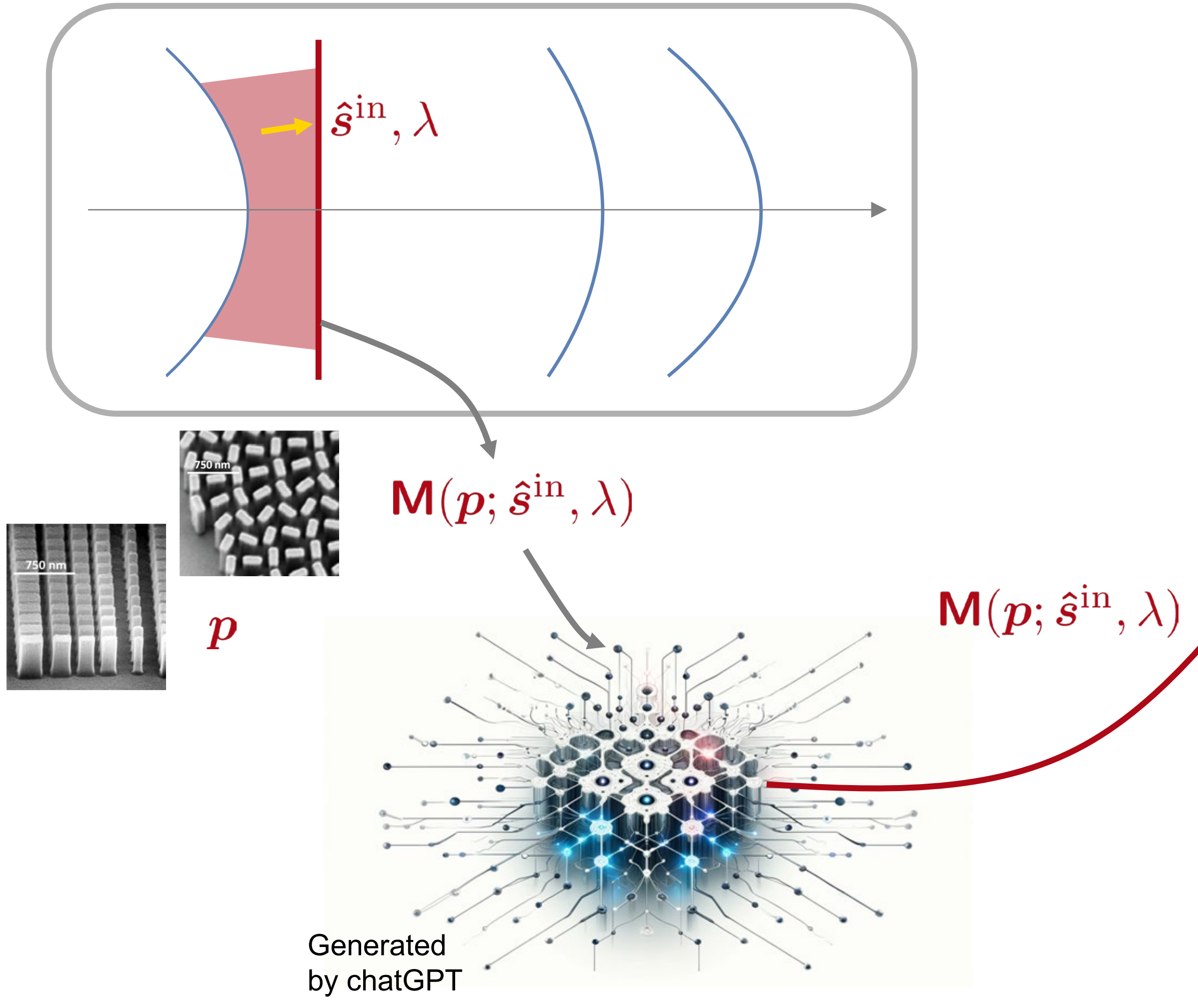

Generated by chatGPT

- Given a particular $\boldsymbol{U}^{\text{in}}$, the network supplies the magnitudes

$$\left|\left\{\mathbf{M}(\boldsymbol{p}; \hat{\boldsymbol{s}}^{\text{in}})\boldsymbol{U}^{\text{in}}\right\}_x\right| \text{ and } \left|\left\{\mathbf{M}(\boldsymbol{p}; \hat{\boldsymbol{s}}^{\text{in}})\boldsymbol{U}^{\text{in}}\right\}_y\right|$$

and the phases

$$\arg\left\{\mathbf{M}(\boldsymbol{p}; \hat{\boldsymbol{s}}^{\text{in}})\boldsymbol{U}^{\text{in}}\right\}_x \text{ and } \arg\left\{\mathbf{M}(\boldsymbol{p}; \hat{\boldsymbol{s}}^{\text{in}})\boldsymbol{U}^{\text{in}}\right\}_y .$$

Effect of a Flat Lens on the Input Field: Examples

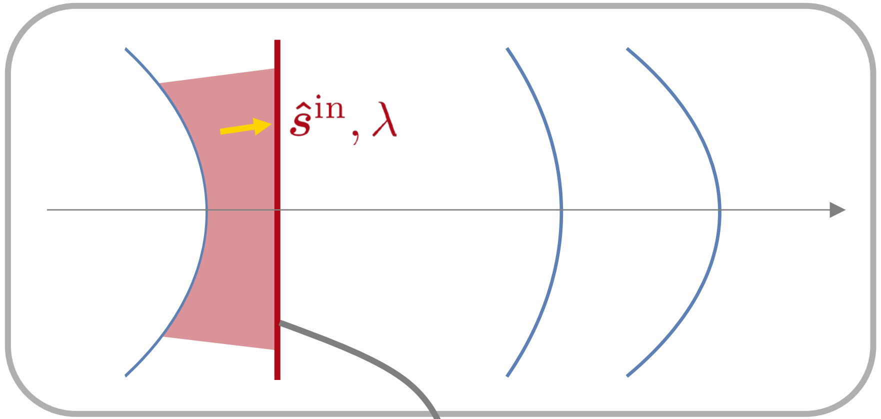

$\mathbf{M}(\boldsymbol{p}; \hat{\boldsymbol{s}}^{\text{in}}, \lambda)$

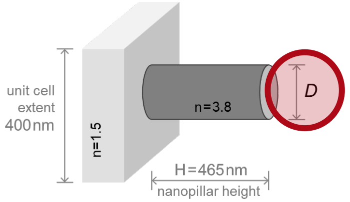

- Refractive index: 3.8 @ 940 nm
- Period: 400 nm
- Height: 465 nm
- Shape: circular
- Diameter: 45 nm - 270 nm

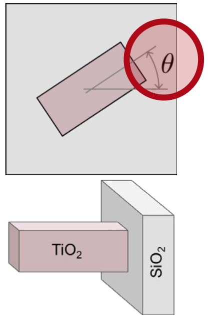

- Refractive index: 2.43 @ 532 nm
- Period: 325 nm
- Height: 600 nm
- Shape: rectangular
- Size: 250 nm x 95 nm
- Rotation angle: 0° - 180°

Effect of a Flat Lens on the Input Field: Examples

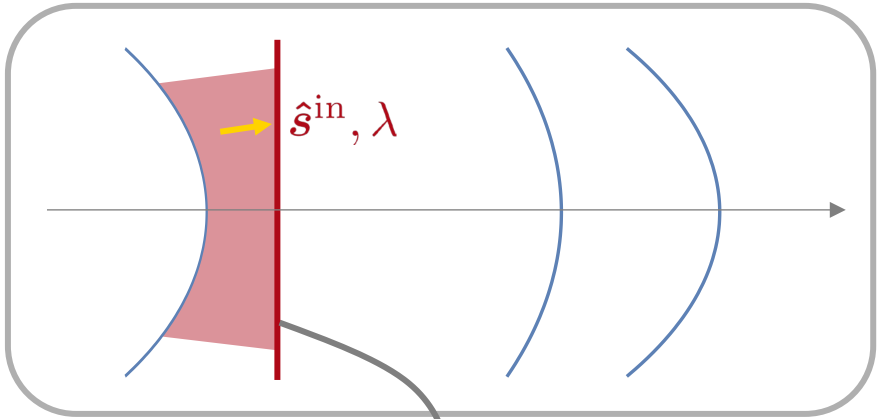

$\mathbf{M}(\boldsymbol{p}; \hat{\boldsymbol{s}}^{\text{in}}, \lambda)$

Example specifications:

- Input field vector: $\boxed{\boldsymbol{U}^{\text{in}} = (1,1)^T}$
- Input direction: $\hat{\boldsymbol{s}}^{\text{in}} = 0$

Magnitudes $\left|\{\mathbf{M}(p)\boldsymbol{U}^{\text{in}}\}_x\right|$ and $\left|\{\mathbf{M}(p)\boldsymbol{U}^{\text{in}}\}_y\right|$

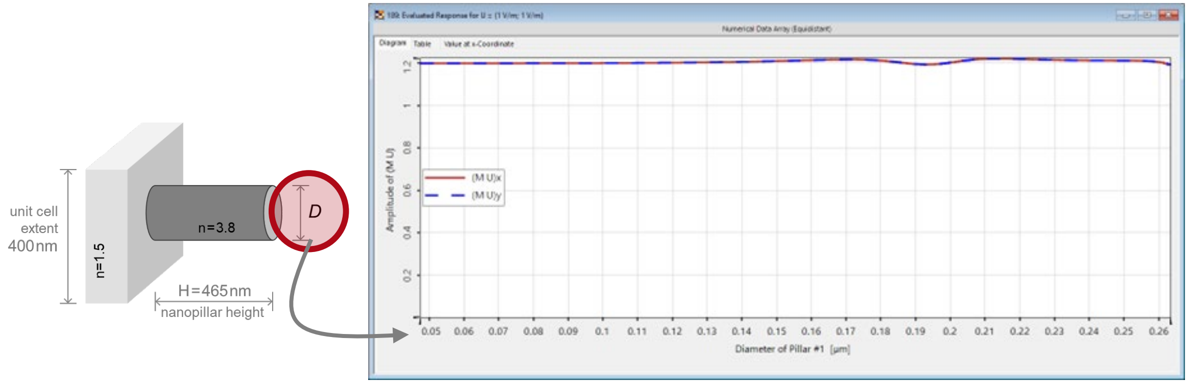

Magnitudes $\left|\{\mathbf{M}(p)\boldsymbol{U}^{\text{in}}\}_x\right|$ and $\left|\{\mathbf{M}(p)\boldsymbol{U}^{\text{in}}\}_y\right|$

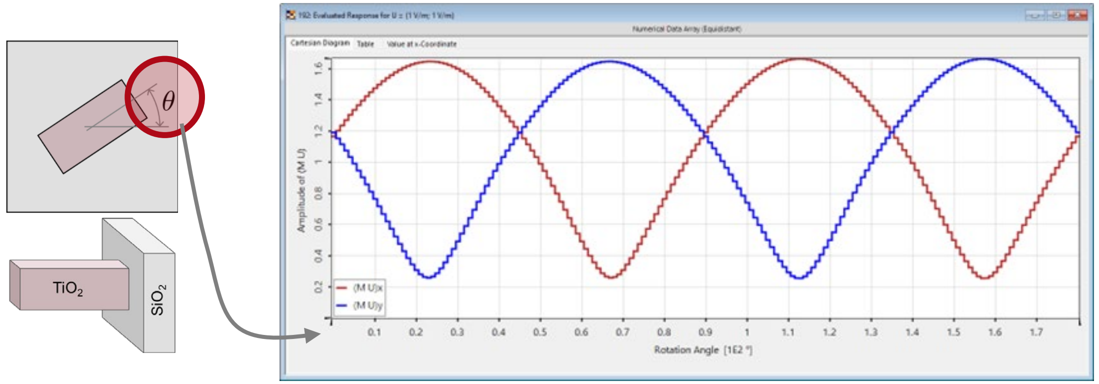

Effect of a Flat Lens on the Input Field: Examples

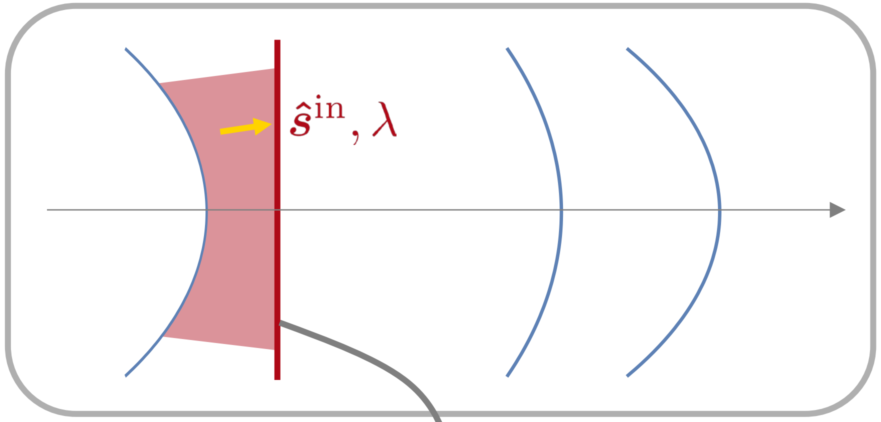

$\mathbf{M}(\boldsymbol{p}; \hat{\boldsymbol{s}}^{\text{in}}, \lambda)$

Example specifications:

- Input field vector: $\boxed{\boldsymbol{U}^{\text{in}} = (1,1)^T}$
- Input direction direction: $\hat{\boldsymbol{s}}^{\text{in}} = 0$

Phases $\arg\left\{\mathbf{M}(p)\boldsymbol{U}^{\text{in}}\right\}_x$ and $\arg\left\{\mathbf{M}(p)\boldsymbol{U}^{\text{in}}\right\}_y$

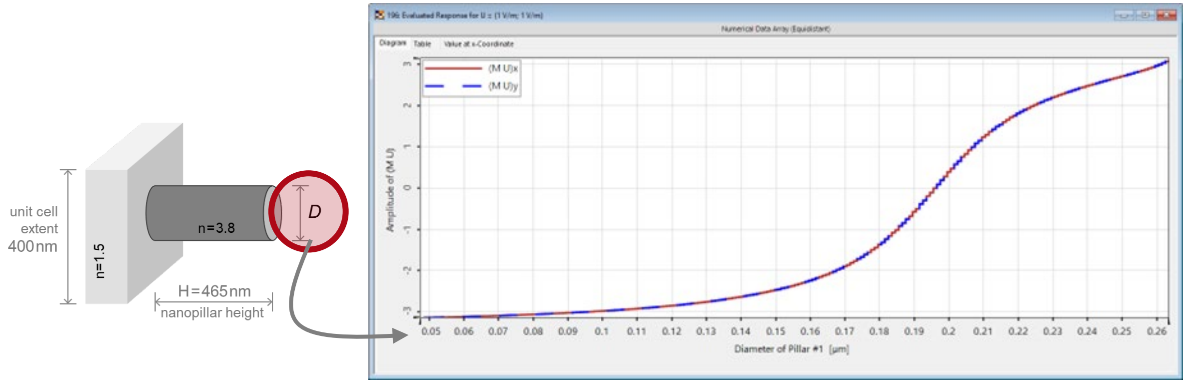

Phases $\arg\left\{\mathbf{M}(p)\boldsymbol{U}^{\text{in}}\right\}_x$ and $\arg\left\{\mathbf{M}(p)\boldsymbol{U}^{\text{in}}\right\}_y$

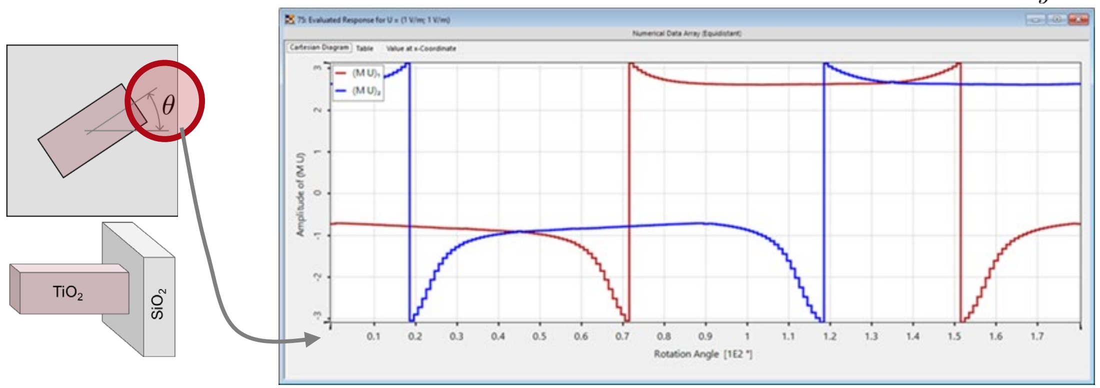

Effect of a Flat Lens on the Input Field: Examples

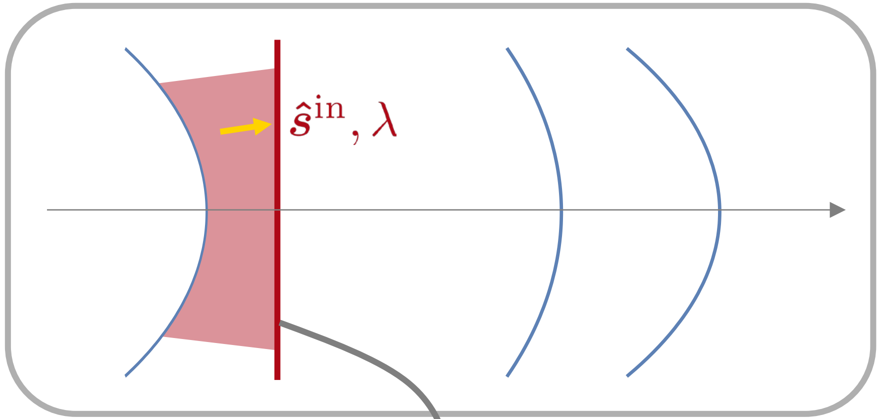

$\mathbf{M}(\boldsymbol{p}; \hat{\boldsymbol{s}}^{\mathrm{in}}, \lambda)$

Magnitudes $\left|\{\mathbf{M}(p)\boldsymbol{U}^{\mathrm{in}}\}_x\right|$ and $\left|\{\mathbf{M}(p)\boldsymbol{U}^{\mathrm{in}}\}_y\right|$

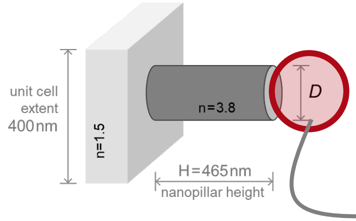

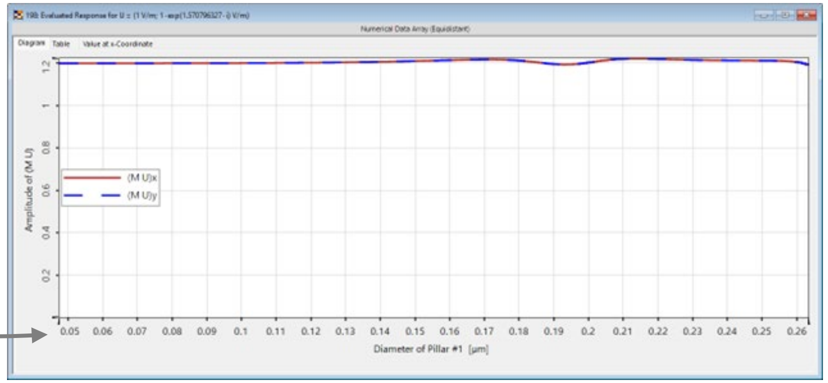

Magnitudes $\left|\{\mathbf{M}(p)\boldsymbol{U}^{\mathrm{in}}\}_x\right|$ and $\left|\{\mathbf{M}(p)\boldsymbol{U}^{\mathrm{in}}\}_y\right|$

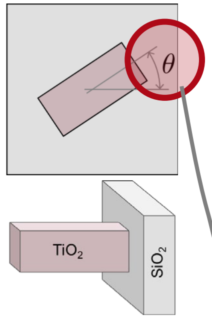

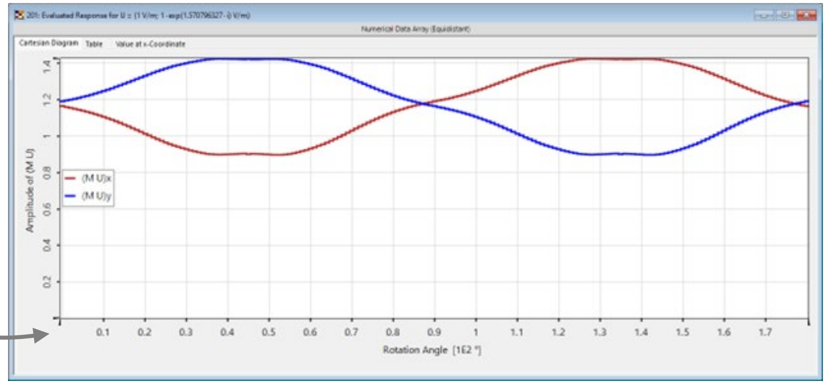

Example specifications:

- Input field vector: $\boxed{\boldsymbol{U}^{\mathrm{in}} = (1, \mathrm{i})^T}$
- Input direction direction: $\hat{\boldsymbol{s}}^{\mathrm{in}} = 0$

Effect of a Flat Lens on the Input Field: Examples

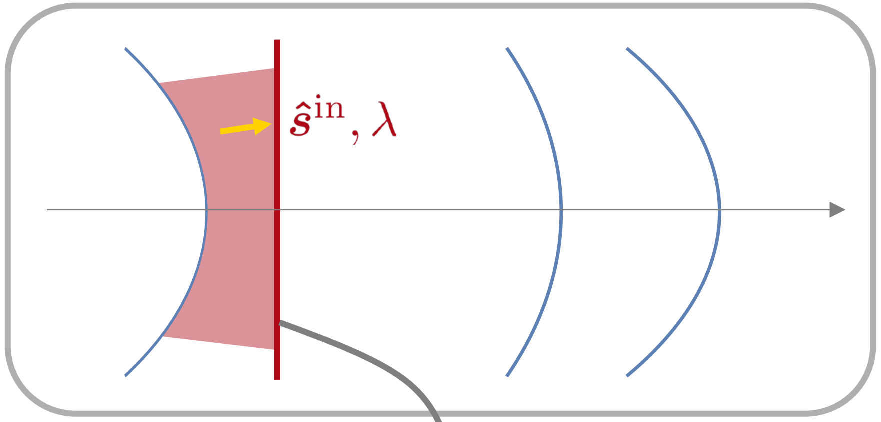

$\mathbf{M}(\boldsymbol{p}; \hat{\boldsymbol{s}}^{\text{in}}, \lambda)$

Example specifications:

- Input field vector: $\boldsymbol{U}^{\text{in}} = (1, \mathrm{i})^T$
- Input direction direction: $\hat{\boldsymbol{s}}^{\text{in}} = 0$

Phases $\arg\{\mathbf{M}(p)\boldsymbol{U}^{\text{in}}\}_x$ and $\arg\{\mathbf{M}(p)\boldsymbol{U}^{\text{in}}\}_y$

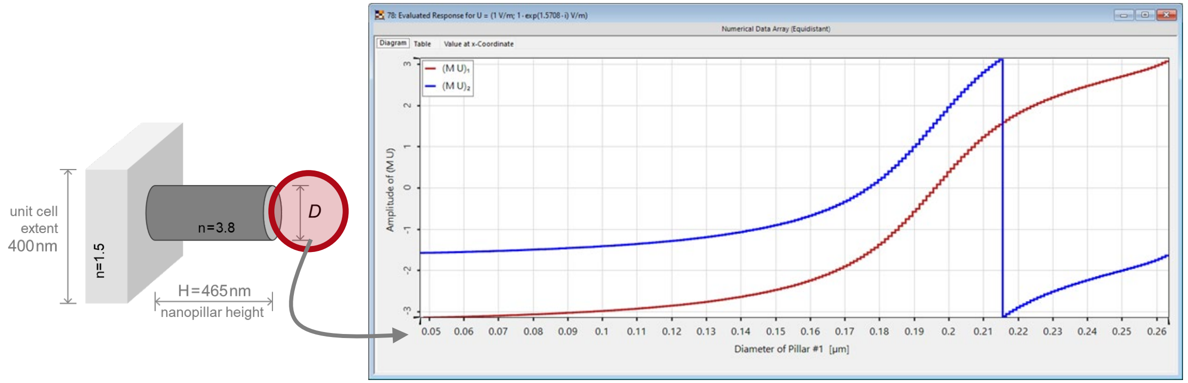

Phases $\arg\{\mathbf{M}(p)\boldsymbol{U}^{\text{in}}\}_x$ and $\arg\{\mathbf{M}(p)\boldsymbol{U}^{\text{in}}\}_y$

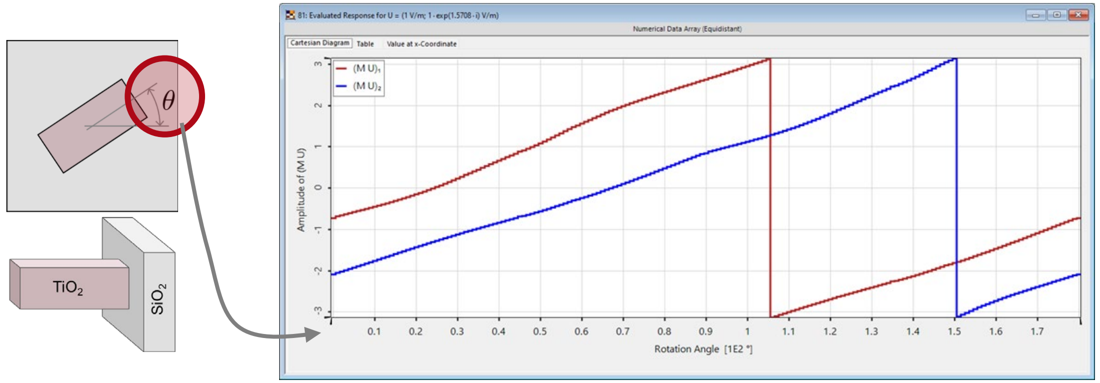

Selecting a Candidate for Wavefront Phase Response

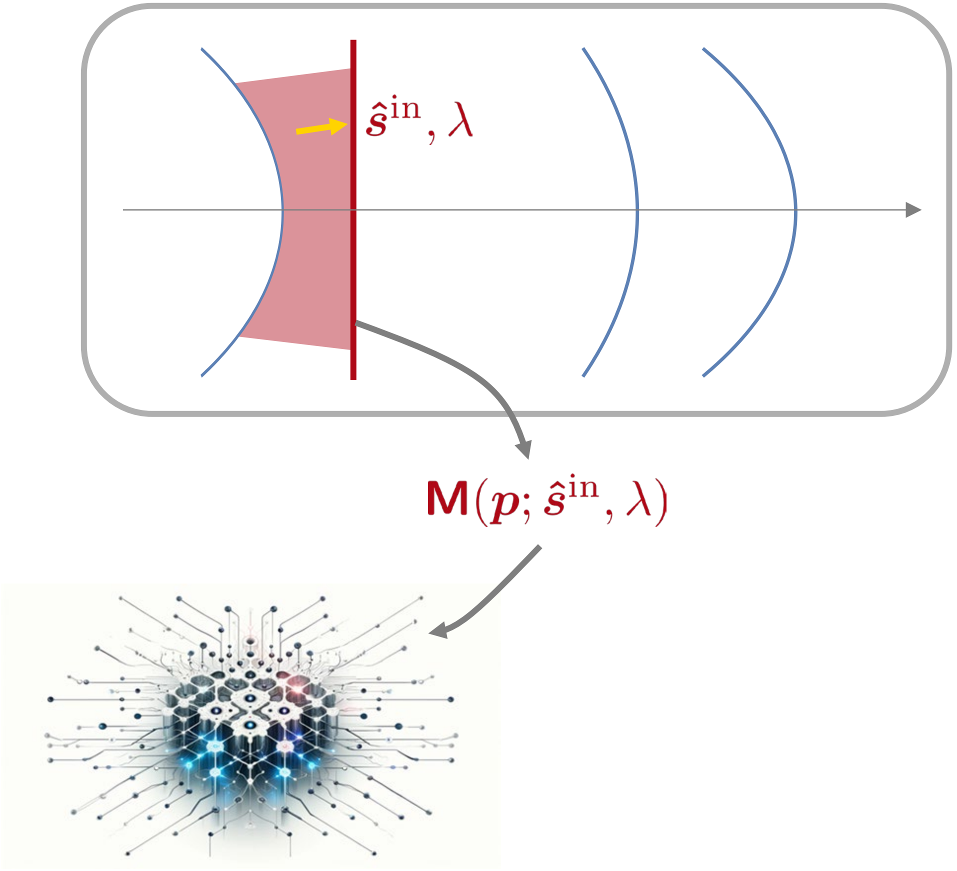

- We must choose a suitable candidate $\Psi^{\mathrm{c.d.}}$ for the wavefront phase response and extract it from the outcome of the matrix multiplication $\mathbf{M}(\boldsymbol{p}; \hat{\boldsymbol{s}}^{\mathrm{in}})\boldsymbol{U}^{\mathrm{in}}$.

- As a result, we obtain the residual phase components

$$\Delta\psi_\ell(\boldsymbol{p}) := \arg\left\{\mathbf{M}(\boldsymbol{p}; \hat{\boldsymbol{s}}^{\mathrm{in}})\, \boldsymbol{U}^{\mathrm{in}}\right\}_\ell - \Psi^{\mathrm{c.d.}}$$

  where $\ell = x, y$.

- The suitability of a candidate is measured by a single metric, denoted as σ^2.

Selecting a Candidate for Wavefront Phase Response

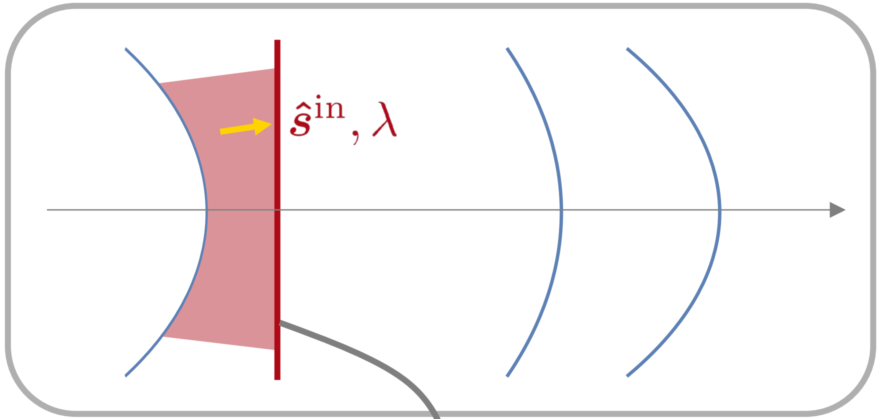

$\mathbf{M}(\boldsymbol{p}; \hat{\boldsymbol{s}}^{\text{in}}, \lambda)$

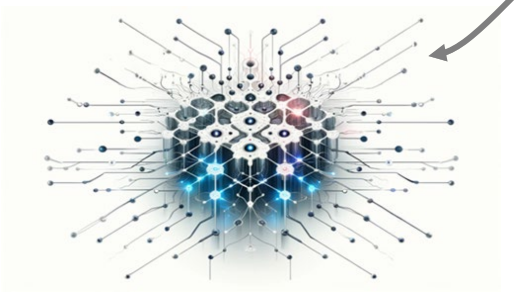

Values for the metric σ^2

	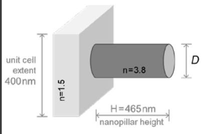		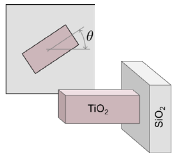	
$\Psi^{\text{c.d.}} = \arg\left\{\mathbf{M}(p)\, \boldsymbol{U}^{\text{in}}\right\}_\ell$ for $\ell = x, y$	x	y	x	y
σ^2 for $\boldsymbol{U}^{\text{in}} = (1,1)^T$	0	0	2.9	2.9
σ^2 for $\boldsymbol{U}^{\text{in}} = (1,\mathrm{i})^T$	0	0	0.04	0.04

Strong polarization dependency.

Selecting a Candidate for Wavefront Phase Response

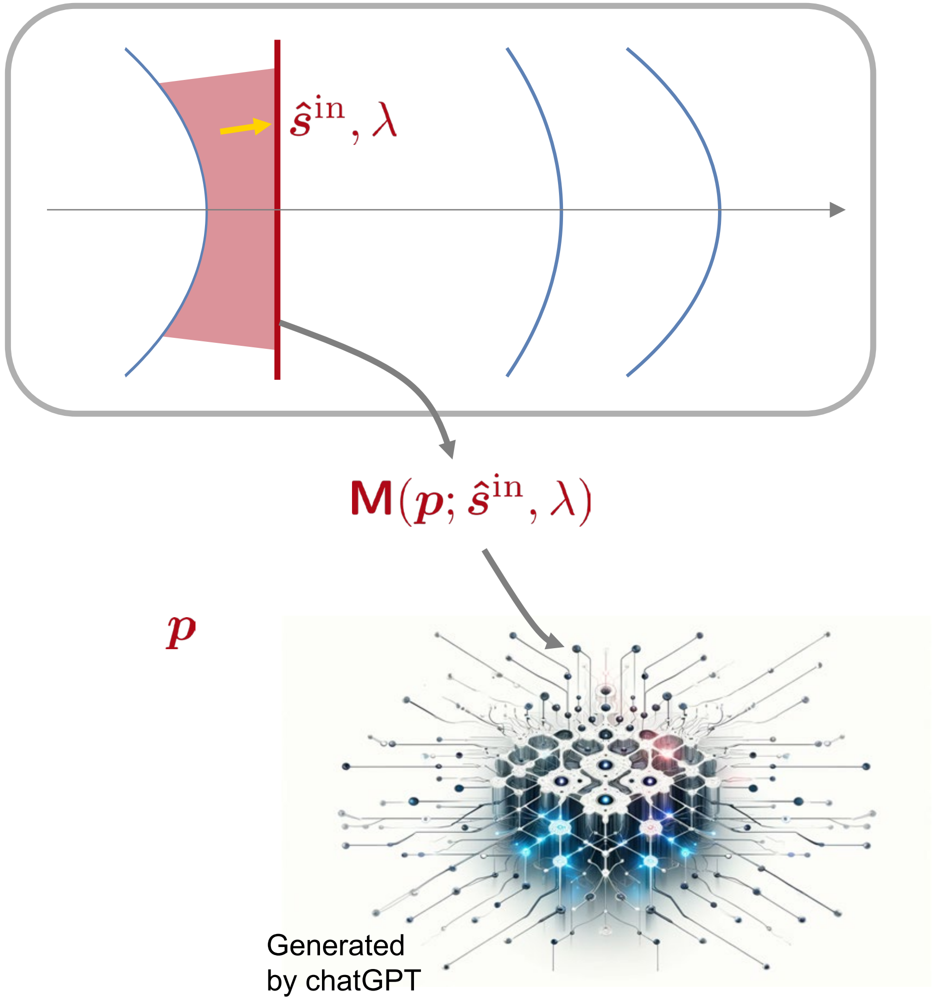

Generated by chatGPT

- This outcome shows that choosing the wavefront phase candidate $\Psi^{\mathrm{c.d.}}$ as the x- or y-component from $\mathbf{M}(\boldsymbol{p}; \hat{\boldsymbol{s}}^{\mathrm{in}})\,\boldsymbol{U}^{\mathrm{in}}$ is inadequate for designing and modeling metalenses in serious software development.
- We propose a technique for the design and simulation of metalenses that fully leverages the capabilities of the established neural network.

Mode Decomposition as a Foundation for Modeling and Design

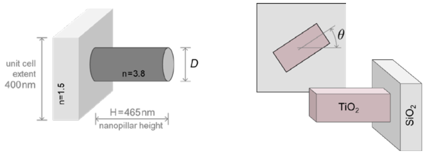

Structure of metacell

Simulation model

Matrix values $\mathbf{M}(\boldsymbol{p}; \hat{\boldsymbol{s}}^{\mathrm{in}}, \lambda)$

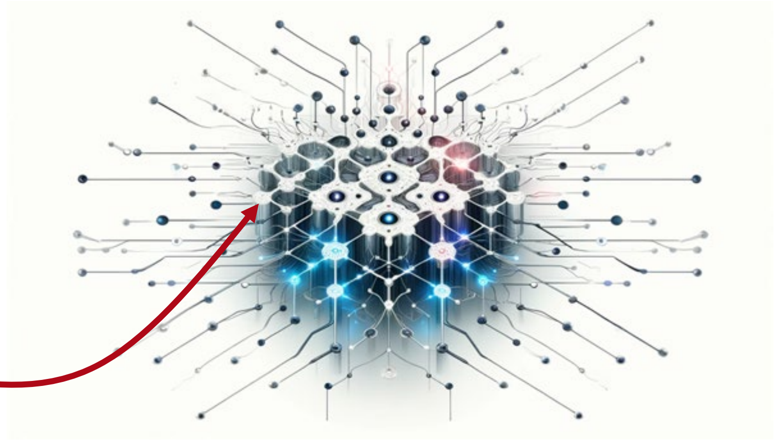

Simulating Metacells Using Periodic Cell Approximation (PCA)

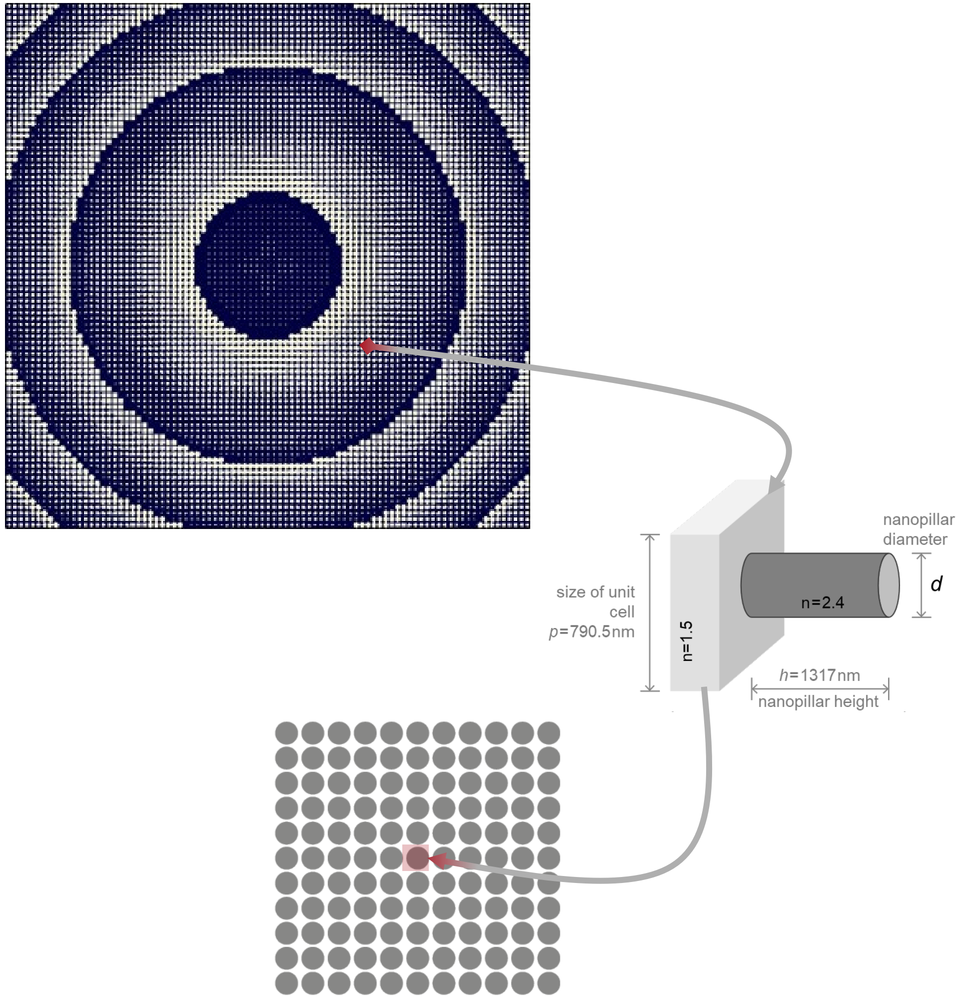

Metacell grating

- Given that each meta-atom is surrounded by neighboring meta-atoms, the matrix analysis is conducted not on a single, isolated meta-atom, but rather on a meta-atom that is replicated periodically.
- This leads to the formation of a sub-wavelength grating, where the metacell serves as the periodic unit for analysis.
- The analysis of this **metacell grating** employs the Fourier Modal Method (FMM), also known as RCWA.
- We call this effective technique the Periodic Cell Approximation (PCA).

Mode Decomposition as a Foundation for Modeling and Design

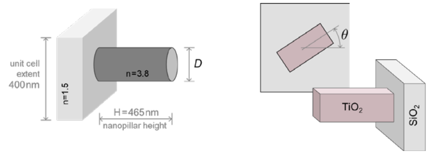

Structure of metacell

Simulation model (PCA)

Matrix values $\mathbf{M}(\boldsymbol{p}; \hat{\boldsymbol{s}}^{\mathrm{in}}, \lambda)$

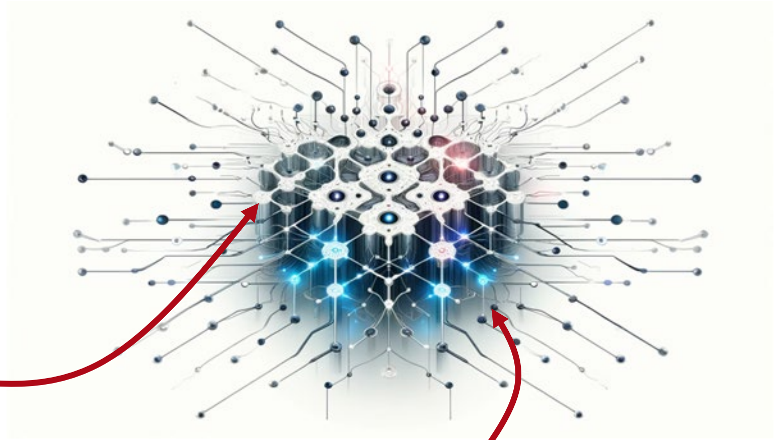

Orthogonal vector basis
$\boldsymbol{W}_1$ and $\boldsymbol{W}_2$

Wavefront phase candidates
$\Psi_1^{\mathrm{c.d.}}$ and $\Psi_2^{\mathrm{c.d.}}$

Training of
neural network

Orthogonal vector basis
$\boldsymbol{W}_1$ and $\boldsymbol{W}_2$

Wavefront phase candidates
$\Psi_1^{\mathrm{c.d.}}$ and $\Psi_2^{\mathrm{c.d.}}$

Mode Decomposition as a Foundation for Modeling and Design

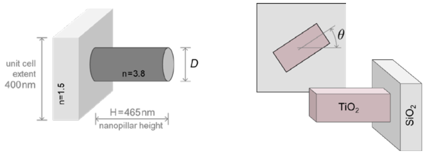

Structure of metacell

Simulation model (PCA)

$$\underbrace{\qquad\qquad\qquad\qquad}$$

Matrix values $\mathbf{M}(\boldsymbol{p}; \hat{\boldsymbol{s}}^{\text{in}}, \lambda)$

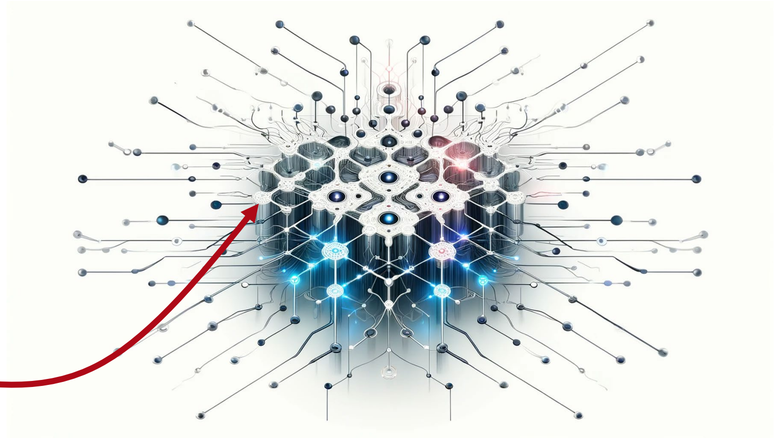

Orthogonal vector basis
$\boldsymbol{W}_1$ and $\boldsymbol{W}_2$

Wavefront phase candidates
$\Psi_1^{\text{c.d.}}$ and $\Psi_2^{\text{c.d.}}$

Training of
neural network ⇨

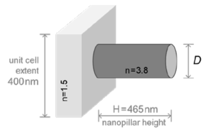	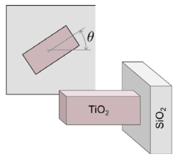
$\boldsymbol{W}_1 = (1,0)^T$ $\boldsymbol{W}_2 = (0,1)^T$	$\boldsymbol{W}_1 = (1,\mathrm{i})^T$ $\boldsymbol{W}_2 = (1,-\mathrm{i})^T$

Using a Trained Neural Network for Modeling

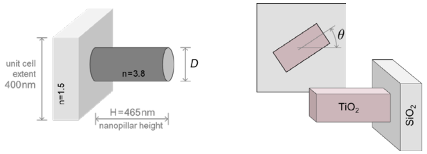

Structure of metacell

Simulation model (PCA)

Matrix values $\mathbf{M}(\boldsymbol{p}; \hat{\boldsymbol{s}}^{\text{in}}, \lambda)$

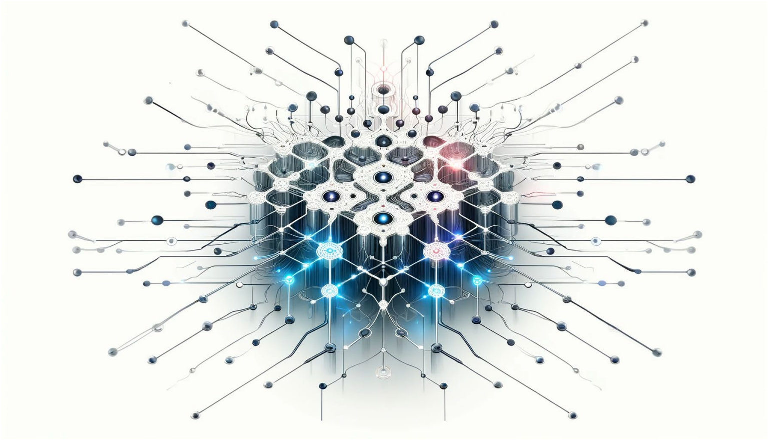

Orthogonal vector basis
$\boldsymbol{W}_1$ and $\boldsymbol{W}_2$

Wavefront phase candidates
$\Psi_1^{\text{c.d.}}$ and $\Psi_2^{\text{c.d.}}$

$$\begin{aligned}\boldsymbol{E}^{\text{in}} &= \boldsymbol{U}^{\text{in}} \exp[\mathrm{i}\psi^{\text{in}}] \\ &= \left\{V_1^{\text{in}}\boldsymbol{W}_1 + V_2^{\text{in}}\boldsymbol{W}_2\right\} \exp[\mathrm{i}\psi^{\text{in}}]\end{aligned}$$

$$\begin{aligned}\boldsymbol{E}^{\text{out}} &= \boldsymbol{U}_1^{\text{out}} \exp[\mathrm{i}\{\psi^{\text{in}} + \Psi_1\}] + \boldsymbol{U}_2^{\text{out}} \exp[\mathrm{i}\{\psi^{\text{in}} + \Psi_2\}] \\ &= \boldsymbol{U}^{\text{out}} \exp[\mathrm{i}\{\psi^{\text{in}} + \Psi\}]\,, \text{if } \Psi_1 = \Psi_2 =: \Psi\end{aligned}$$

From Candidate to Final Wavefront Phase Response

- The phase $\Psi_j^{\text{c.d.}}(\boldsymbol{\rho})$ is not yet in the form of a wavefront phase, since it is in the form of 2π-modulo.
- In addition, it may include some contributions which do not belong to a smooth wavefront phase, e.g., because they cannot be unwrapped like a phase vortex.
- Thus, in a final step the phase $\Psi_j^{\text{c.d.}}(\boldsymbol{\rho})$ is unwrapped and filtered.

$\Psi_j^{\text{c.d.}}(x,y) \bmod 2\pi$ $\qquad$ $\Psi(x,y)$ $\qquad$ $\Psi_j(\boldsymbol{\rho};\Theta) \bmod 2\pi$

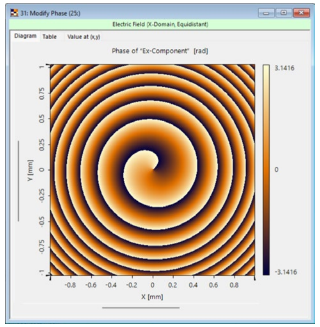

=

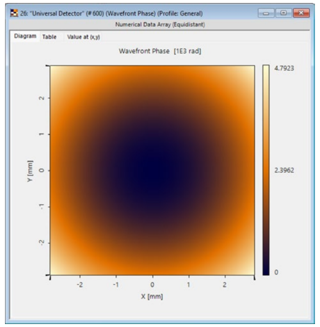

+

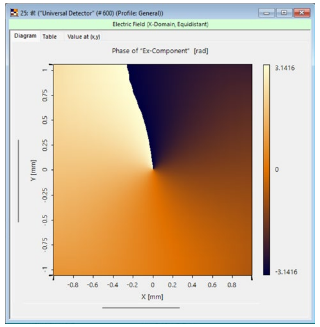

- We refer to this operation as Θ and obtain

$$\left(\Theta\{\Psi_j^{\text{c.d.}} \bmod 2\pi\}(\boldsymbol{\rho})\right) = \Psi_j(\boldsymbol{\rho}) + \Delta\Psi_j(\boldsymbol{\rho};\Theta) \bmod 2\pi\,.$$

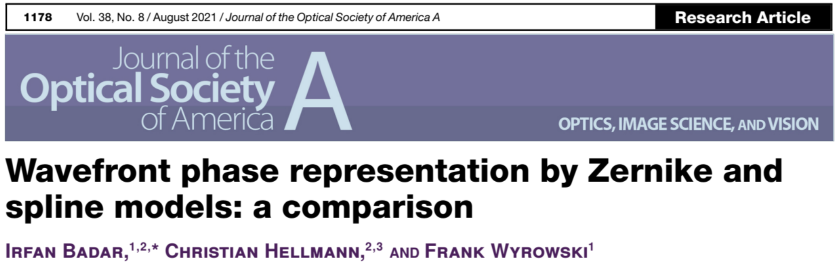
1178 Vol. 38, No. 8 / August 2021 / *Journal of the Optical Society of America A* **Research Article**

Journal of the Optical Society of America A

OPTICS, IMAGE SCIENCE, AND VISION

Wavefront phase representation by Zernike and spline models: a comparison

IRFAN BADAR,[1,2,*] CHRISTIAN HELLMANN,[2,3] AND FRANK WYROWSKI[1]

From Candidate to Final Wavefront Phase Response

- The phase $\Psi_j^{\mathrm{c.d.}}(\boldsymbol{\rho})$ is not yet in the form of a wavefront phase, since it is in the form of 2π-modulo.
- In addition, it may include some contributions which do not belong to a smooth wavefront phase, e.g., because they cannot be unwrapped like a phase vortex.
- Thus, in a final step the phase $\Psi_j^{\mathrm{c.d.}}(\boldsymbol{\rho})$ is unwrapped and filtered.

$\Psi_j^{\mathrm{c.d.}}(x,y) \bmod 2\pi$

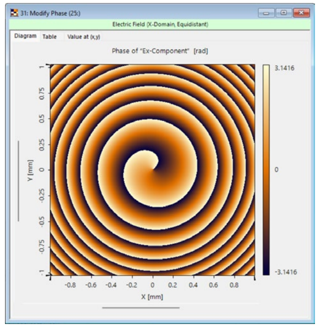

=

$\Psi(x,y)$

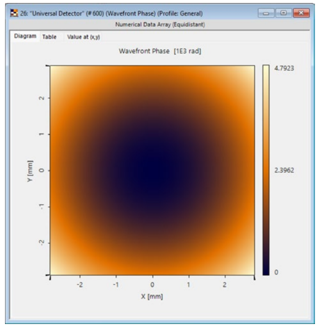

+

$\Psi_j(\boldsymbol{\rho};\Theta) \bmod 2\pi$

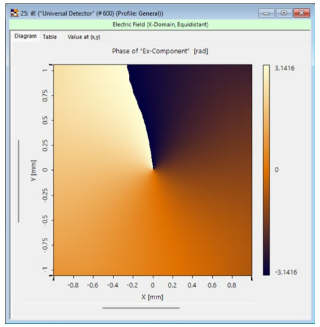

- We refer to this operation as Θ and obtain

$$\left(\Theta\{\Psi_j^{\mathrm{c.d.}} \bmod 2\pi\}(\boldsymbol{\rho})\right) = \Psi_j(\boldsymbol{\rho}) + \Delta\Psi_j(\boldsymbol{\rho};\Theta) \bmod 2\pi\,.$$

- This leads to the output field in form of

$$\boldsymbol{E}_j^{\mathrm{out}}(\boldsymbol{\rho}) = \boldsymbol{U}_j^{\mathrm{out}}(\boldsymbol{\rho})\exp[\mathrm{i}\psi^{\mathrm{in}}(\boldsymbol{\rho}) + \Psi_j(\boldsymbol{\rho})]\,,$$

with the smooth and unwrapped phase $\psi^{\mathrm{out}}(\boldsymbol{\rho}) = \psi^{\mathrm{in}}(\boldsymbol{\rho}) + \Psi(\boldsymbol{\rho})$ and

$$\boldsymbol{U}_j^{\mathrm{out}}(\boldsymbol{\rho}) =$$

$$= V_j(\boldsymbol{\rho})\begin{pmatrix}\left\{\left|(\mathbf{M}\,\boldsymbol{W}_j)_x\right|(\boldsymbol{\rho})\right\}\exp[\mathrm{i}\Delta\psi_{j,x}(\boldsymbol{\rho}) + \mathrm{i}\Delta\Psi_j(\boldsymbol{\rho};\Theta)] \\ \left\{\left|(\mathbf{M}\,\boldsymbol{W}_j)_y\right|(\boldsymbol{\rho})\right\}\exp[\mathrm{i}\Delta\psi_{j,y}(\boldsymbol{\rho}) + \mathrm{i}\Delta\Psi_j(\boldsymbol{\rho};\Theta)]\end{pmatrix}.$$

Design of Metalenses

Using a Trained Neural Network for Designing a Metalens

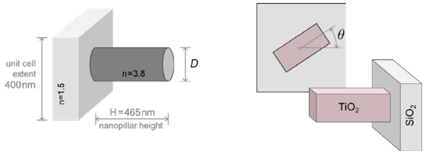

Structure of metacell

Simulation model (PCA)

Matrix values $\mathbf{M}(\boldsymbol{p}; \hat{\boldsymbol{s}}^{\text{in}}, \lambda)$

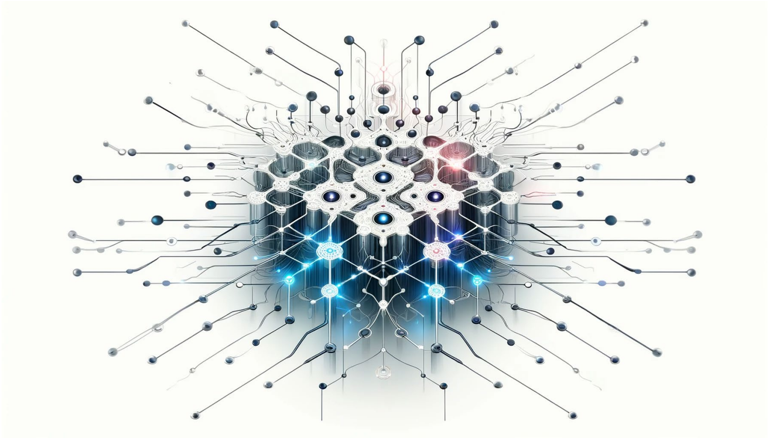

Orthogonal vector basis
$\boldsymbol{W}_1$ and $\boldsymbol{W}_2$

Wavefront phase candidates
$\Psi_1^{\text{c.d.}}$ and $\Psi_2^{\text{c.d.}}$

Select one of the modes for design ⇨ Specify $\Psi(\boldsymbol{\rho})$ ⇨ Neural network performs design ⇨ Export fabrication data, e.g., GSDII

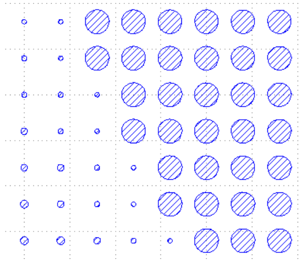

Simulation and Design of Metalenses

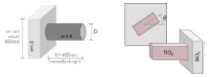

Structure of metacell

Simulation model (PCA)

Matrix values $\mathbf{M}(\boldsymbol{p}; \hat{\boldsymbol{s}}^{\text{in}}, \lambda)$

Orthogonal vector basis
$\boldsymbol{W}_1$ and $\boldsymbol{W}_2$

Wavefront phase candidates
$\Psi_1^{\text{c.d.}}$ and $\Psi_2^{\text{c.d.}}$

$$\begin{aligned}\boldsymbol{E}^{\text{in}} &= \boldsymbol{U}^{\text{in}} \exp[\mathrm{i}\psi^{\text{in}}] \\ &= \{V_1^{\text{in}}\boldsymbol{W}_1 + V_2^{\text{in}}\boldsymbol{W}_2\} \exp[\mathrm{i}\psi^{\text{in}}]\end{aligned}$$

$$\begin{aligned}\boldsymbol{E}^{\text{out}} &= \boldsymbol{U}_1^{\text{out}} \exp[\mathrm{i}\{\psi^{\text{in}} + \Psi_1\}] + \boldsymbol{U}_2^{\text{out}} \exp[\mathrm{i}\{\psi^{\text{in}} + \Psi_2\}] \\ &= \boldsymbol{U}^{\text{out}} \exp[\mathrm{i}\{\psi^{\text{in}} + \Psi\}]\,, \text{ if } \Psi_1 = \Psi_2 =: \Psi\end{aligned}$$

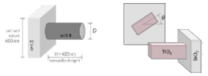

Structure of metacell

Simulation model (PCA)

Matrix values $\mathbf{M}(\boldsymbol{p}; \hat{\boldsymbol{s}}^{\text{in}}, \lambda)$

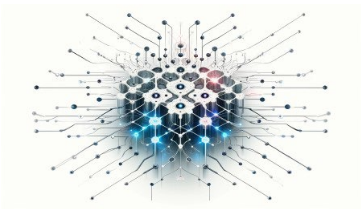

Orthogonal vector basis
$\boldsymbol{W}_1$ and $\boldsymbol{W}_2$

Wavefront phase candidates
$\Psi_1^{\text{c.d.}}$ and $\Psi_2^{\text{c.d.}}$

Select one of the modes for design ⇒ Specify $\Psi(\boldsymbol{\rho})$ ⇒ Neural network performs design ⇒ Export fabrication data, e.g., GSDII

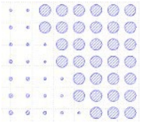

- The simulation and design techniques are incorporated into our proprietary VirtualLab Fusion software.
- These advanced techniques are planned to be released to the public in the upcoming 2024 software updates.

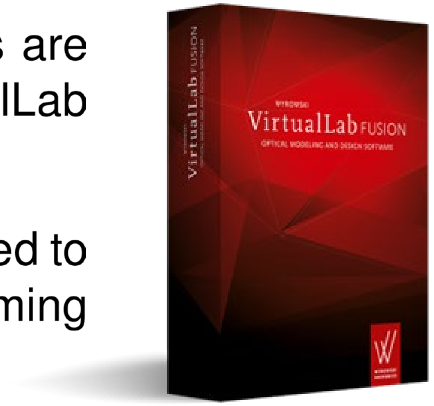

Design Examples and Simulations

Focusing with Pillar-Type Metalens

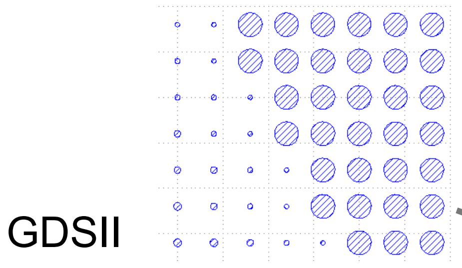

Focusing metalens
- focal length: 7mm
- diameter: 3mm
- nanostructure: pillars
- number of cells: 7501 x 7501
- design time: 2s

Plane incident wave
- 3mm x 3mm diameter
- wavelength: 940nm

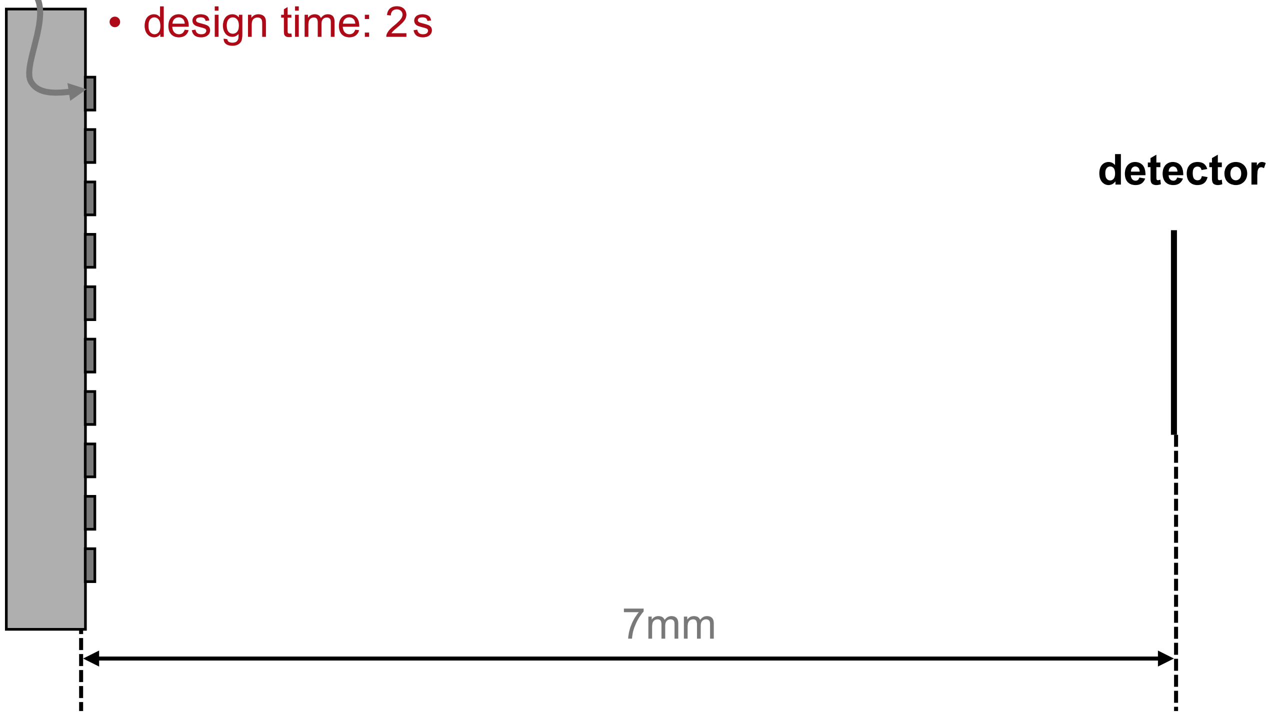

Rays Derived from Multiscale Simulation

Focusing metalens
- focal length: 7mm
- diameter: 3mm
- nanostructure: pillars
- number of cells: 7501 x 7501
- design time: 2s

Plane incident wave
- 3mm x 3mm diameter
- wavelength: 940nm

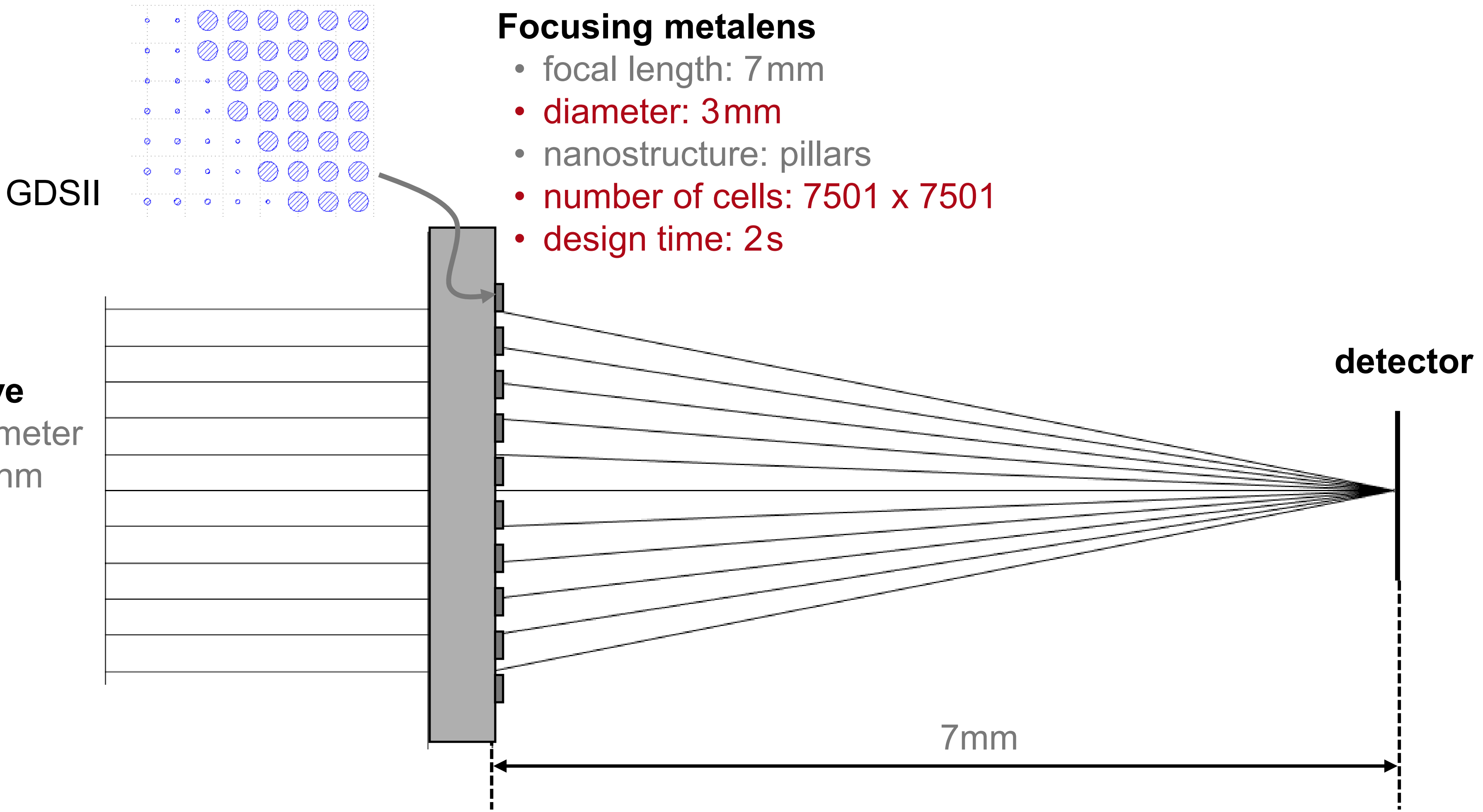

Magnitudes of Focal Point Obtained from Multiscale Simulation

Simulation time ~ 20s
(7501 x 7501 cells)

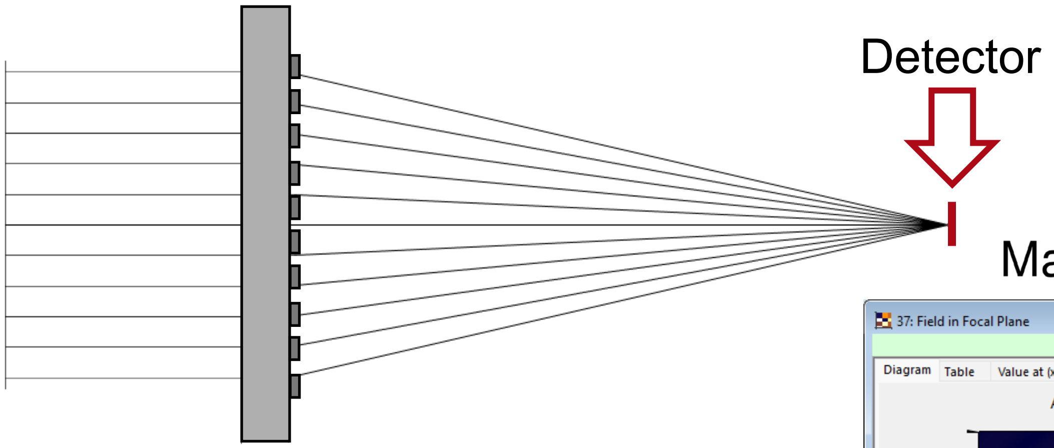

Magnitude $|E_x(\boldsymbol{\rho})|$

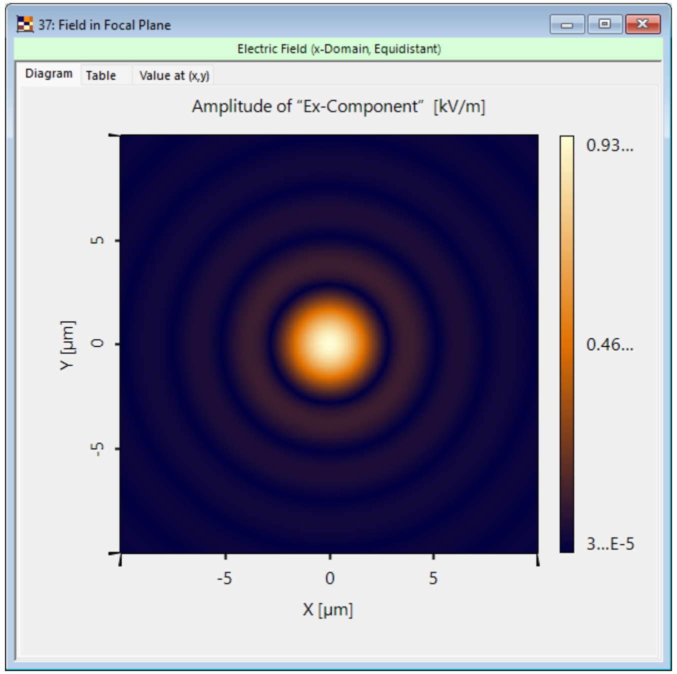

Magnitude $|E_y(\boldsymbol{\rho})|$

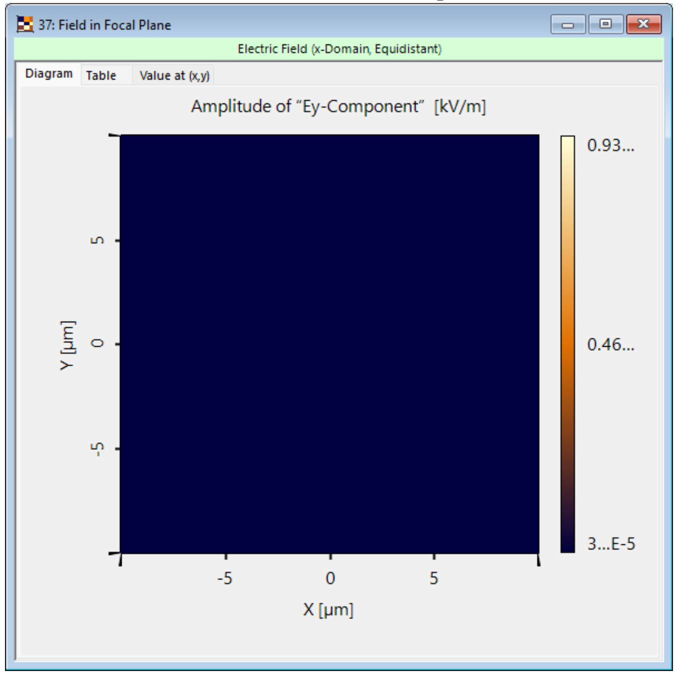

0° Linear Polarization

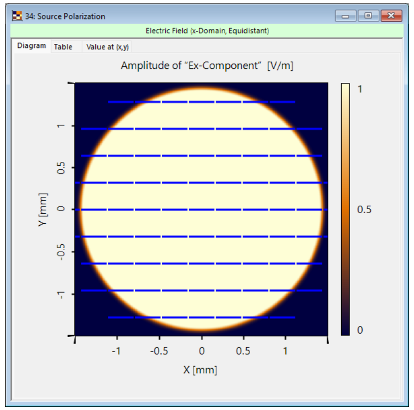

Irradiance of Focal Point Obtained from Multiscale Simulation

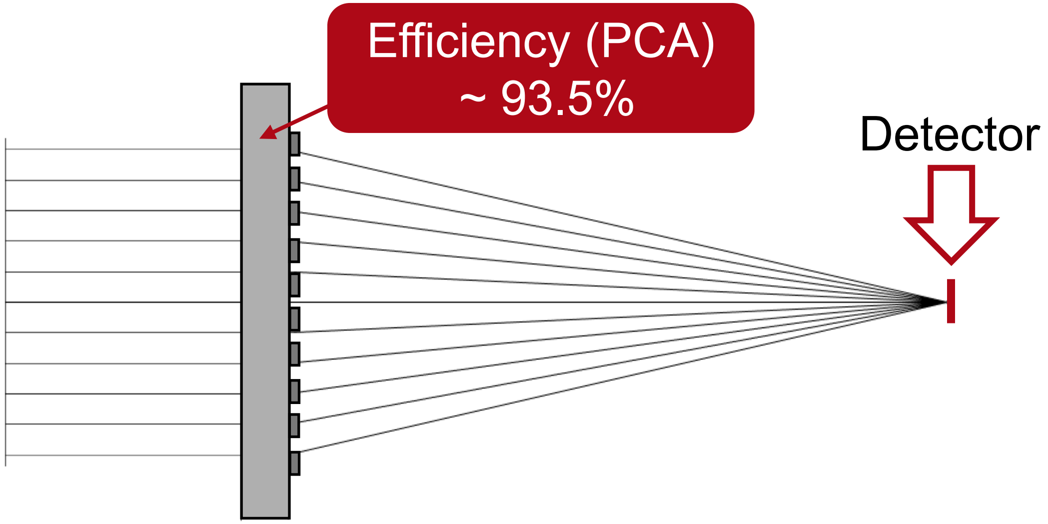

Irradiance $E_e(\boldsymbol{\rho})$

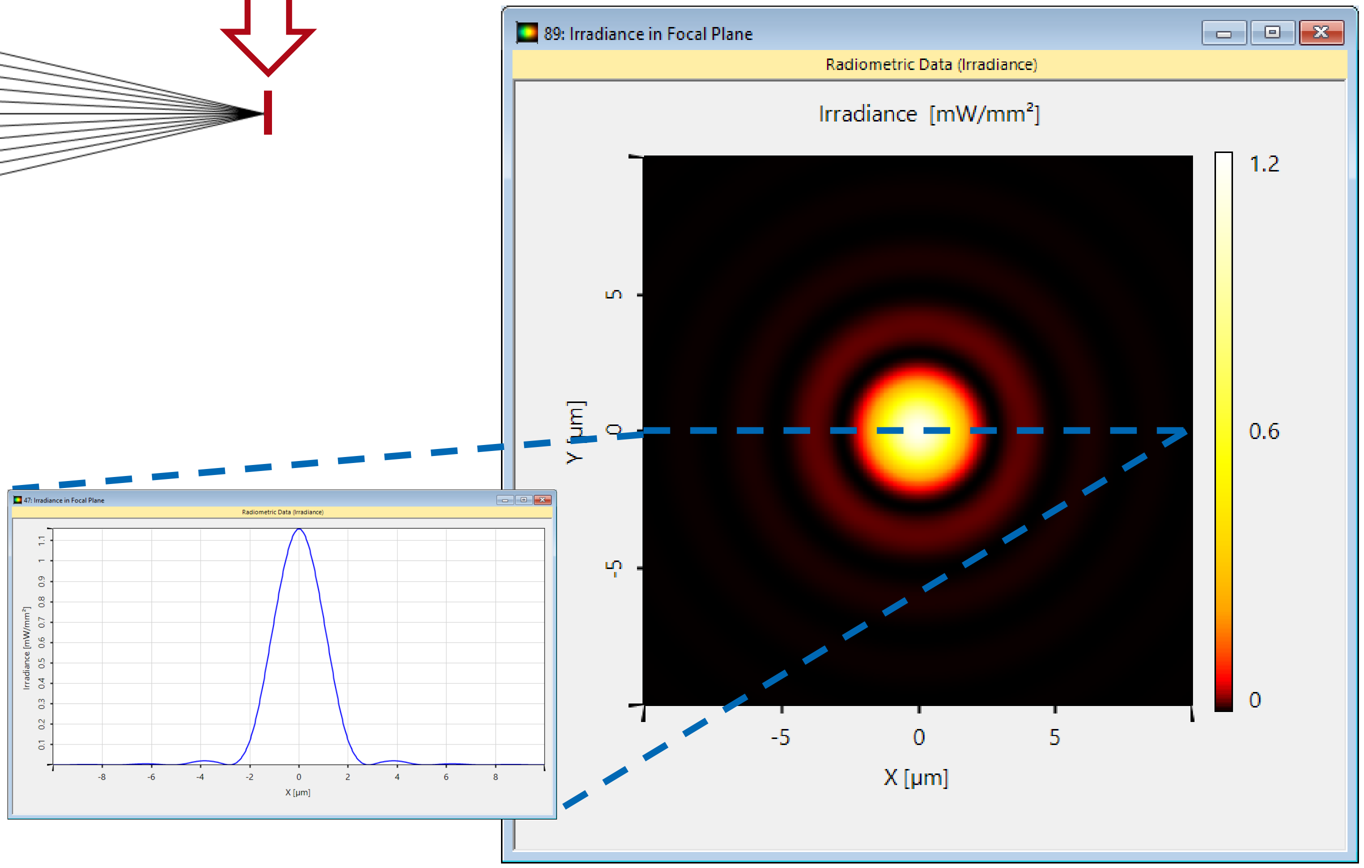

0° Linear Polarization

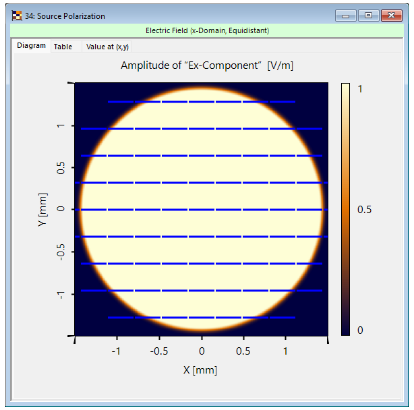

Magnitudes of Focal Point Obtained from Multiscale Simulation

Simulation time ~ 20s
(7501 x 7501 cells)

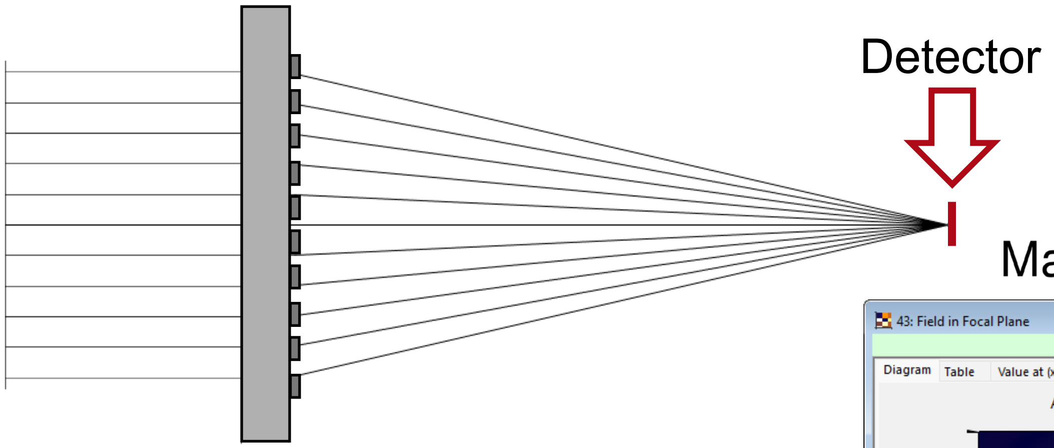

45° Linear Polarization

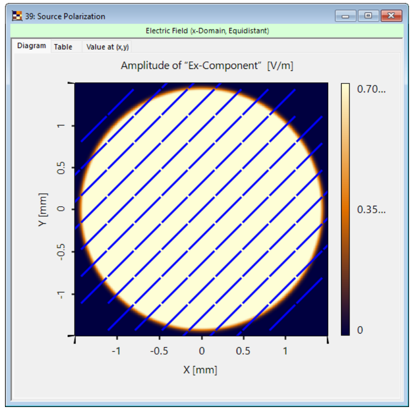

Magnitude $|E_x(\boldsymbol{\rho})|$

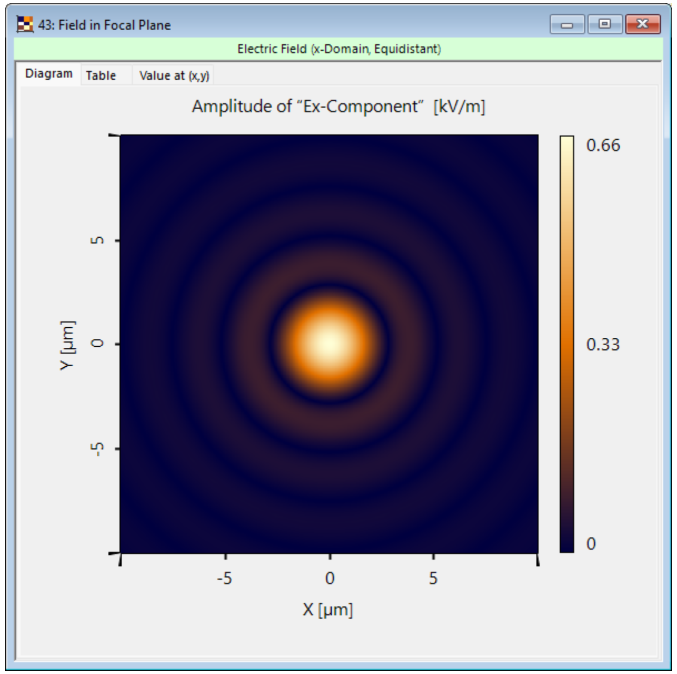

Magnitude $|E_y(\boldsymbol{\rho})|$

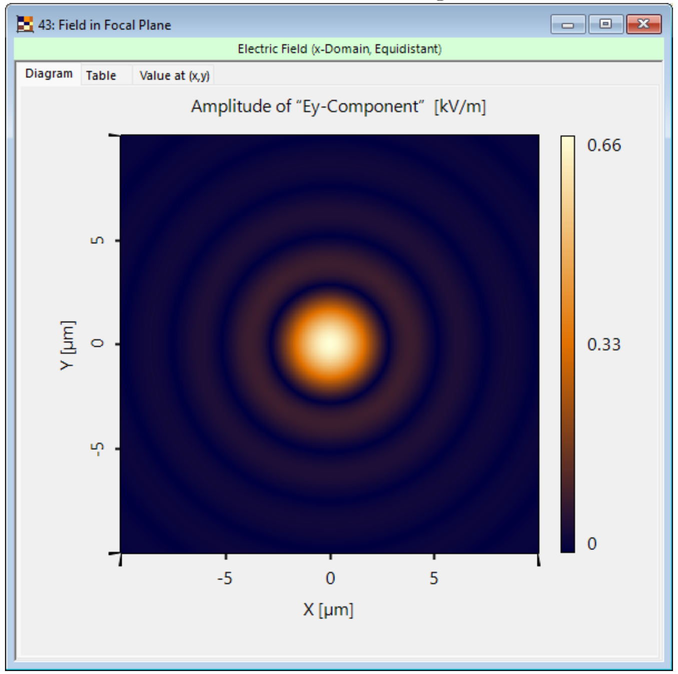

Irradiance of Focal Point Obtained from Multiscale Simulation

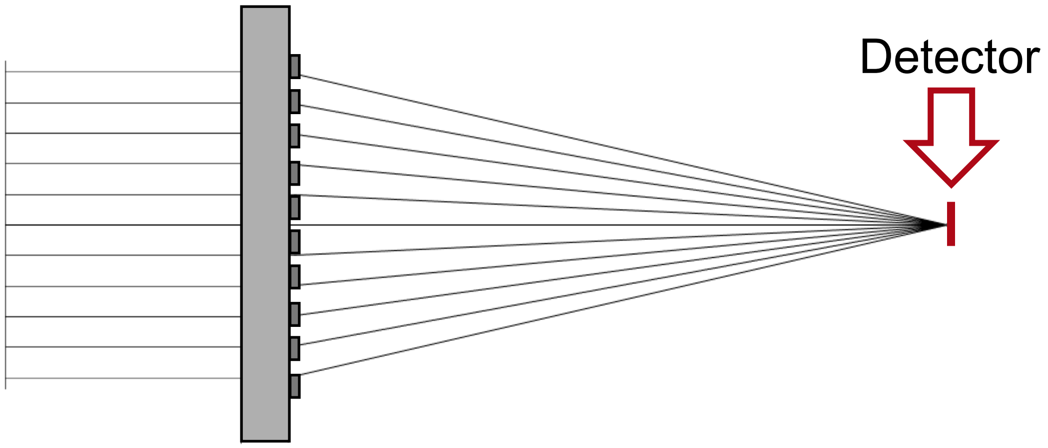

Irradiance $E_e(\boldsymbol{\rho})$

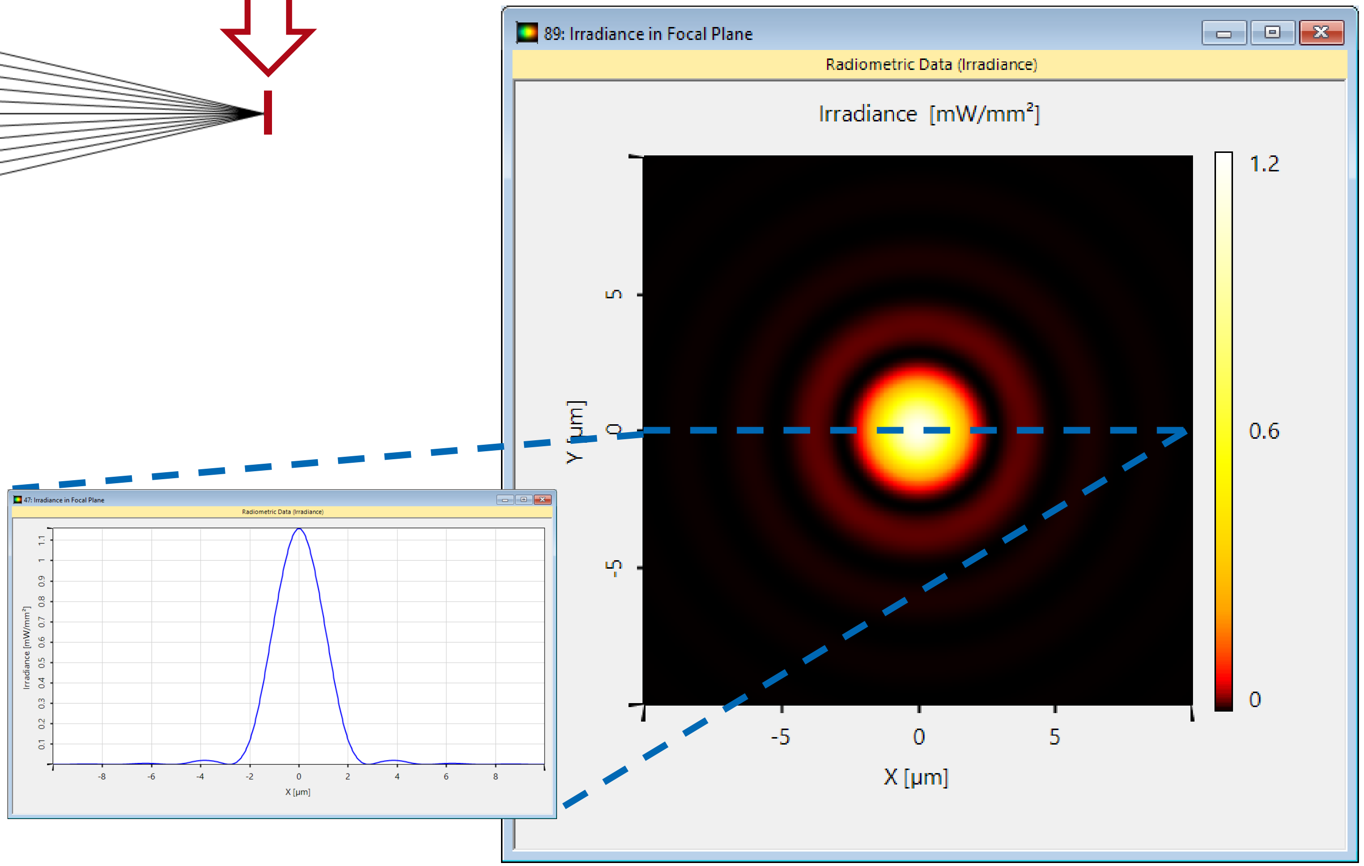

45° Linear Polarization

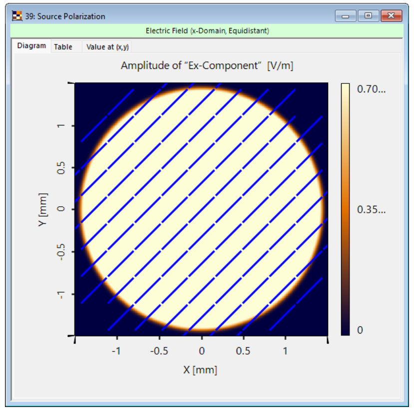

Rays Derived from Multiscale Simulation

Plane incident wave
- 3mm x 3mm diameter
- alpha: 10°
- wavelength: 940nm

Focusing metalens
- focal length: 7mm
- diameter: 3mm
- nanostructure: pillars
- number of cells: 7501 x 7501
- design time: 2s

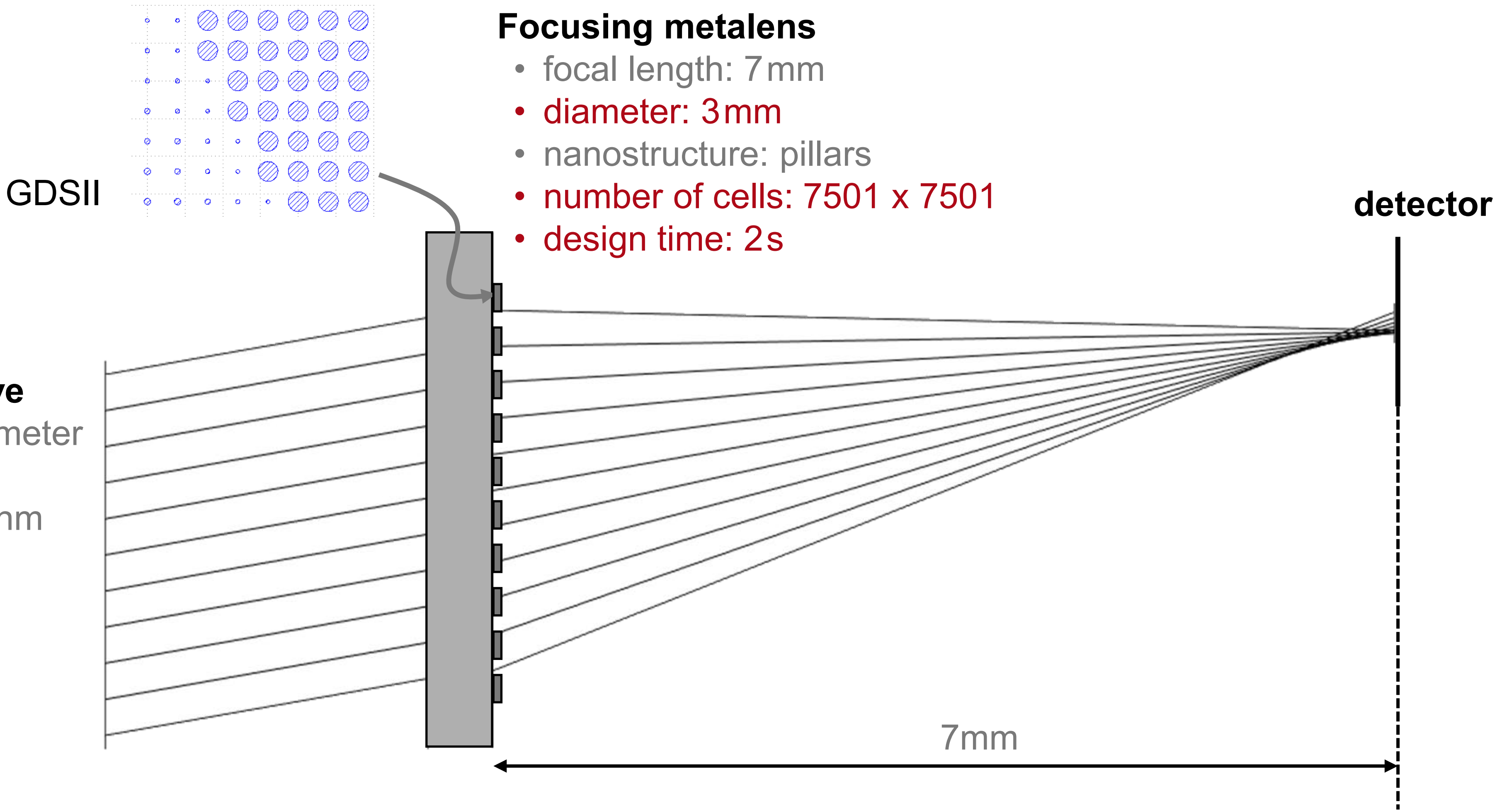

Obtained Wavefront Phase Response of Metalens

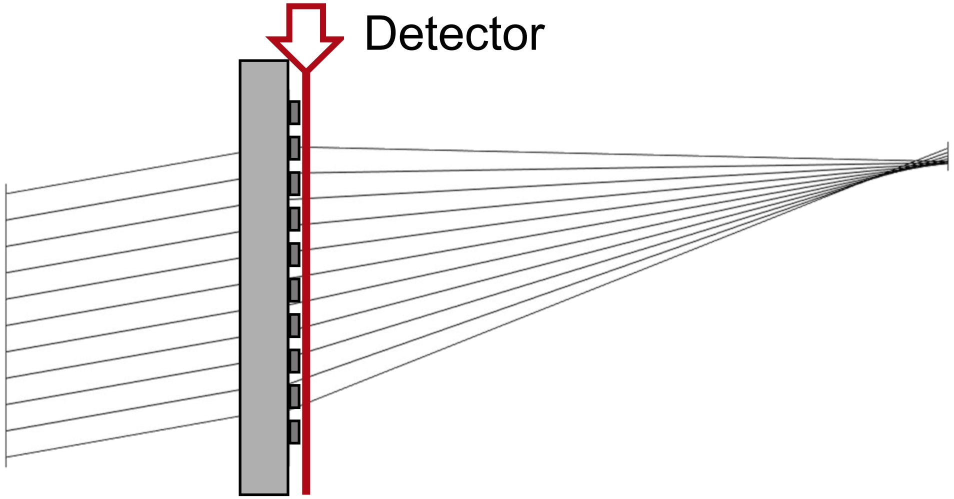

0° Linear Polarization

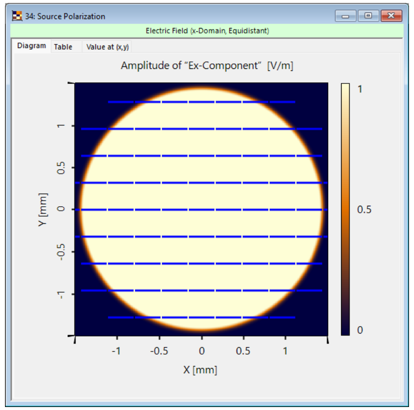

Wavefront Phase Response $\Psi(\rho)$

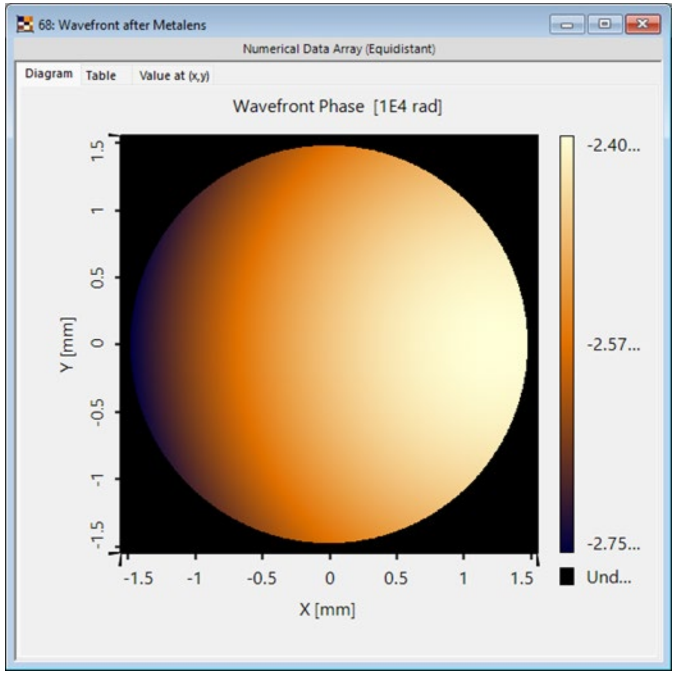

Dot Diagram Derived from Multiscale Simulation

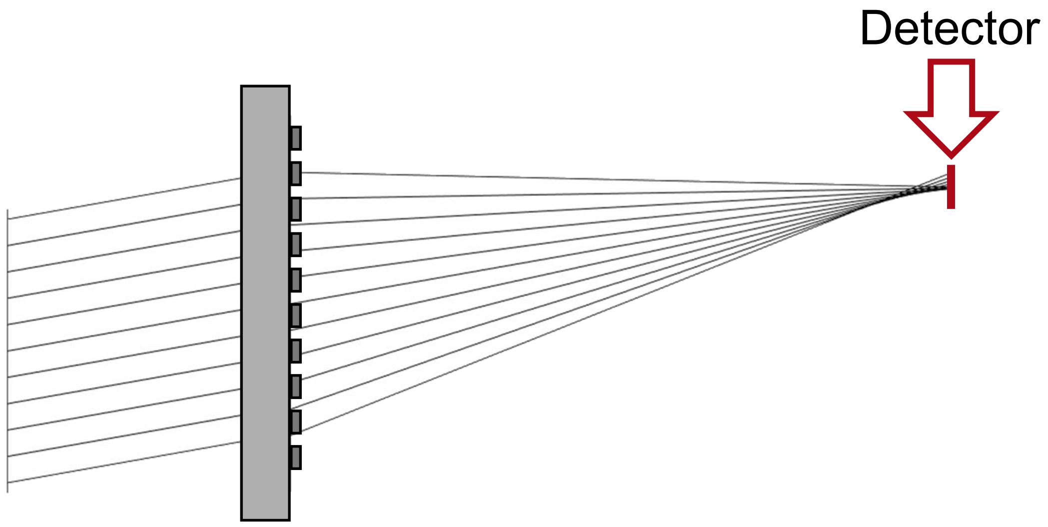

0° Linear Polarization

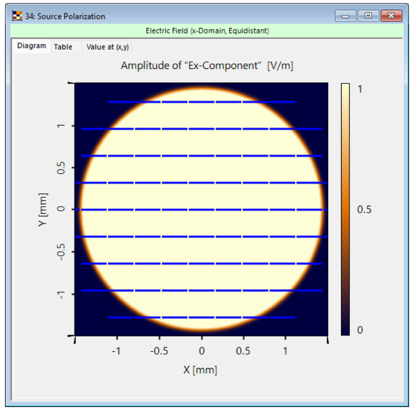

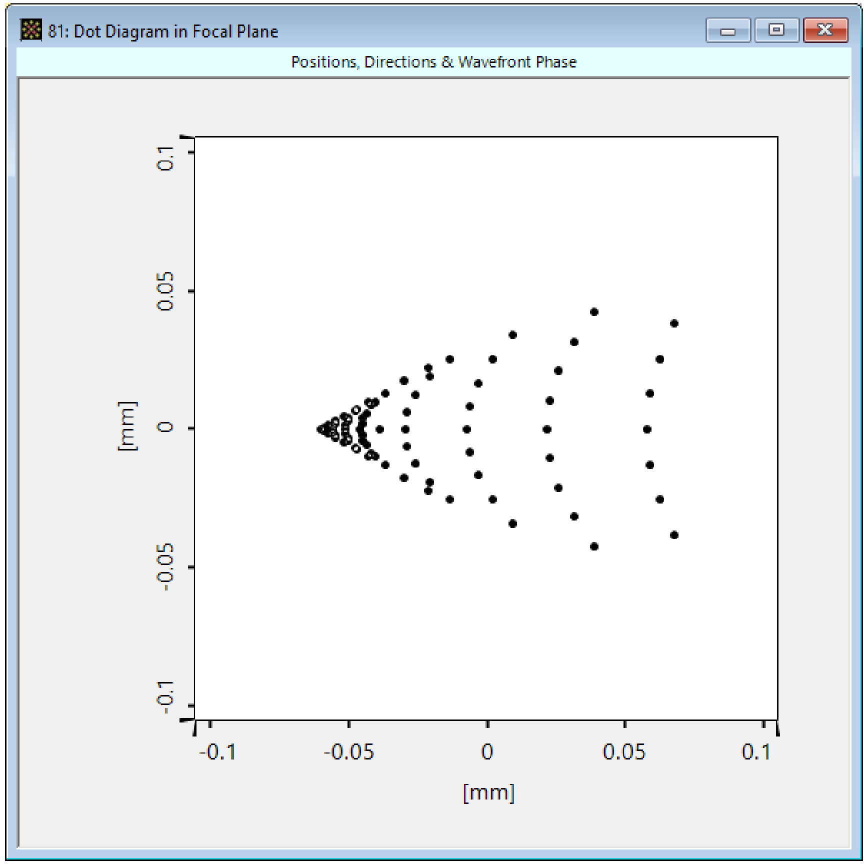

Magnitudes Obtained from Multiscale Simulation

Simulation time ~ 20s
(7501 x 7501 cells)

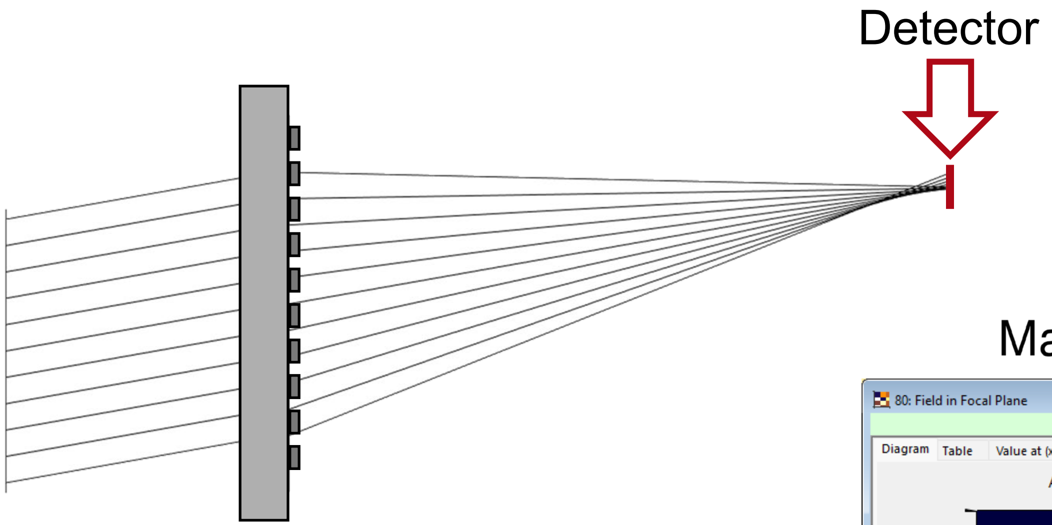

Magnitude $|E_x(\boldsymbol{\rho})|$

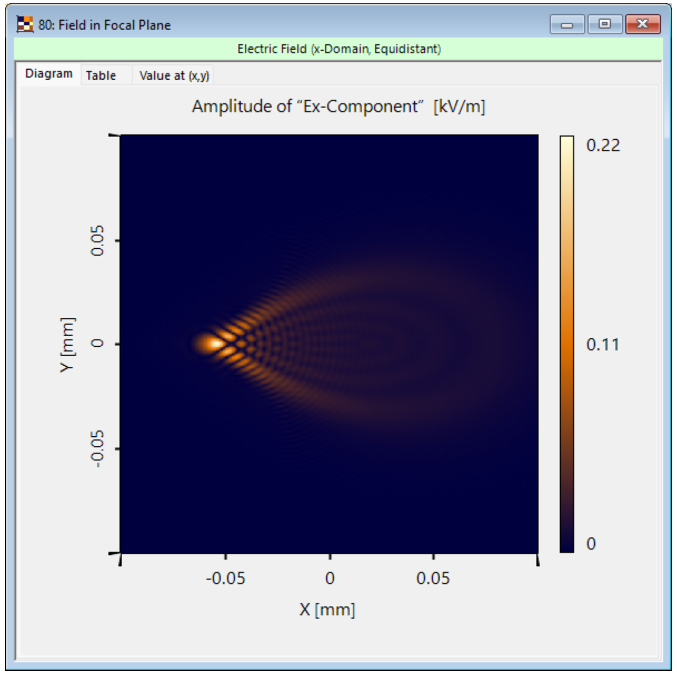

Magnitude $|E_y(\boldsymbol{\rho})|$

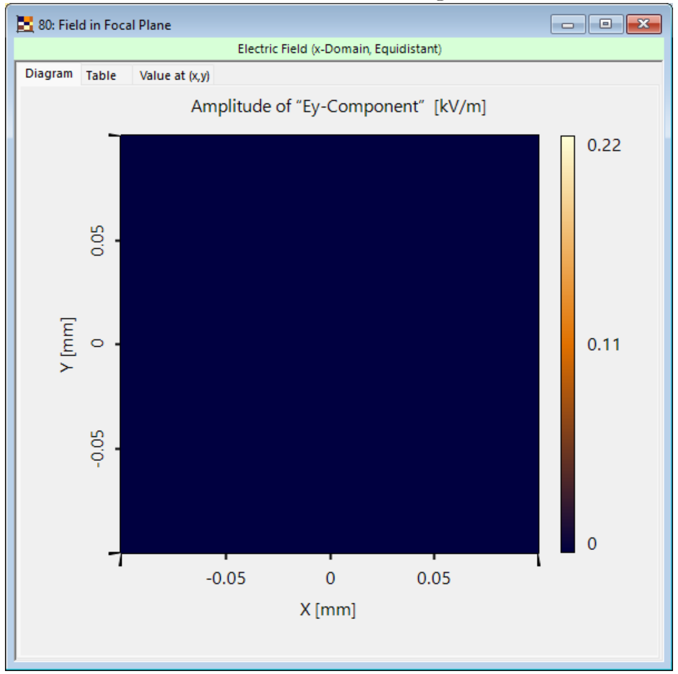

0° Linear Polarization

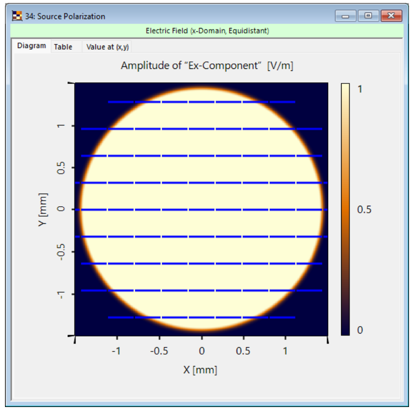

Irradiance from Multiscale Simulation

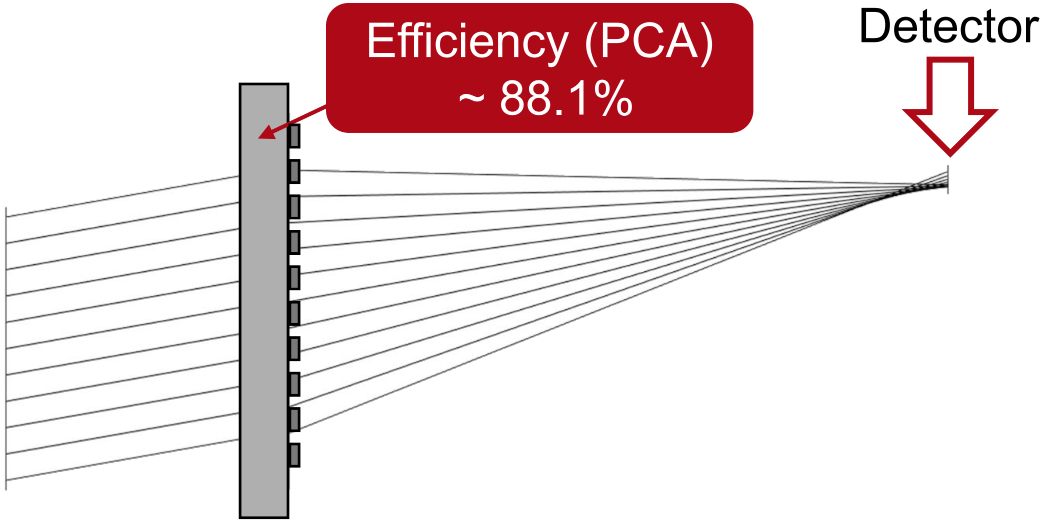

Irradiance $E_e(\boldsymbol{\rho})$

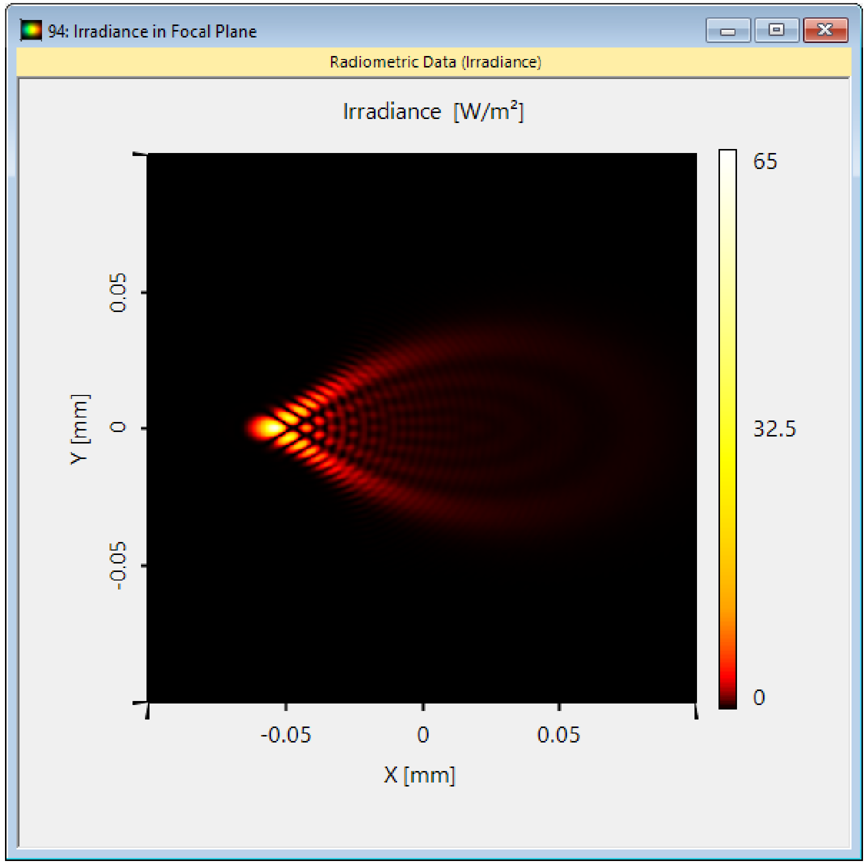

0° Linear Polarization

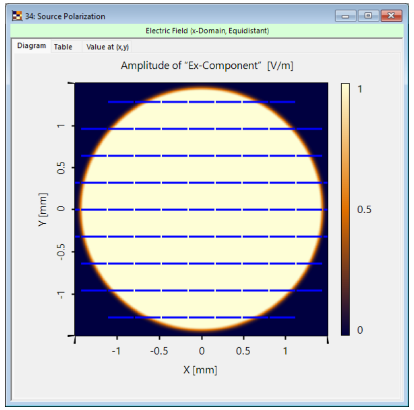

Irradiance and Dot Diagram from Multiscale Simulation

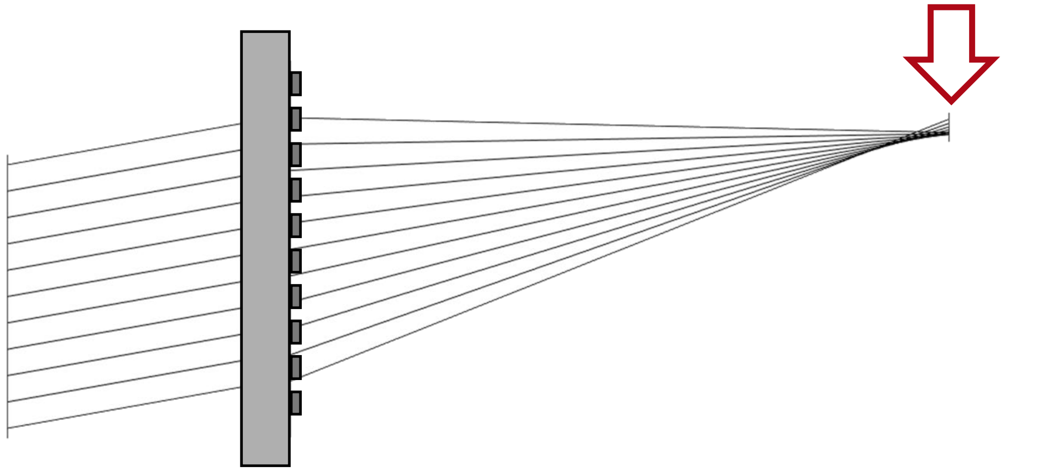

Irradiance $E_{\mathrm{e}}(\boldsymbol{\rho})$ w/ Superimposed Dot Plot

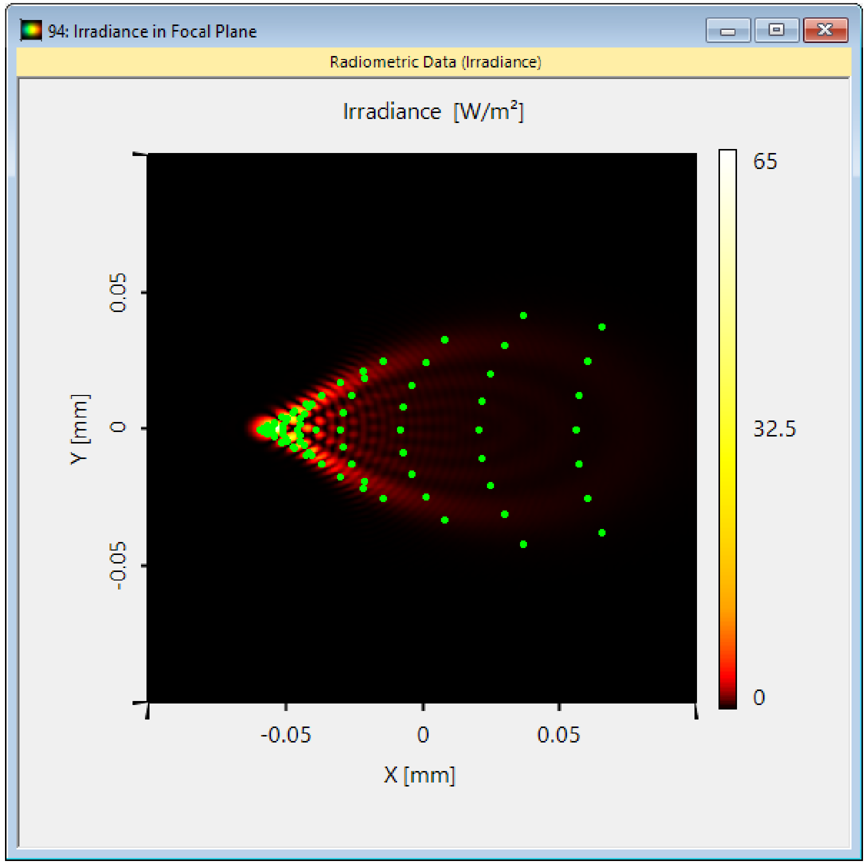

0° Linear Polarization

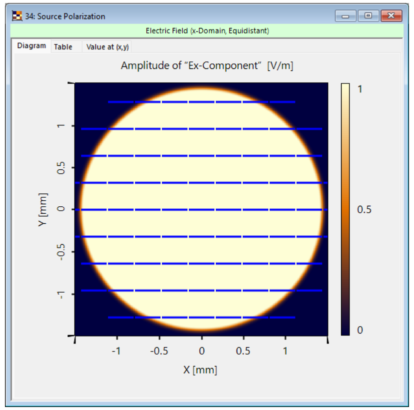

Focusing with Nanofin-Type Metalens

GDSII

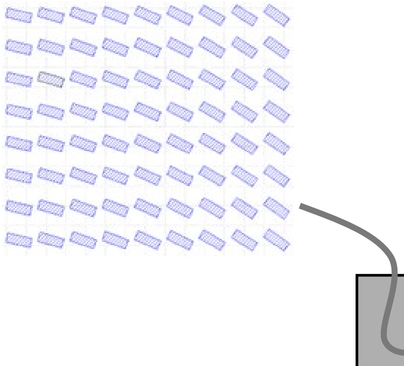

Focusing metalens
- focal length: 7mm
- diameter: 3mm
- nanostructure: nanofins
- number of cells: 9233 x 9233
- design time: 3s

Plane incident wave
- 3mm x 3mm diameter
- wavelength: 532nm

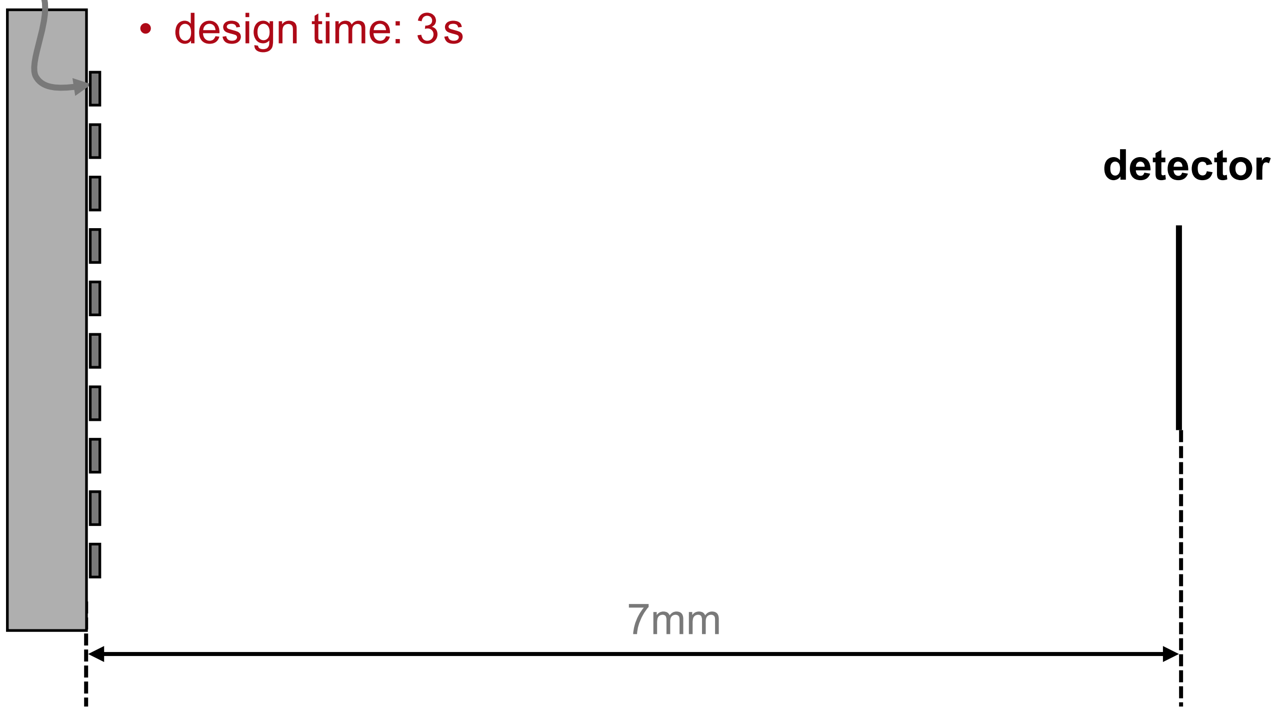

Rays Derived from Multiscale Simulation

Focusing metalens
- focal length: 7mm
- diameter: 3mm
- nanostructure: nanofins
- number of cells: 9233 x 9233
- design time: 3s

Plane incident wave
- 3mm x 3mm diameter
- wavelength: 532nm

Right Circular Polarization

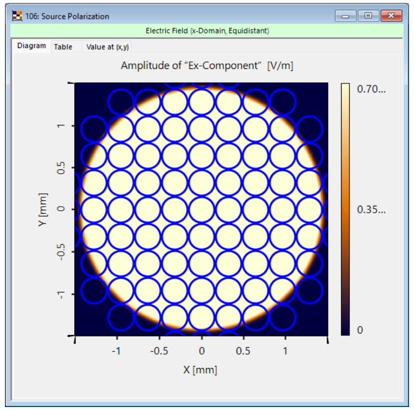

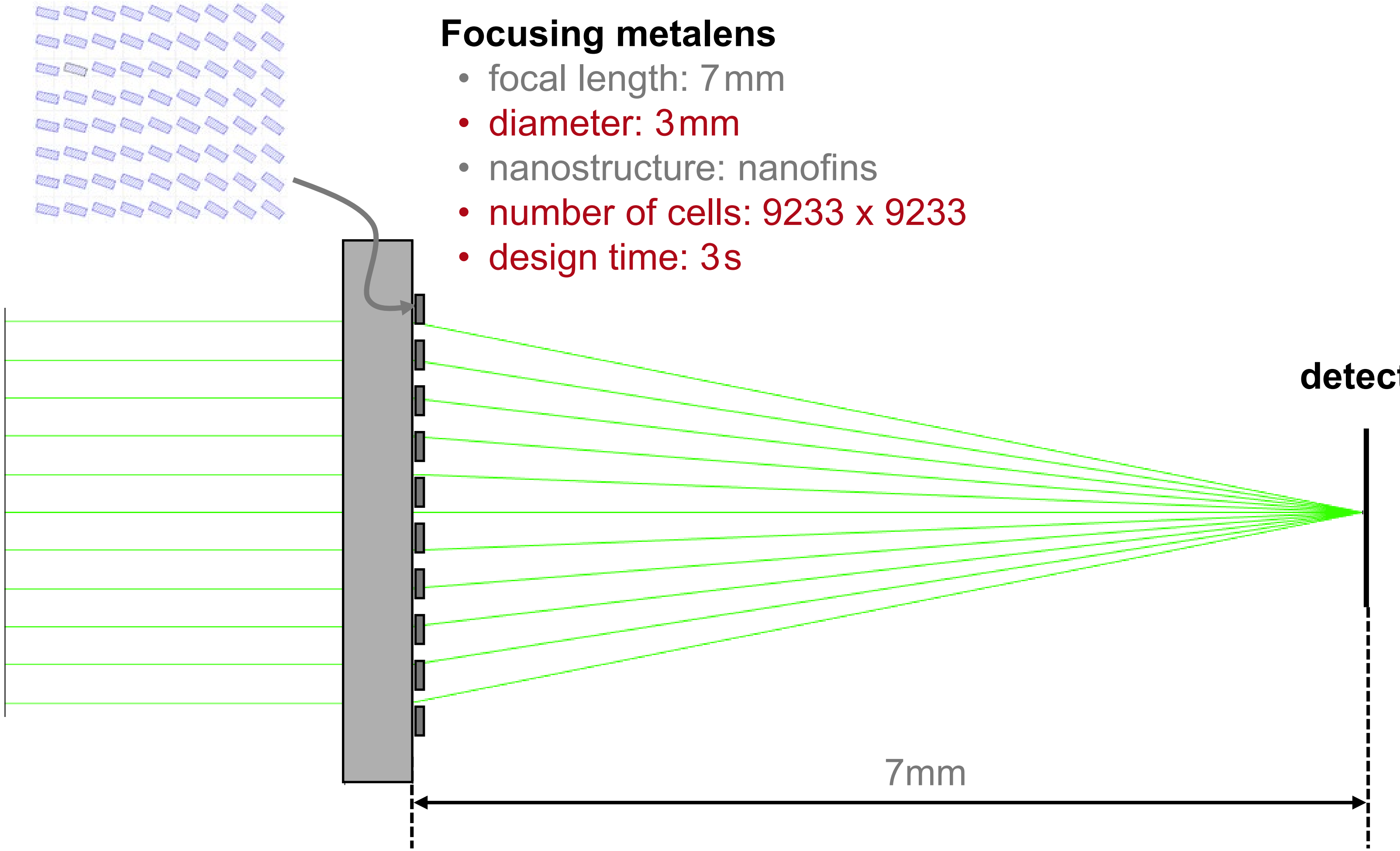

Magnitudes Behind Metalens

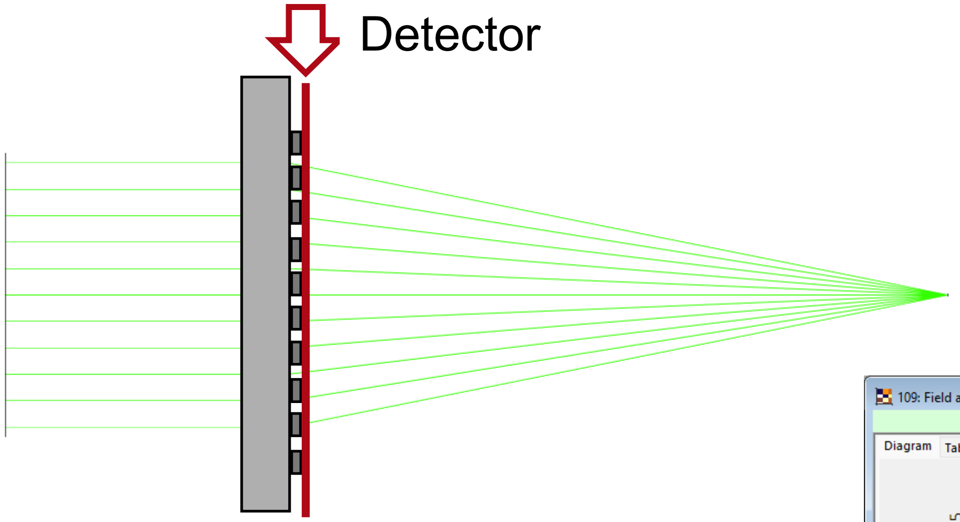

Right Circular Polarization

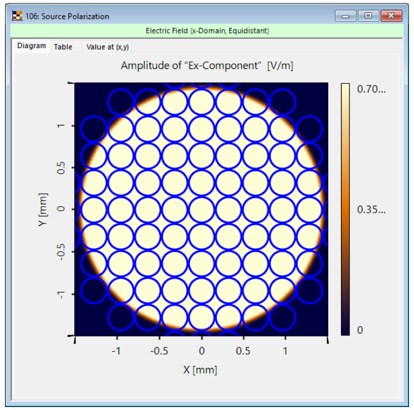

Magnitude $|E_x(\boldsymbol{\rho})|$

Magnitude $|E_y(\boldsymbol{\rho})|$

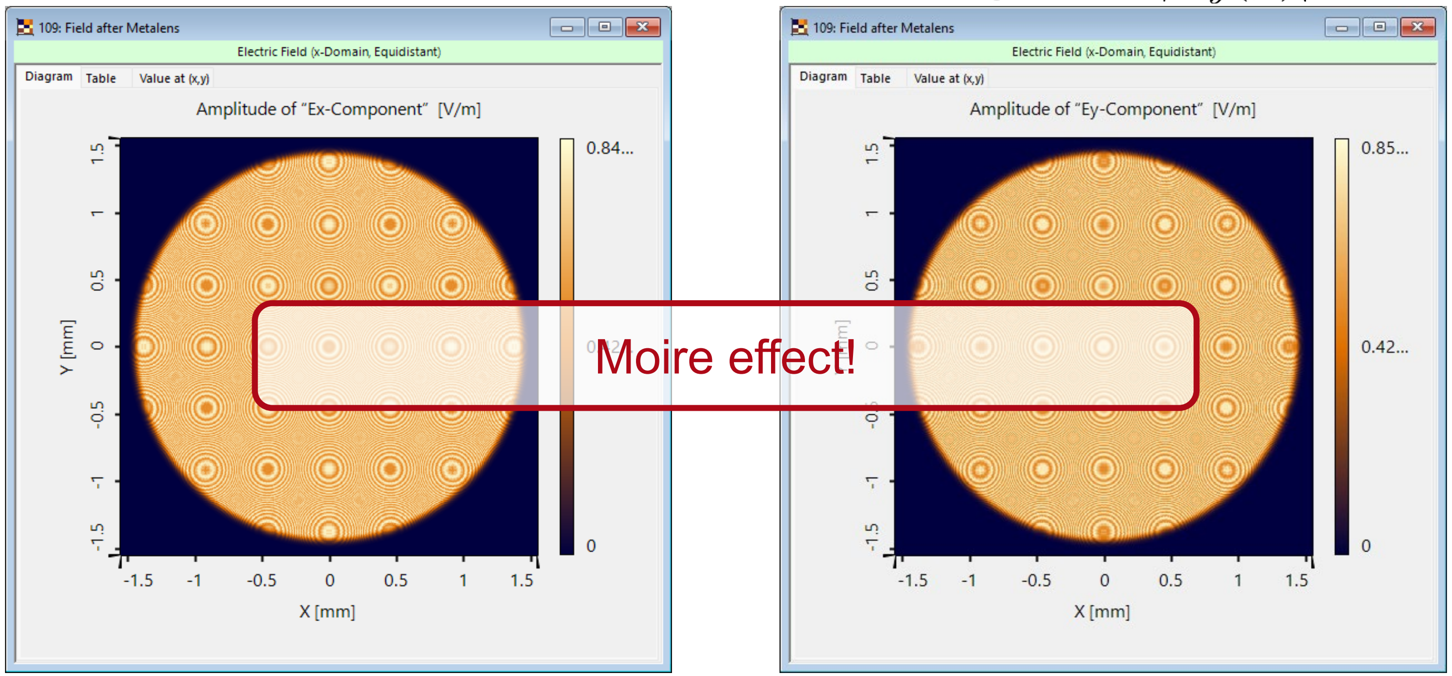

Magnitudes Behind Metalens

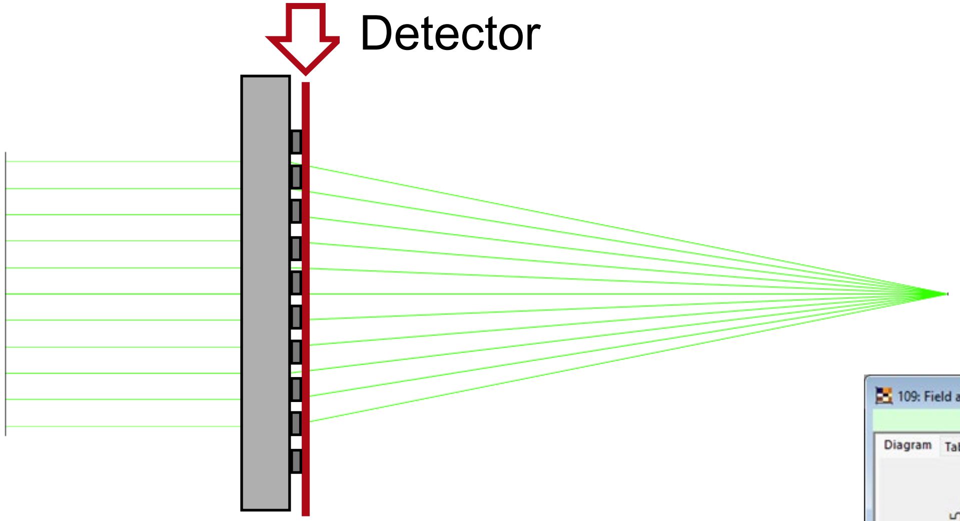

Right Circular Polarization

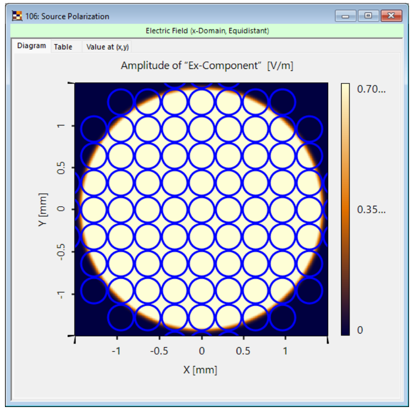

Magnitudes $|\{\mathbf{M}(p)\boldsymbol{U}^{\mathrm{in}}\}_x|$ and $|\{\mathbf{M}(p)\boldsymbol{U}^{\mathrm{in}}\}_y|$

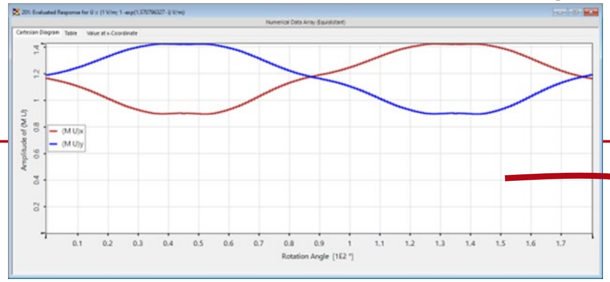

Magnitude $|E_x(\boldsymbol{\rho})|$

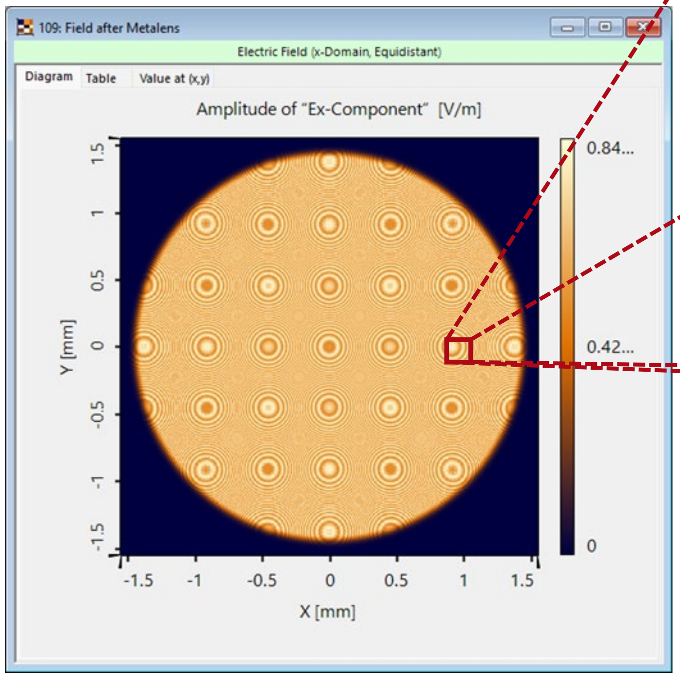

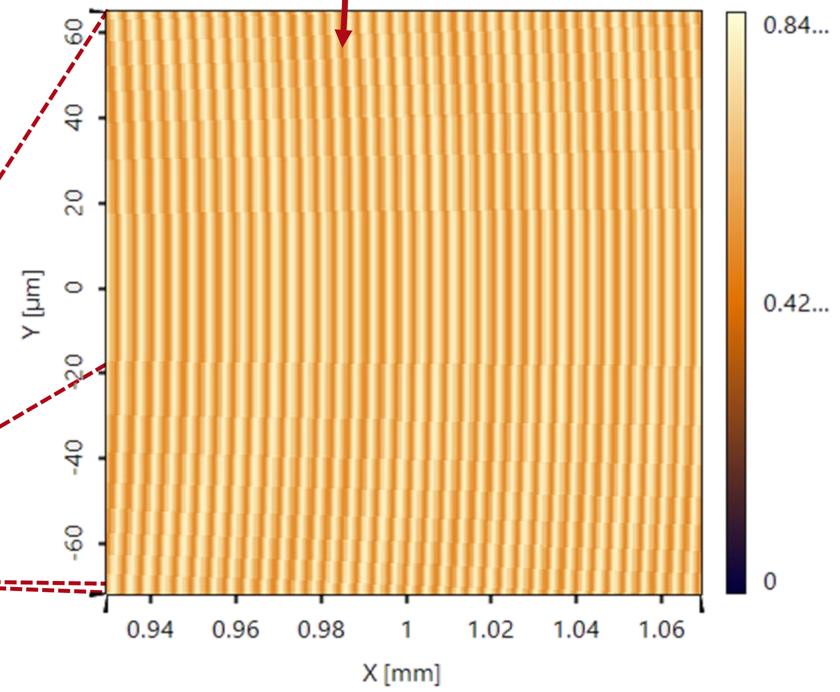

Efficiency (PCA)
~ 89.4 %

Magnitudes Obtained from Multiscale Simulation

Simulation time ~ 27s
(9233 x 9233 cells)

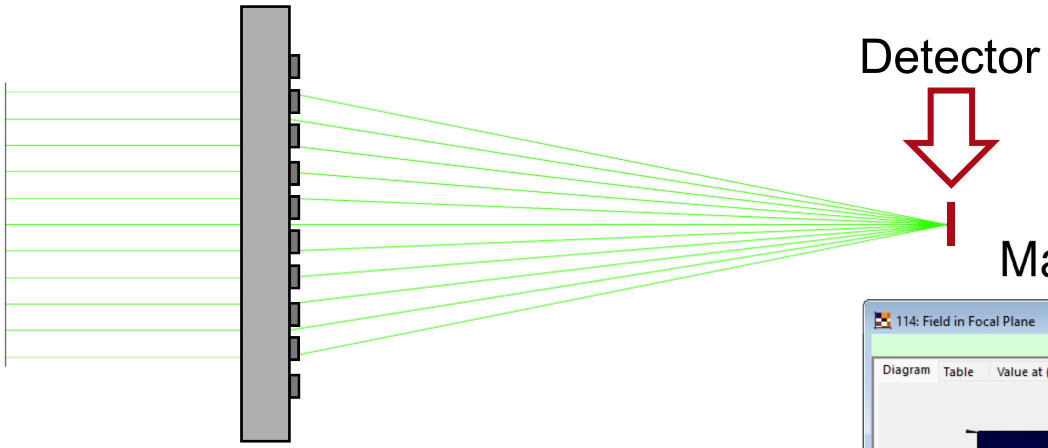

Magnitude $|E_x(\boldsymbol{\rho})|$

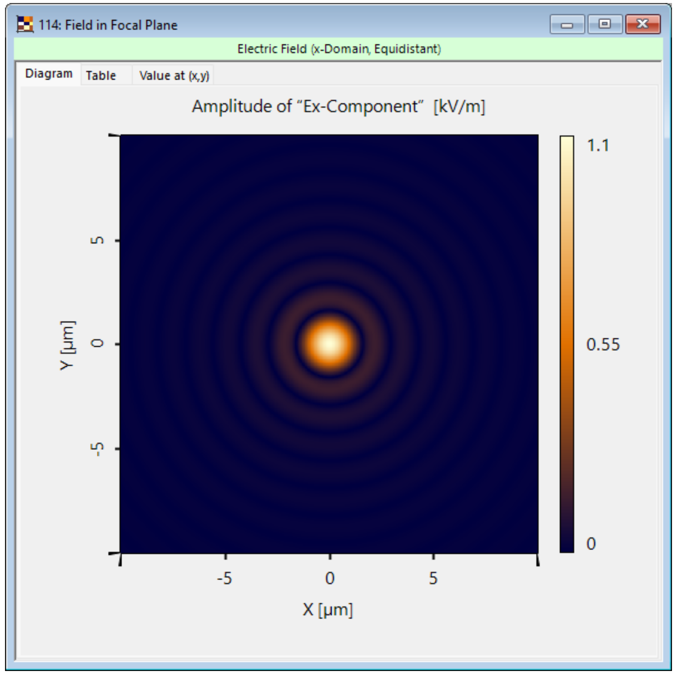

Magnitude $|E_y(\boldsymbol{\rho})|$

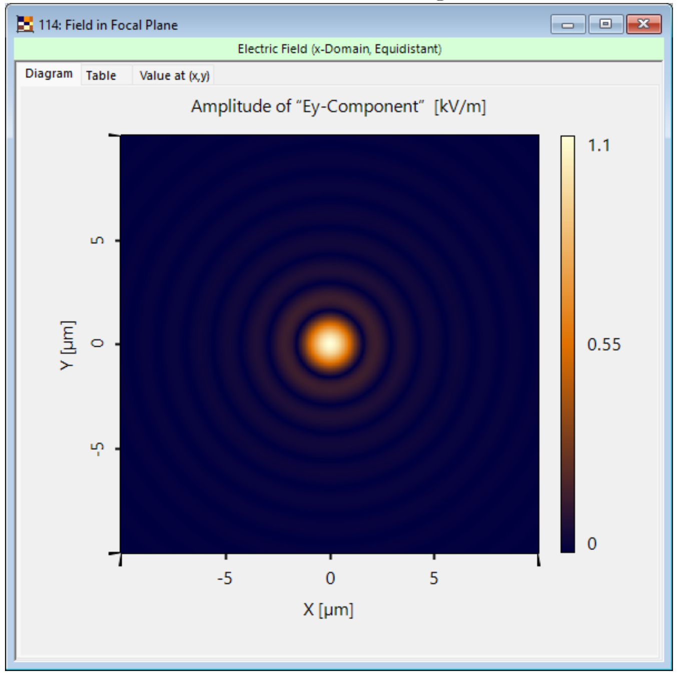

Right Circular Polarization

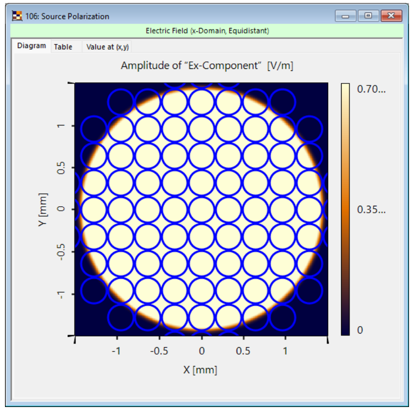

Irradiance of Focal Point Obtained from Multiscale Simulation

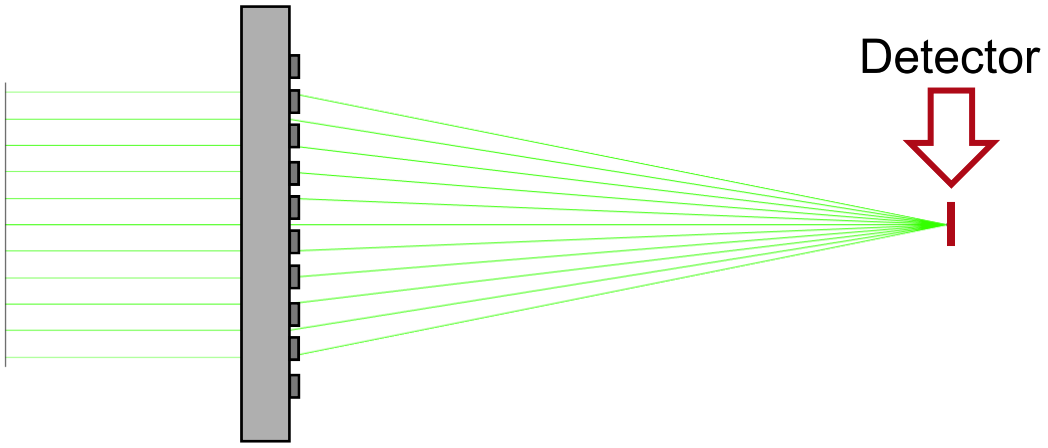

Right Circular Polarization

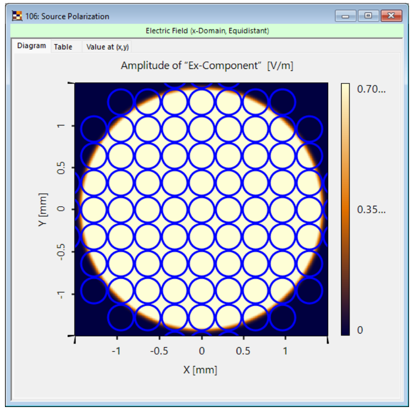

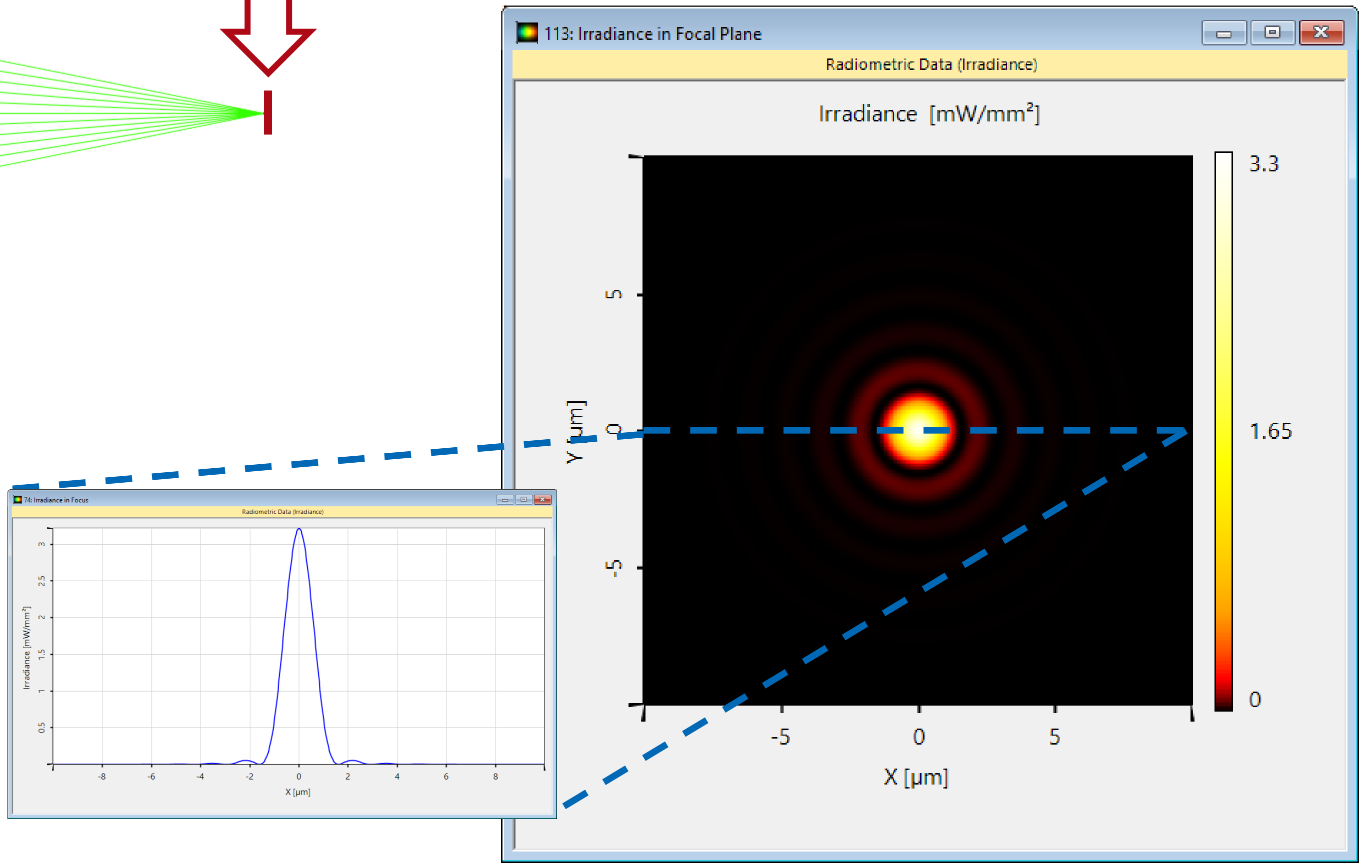

Irradiance

Rays Derived from Multiscale Simulation

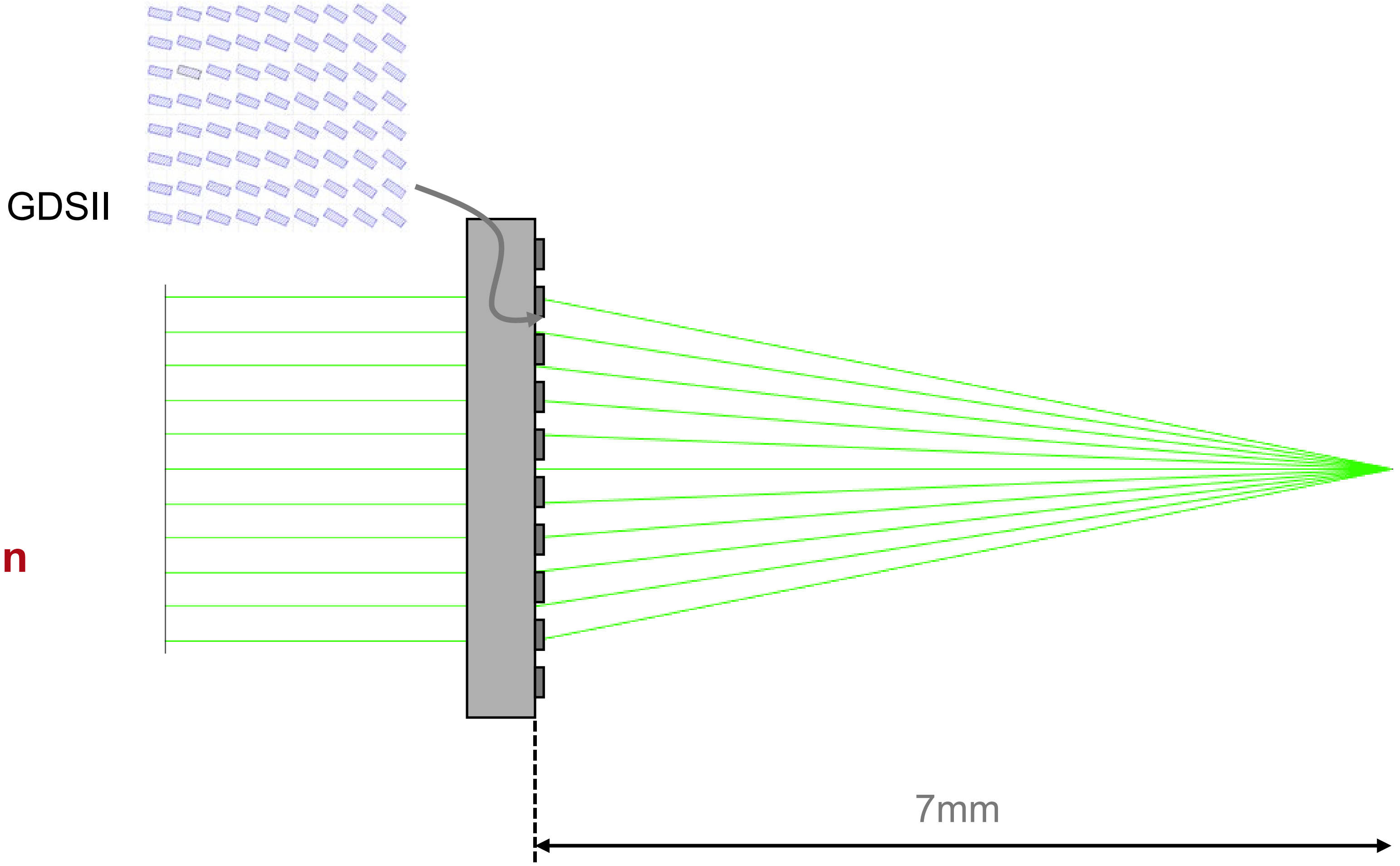

Right Circular Polarization

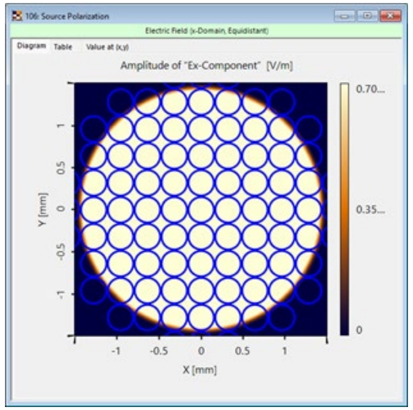

Rays Derived from Multiscale Simulation

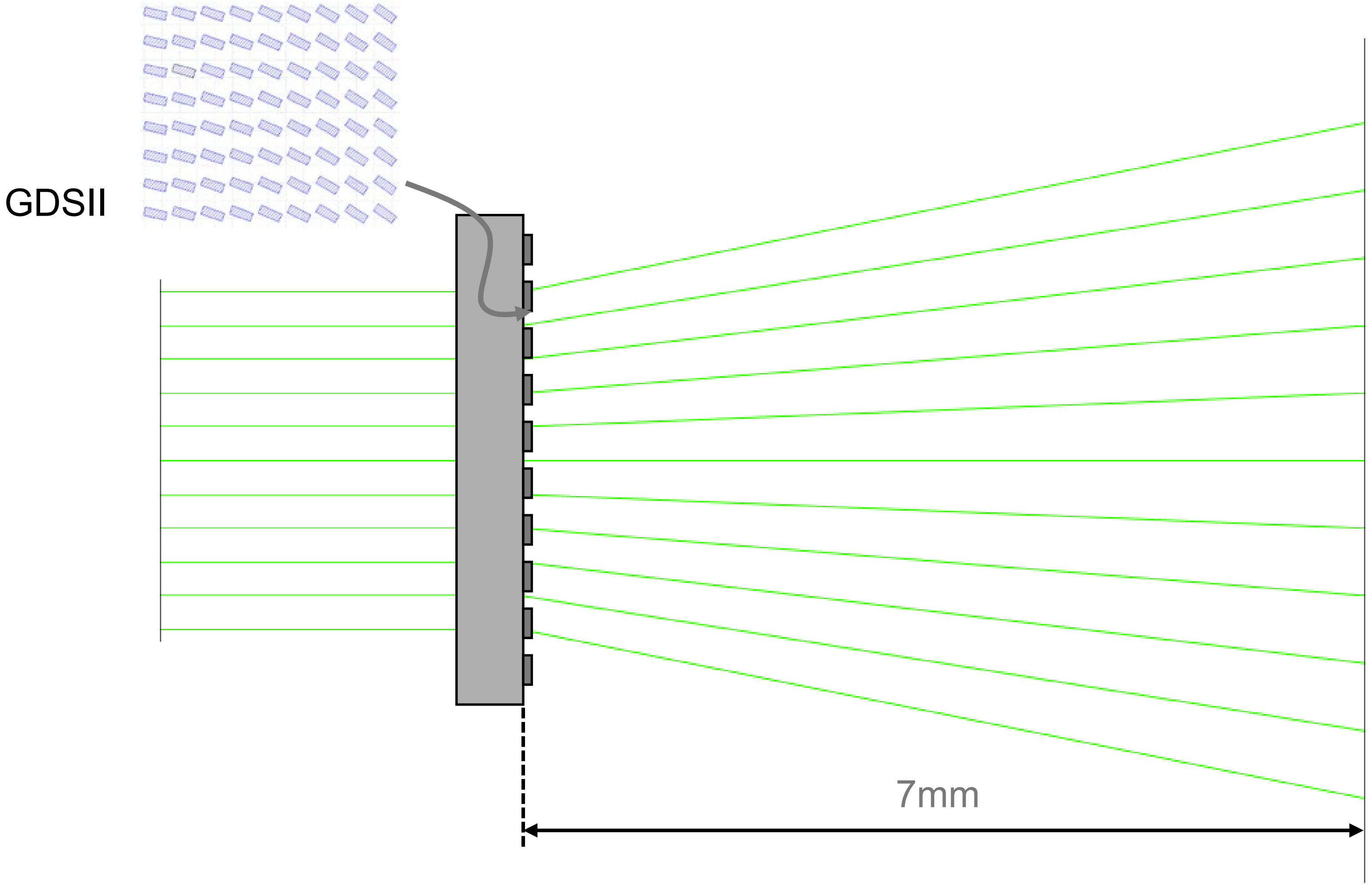

Left Circular Polarization

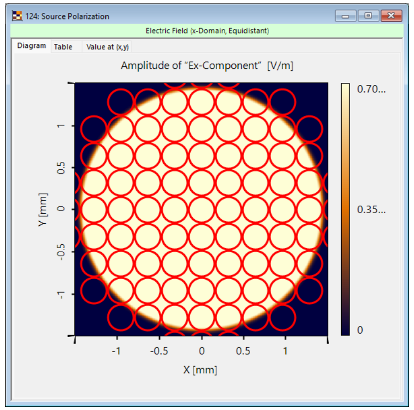

Irradiance Obtained from Multiscale Simulation

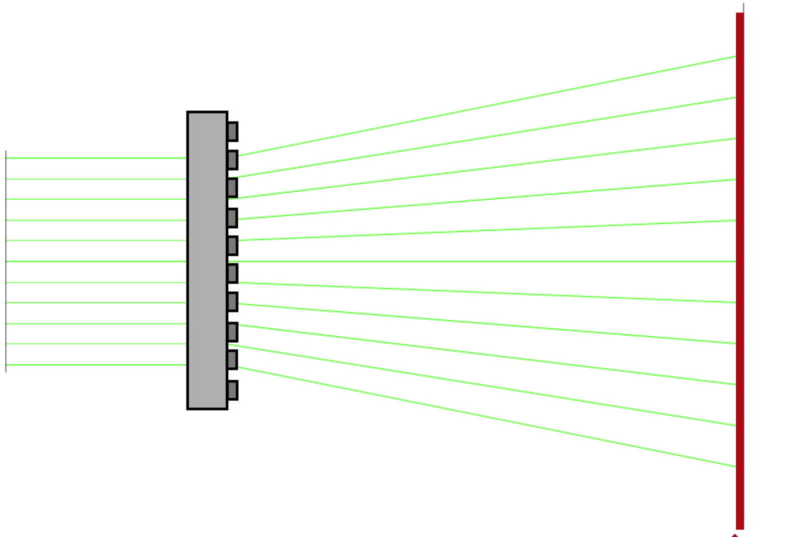

Detector

Left Circular Polarization

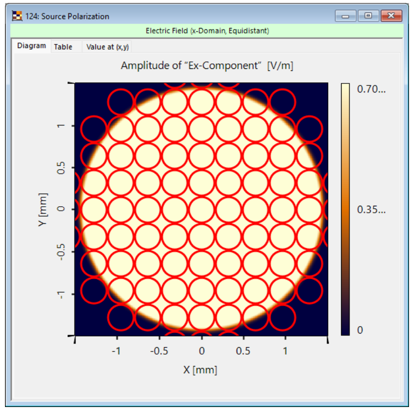

Irradiance $E_\mathrm{e}(\boldsymbol{\rho})$

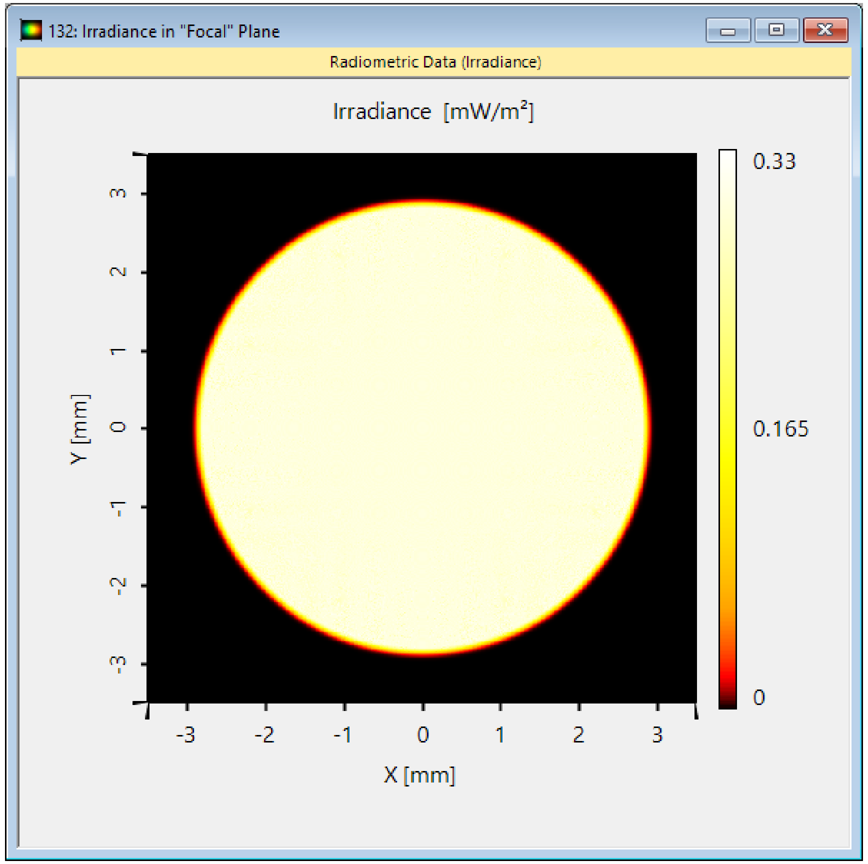

Beam Expander with Aspherical Lens

Rays derived from multiscale simulation

Collimation lens
- diameter: 4.8 mm
- first surface: planar
- second surface: aspherical

Spherical lens
- diameter: 1.5 mm
- focal length: -2.5 mm

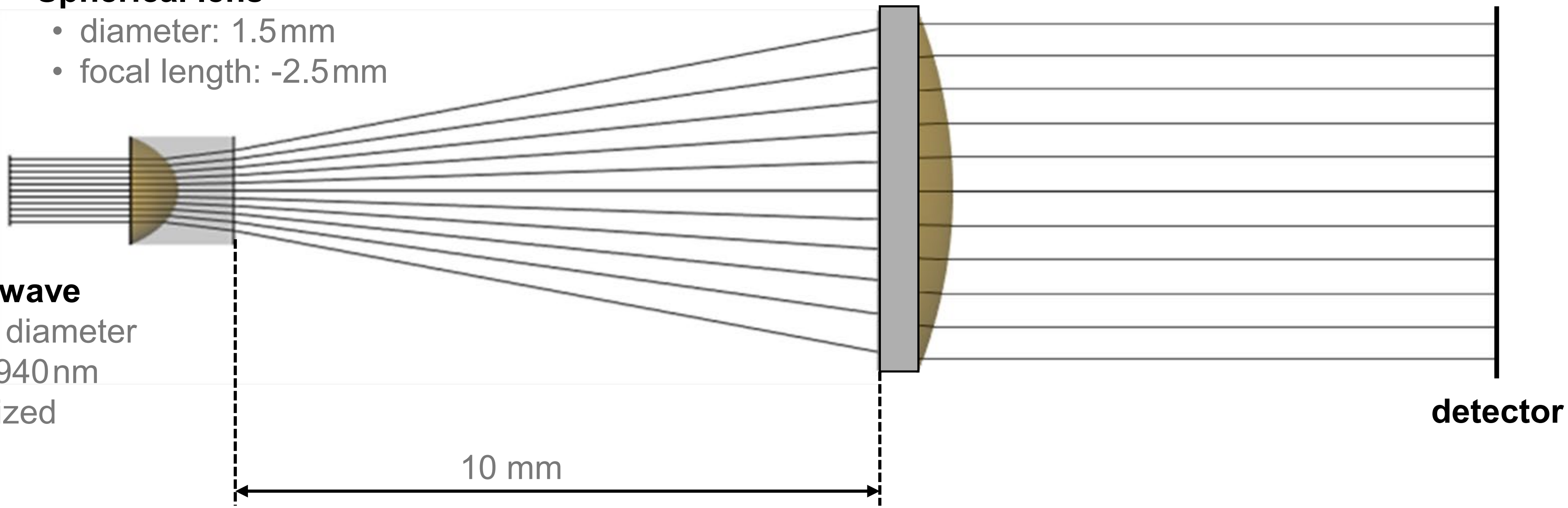

Plane incident wave
- 1 mm x 1 mm diameter
- wavelength: 940 nm
- linearly polarized

Beam Expander with Pillar-Type Metalens

Rays derived from multiscale simulation

GDSII

Collimation metalens
- diameter: 4.8 mm
- nanostructure: pillars
- number of cells: 12001 x 12001
- design time: 7 s

Spherical lens
- diameter: 1.5 mm
- focal length: -2.5 mm

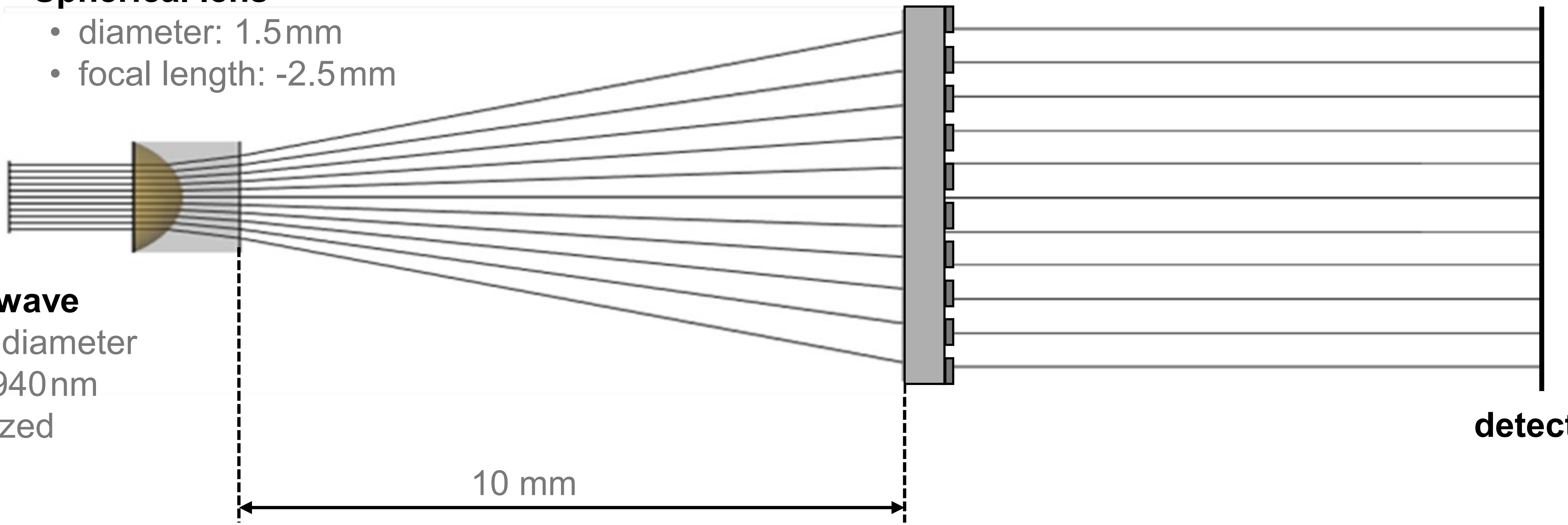

Plane incident wave
- 1 mm x 1 mm diameter
- wavelength: 940 nm
- linearly polarized

Irradiance Obtained from Multiscale Simulation

Efficiency (PCA) ~ 91.2%

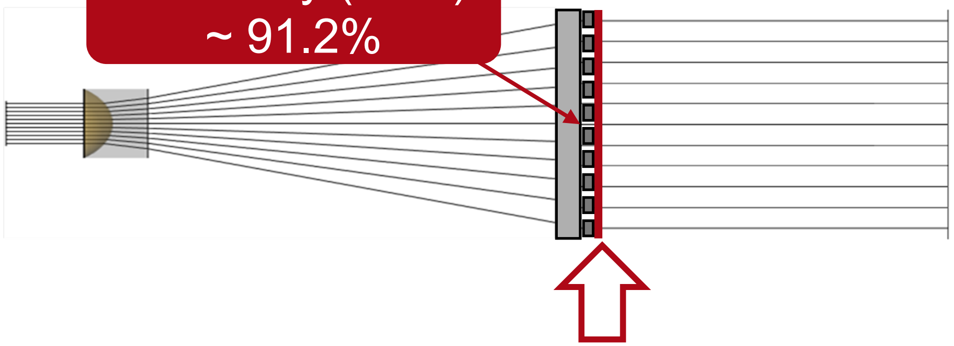

Detector

Simulation time ~ 51s (12001 x 12001cells)

Irradiance $E_{\mathrm{e}}(\boldsymbol{\rho})$

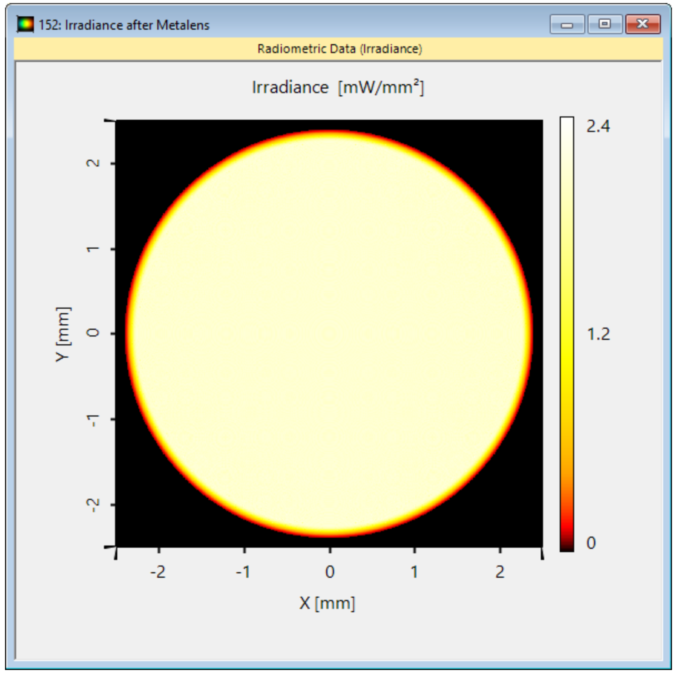

0° Linear Polarization

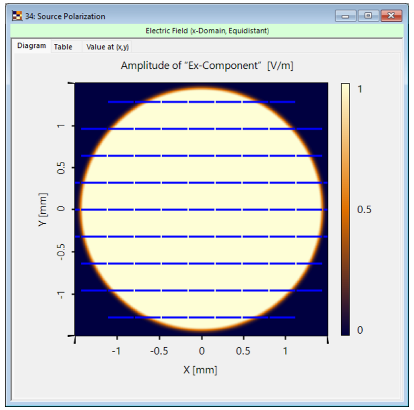

Vectorial PSF Obtained from Multiscale Simulation

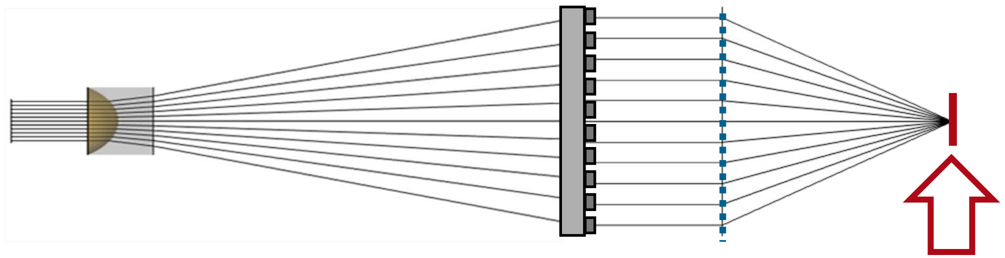

Simulation time ~ 57s
(12001 x 12001cells)

0° Linear Polarization

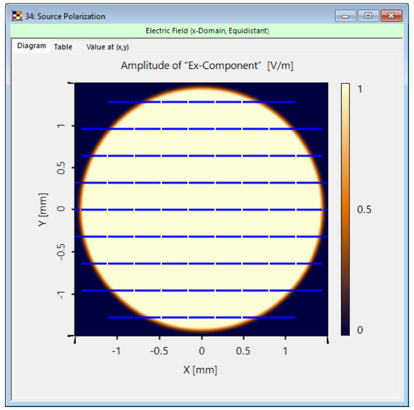

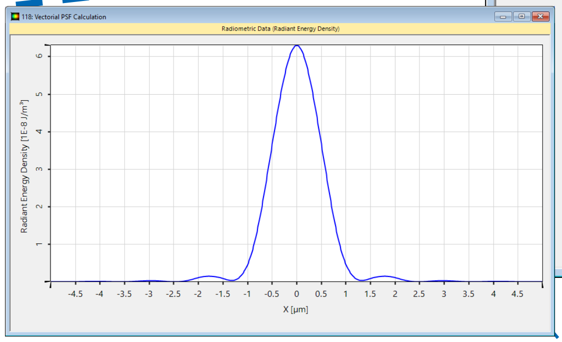

Energy Density $w_{\mathrm{e}}(\boldsymbol{\rho})$

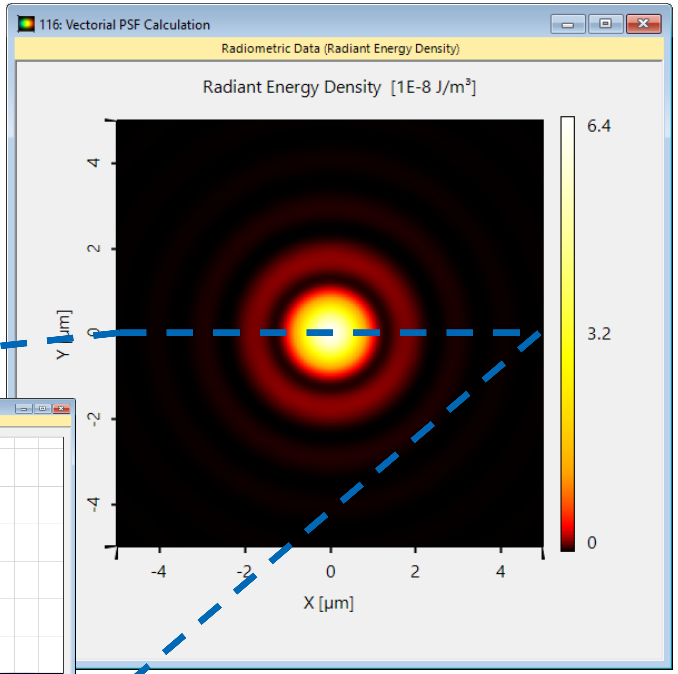

Polarization-Controlled Bifocal System

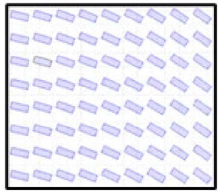

Focusing metalens
- focal length: 60 mm
- diameter: 2 mm
- number of cells: 6153 x 6153
- design time: 2 s

Focusing lens
- focal length: 2 mm

Plane incident wave
- 2 mm x 2 mm diameter
- wavelength: 532 nm

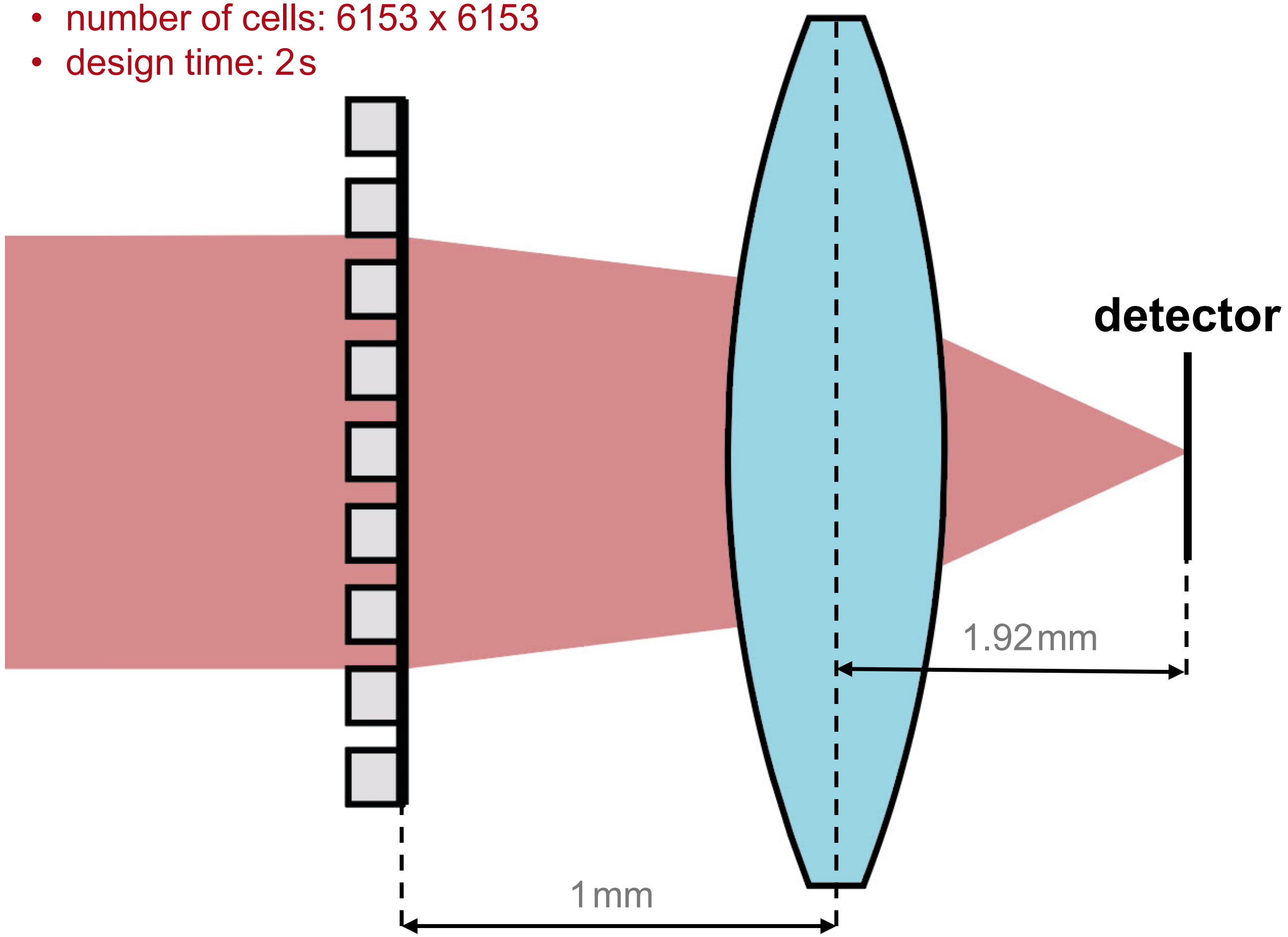

Rays for Spherical Lens

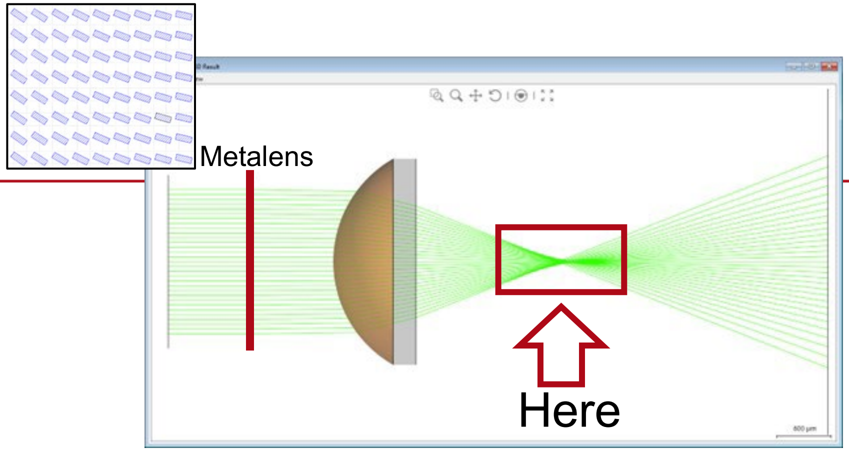

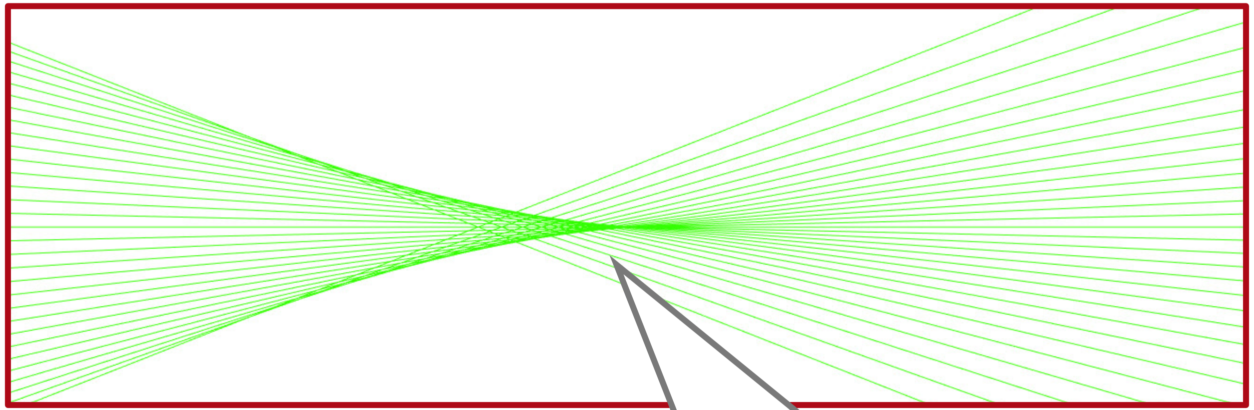

Spherical aberrations

Right Circular Polarization

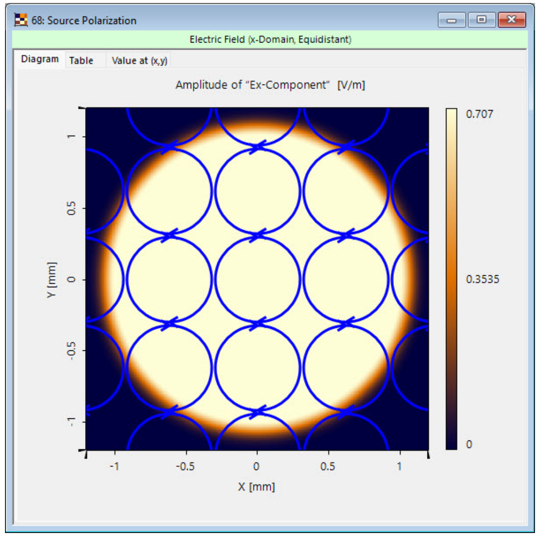

Rays for Spherical Lens

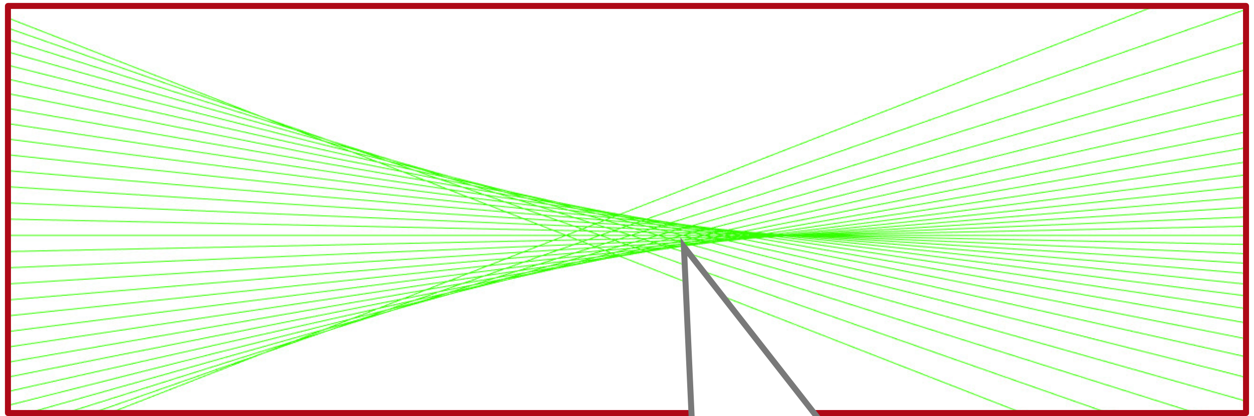

Spherical aberrations

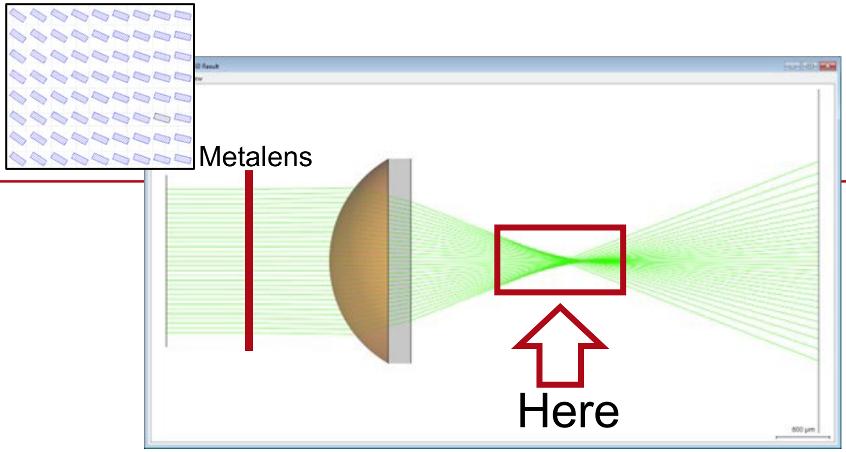

Left Circular Polarization

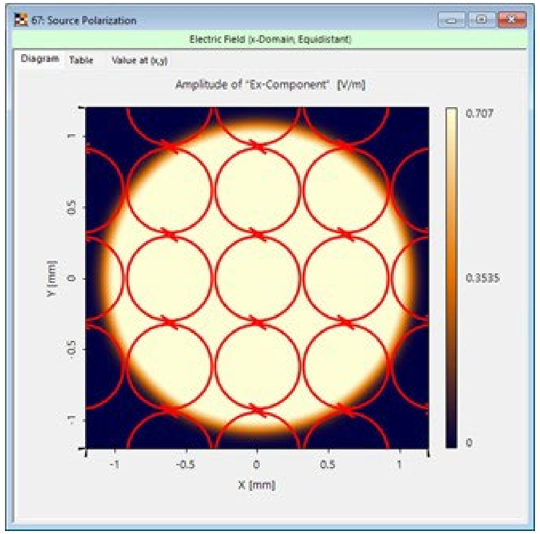

Irradiances for Aspherical Lens

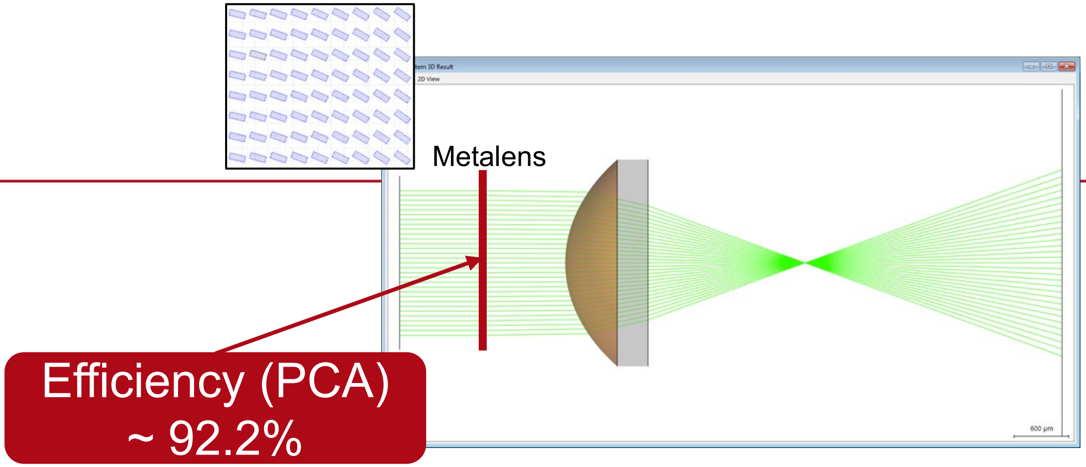

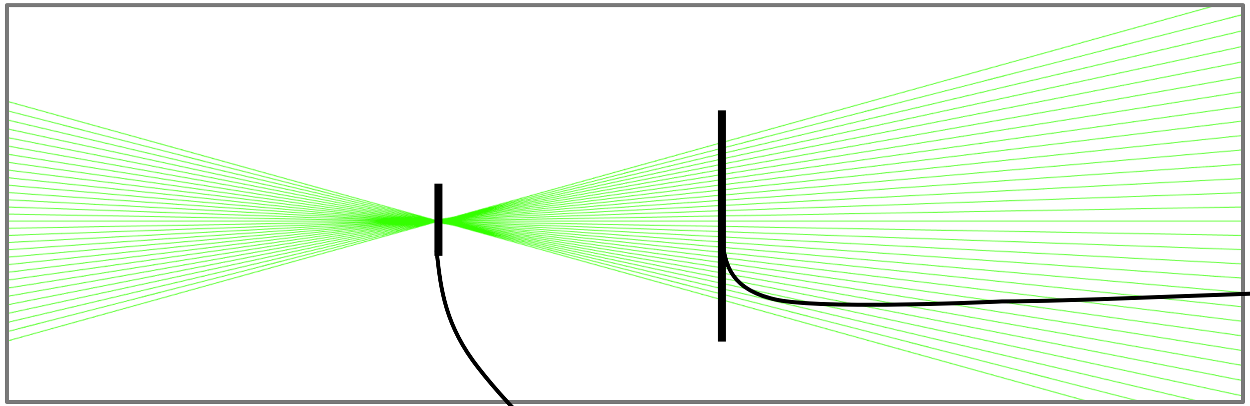

Right Circular Polarization

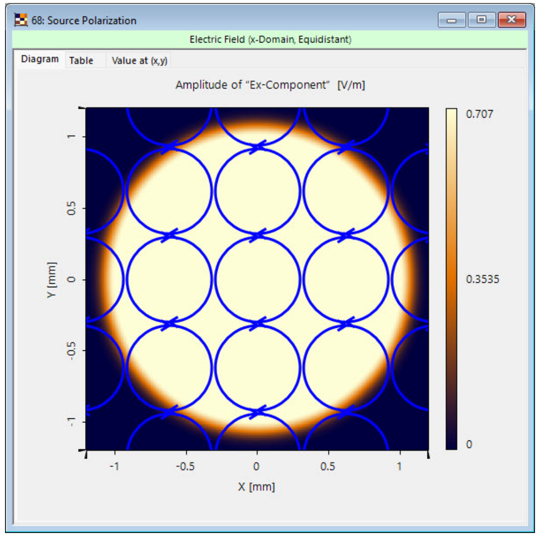

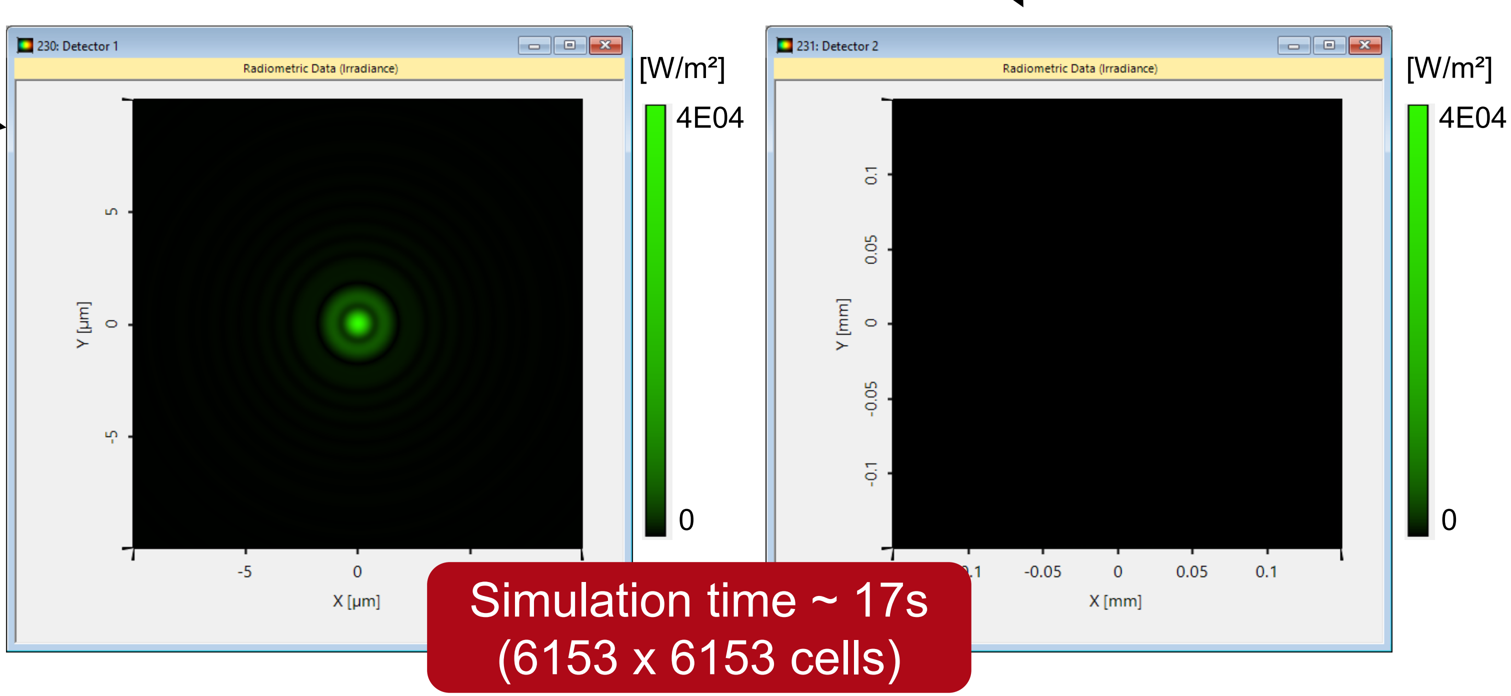

Irradiances for Aspherical Lens

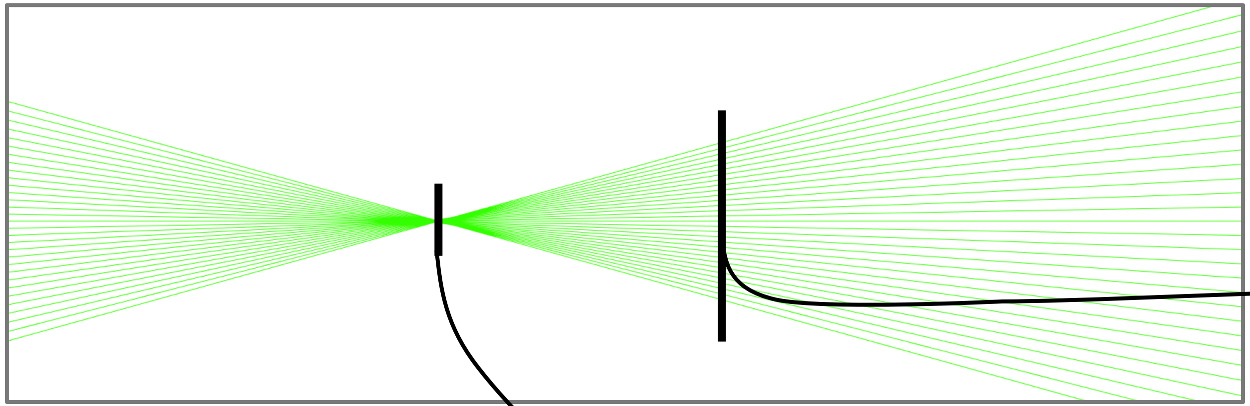

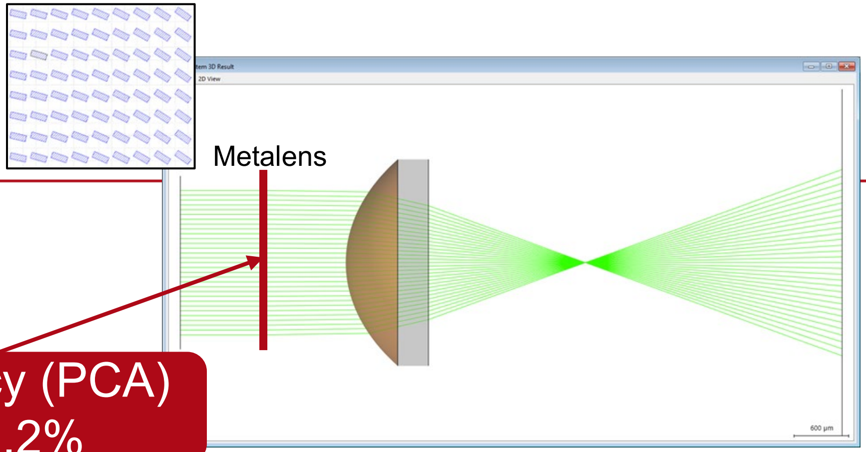

Efficiency (PCA)
~ 92.2%

Right Circular Polarization

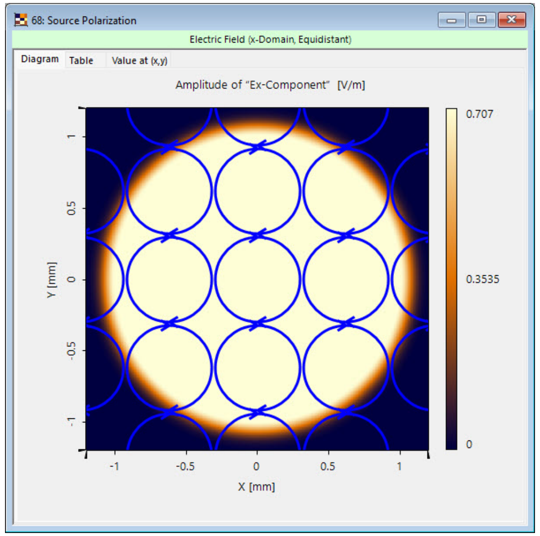

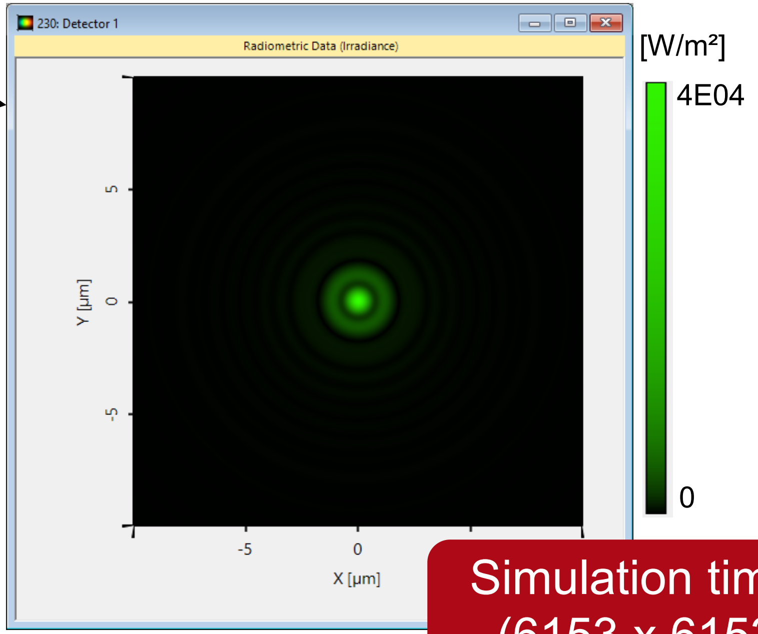

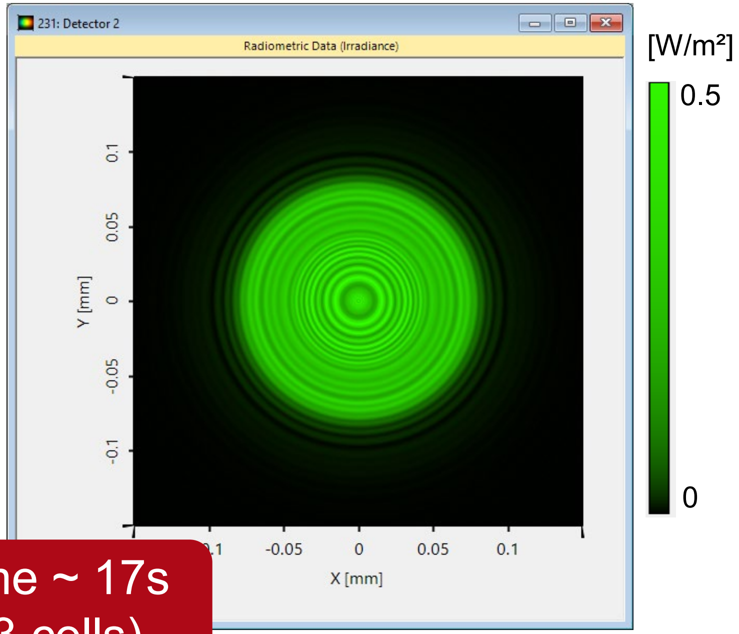

Simulation time ~ 17s
(6153 x 6153 cells)

Irradiances for Aspherical Lens

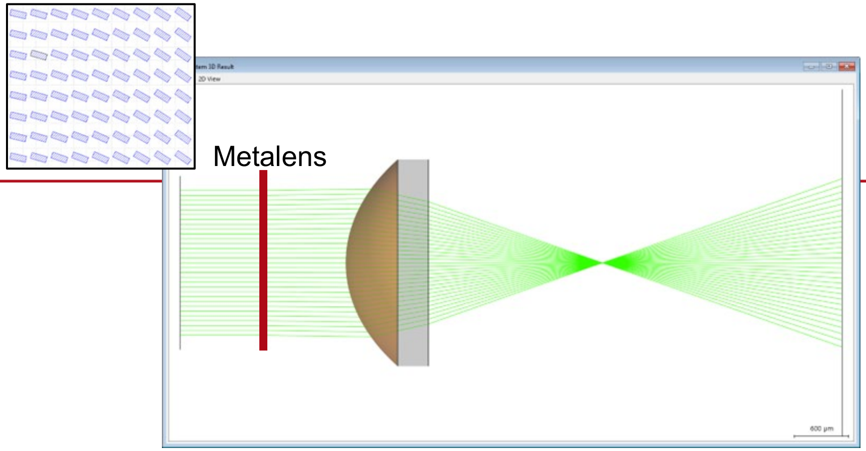

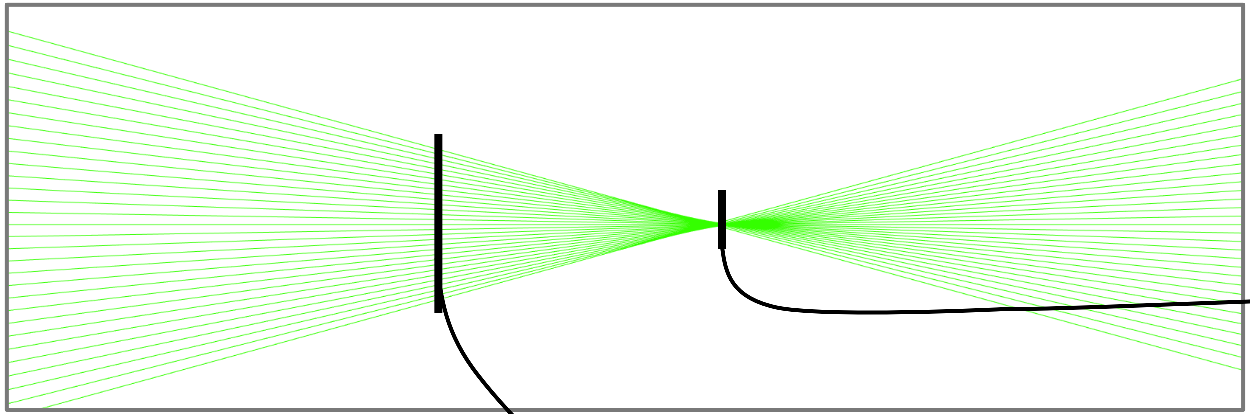

Left Circular Polarization

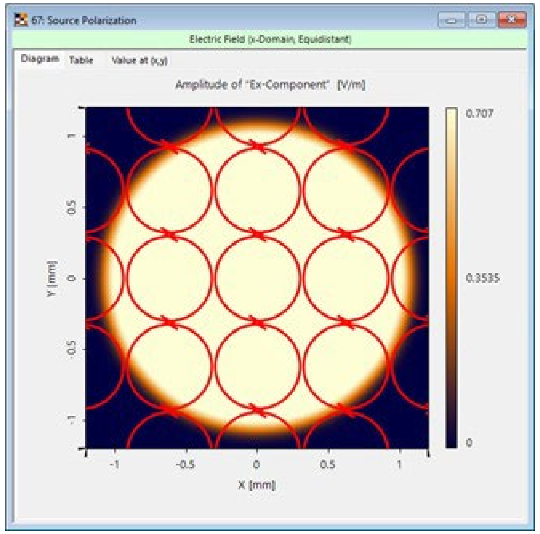

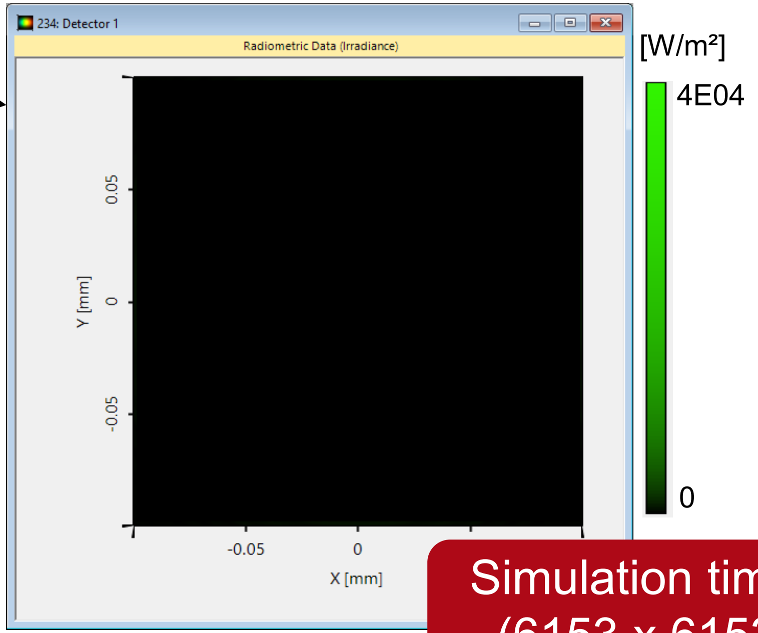

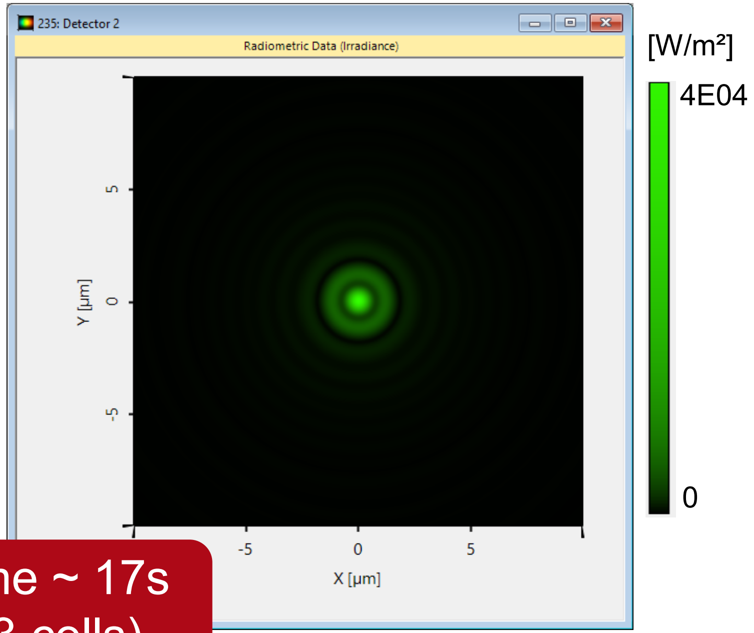

Simulation time ~ 17s
(6153 x 6153 cells)

Irradiances for Aspherical Lens

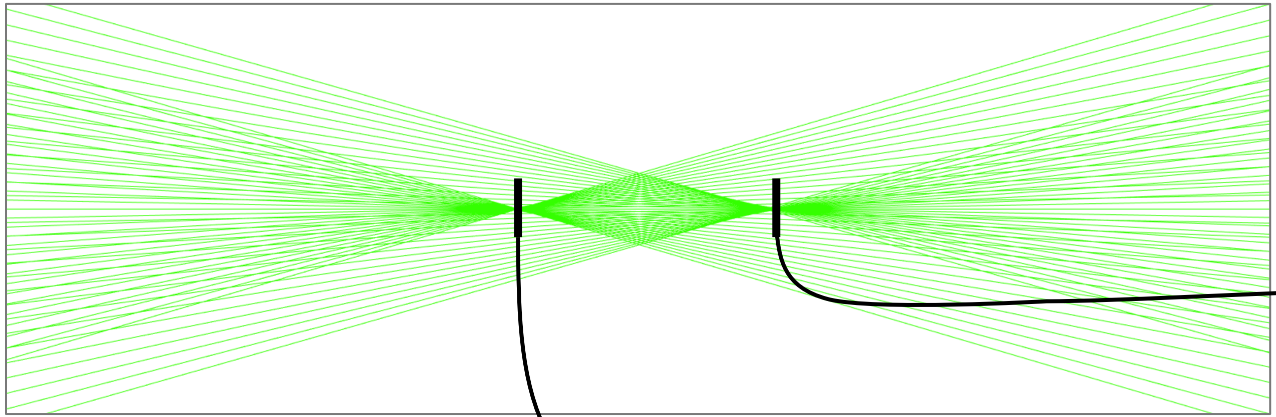

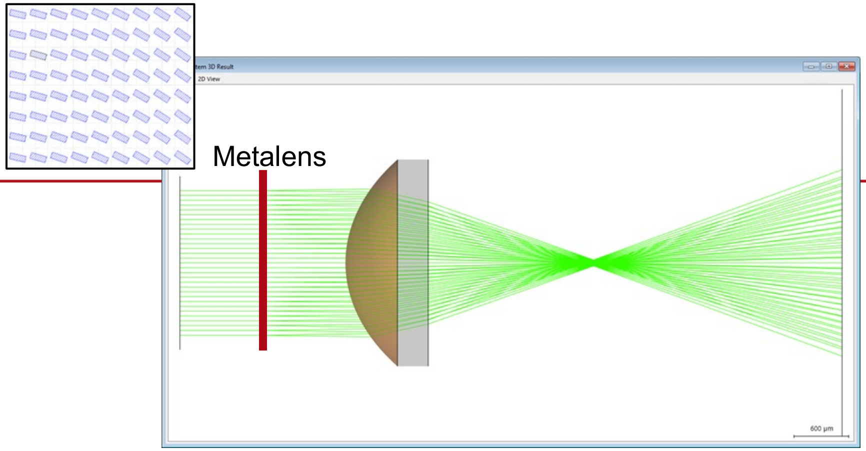

45° Linear Polarization

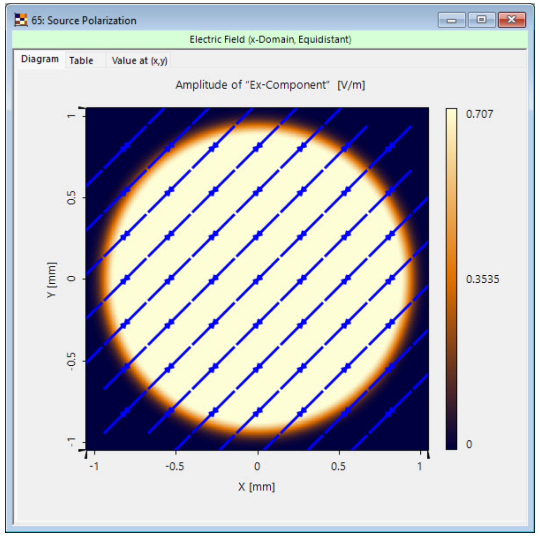

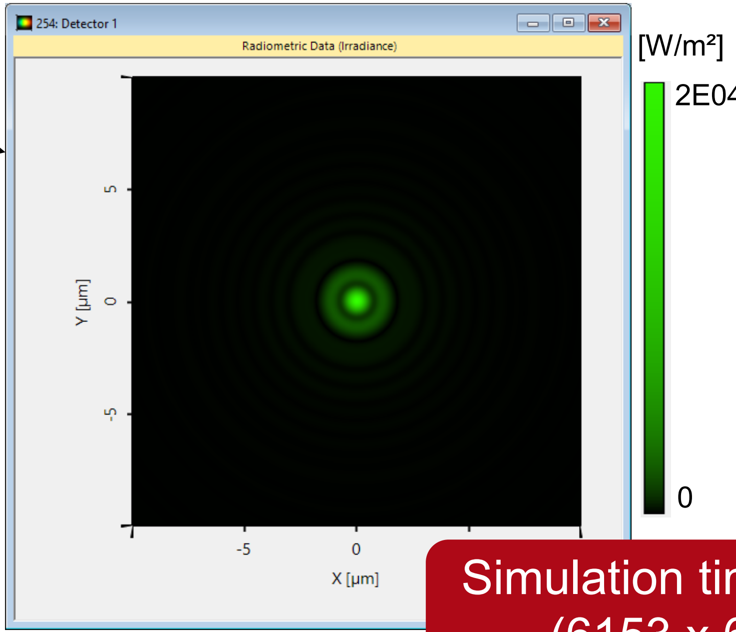

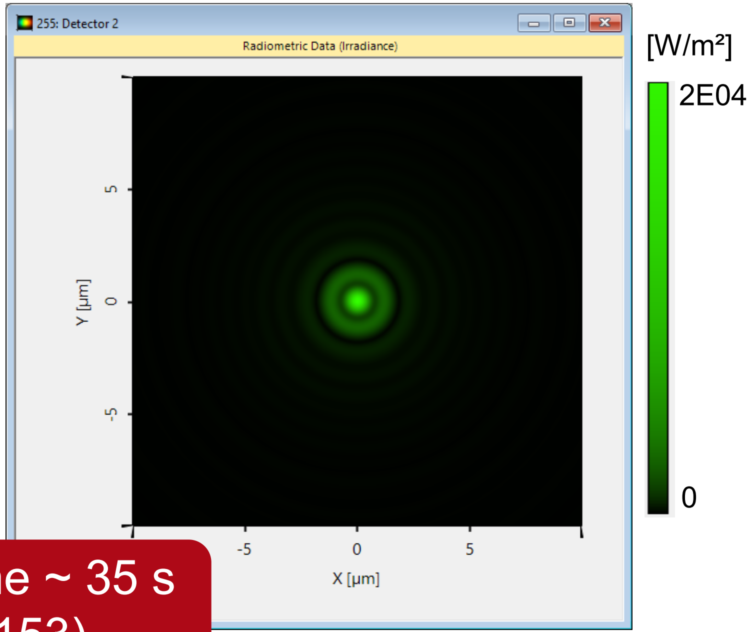

Simulation time ~ 35 s
(6153 x 6153)

Metalens with Encoded Phase Dislocation

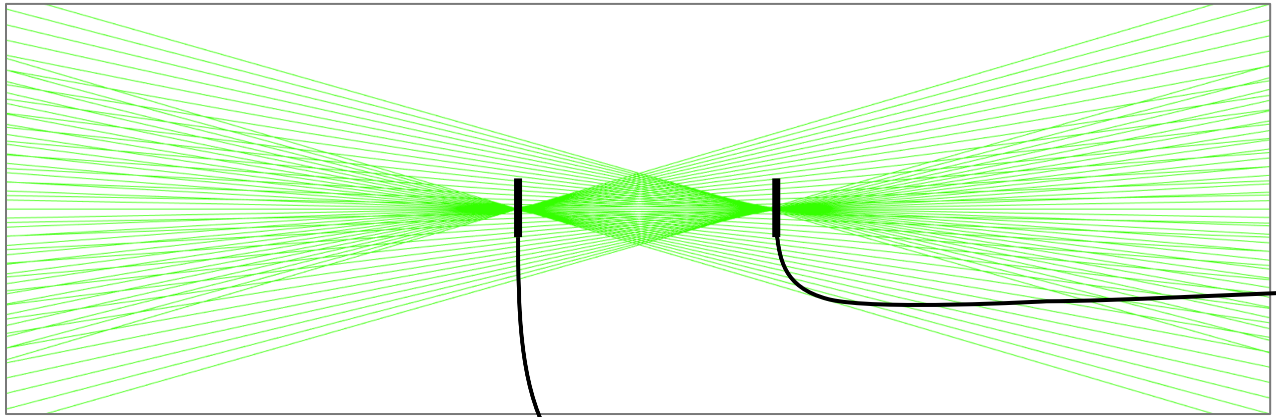

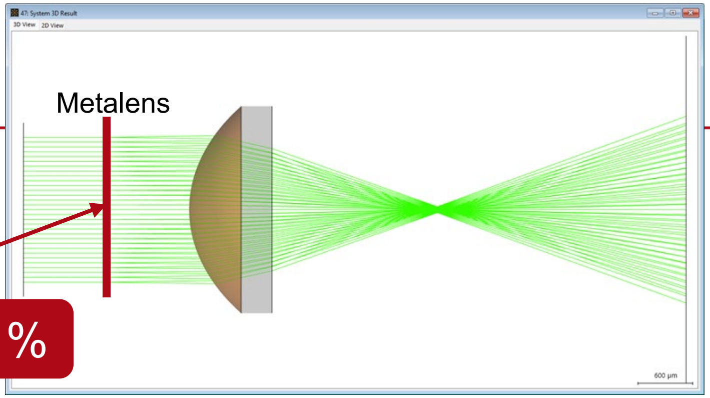

Efficiency ~ 92.1%

45° Linear Polarization

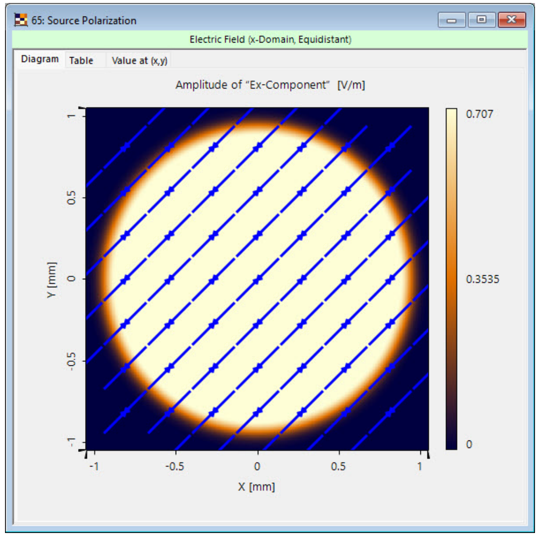

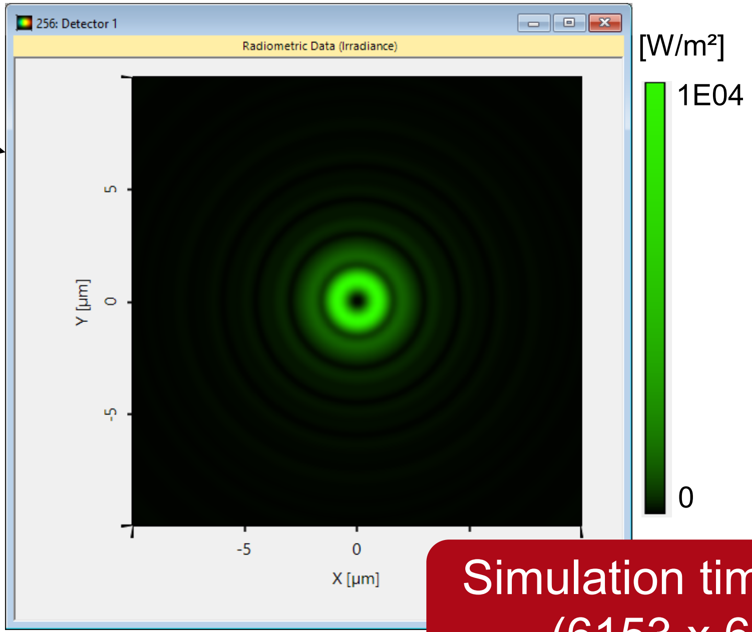

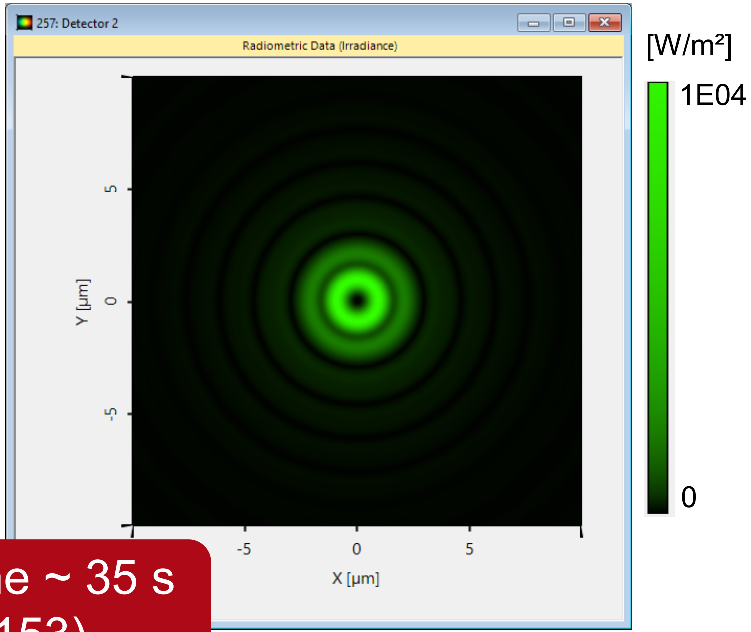

Simulation time ~ 35 s
(6153 x 6153)

Limitations of the PCA Simulation Model and its Further Developments

Constraints of the PCA Simulation Model

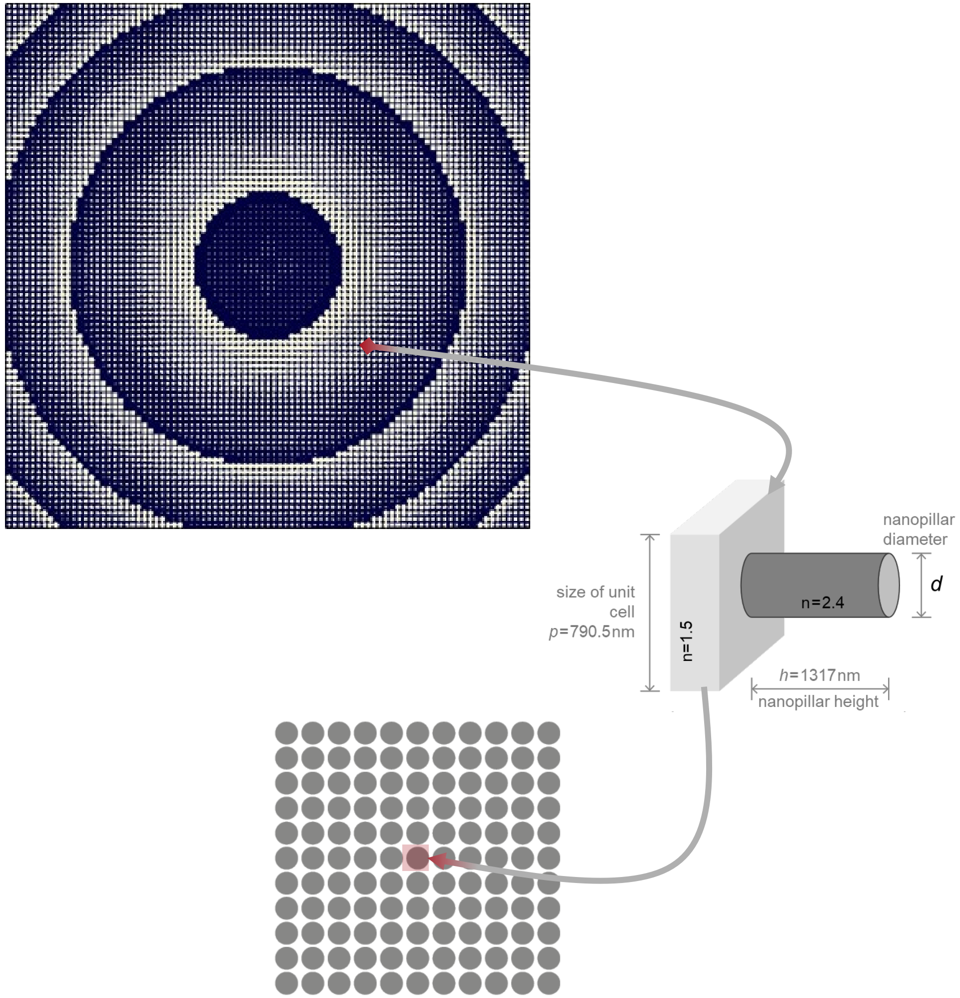

Metacell grating

- In the Periodic Cell Approximation (PCA), it is assumed that neighboring metacells are identical.
- Practically, each metacell is encircled by additional metacells, which differ in structural parameters to varying degrees, thus interrupting the periodic condition to some extent.
- This situation particularly arises when a cycle of the lens zones is completed, causing the structural parameters to revert to their initial values.
- This results in discontinuities in the structure, leading to the production of additional stray light, a phenomenon also well-recognized in diffractive lenses.

Constraints of the PCA Simulation Model

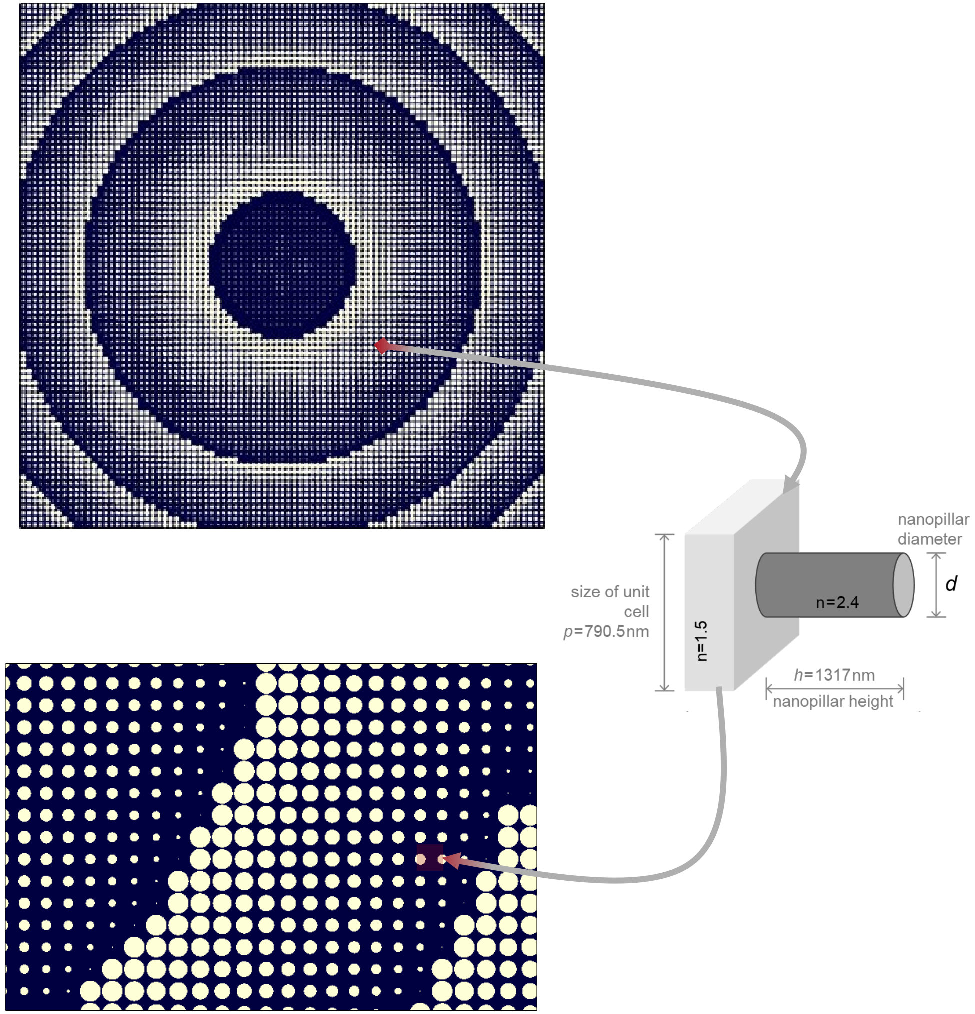

- In the Periodic Cell Approximation (PCA), it is assumed that neighboring metacells are identical.
- Practically, each metacell is encircled by additional metacells, which differ in structural parameters to varying degrees, thus interrupting the periodic condition to some extent.
- This situation particularly arises when a cycle of the lens zones is completed, causing the structural parameters to revert to their initial values.
- This results in discontinuities in the structure, leading to the production of additional stray light, a phenomenon also well-recognized in diffractive lenses.

Local Metagrating Approximation (LMGA)

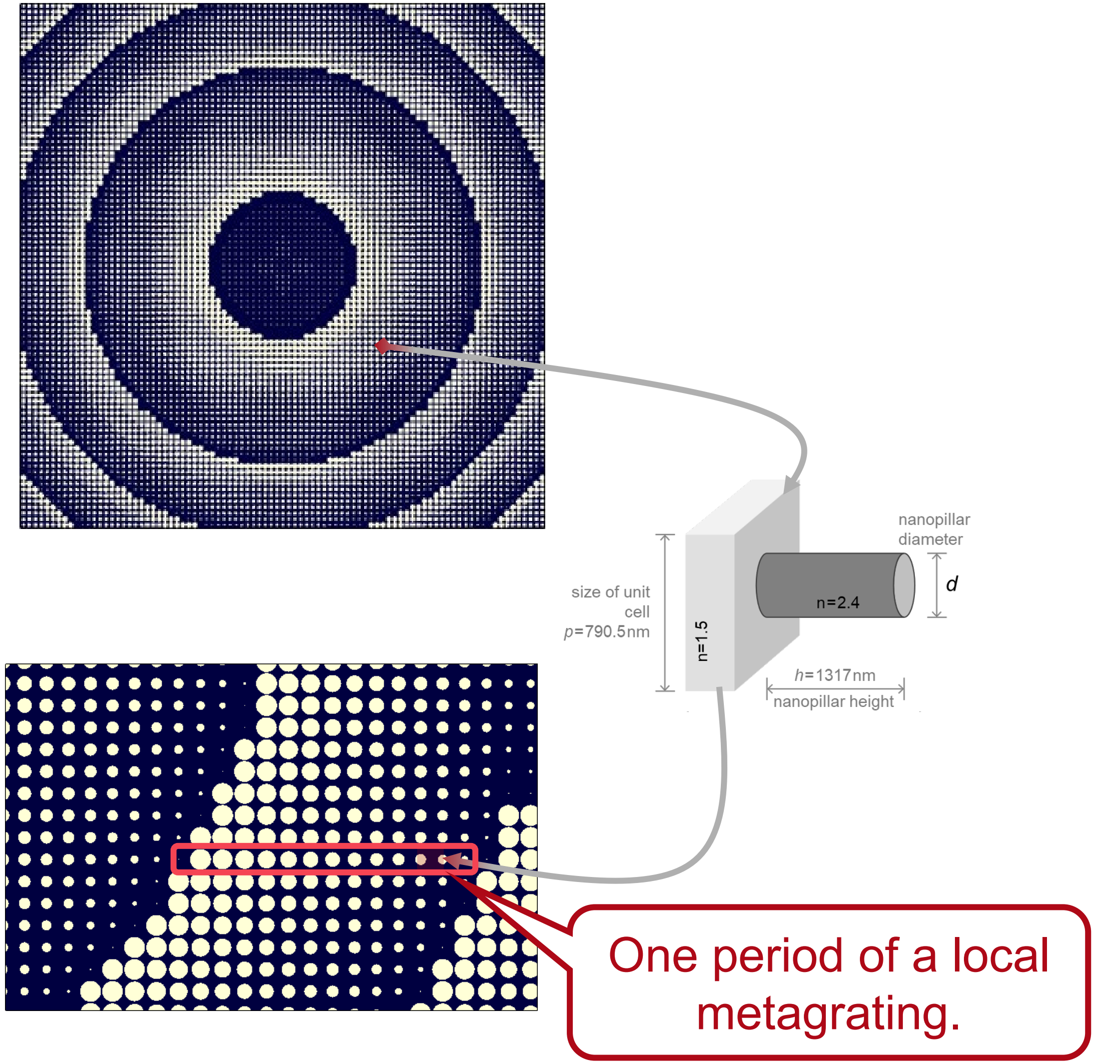

- Thus, the challenge lies in effectively integrating the neighboring metacell in a simulation model to more precisely represent the structural discontinuities.
- We propose using a local metagrating approximation, akin to the modeling of diffractive lenses.
- This method not only provides high computational efficiency but also distinguishes the stray light from the desired light in additional orders.
- These extra orders have clearly defined wavefront phases, allowing them to propagate through the lens system together with the intended light.

Local Metagrating Approximation (LMGA)

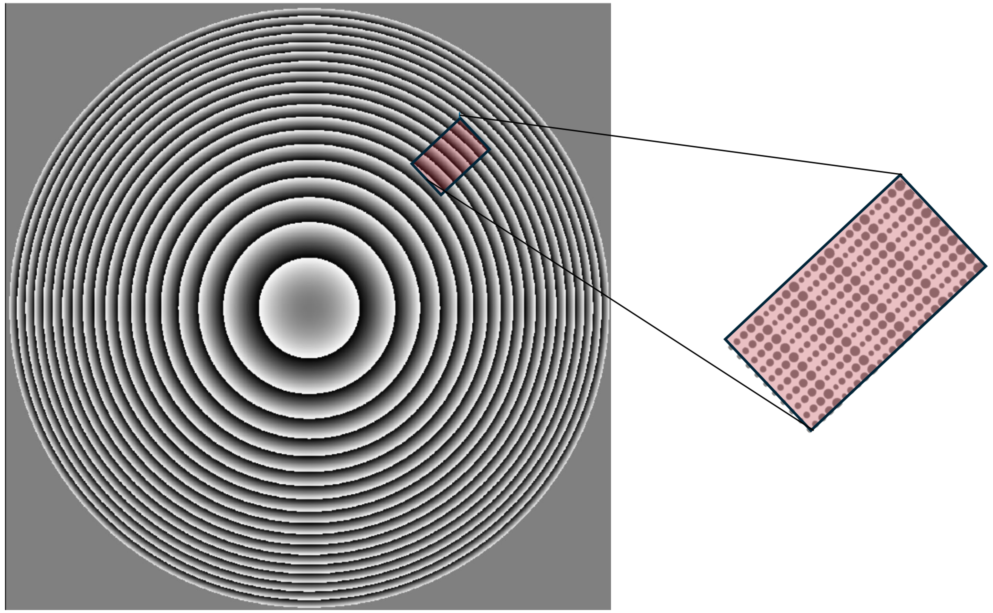

- Thus, the challenge lies in effectively integrating the neighboring metacell in a simulation model to more precisely represent the structural discontinuities.
- We propose using a local metagrating approximation, akin to the modeling of diffractive lenses.
- This method not only provides high computational efficiency but also distinguishes the stray light from the desired light in additional orders.
- These extra orders have clearly defined wavefront phases, allowing them to propagate through the lens system together with the intended light.

Local Metagrating Approximation (LMGA)

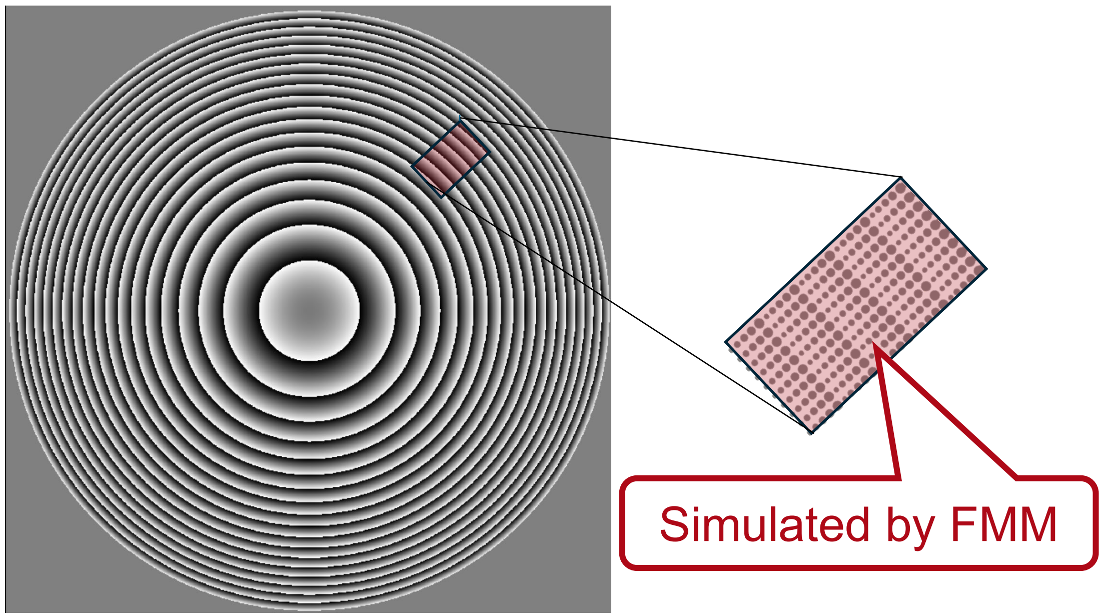

- The rigorous Fourier Modal Method (FMM), also known as RCWA, is employed for analyzing the local gratings.
- The differences in results between PCA and LMGA can be systematically analyzed by generating metagratings with PCA and subsequently simulating them using both FMM and PCA for comparison.

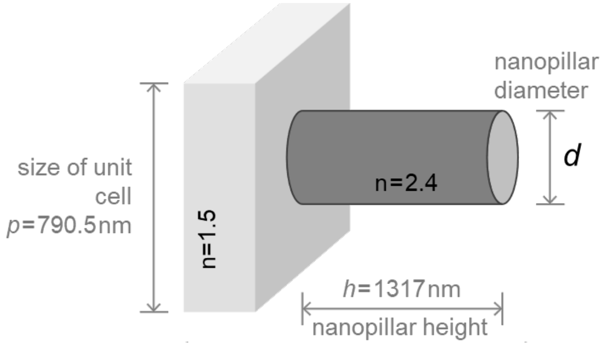

Analysis of Metagratings with PCA and FMM

Period/ Lambda	NA of Lens	Efficiency of Desired Order		Reflected light		Transmitted orders (FMM)
		PCA	FMM	PCA	FMM	
10.6	0.094					
5.3	0.189					
3.2	0.313					
2.9	0.345					
2.1	0.476					
1.3	0.769					

Phase response obtained after one period of metagrating when analyzed using PCA/FMM:

One period of the metagrating

Analysis of Metagratings with PCA and FMM

Period/ Lambda	NA of Lens	Efficiency of Desired Order		Reflected light		Transmitted orders (FMM)
		PCA	FMM	PCA	FMM	
10.6	0.094	95.9 %	94.4 %	4.1 %	3.8 %	1.8 %
5.3	0.189					
3.2	0.313					
2.9	0.345					
2.1	0.476					
1.3	0.769					

Phase response obtained after one period of metagrating when analyzed using **PCA**:

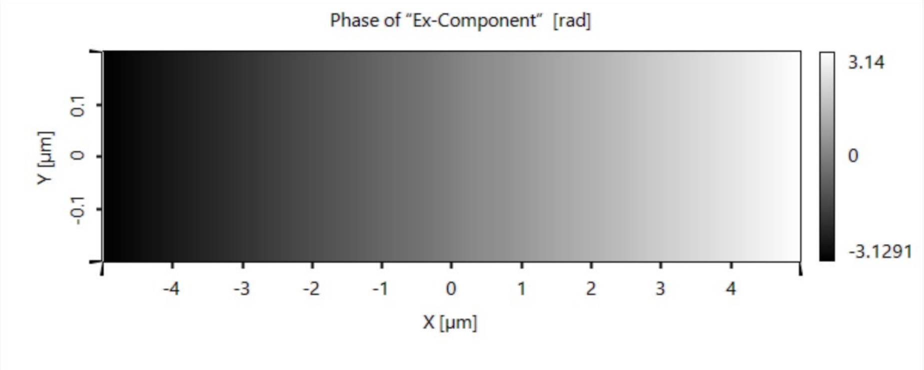

1D Plot

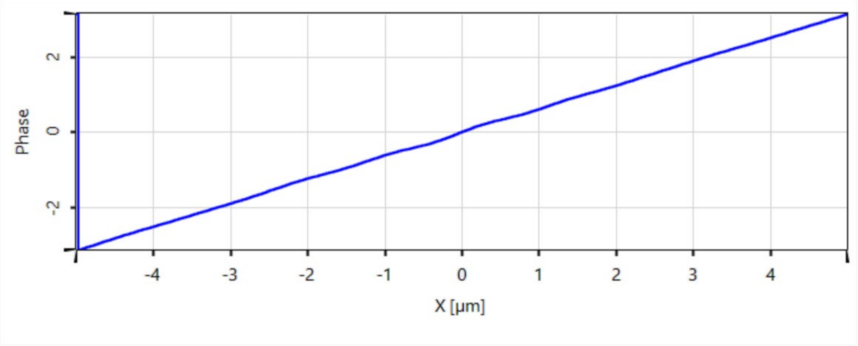

One period of the metagrating

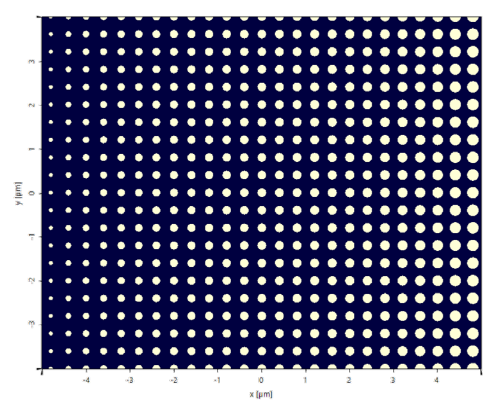

Analysis of Metagratings with PCA and FMM

Period/ Lambda	NA of Lens	Efficiency of Desired Order		Reflected light		Transmitted orders (FMM)
		PCA	FMM	PCA	FMM	
10.6	0.094	95.9 %	94.4 %	4.1 %	3.8 %	1.8 %
5.3	0.189					
3.2	0.313					
2.9	0.345					
2.1	0.476					
1.3	0.769					

Phase response obtained after one period of metagrating when analyzed using **FMM**:

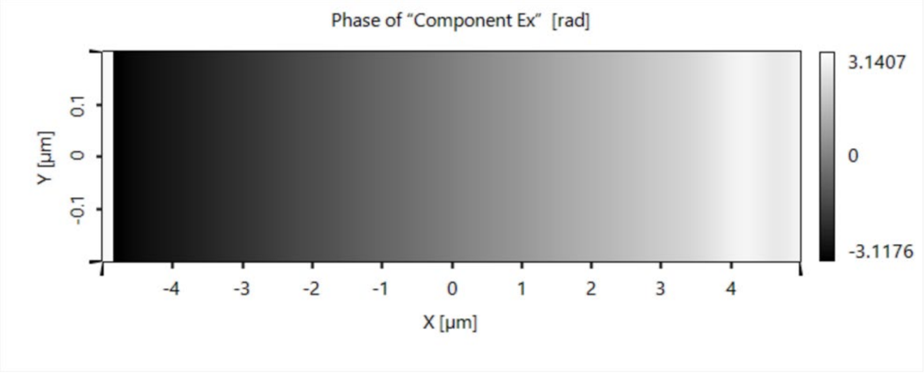

1D Plot

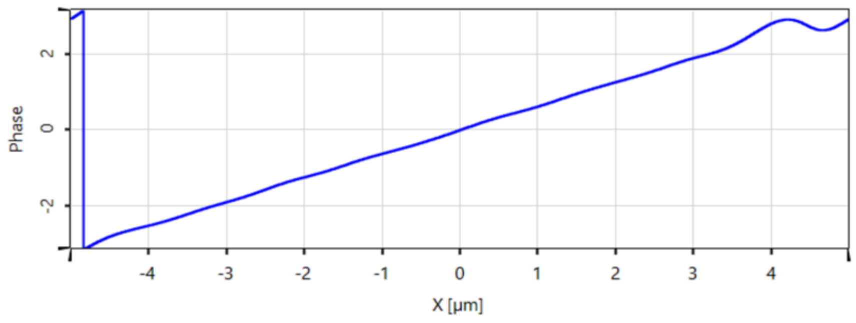

One period of the metagrating

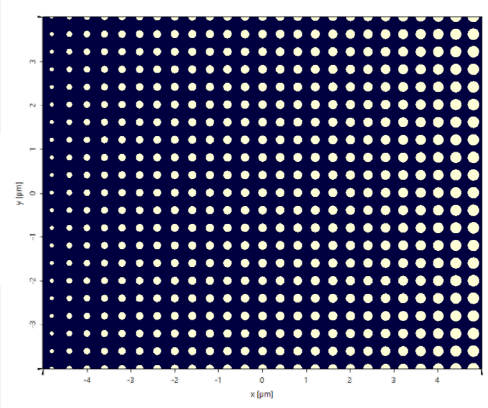

Analysis of Metagratings with PCA and FMM

Period/ Lambda	NA of Lens	Efficiency of Desired Order		Reflected light		Transmitted orders (FMM)
		PCA	FMM	PCA	FMM	
10.6	0.094	95.9 %	94.4 %	4.1 %	3.8 %	1.8 %
5.3	0.189	95.9 %	92.6 %	4.1 %	4.4 %	3 %
3.2	0.313					
2.9	0.345					
2.1	0.476					
1.3	0.769					

Phase response obtained after one period of metagrating when analyzed using **PCA**:

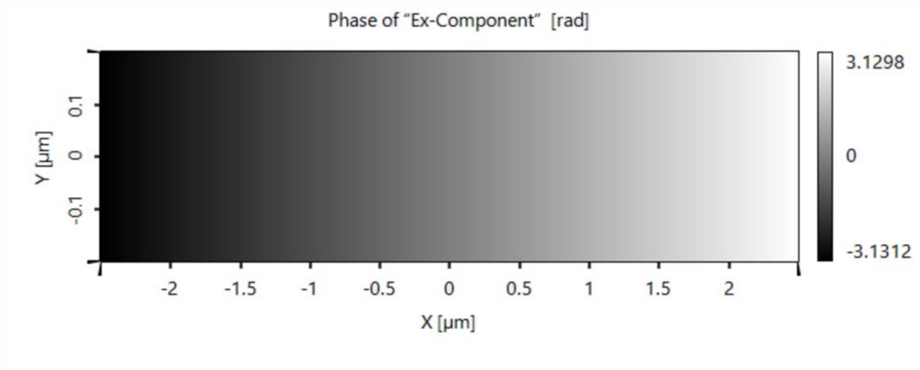

1D Plot

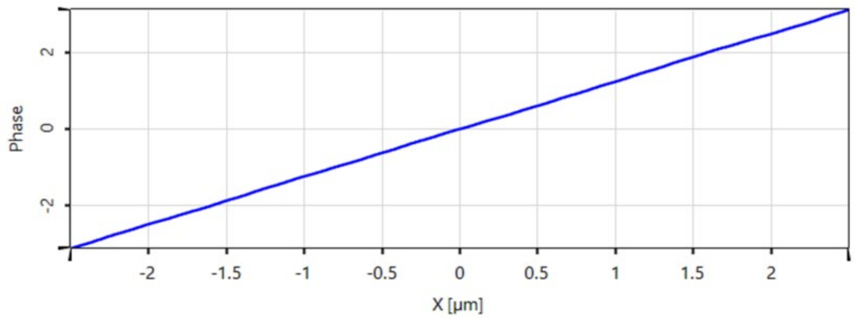

One period of the metagrating

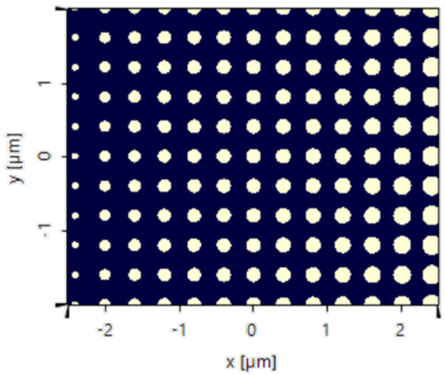

Analysis of Metagratings with PCA and FMM

Period/ Lambda	NA of Lens	Efficiency of Desired Order		Reflected light		Transmitted orders (FMM)
		PCA	FMM	PCA	FMM	
10.6	0.094	95.9 %	94.4 %	4.1 %	3.8 %	1.8 %
5.3	0.189	95.9 %	92.6 %	4.1 %	4.4 %	3 %
3.2	0.313					
2.9	0.345					
2.1	0.476					
1.3	0.769					

Phase response obtained after one period of metagrating when analyzed using **FMM**:

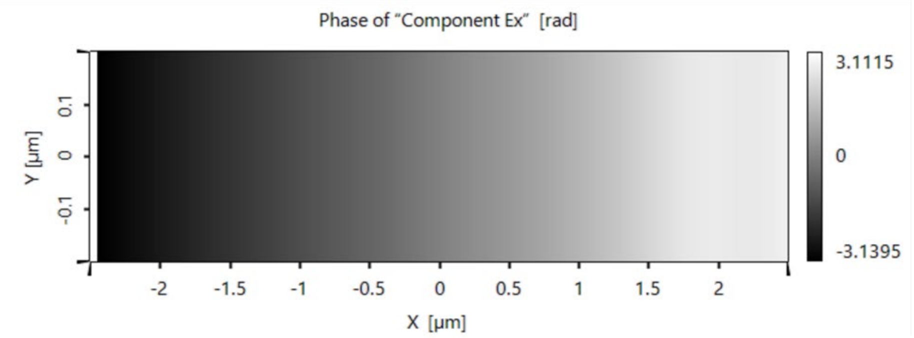

1D Plot

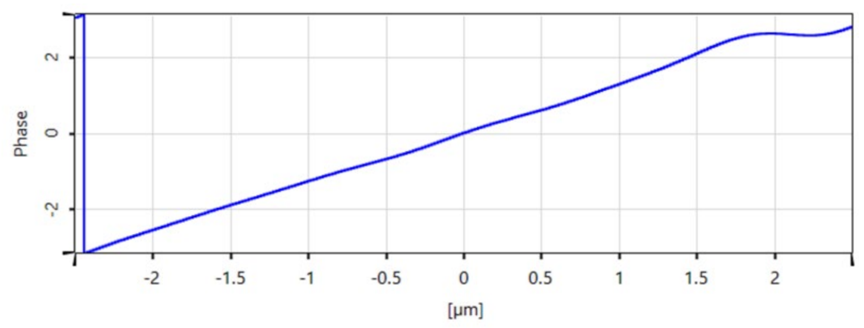

One period of the metagrating

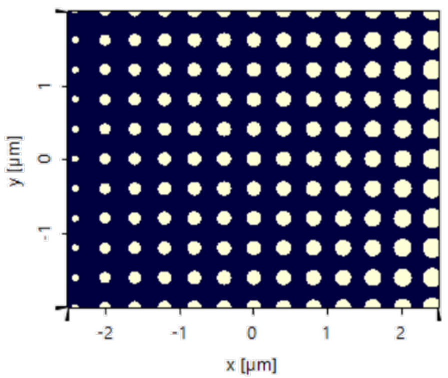

Analysis of Metagratings with PCA and FMM

Period/ Lambda	NA of Lens	Efficiency of Desired Order		Reflected light		Transmitted orders (FMM)
		PCA	FMM	PCA	FMM	
10.6	0.094	95.9 %	94.4 %	4.1 %	3.8 %	1.8 %
5.3	0.189	95.9 %	92.6 %	4.1 %	4.4 %	3 %
3.2	0.313	95.9 %	86.7 %	4.1 %	8.5 %	4.8 %
2.9	0.345					
2.1	0.476					
1.3	0.769					

Phase response obtained after one period of metagrating when analyzed using **PCA**:

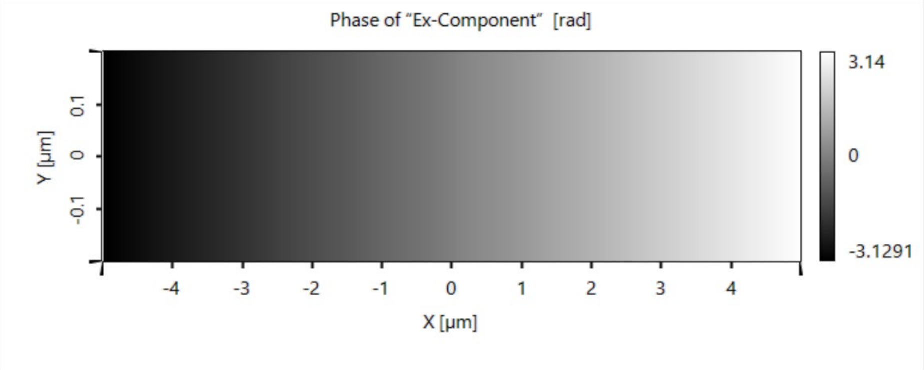

1D Plot

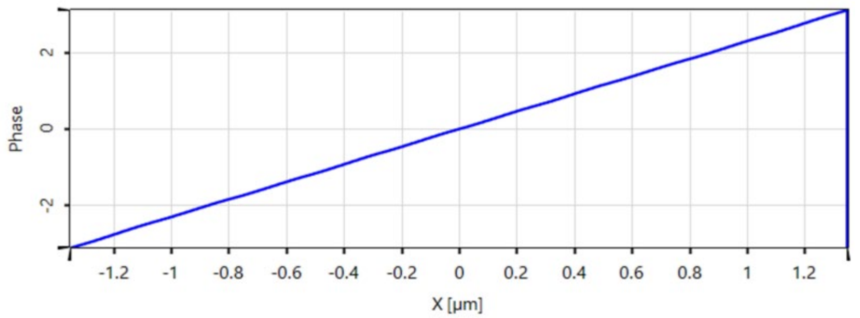

One period of the metagrating

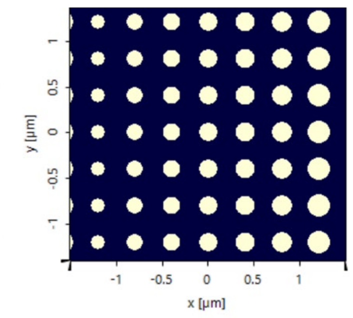

Analysis of Metagratings with PCA and FMM

Period/ Lambda	NA of Lens	Efficiency of Desired Order		Reflected light		Transmitted orders (FMM)
		PCA	FMM	PCA	FMM	
10.6	0.094	95.9 %	94.4 %	4.1 %	3.8 %	1.8 %
5.3	0.189	95.9 %	92.6 %	4.1 %	4.4 %	3 %
3.2	0.313	95.9 %	86.7 %	4.1 %	8.5 %	4.8 %
2.9	0.345					
2.1	0.476					
1.3	0.769					

Phase response obtained after one period of metagrating when analyzed using **FMM**:

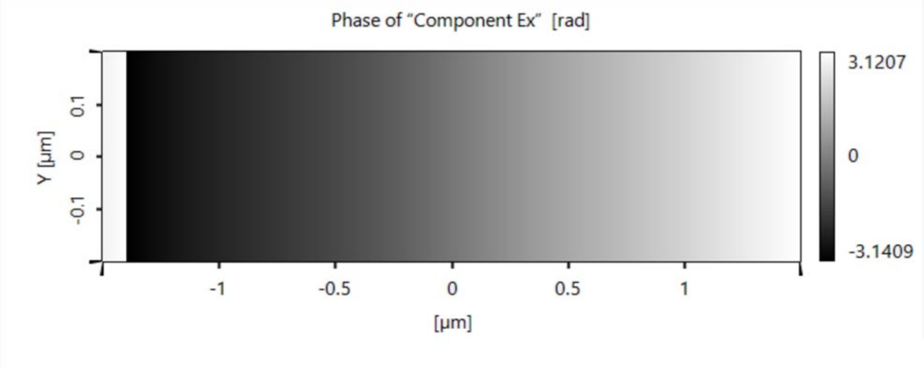

1D Plot

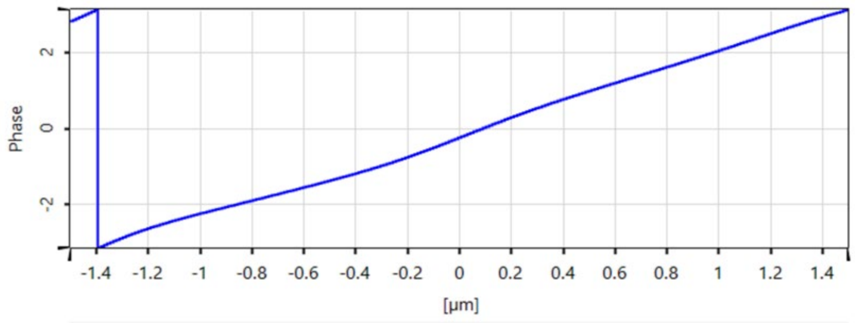

One period of the metagrating

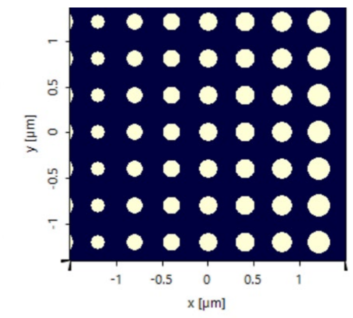

Analysis of Metagratings with PCA and FMM

Period/ Lambda	NA of Lens	Efficiency of Desired Order		Reflected light		Transmitted orders (FMM)
		PCA	FMM	PCA	FMM	
10.6	0.094	95.9 %	94.4 %	4.1 %	3.8 %	1.8 %
5.3	0.189	95.9 %	92.6 %	4.1 %	4.4 %	3 %
3.2	0.313	95.9 %	86.7 %	4.1 %	8.5 %	4.8 %
2.9	0.345	95.9 %	87.6 %	4.1 %	7.5 %	4.9 %
2.1	0.476					
1.3	0.769					

Phase response obtained after one period of metagrating when analyzed using **PCA**:

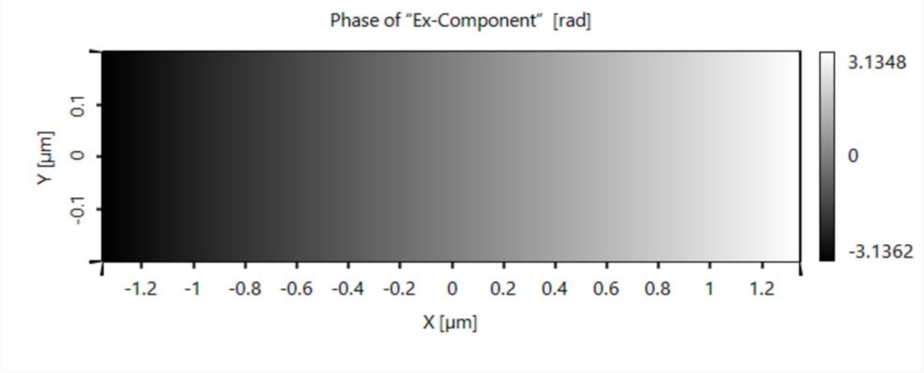

1D Plot

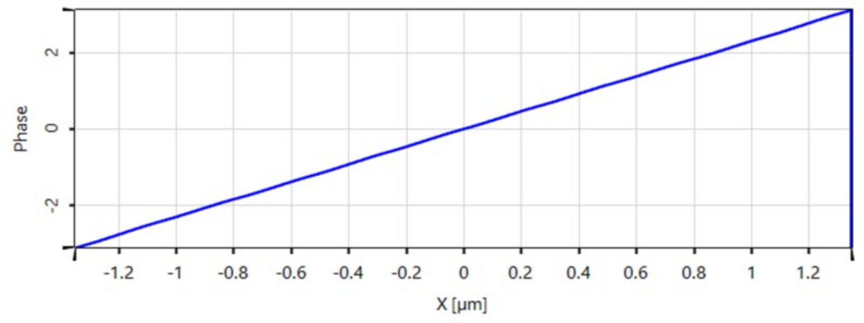

One period of the metagrating

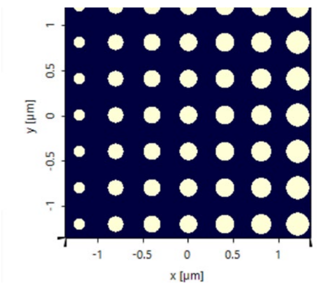

Analysis of Metagratings with PCA and FMM

Period/ Lambda	NA of Lens	Efficiency of Desired Order		Reflected light		Transmitted orders (FMM)
		PCA	FMM	PCA	FMM	
10.6	0.094	95.9 %	94.4 %	4.1 %	3.8 %	1.8 %
5.3	0.189	95.9 %	92.6 %	4.1 %	4.4 %	3 %
3.2	0.313	95.9 %	86.7 %	4.1 %	8.5 %	4.8 %
2.9	0.345	95.9 %	87.6 %	4.1 %	7.5 %	4.9 %
2.1	0.476					
1.3	0.769					

Phase response obtained after one period of metagrating when analyzed using **FMM**:

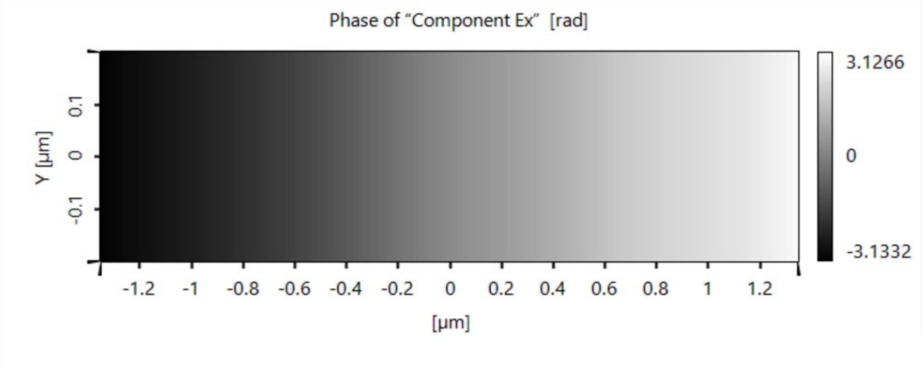

1D Plot

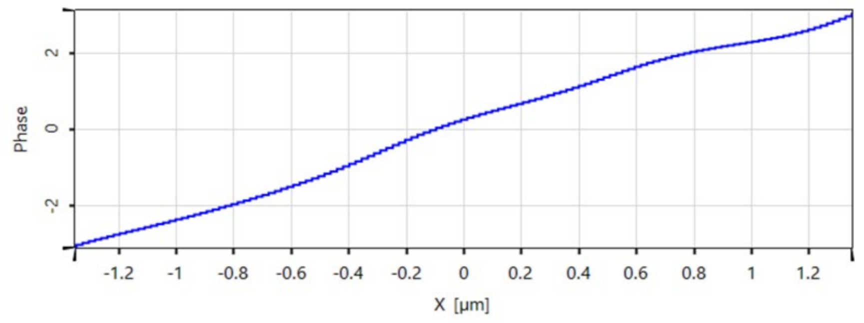

One period of the metagrating

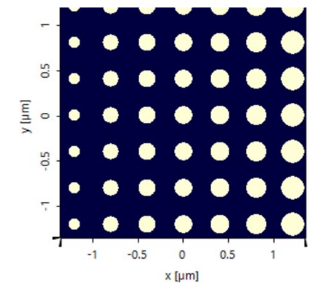

Analysis of Metagratings with PCA and FMM

Period/ Lambda	NA of Lens	Efficiency of Desired Order		Reflected light		Transmitted orders (FMM)
		PCA	FMM	PCA	FMM	
10.6	0.094	95.9 %	94.4 %	4.1 %	3.8 %	1.8 %
5.3	0.189	95.9 %	92.6 %	4.1 %	4.4 %	3 %
3.2	0.313	95.9 %	86.7 %	4.1 %	8.5 %	4.8 %
2.9	0.345	95.9 %	87.6 %	4.1 %	7.5 %	4.9 %
2.1	0.476	95.9 %	82.2 %	4.1 %	12.3 %	5.5 %
1.3	0.769					

Phase response obtained after one period of metagrating when analyzed using **PCA**:

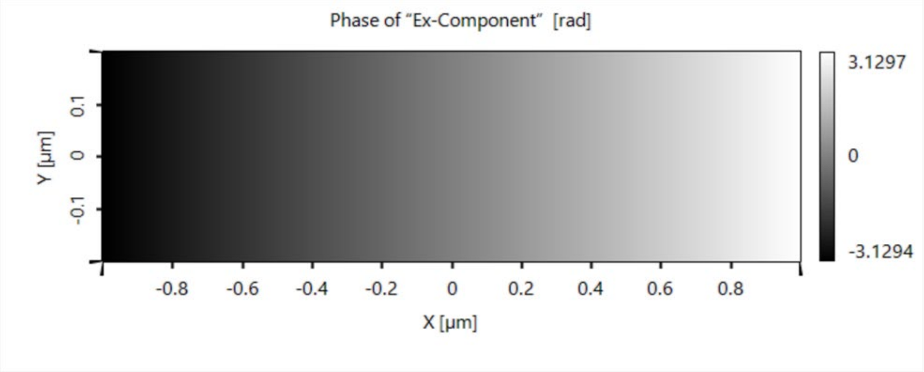

1D Plot

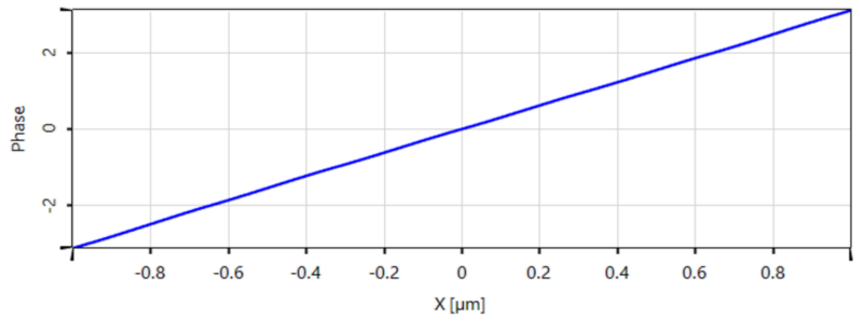

One period of the metagrating

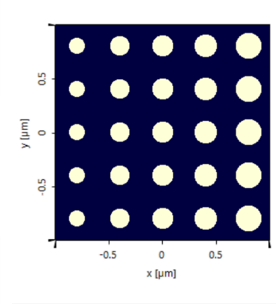

Analysis of Metagratings with PCA and FMM

Period/ Lambda	NA of Lens	Efficiency of Desired Order		Reflected light		Transmitted orders (FMM)
		PCA	FMM	PCA	FMM	
10.6	0.094	95.9 %	94.4 %	4.1 %	3.8 %	1.8 %
5.3	0.189	95.9 %	92.6 %	4.1 %	4.4 %	3 %
3.2	0.313	95.9 %	86.7 %	4.1 %	8.5 %	4.8 %
2.9	0.345	95.9 %	87.6 %	4.1 %	7.5 %	4.9 %
2.1	0.476	95.9 %	82.2 %	4.1 %	12.3 %	5.5 %
1.3	0.769					

Phase response obtained after one period of metagrating when analyzed using **FMM**:

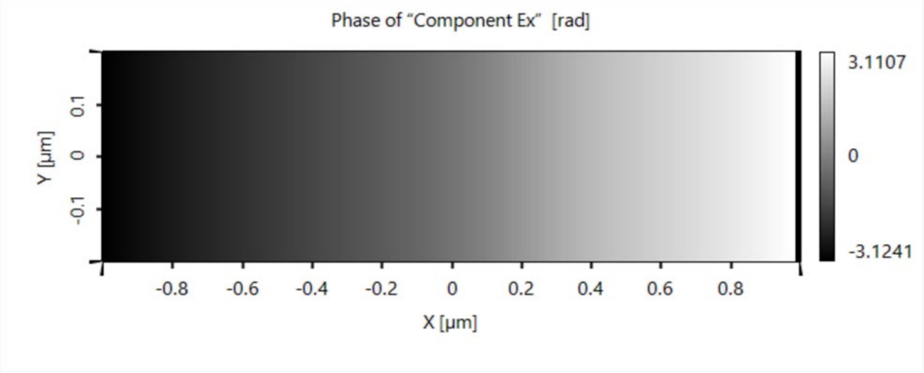

1D Plot

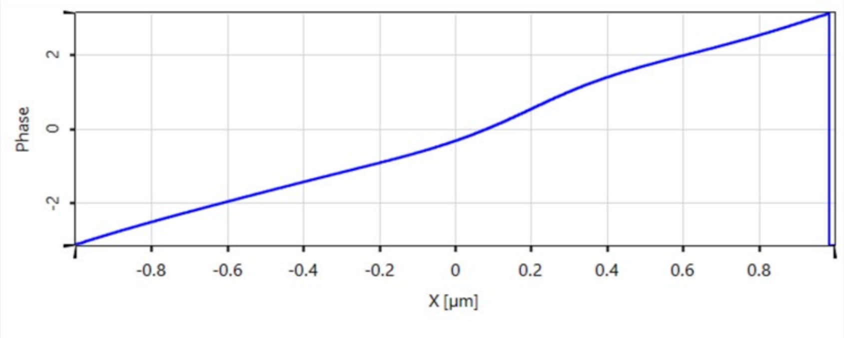

One period of the metagrating

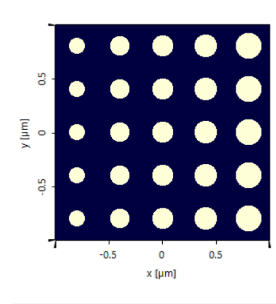

Analysis of Metagratings with PCA and FMM

Linear polarization: x-direction

Period/ Lambda	NA of Lens	Efficiency of Desired Order		Reflected light		Transmitted orders (FMM)
		PCA	FMM	PCA	FMM	
10.6	0.094	95.9 %	94.4 %	4.1 %	3.8 %	1.8 %
5.3	0.189	95.9 %	92.6 %	4.1 %	4.4 %	3 %
3.2	0.313	95.9 %	86.7 %	4.1 %	8.5 %	4.8 %
2.9	0.345	95.9 %	87.6 %	4.1 %	7.5 %	4.9 %
2.1	0.476	95.9 %	82.2 %	4.1 %	12.3 %	5.5 %
1.3	0.769	95.9 %	16.5 %	4.1 %	59.9 %	23.6 %

Phase response obtained after one period of metagrating when analyzed using **PCA**:

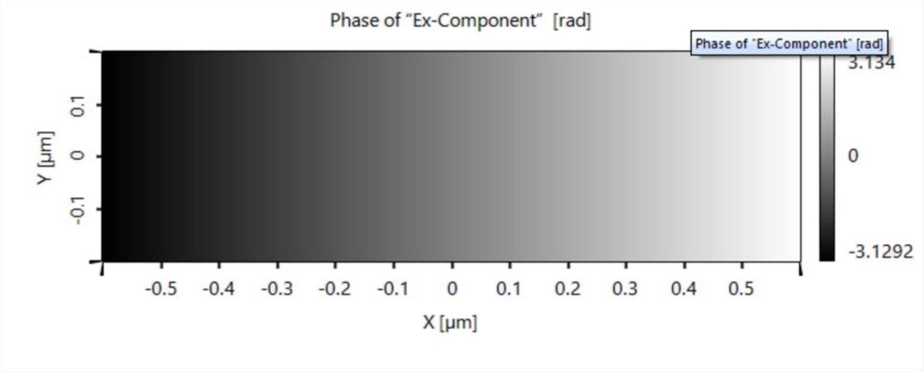

1D Plot

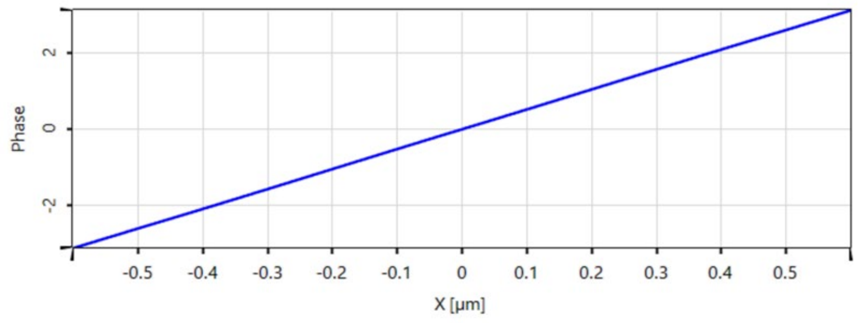

One period of the metagrating

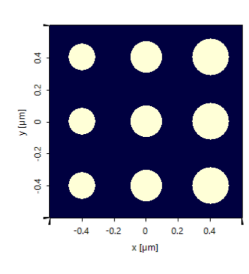

Analysis of Metagratings with PCA and FMM

Linear polarization: x-direction

Period/ Lambda	NA of Lens	Efficiency of Desired Order		Reflected light		Transmitted orders (FMM)
		PCA	FMM	PCA	FMM	
10.6	0.094	95.9 %	94.4 %	4.1 %	3.8 %	1.8 %
5.3	0.189	95.9 %	92.6 %	4.1 %	4.4 %	3 %
3.2	0.313	95.9 %	86.7 %	4.1 %	8.5 %	4.8 %
2.9	0.345	95.9 %	87.6 %	4.1 %	7.5 %	4.9 %
2.1	0.476	95.9 %	82.2 %	4.1 %	12.3 %	5.5 %
1.3	0.769	95.9 %	16.5 %	4.1 %	59.9 %	23.6 %

One period of the metagrating

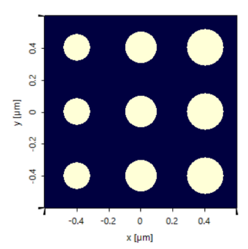

Phase response obtained after one period of metagrating when analyzed using **FMM**:

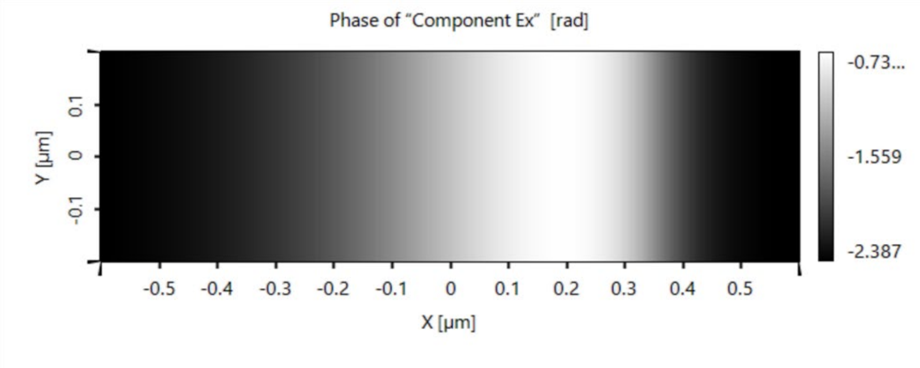

1D Plot

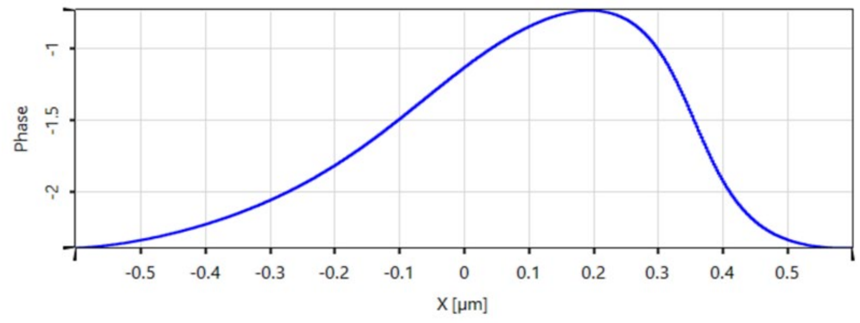

Analysis of Metagratings with PCA and FMM

Linear polarization: y-direction

Period/ Lambda	NA of Lens	Efficiency of Desired Order		Reflected light		Transmitted orders (FMM)
		PCA	FMM	PCA	FMM	
10.6	0.094	95.9 %	94.4 %	4.1 %	3.8 %	1.8 %
5.3	0.189	95.9 %	92.6 %	4.1 %	4.4 %	3 %
3.2	0.313	95.9 %	86.7 %	4.1 %	8.5 %	4.8 %
2.9	0.345	95.9 %	87.6 %	4.1 %	7.5 %	4.9 %
2.1	0.476	95.9 %	82.2 %	4.1 %	12.3 %	5.5 %
1.3	0.769	95.9 %	76.6 %	4.1 %	19.6 %	3.8 %

Phase response obtained after one period of metagrating when analyzed using **FMM**:

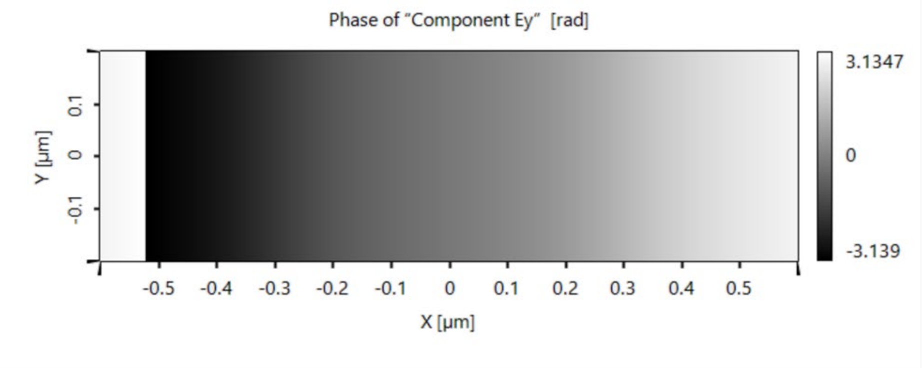

1D Plot

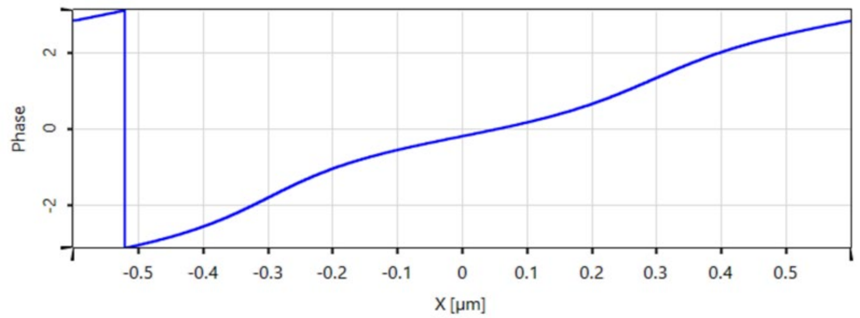

One period of the metagrating

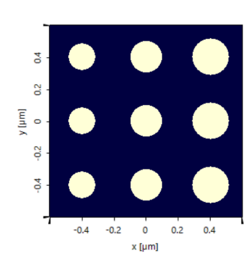

Analysis of Metagratings with PCA and FMM: Summary

Period/ Lambda	NA of Lens	Efficiency of Desired Order		Reflected light		Transmitted orders (FMM)
		PCA	FMM	PCA	FMM	
10.6	0.094	95.9 %	94.4 %	4.1 %	3.8 %	1.8 %
5.3	0.189	95.9 %	92.6 %	4.1 %	4.4 %	3 %
3.2	0.313	95.9 %	86.7 %	4.1 %	8.5 %	4.8 %
2.9	0.345	95.9 %	87.6 %	4.1 %	7.5 %	4.9 %
2.1	0.476	95.9 %	82.2 %	4.1 %	12.3 %	5.5 %
1.3	0.769	95.9 %	76.6 %	4.1 %	19.6 %	3.8 %

Resonance domain; typically not suitable for lens design

- The PCA offers high precision in phase modeling and design outside of the resonance domain of local gratings.
- PCA is unable to forecast the emergence of stray light in higher-order reflections and transmissions.
- The Local Metagrating Approximation (LMGA) can achieve this.

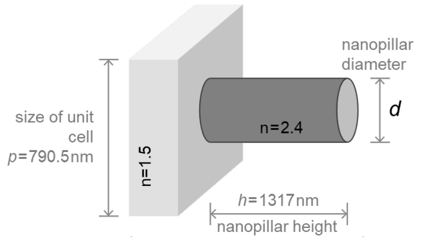

Using a Trained Neural Network for Modeling

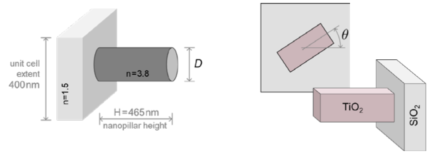

Structure of metacell

Simulation model (PCA)

Matrix values $\mathbf{M}(\boldsymbol{p}; \hat{\boldsymbol{s}}^{\mathrm{in}}, \lambda)$

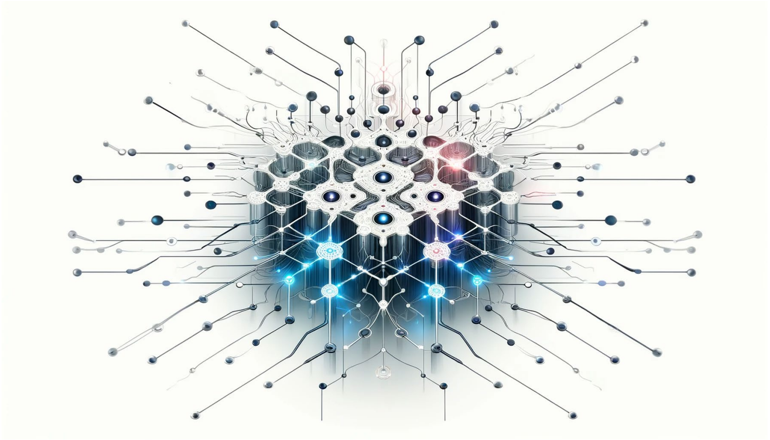

Orthogonal vector basis
$\boldsymbol{W}_1$ and $\boldsymbol{W}_2$

Wavefront phase candidates
$\Psi_1^{\mathrm{c.d.}}$ and $\Psi_2^{\mathrm{c.d.}}$

$$\begin{aligned}\boldsymbol{E}^{\mathrm{in}} &= \boldsymbol{U}^{\mathrm{in}} \exp[\mathrm{i}\psi^{\mathrm{in}}] \\ &= \{V_1^{\mathrm{in}} \boldsymbol{W}_1 + V_2^{\mathrm{in}} \boldsymbol{W}_2\} \exp[\mathrm{i}\psi^{\mathrm{in}}]\end{aligned}$$

$$\Rightarrow$$

$$\begin{aligned}\boldsymbol{E}^{\mathrm{out}} &= \boldsymbol{U}_1^{\mathrm{out}} \exp[\mathrm{i}\{\psi^{\mathrm{in}} + \Psi_1\}] + \boldsymbol{U}_2^{\mathrm{out}} \exp[\mathrm{i}\{\psi^{\mathrm{in}} + \Psi_2\}] \\ &= \boldsymbol{U}^{\mathrm{out}} \exp[\mathrm{i}\{\psi^{\mathrm{in}} + \Psi\}]\,, \text{if } \Psi_1 = \Psi_2 =: \Psi\end{aligned}$$

Using a Trained Neural Network for Modeling

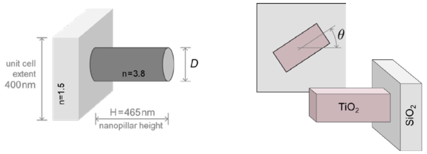

Structure of metacell

Simulation models:
PCA and LMGA

Matrix values $\mathbf{M}(\boldsymbol{p};\hat{\boldsymbol{s}}^{\mathrm{in}},\lambda)$

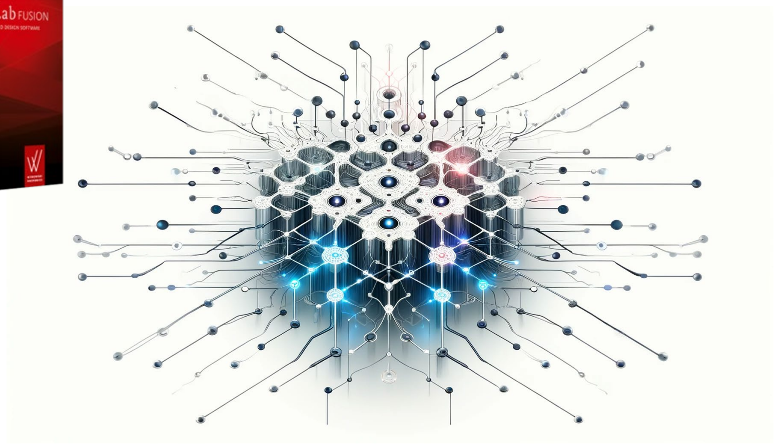

Orthogonal vector basis
$\boldsymbol{W}_1$ and $\boldsymbol{W}_2$

Wavefront phase candidates
$\Psi_1^{\mathrm{c.d.}}$ and $\Psi_2^{\mathrm{c.d.}}$

$$\begin{aligned}\boldsymbol{E}^{\mathrm{in}} &= \boldsymbol{U}^{\mathrm{in}}\exp[\mathrm{i}\psi^{\mathrm{in}}]\\ &= \left\{V_1^{\mathrm{in}}\boldsymbol{W}_1 + V_2^{\mathrm{in}}\boldsymbol{W}_2\right\}\exp[\mathrm{i}\psi^{\mathrm{in}}]\end{aligned}$$

$$\Rightarrow$$

$$\begin{aligned}\boldsymbol{E}^{\mathrm{out}} &= \boldsymbol{U}_1^{\mathrm{out}}\exp[\mathrm{i}\{\psi^{\mathrm{in}}+\Psi_1\}] + \boldsymbol{U}_2^{\mathrm{out}}\exp[\mathrm{i}\{\psi^{\mathrm{in}}+\Psi_2\}]\\ &= \boldsymbol{U}^{\mathrm{out}}\exp[\mathrm{i}\{\psi^{\mathrm{in}}+\Psi\}]\,,\text{ if } \Psi_1=\Psi_2=:\Psi\end{aligned}$$

“Roughness” of Metalenses

“Roughness” of Metalenses

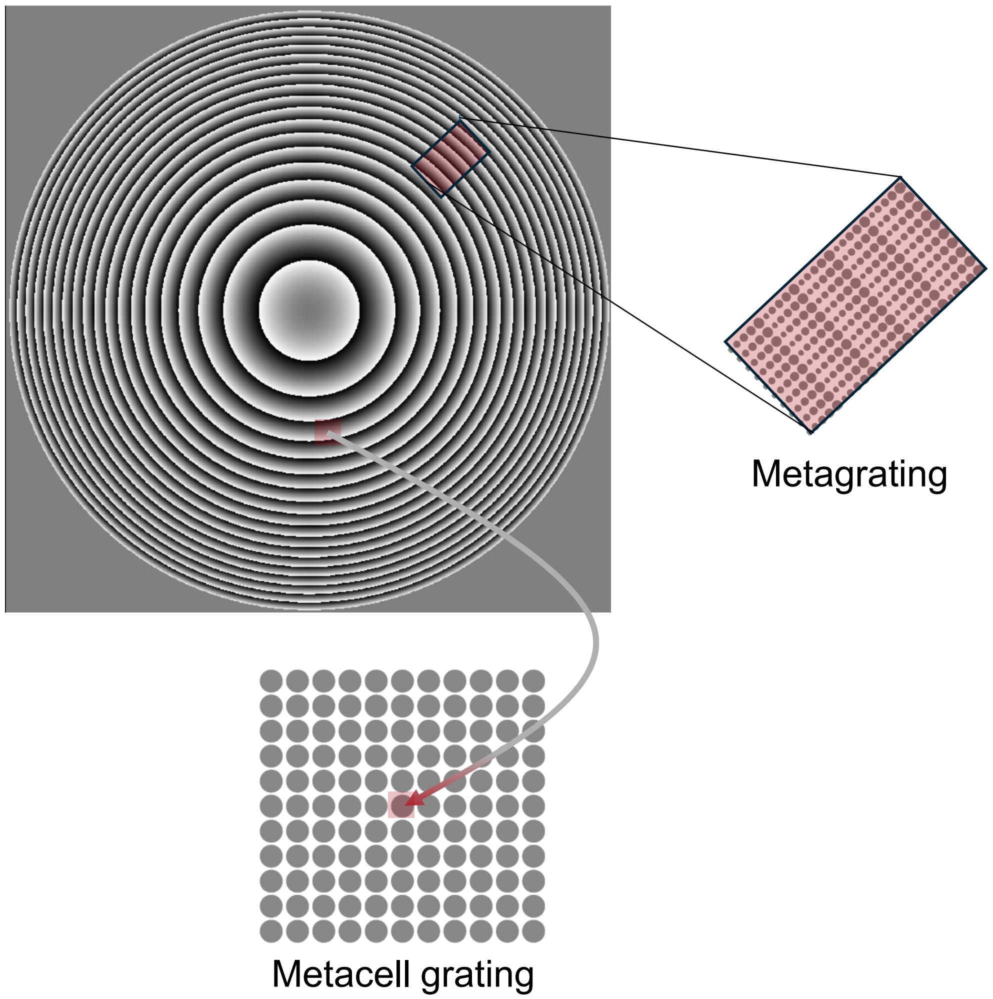

- Combining the PCA and LMGA simulation models with the neural network approach provides an excellent trade-off between precision and efficiency for simulating flat lenses in lens systems.
- Nevertheless, they do not completely consider the specific grid arrangement of the metacells.
- From a modeling standpoint, this phenomenon results in a slight increase in stray light, which can be interpreted as a consequence of the metalens’s intrinsic "roughness."
- This intrinsic "roughness" plays a similar role in metalens modeling as modeling the roughness and other defects of lens surfaces.

“Roughness” of Metalenses

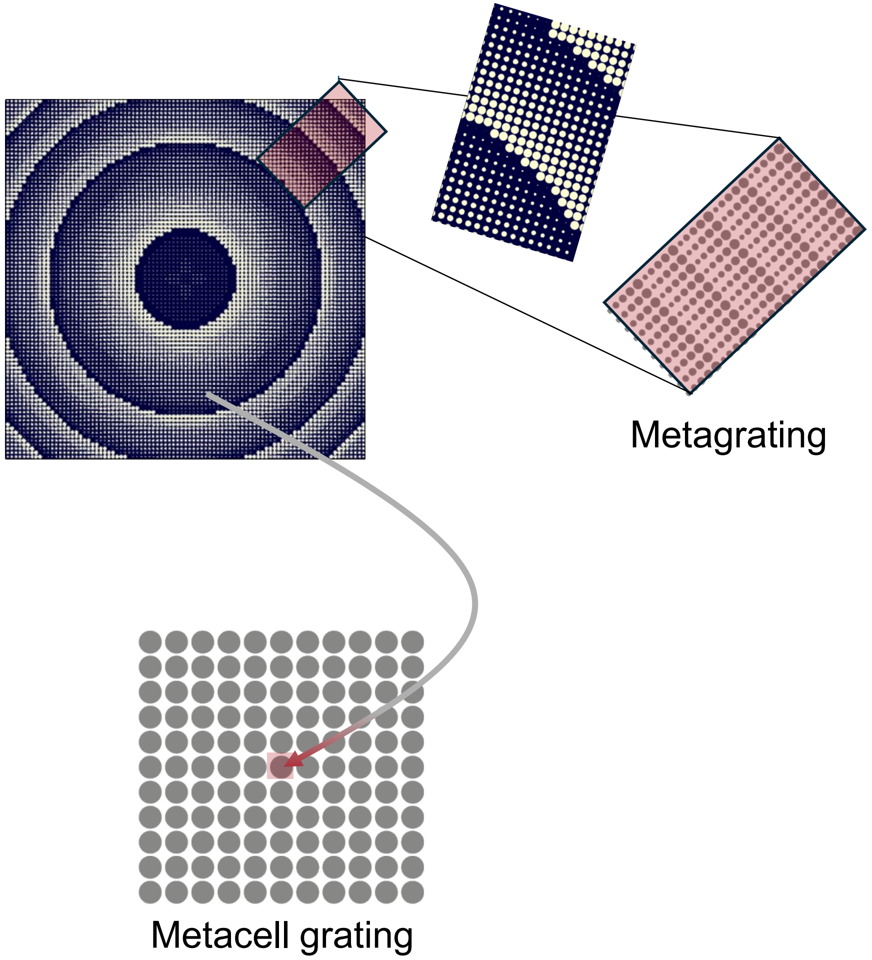

- Combining the PCA and LMGA simulation models with the neural network approach provides an excellent trade-off between precision and efficiency for simulating flat lenses in lens systems.
- Nevertheless, they do not completely consider the specific grid arrangement of the metacells.
- From a modeling standpoint, this phenomenon results in a slight increase in stray light, which can be interpreted as a consequence of the metalens’s intrinsic "roughness."
- This intrinsic "roughness" plays a similar role in metalens modeling as modeling the roughness and other defects of lens surfaces.

Field Decomposition, FMM/PML, and Distributed Computing

Metasurface

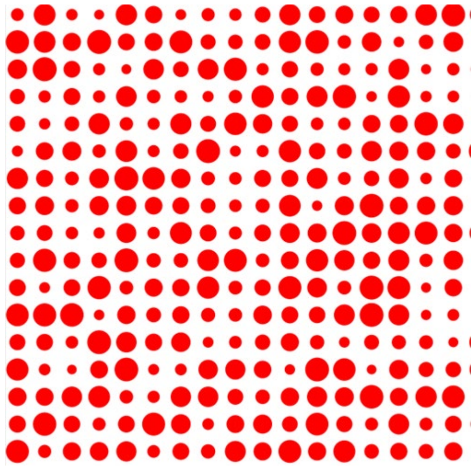

Field Decomposition, FMM/PML, and Distributed Computing

Illuminate metalens with subfields

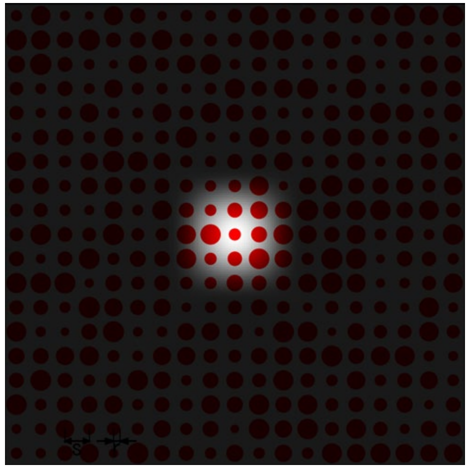

Subfields

Simulation with FMM and Perfect Matched Layer (PML)

Distribute FMM/PML subfield simulations over a computer network.

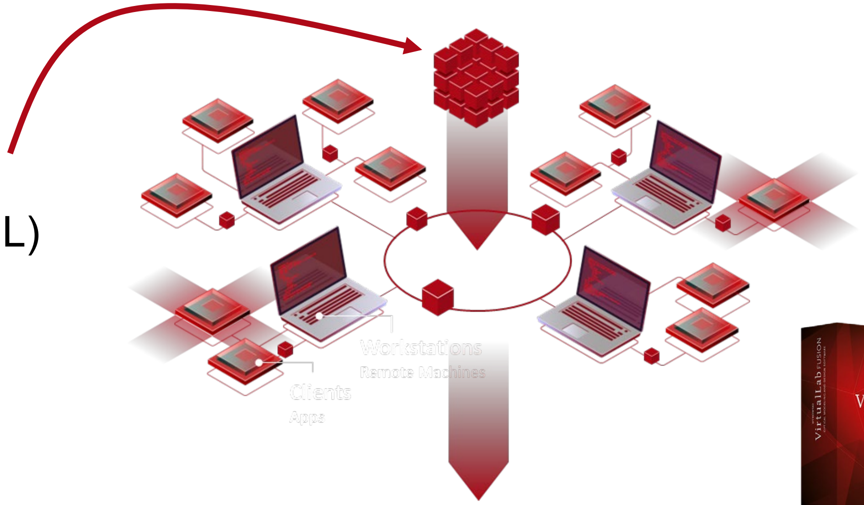

Simulation result for entire metalens

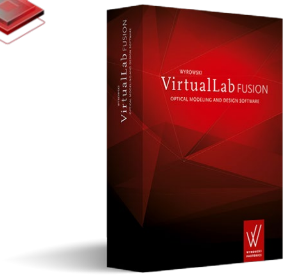

Conclusion

Summary

- Flat lenses represent a significant and fascinating enhancement to the toolkit available for optical design, particularly in the fields of imaging and illumination.
- Ultimately, it is essential to incorporate flat lens technology into lens design workflows to fully grasp and take advantage of their potential.
- In this year's forthcoming software updates, we will be incorporating the flat lens technologies showcased in this webinar, allowing you to use them directly.

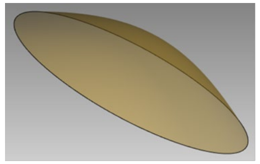

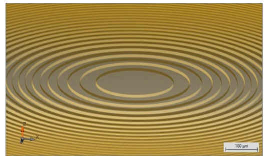

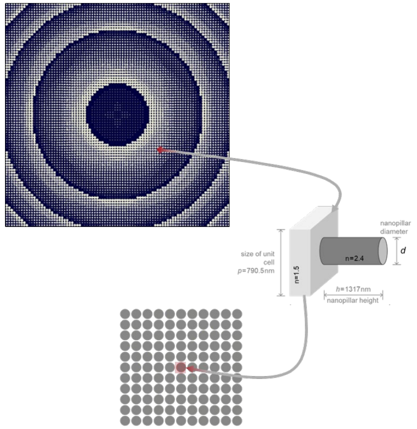

Metacell grating

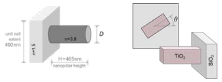

Structure of metacell

Simulation models:
PCA and LMGA

Matrix values $\mathbf{M}(\boldsymbol{p}; \hat{\boldsymbol{s}}^{\text{in}}, \lambda)$

Orthogonal vector basis
$\boldsymbol{W}_1$ and $\boldsymbol{W}_2$

Wavefront phase candidates
$\Psi_1^{\text{c.d.}}$ and $\Psi_2^{\text{c.d.}}$